Structure-Preserving Model Reduction on Subspaces and Manifolds

Patrick Buchfink

Structure-Preserving Model Reduction on Subspaces and Manifolds

Von der Fakultät Mathematik und Physik und dem
Stuttgarter Zentrum für Simulationswissenschaft (SC SimTech)
der Universität Stuttgart zur Erlangung der Würde eines
Doktors der Naturwissenschaften (Dr. rer. nat.)
genehmigte Abhandlung

vorgelegt von

Patrick Buchfink

aus Backnang

Hauptberichter:	Prof. Dr. Bernard Haasdonk
Mitberichter:	Prof. Dr. Tatjana Stykel
	Prof. Dr. Boris Krämer

Tag der mündlichen Prüfung: 15. März 2024

Institut für Angewandte Analysis und Numerische Simulation,
Universität Stuttgart

2024

University of Stuttgart
Germany

SimTech

Acknowledgements

Contents

Abstract

Mathematical models are a key enabler to understand complex processes across all branches of research and development since such models allow us to simulate the behavior of the process without physically realizing it. However, detailed models are computationally demanding and, thus, are frequently prohibited from being evaluated (a) multiple times for different parameters, (b) in real time or (c) on hardware with low computational power. The field of model (order) reduction (MOR) aims to approximate such detailed models with more efficient surrogate models that are suitable for the tasks (a-c). In classical MOR, the solutions of the detailed model are approximated in a problem-specific, low-dimensional subspace, which is why we refer to it as MOR on subspaces. The subspace is characterized by a reduced basis that can be computed from given data with a so-called basis generation technique.

The two key aspects in this thesis are: (i) structure-preserving MOR techniques and (ii) MOR on manifolds. Preserving given structures throughout the reduction is important to obtain physically consistent reduced models. We demonstrate this for Lagrangian and Hamiltonian systems, which are dynamical systems that guarantee preservation of energy over time. MOR on manifolds, on the other hand, broadens the applicability of MOR to problems that cannot be treated efficiently with MOR on subspaces.

The first part of this thesis introduces and analyzes new basis generation techniques for structure-preserving MOR of Hamiltonian systems. The introduced methods are able to compute a non-orthogonal basis, which allows deriving more concise reduced models compared to existing approaches. Moreover, we introduce a structure-preserving greedy procedure and a provably optimal basis generation technique for a special case.

The second part of this thesis develops an expressive framework to formulate structure-preserving MOR on manifolds with differential geometry. The structure of both Lagrangian and Hamiltonian systems can be treated in this formalism and many existing nonlinear dimension reduction techniques are reflected in our framework. Specifically for structure-preserving MOR on manifolds for Hamiltonian systems, we prove preservation of energy over time and preservation of Lyapunov-stable points. Moreover, we present an algorithm for structure-preserving MOR on manifolds of Hamiltonian systems based on so-called autoencoders. In the numerical experiment of this part, we consider a model that is hard to treat with MOR on subspaces and show that both (i) structure-preservation and (ii) MOR on manifolds improve the accuracy and robustness of the reduced models.

Zusammenfassung

Mathematische Modelle sind in Forschung und Entwicklung unerlässlich, um komplexe Prozesse zu verstehen, da solche Modelle das Systemverhalten vorhersagen können. Allerdings benötigen detaillierte Modelle viele Rechenressourcen und können deshalb oft nicht (a) mehrfach für verschiedene Parameter ausgewertet werden, (b) in Echtzeit reagieren, oder (c) auf Hardware mit geringer Rechenleistung operieren. Die Modell(-ordnungs-)reduktion (MOR) hat zum Ziel, solche rechenintensive Modelle mit effizienteren Ersatzmodellen zu approximieren und somit die oben beschriebenen Aufgaben (a-c) zu ermöglichen. Die klassische MOR approximiert dazu Lösungen des detaillierten Modells in einem niedrigdimensionalen, problemspezifischen Unterraum, weshalb wir diese als MOR auf Unterräumen bezeichnen. Der Unterraum kann durch eine reduzierte Basis charakterisiert werden, die wiederum mit einem sogenannten Basisgenerierungsverfahren berechnet werden kann.

Die zwei Hauptaspekte dieser Arbeit sind: (i) Strukturerhaltung und (ii) Modellreduktion auf Mannigfaltigkeiten. Strukturen während der Reduktion zu erhalten ist wichtig, um konsistente reduzierte Modelle zu erhalten. Wir zeigen dies anhand von Lagrangeschen und Hamiltonschen Systemen, welches dynamische Systeme sind, die die Erhaltung einer Energie garantieren. MOR auf Mannigfaltigkeiten hingegen erweitern die Anwendbarkeit von MOR auf Probleme, die mit MOR auf Unterräumen nicht effizient reduziert werden können.

Der erste Teil der Thesis führt neue Basisgenerierungsverfahren zur strukturerhaltenden MOR für Hamiltonsche Systeme ein und analysiert diese. Das beinhaltet ein Verfahren zur Generierung nicht-orthogonaler Basen, ein strukturerhaltendes Greedy-Verfahren und ein beweisbar optimales Verfahren für einen Spezialfall.

Der zweite Teil dieser Thesis entwickelt ein umfassendes Framework, um strukturerhaltende MOR auf Mannigfaltigkeiten mit Differentialgeometrie zu formulieren. Sowohl Lagrangesche als auch Hamiltonsche Systeme sind mit dem Framework abgedeckt. Ferner können vielseitige Methoden der nichtlinearen Dimensionsreduktion in dem Framework verwendet werden. Anschließend vertiefen wir die strukturerhaltende MOR für Hamiltonsche Systeme und führen dafür einen Algorithmus ein, der auf sogenannten Autoencodern basiert. In den numerischen Experimenten betrachten wir ein Modell, das sich nicht sinnvoll mit MOR auf Unterräumen reduzieren lässt und zeigen, dass beide Hauptaspekte dieser Thesis, (i) Strukturerhaltung und (ii) MOR auf Mannigfaltigkeiten, die Genauigkeit und Robustheit der reduzierten Modelle erhöht.

Introduction

<div align="right">

1

</div>

1.1 Motivation

Model (order) reduction (MOR) is a research area in the field of surrogate modelling. The challenge is to approximate the set of all solutions of a computationally demanding, high-dimensional model with a more efficient replacement. In the scope of MOR, we call these models the full(-order) model (FOM) and the reduced(-order) model (ROM) accordingly. Such surrogate modelling techniques are essential in research and development as the demand occurs naturally if (a) the FOM needs to be evaluated for many parameters (e.g. in parameter studies or sampling-based uncertainty quantification), (b) the FOM is required to be evaluated in real-time (e.g. in control problems or interactive simulations), or (c) the FOM is run on devices with low computational power (e.g. simulations on embedded devices based on microcontrollers). A subclass in MOR is projection-based MOR. The idea there is to project the FOM on a low-dimensional, problem-specific (linear) subspace to obtain the ROM. This subspace is typically characterized by a reduced(-order) basis (ROB) which is computed with a basis generation technique. The two main aspects of MOR investigated in the present thesis are (1.) structure-preserving MOR techniques and (2.) MOR on (sub-)manifolds:

1. In regard of the first aspect, a "structure" is any kind of mathematical property or object (e.g. a specific bilinear form, linearity, or block-structure of certain matrices). Assuming additional structures in the FOM allows guaranteeing desirable mathematical and physical properties, e.g., that the FOM solutions conserve energy over time. In this thesis, we are mostly interested in Hamiltonian systems, which are based on a so-called symplectic structure and guarantee the mentioned conservation of energy. The

goal of structure-preserving MOR is then to preserve these structures throughout the reduction and, thus, guarantee the corresponding mathematical and physical properties for the ROM. In that regard, structure-preserving MOR is physics-preserving, which is important to obtain physically consistent surrogate models.

2. Classical MOR approximates a solution on a low-dimensional (linear) subspace. Thus, we refer to it also as "MOR on subspaces". In contrast, MOR on manifolds approximates the solution on a low-dimensional submanifold. This is advantageous since the approximation quality of MOR on subspaces is known to be bounded from below by the so-called Kolmogorov n-widths of the set of all solutions [92]. If these Kolmogorov n-widths decay slowly, MOR on subspaces can thus not obtain efficient ROMs. It has been shown [44, 92] that especially for FOMs with transport-dominated solutions this is the case and thus such FOMs are problematic for MOR on subspaces, while MOR on manifolds does in general not suffer from this limitation (e.g. [91]). So the idea of MOR on manifolds is to broaden the applicability of MOR in general.

1.2 Structure of the Thesis

The thesis is split in two parts. Part I investigates structure-preserving MOR on subspaces for Hamiltonian system, which is typically referred to as symplectic MOR (on subspaces). In particular, new symplectic basis generation techniques are presented and analyzed. The goal is to compute smaller ROBs than existing techniques, which yields more efficient ROMs. To understand our contributions, we formulate the fundamentals of MOR on subspaces in Chapter 2 with slightly more emphasis on the underlying structures than usual. We start presenting our work by introducing a non-orthonormal, symplectic basis generation technique, the PSD SVD-like decomposition, in Chapter 3. Subsequently, we present in Chapter 4 the PSD-greedy, a greedy procedure for symplectic basis generation. Lastly, we demonstrate in Chapter 5 how to obtain a provably optimal symplectic ROB in the special case of a canonizable Hamiltonian system with periodic solutions.

Part II concerns structure-preserving MOR on manifolds to strive for more general physics-preserving surrogate models. We introduce an extensive framework for structure-preserving MOR on manifolds based on differential geometry in Chapter 6. Moreover, we show that structure-preserving MOR on subspaces and manifolds is reflected in this framework as well as various existing approaches that rely on nonlinear dimension reduction techniques.

Subsequently, we intensify the analysis for structure-preserving MOR on manifolds for Hamiltonian systems in Chapter 7. We prove theoretical findings on preservation of energy and stability as well as an error bound. Moreover, we modify autoencoders, a technique from machine learning, to (approximately) preserve the symplectic structure. In a numerical example, we show for a FOM with transport-dominated solution that both aspects of this thesis, (i) structure-preservation and (ii) MOR on manifolds, improve the accuracy and robustness of the surrogate models.

Remark 1.1 (Distinction to the Master's thesis [18])**:** *In previous work [18], we worked on orthosymplectic basis generation techniques, which is related to the work presented in Chapter 3. For a transparent separation of [18] with the present thesis, we briefly highlight the (i) similarities and (ii) differences: (i) In the numerical example, both works use a similar two-dimensional linear elasticity model of a cantilever beam and the same implementation for the FOM, orthosymplectic basis generation techniques and evaluation framework of ROMs. (ii) All theoretical results presented in Chapter 3 are disjoint from the Master's thesis. Moreover, all numerical results related to the newly developed PSD SVD-like decomposition are disjoint from [18].*

1.3 Publications

During the course of this thesis several publications were authored in cooperation with different coworkers. In the following all publications are listed chronologically together with a small summary or a reference to a section within this thesis. The following publications fall within the scope of this thesis:

[20] P. Buchfink, A. Bhatt, and B. Haasdonk. *Symplectic model order reduction with non-orthonormal bases.* Mathematical and Computational Applications 24.2 (2019). DOI: 10.3390/mca24020043
▷ see Chapter 3

[26] P. Buchfink, B. Haasdonk, and S. Rave. *PSD-greedy basis generation for structure-preserving model order reduction of Hamiltonian systems.* Proceedings of the conference Algoritmy 2020. http://www.iam.fmph.uniba.sk/amuc/ojs/index.php/algoritmy/article/view/1577/829 (last accessed 5-Dec-2023). Vydavateľstvo SPEKTRUM, 2020, pp. 151–160
▷ see Chapter 4

[21] P. Buchfink, S. Glas, and B. Haasdonk. *Optimal bases for symplectic model order reduction of canonizable linear Hamiltonian systems.* Proceedings of MATHMOD 2022. Vol. 55. 20. 2022, pp. 463–468. DOI: 10.1016/j.ifacol.2022.09.138
▷ see Chapter 5

[22] P. Buchfink, S. Glas, and B. Haasdonk. *Symplectic model reduction of Hamiltonian systems on nonlinear manifolds and approximation with weakly symplectic autoencoder.* SIAM Journal on Scientific Computing 45.2 (2023), A289–A311. DOI: 10.1137/21M1466657
▷ see Chapter 7

[24] P. Buchfink, S. Glas, B. Haasdonk, and B. Unger. *Model reduction on manifolds: A differential geometric framework.* Preprint. 2023. arXiv: 2312.01963 [math.NA]
▷ see Chapter 6

Outside the scope of the present thesis, the following publications were coauthored:

[25] P. Buchfink and B. Haasdonk. *Experimental comparison of symplectic and non-symplectic model order reduction on an uncertainty quantification problem.* Numerical mathematics and advanced applications ENUMATH 2019. Springer International Publishing, 2020. DOI: 10.1007/978-3-030-55874-1_19
▷ This paper compares different (non-)structure-preserving MOR techniques on subspaces in a numerical experiment in the context of Uncertainty Quantification.

[77] R. Leiteritz, P. Buchfink, B. Haasdonk, and D. Pflüger. *Surrogate-data-enriched physics-aware neural networks.* Proceedings of the northern lights deep learning workshop 2022. Vol. 3. 2022. DOI: 10.7557/18.6268
▷ This work investigates how physics-informed neural networks (PINNs) can be enriched with inexact data from other surrogate models like reduced-order models. The novelty is how to transfer the error estimates from MOR to the training of PINNs such that the inexact data is only trusted up to the error estimate.

[110] S. Shuva, P. Buchfink, O. Röhrle, and B. Haasdonk. *Reduced basis methods for efficient simulation of a rigid robot hand interacting with soft tissue.* Large-scale scientific computing. Springer International Publishing, 2022, pp. 402–409. DOI: 10.1007/978-3-030-97549-4_46
▷ In this publication, we apply different MOR techniques to a control problem from soft tissue modelling. Very positively, the structure-preserving basis generation with the PSD SVD-like decomposition gives the best results.

[23] P. Buchfink, S. Glas, and B. Haasdonk. *Approximation bounds for model reduction on polynomially mapped manifolds.* Comptes Rendus. Mathématique (2024)
▷ In this work, we introduce an analogue to the Kolmogorov n-widths for approximations based on polynomial embeddings. Moreover, we show that this quantity is bounded by Kolmogorov widths from below.

[53] R. Herkert, P. Buchfink, and B. Haasdonk. *Dictionary-based online-adaptive structure-preserving model order reduction for parametric Hamiltonian systems.* Proceedings of Model Reduction and Surrogate Modeling (MORE 2022). 2024
▷ In this publication, we formulate structure-preserving MOR for Hamiltonian systems with a dictionary-based approach.

[54] R. Herkert et al. *Randomized symplectic model order reduction for Hamiltonian systems.* Large-scale scientific computing. Springer International Publishing, 2024
▷ In this publication, we investigate techniques from randomized linear algebra for symplectic basis generation with the PSD complex SVD and the PSD SVD-like decomposition.

[103] J. Rettberg et al. *Port-Hamiltonian fluid–structure interaction modelling and structure-preserving model order reduction of a classical guitar.* Mathematical and Computer Modelling of Dynamical Systems 29.1 (2023), pp. 116–148. DOI: 10.1080/13873954.2023.2173238
▷ This publication investigates structure-preserving MOR on subspaces for a port-Hamiltonian formulation of a multiphysical model describing a guitar body.

[104] J. Rettberg et al. *Improved a posteriori error bounds for reduced port-Hamiltonian systems.* Preprint. 2023. arXiv: 2303.17329 [math.NA]
▷ In this preprint, we investigate two a posteriori error bounds, namely a hierarchical error bound and an error bound based on a so-called auxiliary linear problem.

[108] H. Sharma et al. *Symplectic model reduction of Hamiltonian systems using data-driven quadratic manifolds.* Computer Methods in Applied Mechanics and Engineering 417 (2023), p. 116402. DOI: 10.1016/j.cma.2023.116402
▷ In this publication, we develop structure-preserving MOR on manifolds for Hamiltonian system with quadratic embeddings.

1.4 Software

Within the scope of this thesis, different software frameworks have been implemented or modified by the author. A chronological overview is given here:

- Symplectic MOR in `RBmatlab`: An add-on for the existing open-source MOR library `RBmatlab` (v1.16.09) was implemented to provide symplectic MOR, which is used for the experiments of Chapter 3. It is publicly available: https://doi.org/10.5281/zenodo.2578078 (last accessed 5-Dec-2023).

- Symplectic MOR & three-dimensional linear elasticity in `pyMOR`: Symplectic MOR was implemented in the open-source library `pyMOR` [87] and a three-dimensional linear elasticity model has been formulated via `FEnics` [71] for the experiments of Chapter 4. The essential part of the code is included in `pyMOR 2022.1`. The contribution is documented in the release note: https://docs.pymor.org/2023-1-1/release_notes/all.html#pymor-2022-1-july-21-2022 (last accessed 5-Dec-2023).

- Hamiltonian systems in `python`: For a supervised Bachelor's thesis and the experiments in Chapter 7, a collection of Hamiltonian systems was implemented in `python`. The package is publicly available: https://github.com/pbuchfink/hamiltonian-models (last accessed 5-Dec-2023).

- Structure-preserving MOR on manifolds in `python`: A software package for MOR on manifolds was implemented in `python` using `pyTorch` [96]. It was used for the experiments of Chapter 7. The package is publicly available: https://github.com/pbuchfink/manifold-mor-wave (last accessed 5-Dec-2023).

Part I
Symplectic MOR on Subspaces and Symplectic Basis Generation

Fundamentals

2

In the following, we give a brief introduction to the fundamentals in order to understand our contributions in the field of symplectic MOR on subspaces. The fundamentals include linear algebra and calculus (Section 2.1), classical projection-based MOR (Section 2.2), symplectic vector spaces and Hamiltonian systems (Section 2.3), and symplectic MOR (Section 2.4).

2.1 Linear Algebra and Calculus

We give a very brief introduction to our notation of linear algebra. For more details, we refer to a basic algebra textbook like [65]. As the underlying field, we consider the real numbers $\mathbb{R}$.[1] In the following, we distinguish between coordinate representations in $\mathbb{R}^N$ with bold letters and general $\mathbb{R}$ vector spaces. This is slightly repetitive. However, this helps to understand the parallels to the formulation on manifolds in Part II.

Consider $N \in \mathbb{N}$. An element $\boldsymbol{v} \in \mathbb{R}^N$ is called a *vector* and $\boldsymbol{A} \in \mathbb{R}^{M \times N}$ a *matrix*. Special vectors are (a) the *i-th unit vector* $\boldsymbol{e}_i = (0, \dots, 0, 1, 0, \dots 0)^\top \in \mathbb{R}^N$, for $1 \leq i \leq N$, and (b) the *vector of all zeros* $\boldsymbol{0}_{N \times 1} \in \mathbb{R}^N$, while special matrices are (a) the *matrix of all zeros* $\boldsymbol{0}_{M \times N} \in \mathbb{R}^{M \times N}$ and (b), for $M = N$, the *identity matrix* $\boldsymbol{I}_N = [\boldsymbol{e}_1, \dots, \boldsymbol{e}_N] \in \mathbb{R}^{N \times N}$. For vectors $\boldsymbol{v} \in \mathbb{R}^N$ and matrices $\boldsymbol{A} \in \mathbb{R}^{M \times N}$, the *components* of $\boldsymbol{v}$ and $\boldsymbol{A}$ are denoted with $[\boldsymbol{v}]_i \in \mathbb{R}$ for $1 \leq i \leq N$ and $[\boldsymbol{A}]_{ij} \in \mathbb{R}$ for $1 \leq i \leq M, 1 \leq j \leq N$. Slightly abusing the notation, we use the same brackets for the inverse operation, i.e. for $\alpha_i \in \mathbb{R}$ with $1 \leq i \leq N$, $[\alpha_i]_{i=1}^N \in \mathbb{R}^N$ and for $A_{ij} \in \mathbb{R}$ with $1 \leq i \leq M, 1 \leq j \leq N$, $[A_{ij}]_{\substack{1 \leq i \leq M \\ 1 \leq j \leq N}} \in \mathbb{R}^{M \times N}$. Moreover, we may *stack* vectors $\boldsymbol{v}_1, \dots, \boldsymbol{v}_k \in \mathbb{R}^N$ and matrices $\boldsymbol{M}_i \in \mathbb{R}^{N \times n_i}$ for $1 \leq i \leq l$ to obtain a

---

[1]Occasionally, vector spaces over the complex numbers $\mathbb{C}$ occur. In this case $\mathrm{i} \in \mathbb{C}$ denotes the imaginary unit.

matrix $[\boldsymbol{v}_1, \dots, \boldsymbol{v}_k] = [\boldsymbol{v}_i]_{i=1}^k \in \mathbb{R}^{N \times k}$ or $[\boldsymbol{M}_1, \dots, \boldsymbol{M}_l] = [\boldsymbol{M}_i]_{i=1}^l \in \mathbb{R}^{N \times \sum_{i=1}^l n_i}$, respectively. For a vector $\boldsymbol{v} \in \mathbb{R}^N$ and a matrix $\boldsymbol{A} \in \mathbb{R}^{M \times N}$, the *transposed* is denoted with $\boldsymbol{v}^\top \in \mathbb{R}^{1 \times N}$ and $\boldsymbol{A}^\top \in \mathbb{R}^{N \times M}$. A matrix $\boldsymbol{A} \in \mathbb{R}^{N \times N}$ with $\boldsymbol{A}^\top = \boldsymbol{A}$ is called *symmetric*. For vectors $\boldsymbol{v} \in \mathbb{R}^N$, we may use the *two-norm* $\|\boldsymbol{v}\|_2 := \sqrt{\boldsymbol{v}^\top \boldsymbol{v}}$ and for matrices $\boldsymbol{A} \in \mathbb{R}^{M \times N}$ the *Frobenius norm* $\|\boldsymbol{A}\|_{\mathrm{F}} := \sqrt{\sum_{\substack{1 \le i \le M \\ 1 \le j \le N}} |[\boldsymbol{A}]_{ij}|^2} = \sqrt{\operatorname{trace}(\boldsymbol{A}^\top \boldsymbol{A})}$ with $\operatorname{trace}(\boldsymbol{M}) = \sum_{i=1}^N [\boldsymbol{M}]_{ii}$ for $\boldsymbol{M} \in \mathbb{R}^{N \times N}$. For matrices $\boldsymbol{A} \in \mathbb{R}^{M \times N}$, we may use the *Python notation for slicing matrices* $\boldsymbol{A}[:, : n] \in \mathbb{R}^{M \times n}$ to select the first n columns of $\boldsymbol{A}$. For square matrices, we denote the *determinant* with $\det(\cdot) : \mathbb{R}^{M \times M} \to \mathbb{R}$.

In the scope of this thesis, we consider finite-dimensional *vector spaces $\mathbb{V}$ over $\mathbb{R}$*, also denoted as *$\mathbb{R}$-vector-spaces*. The *dimension* of the vector space is denoted with $\dim(\mathbb{V})$. In the following, we consider an $\mathbb{R}$-vector-space of dimension $N := \dim(\mathbb{V})$. Each element $v \in \mathbb{V}$ is called a *vector* and elements of the underlying field $\alpha \in \mathbb{R}$ are called *scalars*. For a given *(ordered) basis* $\{v_i\}_{i=1}^N \subset \mathbb{V}$, the *span* is denoted with $\mathbb{V} = \operatorname{span}\{v_i\}_{i=1}^N$. Moreover, for a vector $v = \sum_{i=1}^N \lambda_i v_i$ the *coordinates* $\lambda_i \in \mathbb{R}$ are collected in the *coordinate vector* $\boldsymbol{v} := [\lambda_i]_{i=1}^N \in \mathbb{R}^N$ which we denote in the corresponding bold symbol which we refer to as *bold notation*. Choosing a basis is equivalent to choosing a *coordinate mapping* as a linear bijective map $\varphi : \mathbb{V} \to \mathbb{R}^N$, which assigns a vector the corresponding coordinate vector, i.e.

$$\begin{aligned}
\text{basis formulation:} \qquad & v = \sum_{i=1}^N \lambda_i v_i \in \mathbb{V}, \quad \boldsymbol{v} = [\lambda_i]_{i=1}^N \in \mathbb{R}^N, \\
\text{coordinate mapping formulation:} \quad & v = \varphi^{-1}(\boldsymbol{v}) \in \mathbb{V}, \quad \boldsymbol{v} = \varphi(v) \in \mathbb{R}^N.
\end{aligned} \tag{2.1}$$

We use the two formulations synonymously depending on the context.

The *space of linear maps between two vector spaces $\mathbb{V}, \hat{\mathbb{V}}$* of dimensions $N, \hat{N}$ is denoted with $L(\mathbb{V}; \hat{\mathbb{V}})$. For given coordinate mappings φ and $\hat{\varphi}$ of $\mathbb{V}$ and $\hat{\mathbb{V}}$, a linear map $A \in L(\mathbb{V}; \hat{\mathbb{V}})$ is represented by its *coordinate matrix* $\boldsymbol{A} \in \mathbb{R}^{\hat{N} \times N}$ with $[\boldsymbol{A}]_{ij} = \left[\left(\hat{\varphi} \circ A \circ \varphi^{-1}\right)(\boldsymbol{e}_j)\right]_i$ such that for all $\boldsymbol{v} \in \mathbb{R}^N$: $\left(\hat{\varphi} \circ A \circ \varphi^{-1}\right)(\boldsymbol{v}) = \boldsymbol{A}\boldsymbol{v}$. Special linear maps are (a) the *identity map* $\mathrm{id} : \mathbb{V} \to \mathbb{V}, \ v \mapsto v$ with coefficient matrix $\boldsymbol{I}_N \in \mathbb{R}^{N \times N}$ if $\hat{\varphi} \equiv \varphi$, and (b) the *zero map* $\mathrm{zero} : \mathbb{V} \to \hat{\mathbb{V}}, \ v \mapsto 0 \in \hat{\mathbb{V}}$ with coefficient matrix $\boldsymbol{0}_{N \times \hat{N}} \in \mathbb{R}^{N \times \hat{N}}$. A linear map is called a *(linear) isomorphism*, if it is bijective. For an isomorphism $A \in L(\mathbb{V}; \hat{\mathbb{V}})$, its *inverse* is a linear map $A^{-1} \in L(\hat{\mathbb{V}}; \mathbb{V})$. For the special case of $\mathbb{V} = \hat{\mathbb{V}}$, a bijective linear map is referred to as an *automorphism*, which build the *group of automorphisms of $\mathbb{V}$* $\mathrm{GL}(\mathbb{V}) \subset L(\mathbb{V}; \mathbb{V})$. Bijectivity of a linear map is equivalent to the coordinate matrix being invertible, which we denote with

$\boldsymbol{A} \in \mathrm{GL}(N, \mathbb{R})$. Since $(\cdot)^{\top}$ and $(\cdot)^{-1}$ commute, we write $\boldsymbol{A}^{-\top} := \left(\boldsymbol{A}^{\top}\right)^{-1} = \left(\boldsymbol{A}^{-1}\right)^{\top}$.

A function $a : \mathbb{V} \times \mathbb{V} \to \mathbb{R}$ is called a *bilinear form* if a is linear in both arguments separately. We denote the *space of bilinear forms* as $\mathrm{Bil}(\mathbb{V})$. Its *coordinate matrix* is denoted as $\boldsymbol{a} \in \mathbb{R}^{N \times N}$ such that for all $u, v \in \mathbb{V}$: $a(u, v) = a(\varphi^{-1}(\boldsymbol{u}), \varphi^{-1}(\boldsymbol{v})) = \boldsymbol{u}^{\top} \boldsymbol{a} \boldsymbol{v} \in \mathbb{R}$. A bilinear form is called *nondegenerate* if

$$a(v, u) = 0 \quad \forall u \in \mathbb{V} \quad \implies \quad v = 0 \tag{2.2}$$

or, equivalently, if the coordinate matrix $\boldsymbol{a}$ is invertible. A bilinear form $g \in \mathrm{Bil}(\mathbb{V})$ is called an *inner product* if it is *symmetric* (i.e. $\forall u, v \in \mathbb{V} : g(u, v) = g(v, u)$) and *positive-definite* (i.e. $\forall v \in \mathbb{V} \setminus \{0\} : g(v, v) > 0$). We call the tuple $(\mathbb{V}, g)$ an *inner product space*. Moreover, an inner product defines an *induced norm* $\|\cdot\|_{g} : \mathbb{V} \to \mathbb{R}_{\geq 0}, \ v \mapsto \sqrt{g(v, v)}$. The coordinate matrix $\boldsymbol{g} \in \mathbb{R}^{N \times N}$ is called the *inner product matrix*, and it is symmetric ($\boldsymbol{g}^{\top} = \boldsymbol{g}$) and positive-definite ($\forall \boldsymbol{v} \in \mathbb{R}^{N} \setminus \{\boldsymbol{0}_{N \times 1}\} : \boldsymbol{v}^{\top} \boldsymbol{g} \boldsymbol{v} > 0$). For an inner product matrix $\boldsymbol{g} \in \mathbb{R}^{N \times N}$, its *matrix square root* $\boldsymbol{g}^{1/2} \in \mathbb{R}^{N \times N}$ is well-defined such that $\boldsymbol{g} = \boldsymbol{g}^{1/2} \boldsymbol{g}^{1/2}$. The matrix square root of an inner product matrix and its inverse are again symmetric and can be chosen to be positive-definite. Thus, $\left(\boldsymbol{g}^{-1/2}\right)^{\top} = \boldsymbol{g}^{-1/2}$.

For a vector space $\mathbb{V}$ with basis $\{v_i\}_{i=1}^{N}$ and corresponding coordinate mapping φ, a *change of basis* can be performed to switch to another basis $\{\hat{v}_i\}_{i=1}^{N}$ or, alternatively, to choose another coordinate mapping $\hat{\varphi}$. The *change-of-basis matrix* $\boldsymbol{B} \in \mathrm{GL}(N, \mathbb{R})$ represents the change of basis such that for all $\boldsymbol{v} \in \mathbb{R}^{N}$: $(\hat{\varphi} \circ \varphi^{-1})(\boldsymbol{v}) = \boldsymbol{B} \boldsymbol{v} = \hat{\boldsymbol{v}}$. The coefficient matrix of a linear map $A \in L(\mathbb{V}; \mathbb{V})$ transforms with $\boldsymbol{A} = \boldsymbol{B}^{-1} \hat{\boldsymbol{A}} \boldsymbol{B}$ since

$$\boldsymbol{A} \boldsymbol{u} = (\varphi \circ A \circ \varphi^{-1})(\boldsymbol{u}) = \left((\varphi \circ \hat{\varphi}^{-1}) \circ (\hat{\varphi} \circ A \circ \hat{\varphi}^{-1}) \circ (\hat{\varphi} \circ \varphi^{-1})\right)(\boldsymbol{u}) = \boldsymbol{B}^{-1} \hat{\boldsymbol{A}} \boldsymbol{B} \boldsymbol{u},$$

the coefficient matrix of a bilinear form $a \in \mathrm{Bil}(\mathbb{V})$ transforms with $\boldsymbol{a} = \boldsymbol{B}^{\top} \hat{\boldsymbol{a}} \boldsymbol{B}$ since

$$\begin{aligned} \boldsymbol{u}^{\top} \boldsymbol{a} \boldsymbol{v} &= a(\varphi^{-1}(\boldsymbol{u}), \varphi^{-1}(\boldsymbol{v})) = a(\hat{\varphi}^{-1}\left((\hat{\varphi} \circ \varphi^{-1})(\boldsymbol{u})\right), \hat{\varphi}^{-1}\left((\hat{\varphi} \circ \varphi^{-1})(\boldsymbol{v})\right)) \\ &= \boldsymbol{u}^{\top} \boldsymbol{B}^{\top} \hat{\boldsymbol{a}} \boldsymbol{B} \boldsymbol{v}, \end{aligned} \tag{2.3}$$

which reflects the concepts typically referred to as matrix similarity and matrix congruence.

The *dual space of* $\mathbb{V}$ is the set of all linear functionals $\mathbb{V}^{*} := L(\mathbb{V}; \mathbb{R})$. It is a vector space of dimension $\dim(\mathbb{V}^{*}) = \dim(\mathbb{V}) = N$ [65, Prop. 2.19]. As a linear function $w \in L(\mathbb{V}; \mathbb{R})$, the coordinate matrix $\boldsymbol{w}^{\top} \in \mathbb{R}^{1 \times N}$ is a row vector (which we indicate by transposing a

column vector $\boldsymbol{w} \in \mathbb{R}^N$). For the sake of notation, we introduce the *dual coordinate mapping* $\psi : \mathbb{V}^* \to \mathbb{R}^{1 \times N}, \ w \mapsto \left[(w \circ \varphi^{-1})(\boldsymbol{e}_i) \right]^\top_{1 \leq i \leq N}$ which assigns a linear functional its coordinate vector. This coordinate mapping is invertible since φ is invertible. Then, the dual product in coordinates is $w(v) = \boldsymbol{w}^\top \boldsymbol{v} \in \mathbb{R}$.

If there is additional structure in the form of a nondegenerate bilinear form $a \in \text{Bil}(\mathbb{V})$, it is possible to define an isomorphism $\flat_a \in L(\mathbb{V}; \mathbb{V}^*), \ v \mapsto a(\cdot, v)$ [65, p. 115]. We denote the inverse with $\sharp_a := \flat_a^{-1}$. In coordinates, it holds for all $v \in \mathbb{V}$ and $w \in \mathbb{V}^*$

$$\flat_{\boldsymbol{a}}(\boldsymbol{v}) := (\psi \circ \flat_a \circ \varphi^{-1})(\boldsymbol{v}) = \left[a(\varphi^{-1}(\boldsymbol{e}_i), \varphi^{-1}(\boldsymbol{v})) \right]^\top_{1 \leq i \leq N} = \boldsymbol{v}^\top \boldsymbol{a}^\top,$$

$$\sharp_{\boldsymbol{a}}(\boldsymbol{w}^\top) := \flat_{\boldsymbol{a}}^{-1}(\boldsymbol{w}^\top) = \boldsymbol{a}^{-1} \boldsymbol{w}.$$

A subset $\tilde{\mathbb{V}} \subset \mathbb{V}$ is called a *(linear) subspace*, if it is a vector space. Consider $\mathbb{R}$-vector-spaces $\mathbb{V}$ and $\check{\mathbb{V}}$ of dimension N and $n \leq N$. We call a linear map $V \in L(\check{\mathbb{V}}; \mathbb{V})$ an *embedding*, if it is linear and injective, such that it is an isomorphism on its image $V(\check{\mathbb{V}}) \subset \mathbb{V}$. Every subspace $\tilde{\mathbb{V}} \subset \mathbb{V}$ can be characterized by (i) an embedding $V \in L(\check{\mathbb{V}}; \mathbb{V})$ with $\tilde{\mathbb{V}} = V(\check{\mathbb{V}})$ or (ii) by a *reduced(-order) basis (ROB)* $\{\tilde{v}_i\}_{1 \leq i \leq n} \subset \mathbb{V}$ with $\tilde{\mathbb{V}} = \text{span} \{\tilde{v}_i\}_{1 \leq i \leq n}$. For $\check{\mathbb{V}} = \mathbb{R}^n$, the two characterizations relate by superposition $V(\check{\boldsymbol{x}}) = \sum_{i=1}^n [\check{\boldsymbol{x}}]_i \, \tilde{v}_i$. The coordinate matrix $\boldsymbol{V} \in \mathbb{R}^{N \times n}$ of V is referred to as the *ROB matrix*, the space $\check{\mathbb{V}}$ as *reduced space*, a coordinate vector $\check{\boldsymbol{v}} \in \mathbb{R}^n$ as a *reduced coordinate vector* and $V(\check{v}) \in \tilde{\mathbb{V}}$ a *reconstructed vector*. The reduced space $\check{\mathbb{V}}$ can inherit structure from the full space $\mathbb{V}$. Firstly, the so-called *pullback (of a linear functional)* $V^* : \mathbb{V}^* \to \check{\mathbb{V}}^*, \ w \mapsto w \circ V$ defines a *reduced linear functional* $\check{w} := w \circ V \in \check{\mathbb{V}}^*$ on $\check{\mathbb{V}}$ which reads in coordinates $\check{\boldsymbol{w}}^\top = \boldsymbol{w}^\top \boldsymbol{V}^\top \in \mathbb{R}^{1 \times n}$. Secondly, a bilinear form $a \in \text{Bil}(\mathbb{V})$ defines a *reduced bilinear form* $\check{a} := a(V(\cdot), V(\cdot)) \in \text{Bil}(\check{\mathbb{V}})$, which reads in coordinates $\check{\boldsymbol{a}} = \boldsymbol{V}^\top \boldsymbol{a} \boldsymbol{V} \in \mathbb{R}^{n \times n}$ such that $\check{a}(\check{v}, \check{u}) = a(V(\check{v}), V(\check{u})) = \check{\boldsymbol{v}}^\top \boldsymbol{V}^\top \boldsymbol{a} \boldsymbol{V} \check{\boldsymbol{u}} = \check{\boldsymbol{v}}^\top \check{\boldsymbol{a}} \check{\boldsymbol{u}}$. For a given nondegenerate bilinear form $a \in \text{Bil}(\mathbb{V})$, we call a subspace $\tilde{\mathbb{V}}$ *compatible with a* if the corresponding reduced bilinear form $\check{a}$ is again nondegenerate. If $g \in \text{Bil}(\mathbb{V})$ is an inner product, this property is fulfilled automatically.

A linear map $\Pi \in L(\mathbb{V}; \tilde{\mathbb{V}})$ with $\Pi \circ \Pi = \Pi$ is called a *projection*. Given an embedding $V \in L(\check{\mathbb{V}}; \mathbb{V})$, which characterizes the subspace $\tilde{\mathbb{V}} = V(\check{\mathbb{V}}) \subset \mathbb{V}$, and a nondegenerate bilinear form $a \in \text{Bil}(\mathbb{V})$ such that $\tilde{\mathbb{V}}$ and a are compatible (i.e. $\check{\boldsymbol{a}} \in \text{GL}(n, \mathbb{R})$), we define the *a-based projection*

$$\Pi_{a,\tilde{\mathbb{V}}} := V \circ \sharp_{\check{a}} \circ V^* \circ \flat_a \in L(\mathbb{V}; \tilde{\mathbb{V}}) \qquad \text{with} \qquad \boldsymbol{\Pi}_{a,\tilde{\mathbb{V}}} = \boldsymbol{V} \check{\boldsymbol{a}}^{-1} \boldsymbol{V}^\top \boldsymbol{a}, \qquad (2.4)$$

Figure 2.1: Projection to a subspace $\check{\mathbb{V}} \subset \mathbb{V}$ via a nondegenerate bilinear form $a \in \mathrm{Bil}(\mathbb{V})$ fulfilling the compatibility condition.

see Figure 2.1. In the following it will also be interesting to consider $V^{-1} \circ \Pi_{a,\tilde{\mathbb{V}}} : \mathbb{V} \to \check{\mathbb{V}}$, which projects a vector $v \in \mathbb{V}$ to a reduced vector $(V^{-1} \circ \Pi_{a,\tilde{\mathbb{V}}})(v) \in \check{\mathbb{V}}$. For a given norm $\|\cdot\| : \mathbb{V} \to \mathbb{R}_{\geq 0}$, we define the *projection error* $e_{a,\tilde{\mathbb{V}}} : \mathbb{V} \to \mathbb{R}_{\geq 0}, \ v \mapsto \left\| v - \Pi_{a,\tilde{\mathbb{V}}}(v) \right\|$.

For two given inner product spaces $(\mathbb{V}, g)$ and $(\check{\mathbb{V}}, \check{g})$, an embedding $V \in L(\check{\mathbb{V}}; \mathbb{V})$ is called *orthogonal* if $g(V(\check{u}), \ V(\check{v})) = \check{g}(\check{u}, \check{v})$ for all $\check{u}, \check{v} \in \check{\mathbb{V}}$. For the ROB matrix, this condition is equivalent to $\boldsymbol{V}^{\top} \boldsymbol{g} \boldsymbol{V} = \check{\boldsymbol{g}}$. The ROB matrix is said to have *orthonormal columns* if $\check{\boldsymbol{g}} = \boldsymbol{I}_n$. Moreover, for the case of $\boldsymbol{g} = \boldsymbol{I}_N$, the set $V_n(\mathbb{R}^N) := \{\boldsymbol{V} \in \mathbb{R}^{N \times n} \,|\, \boldsymbol{V}^{\top} \boldsymbol{V} = \boldsymbol{I}_n\}$ of ROB matrices with orthonormal columns is called the *Stiefel manifold*.

We consider two $\mathbb{R}$-vector-spaces $\mathbb{V}, \hat{\mathbb{V}}$ with $\dim(\mathbb{V}) = N$ and $\dim(\hat{\mathbb{V}}) = \hat{N}$. For open subsets $U \subset \mathbb{V}, \hat{U} \subset \hat{\mathbb{V}}$, we denote a (potentially nonlinear) mapping $f : U \to \hat{U}$ *in coordinates* as a bold symbol $\boldsymbol{f} := \hat{\varphi} \circ f \circ \varphi^{-1}$. Moreover, the *space of k-times differentiable mappings* for $k \in \mathbb{N} \cup \{\infty\}$ is denoted with $C^k(U, \hat{\mathbb{V}})$. For scalar-valued functions, we abbreviate $C^k(U) := C^k(U, \mathbb{R})$. For a mapping $f \in C^k(U, \hat{\mathbb{V}})$, the *derivative at $u \in U$* $\mathrm{d}f|_u \in L(\mathbb{V}; \hat{\mathbb{V}})$ is a linear map from $\mathbb{V}$ to $\hat{\mathbb{V}}$. The coefficient matrix $\mathbf{D}\boldsymbol{f}|_{\boldsymbol{u}} \in \mathbb{R}^{\hat{N} \times N}$ is called the *Jacobian matrix*. The differential satisfies the *chain rule*, i.e., for three vector spaces $\mathbb{V}, \hat{\mathbb{V}}, \overline{\mathbb{V}}$, an open subset $U \subset \mathbb{V}$, and mappings $f \in C^1(U, \hat{\mathbb{V}})$, and $g \in C^1(f(U), \overline{\mathbb{V}})$, it holds for all $u \in U$ and $v \in \mathbb{V}$

$$\mathrm{d}(g \circ f)|_u (v) = \mathrm{d}g|_{f(u)} \left(\mathrm{d}f|_u (v) \right) \in \overline{\mathbb{V}}. \tag{2.5}$$

For a curve $\gamma \in C^1(I_t, \mathbb{V})$ defined on an interval $I_t \subset \mathbb{R}$, we denote its derivative with $\frac{\mathrm{d}}{\mathrm{d}t}\gamma(t) := \mathrm{d}\gamma|_t$ by custom. The derivative of a scalar-valued function $f \in C^1(\mathbb{V})$ is a linear functional on $\mathbb{V}$, i.e. $\mathrm{d}f|_u \in L(\mathbb{V}; \mathbb{R})$. Thus, it can be understood as an element in the dual space $\mathbb{V}^*$. In that context, we refer to it as the *gradient of f* $\nabla f|_u \in \mathbb{V}^*$ with $\nabla \boldsymbol{f}|_{\boldsymbol{u}} = \mathbf{D}\boldsymbol{f}|_{\boldsymbol{u}}^{\top}$.

2.2 (Classical) Model Order Reduction on Subspaces

Essentially, the idea of projection-based MOR (for dynamical systems) is to project a high-dimensional dynamical system to a low-dimensional, problem-specific subspace. To this end, we introduce the high-dimensional dynamical system (Section 2.2.1), the projection of a dynamical system to a subspace (Section 2.2.2) and data-based methods to identify low-dimensional problem-specific subspaces with a basis generation technique (Section 2.2.3).

2.2.1 Full-Order Model (FOM)

In the scope of this work, we consider a general high-dimensional initial value problem as full-order model of interest. Such systems frequently appear when PDEs are semi-discretized in space, as discussed later in the numerical examples. In the following, $x \in \mathbb{V}$ denotes a point in $\mathbb{V}$ and $x(\cdot) : I_t \to \mathbb{V}$ is used to indicate a curve (or trajectory) in $\mathbb{V}$.

Definition 2.1 (Full-Order Model (FOM)): *Given an N-dimensional $\mathbb{R}$-vector-space $\mathbb{V}$, a time interval $\emptyset \neq I_t = [t_0, t_{\mathrm{end}}]$, a parameter domain $P \subset \mathbb{R}^{n_{\mathrm{p}}}$, an arbitrary, but fixed, parameter vector $\boldsymbol{\mu} \in P$, a right-hand side $f(\cdot, \cdot; \boldsymbol{\mu}) : \mathbb{V} \times I_t \to \mathbb{V}$, which is Lipschitz continuous in the first argument, and an initial value $x_0(\boldsymbol{\mu}) \in \mathbb{V}$, the solution of the full-order model (solution of the FOM or FOM solution) $x(\cdot; \boldsymbol{\mu}) \in C^1(I_t, \mathbb{V})$ satisfies the initial-value problem (IVP)*

$$\frac{\mathrm{d}}{\mathrm{d}t} x(t; \boldsymbol{\mu}) = f(x(t; \boldsymbol{\mu}), t; \boldsymbol{\mu}) \in \mathbb{V} \quad \forall t \in I_t, \qquad x(t_0; \boldsymbol{\mu}) = x_0(\boldsymbol{\mu}). \qquad (2.6)$$

We call N the dimension of the FOM or the high dimension.

Remark 2.2 (Existence and uniqueness of FOM solution): *We assume the right-hand side to be Lipschitz in the first argument and the length of the time interval $|t_{\mathrm{end}} - t_0|$ to be small enough, such that there the exists a unique solution of the FOM (2.6), see e.g. [46, Sec. 3.3].*

Remark 2.3 (Solution via time integration scheme): *In practice, the FOM is solved numerically with a time discretization scheme. In this thesis, we consider time stepping schemes with a fixed time stepping width $\Delta t > 0$ and $(K + 1) \in \mathbb{N}$ time steps $t_k = t_0 + k\Delta t \in I_t$, $0 \leq k \leq K$, $t_{\mathrm{end}} = K\Delta t$. The numerical solution is denoted with $x_k(\boldsymbol{\mu}) \approx x(t_k; \boldsymbol{\mu}) \in \mathbb{V}$.*

Definition 2.4 (Linear (time-invariant) FOM): *We call the FOM linear if the right-hand side is affine in the first argument, i.e. there exists $A : I_t \times P \to L(\mathbb{V}; \mathbb{V})$ and $b : I_t \times P \to \mathbb{V}$*

such that $f(x, t; \boldsymbol{\mu}) = (A(t; \boldsymbol{\mu}))(x) + b(t; \boldsymbol{\mu})$, where the coefficient matrix $\boldsymbol{A}(t; \boldsymbol{\mu}) \in \mathbb{R}^{N \times N}$ is called the system matrix. We call the FOM linear and time-invariant if $A(t; \boldsymbol{\mu}) \equiv A(\boldsymbol{\mu})$ and $b(t; \boldsymbol{\mu}) \equiv b(\boldsymbol{\mu})$ are constant in time.

Definition 2.5 (Flow of an IVP): *Assume there exists $M \subset \mathbb{V}$ such that all solutions $x(t; \boldsymbol{\mu}; x_0)$ of the IVP (2.6) exist for $x_0 \in M$. Then, the flow $\theta_t(\cdot; \boldsymbol{\mu}) \in C^1(M, \mathbb{V})$ evolves the initial state $x_0 \in M$ to the corresponding solution $x(t; \boldsymbol{\mu}; x_0)$ such that $\theta_t(x_0; \boldsymbol{\mu}) := x(t; \boldsymbol{\mu}; x_0)$.*

Remark 2.6 (Other settings for FOMs): *We note that the following techniques can also be useful to solve other parametric, high-dimensional problems like systems of linear equations [48, Ex. 2.8] as they may arise from the discretization of stationary PDEs. In the scope of this work, however, we only consider high-dimensional initial value problems of the form (2.6).*

Definition 2.7 (Set of all solutions): *The set of all solutions is the set*

$$S := \left\{ x(t; \boldsymbol{\mu}) \in \mathbb{V} \mid (t, \boldsymbol{\mu}) \in I_t \times P, \ x(t; \boldsymbol{\mu}) \text{ is a FOM solution of } (2.6) \right\} \subset \mathbb{V} \qquad (2.7)$$

which consists of all solutions of (2.6) over $I_t \times P$.

Remark 2.8 (Solution "manifold"): *The set of all solutions is frequently denoted as the so-called solution manifold. However, the set of all solutions is not necessarily a manifold (i.e. locally homeomorphic to some $\mathbb{R}^N$, see Part II). The solution $x(t; \boldsymbol{\mu})$ might actually be arbitrarily complex in the parameter $\boldsymbol{\mu}$. This can be seen by following the idea in [48, Ex. 2.9] from the context of reduced basis methods. Assume to be given a mapping $y : I_t \times P \to \mathbb{V}$ such that $y(\cdot; \boldsymbol{\mu}) \in C^1(I_t, \mathbb{V})$ for all $\boldsymbol{\mu} \in P$. This allows the mapping $\boldsymbol{\mu} \mapsto y(\cdot; \boldsymbol{\mu})$ to be arbitrarily complex. Consider the FOM (2.6) with the right-hand side $f(x, t; \boldsymbol{\mu}) = \frac{d}{dt}y(t; \boldsymbol{\mu})$ and initial value $x_0(\boldsymbol{\mu}) = y(t_0; \boldsymbol{\mu})$. Then, by definition, $x \equiv y$ solves this FOM and the set of all solutions for $n_p = 1$ is not a manifold if we e.g. choose $y(t; \boldsymbol{\mu}) \equiv c(\boldsymbol{\mu})$ as a constant $c(\boldsymbol{\mu}) \in \mathbb{R}$ for each $\boldsymbol{\mu} \in P$ such that $\boldsymbol{\mu} \mapsto y(\cdot; \boldsymbol{\mu})$ describes a self-intersecting line.*

2.2.2 Projection-based MOR and Reduced-Order Model (ROM)

We assume that there exists a low-dimensional subspace $\tilde{\mathbb{V}} \subset \mathbb{V}$, $\dim(\tilde{\mathbb{V}}) = n \ll N$, (characterized by a reduced space $\check{\mathbb{V}}$ and an embedding $V \in L(\check{\mathbb{V}}; \mathbb{V})$) that approximates the set of all solutions $S \subset \mathbb{V}$ well. The FOM solution $x(\cdot; \boldsymbol{\mu}) \in C^1(I_t, \mathbb{V})$ is approximated with

$$x(t; \boldsymbol{\mu}) \approx \tilde{x}(t; \boldsymbol{\mu}) := V(\check{x}(t; \boldsymbol{\mu})), \qquad (2.8)$$

where we refer to $\check{x}(\cdot; \boldsymbol{\mu}) \in C^1(I_t, \check{\mathbb{V}})$ as the *reduced trajectory* and to $\tilde{x}(\cdot; \boldsymbol{\mu}) \in C^1(I_t, \tilde{\mathbb{V}})$ as the *reconstructed solution*. The reduced trajectory is determined from a dynamical system by projecting the FOM dynamics on $\check{\mathbb{V}}$. To this end, we insert the approximation (2.8) into the FOM (2.6), which defines the *residual*

$$r : I_t \times P \to \mathbb{V}, \ (t; \boldsymbol{\mu}) \mapsto \tfrac{\mathrm{d}}{\mathrm{d}t} V(\tilde{x}(t; \boldsymbol{\mu})) - f(V(\tilde{x}(t; \boldsymbol{\mu})), t; \boldsymbol{\mu}) \in \mathbb{V}.$$

The reduced trajectory $\check{x}(\cdot; \boldsymbol{\mu})$ is chosen to make the a-based projection (2.4) of the residual onto $\tilde{\mathbb{V}}$ vanish for all $(t, \boldsymbol{\mu}) \in I_t \times P$, i.e.

$$\check{\mathbb{V}} \ni 0 = (V^{-1} \circ \Pi_{a,\tilde{\mathbb{V}}})(r(t; \boldsymbol{\mu})) = \tfrac{\mathrm{d}}{\mathrm{d}t}\check{x}(t; \boldsymbol{\mu}) - (V^{-1} \circ \Pi_{a,\tilde{\mathbb{V}}})(f(V(\check{x}(t; \boldsymbol{\mu})), t; \boldsymbol{\mu})) \quad (2.9)$$

This defines the following reduced model.

Definition 2.9 (a-based Reduced-Order Model (a-ROM)): *Assume to be given a FOM (2.6), a nondegenerate bilinear form $a \in \mathrm{Bil}(\mathbb{V})$, and an n-dimensional subspace $\tilde{\mathbb{V}} \subset \mathbb{V}$ (characterized by a reduced space $\check{\mathbb{V}}$ and an embedding $V \in L(\check{\mathbb{V}}; \mathbb{V})$) such that a and $\tilde{\mathbb{V}}$ are compatible. The* solution of the reduced-order model (solution of the ROM or ROM solution) *$\check{x}(\cdot; \boldsymbol{\mu}) \in C^1(I_t, \check{\mathbb{V}})$ satisfies the IVP*

$$\tfrac{\mathrm{d}}{\mathrm{d}t}\check{x}(t; \boldsymbol{\mu}) = \check{f}(\check{x}(t; \boldsymbol{\mu}), t; \boldsymbol{\mu}) \in \check{\mathbb{V}} \quad \forall t \in I_t, \qquad\qquad \check{x}(t_0; \boldsymbol{\mu}) = \check{x}_0(\boldsymbol{\mu}), \qquad (2.10)$$

with the reduced right-hand side *and the* reduced initial value

$$\check{f}(\check{x}, t; \boldsymbol{\mu}) := (V^{-1} \circ \Pi_{a,\tilde{\mathbb{V}}})(f(V(\check{x}), t; \boldsymbol{\mu})) \quad \text{and} \quad \check{x}_0(\boldsymbol{\mu}) := (V^{-1} \circ \Pi_{a,\tilde{\mathbb{V}}})(x_0(\boldsymbol{\mu})). \quad (2.11)$$

We refer to n as the dimension of the ROM *or the* reduced dimension.

The most popular approach is the Galerkin ROM, which uses an inner product as bilinear form.

Definition 2.10 (Galerkin ROM (g-ROM), e.g. [115, Cha. 3]): *Let $(\mathbb{V}, g)$ be an inner product space. The* Galerkin ROM (g-ROM) *is a special case of the a-ROM (Definition 2.9) with $a = g$.*

For computational efficient evaluations of the ROM (2.10), it still lacks another ingredient. Although the ROM is of low dimension $n \ll N$, it will in general still be computationally expensive to evaluate the reduced right-hand side (2.11) since it requires to evaluate the

original right-hand side f and to perform the projection with $V^{-1} \circ \Pi_{a,\check{\mathbb{V}}}$. To obtain efficient ROMs, the concept of an offline–online decomposition is introduced and it is briefly discussed how to achieve it.

Definition 2.11 (Offline–online decomposition): *We call a ROM offline–online decomposable if the computation of the ROM can be decomposed in two sequential phases: (i) a (possibly computationally expensive) offline phase, which includes operations scaling with the high dimension N, and (ii) an online phase which allows to evaluate the ROM for arbitrary parameter vectors $\boldsymbol{\mu} \in P$ while requiring only operations that scale with the reduced dimension n (i.e. no operations scaling with the high-dimension N).*

Remark 2.12 (Offline–online decomp. for parameter-separable, linear FOMs, e.g. [50]): *We refer to a linear FOM (see Definition 2.4) as parameter-separable if*

$$A(t; \boldsymbol{\mu}) = \sum_{q_A=1}^{n_A} \theta_{A,q_A}(t; \boldsymbol{\mu}) A_{q_A} \in L(\mathbb{V}; \mathbb{V}) \qquad b(t; \boldsymbol{\mu}) = \sum_{q_b=1}^{n_b} \theta_{b,q_b}(t; \boldsymbol{\mu}) b_{q_b} \in \mathbb{V}$$

with the constant components of A (and b) $A_{q_A} \in L(\mathbb{V}; \mathbb{V})$ (and $b_{q_b} \in \mathbb{V}$) and the coefficients of A (and b) $\theta_{A,q_A}(t; \boldsymbol{\mu}) \in \mathbb{R}$, (and $\theta_{b,q_b}(t; \boldsymbol{\mu}) \in \mathbb{R}$) for $1 \leq q_A \leq n_A$ (and $1 \leq q_b \leq n_b$, respectively). This system is offline–online decomposable by computing and storing the reduced components of A (and b),

$$\check{A}_{q_A} := V^{-1} \circ \Pi_{a,\tilde{\mathbb{V}}} \circ A_{q_A} \circ V \in L(\check{\mathbb{V}}; \check{\mathbb{V}}), \qquad \check{b}_{q_b} := (V^{-1} \circ \Pi_{a,\tilde{\mathbb{V}}})(b_{q_b}) \in \check{\mathbb{V}},$$

for $1 \leq q_A \leq n_A$ (and $1 \leq q_b \leq n_b$) in the offline phase and assembling the reduced right-hand side $\check{f}(\check{x}, t; \boldsymbol{\mu}) = \left(\check{A}(t; \boldsymbol{\mu}) \right)(\check{x}) + \check{b}(t; \boldsymbol{\mu})$ for a given parameter $\boldsymbol{\mu} \in P$ in the online phase

$$\check{A}(t; \boldsymbol{\mu}) = \sum_{q_A=1}^{n_A} \theta_{A,q_A}(t; \boldsymbol{\mu}) \check{A}_{q_A}, \qquad \check{b}(t; \boldsymbol{\mu}) = \sum_{q_b=1}^{n_b} \theta_{b,q_b}(t; \boldsymbol{\mu}) \check{b}_{q_b},$$

which is independent of the high-dimension N if $n_A, n_b \ll N$.

Remark 2.13 (Hyperreduction): *For (a) nonlinear or (b) affine but non-parameter-separable contributions to the right-hand side, the (discrete) empirical interpolation method ((D)EIM) [7, 32] can be used to derive an approximation of the right-hand side, which is parameter-separable. This, however, requires to be able to evaluate single components of the concerning terms efficiently.*

In the following two remarks, we briefly highlight two concepts important in MOR, which are, however, outside the scope of this thesis.

Remark 2.14 (Intrusive and nonintrusive MOR): *To assemble the reduced right-hand side (2.11), access to the full right-hand side f of the FOM is required. In general, this needs access to the governing equations, discretization, and the solver, which may be unavailable, e.g., when working with commercial software. This is called an intrusive MOR technique. In contrast, non-intrusive methods avoid accessing such information. For more details see, e.g., [13, 97, 98].*

Remark 2.15 (Discretize-then-reduce vs. reduce-then-discretize): *The projection of the residual (2.9) does in general not commute with the time integration scheme. In that regard, it has to be differentiated if the projection is applied before or after time discretization. An example for the latter is the so-called Least-Squares Petrov–Galerkin method [29]. In the present work, however, we focus on projection-based techniques applied before time integration (reduce-then-discretize).*

To conclude this subsection, we want to briefly discuss the fundamental assumption of projection-based MOR that the set of all solutions (2.7) can be approximated sufficiently accurate with a low-dimensional subspace $\tilde{\mathbb{V}} \subset \mathbb{V}$, $\dim(\tilde{\mathbb{V}}) = n \ll N$. A quantity to measure this property are the Kolmogorov n-widths:

Definition 2.16 (Kolmogorov n-width [66]): *Let $(\mathbb{V}, g)$ be an inner product space with the induced norm $\|\cdot\|_g : \mathbb{V} \to \mathbb{R}_{\geq 0}$ and let $M \subset \mathbb{V}$ be a subset. For a subspace $\tilde{\mathbb{V}} \subset \mathbb{V}$, we denote the worst best-approximation error of M in $\tilde{\mathbb{V}}$ with $d(M, \tilde{\mathbb{V}}) := \sup_{x \in M} \inf_{u \in \tilde{\mathbb{V}}} \|x - u\|_g$. Then, the Kolmogorov n-width*

$$d_n(M) := \inf_{\substack{\tilde{\mathbb{V}} \subset \mathbb{V} \text{ subspace} \\ \dim(\tilde{\mathbb{V}}) \leq n}} d(M, \tilde{\mathbb{V}}) \tag{2.12}$$

measures the theoretically optimal worst best-approximation error of M achievable by some subspace $\tilde{\mathbb{V}}$ of $\mathbb{V}$ with dimension $\dim(\tilde{\mathbb{V}}) \leq n$.

The decay of the Kolmogorov n-widths is important for MOR, as it quantifies how well the approximation based on an n-dimensional subspace $\tilde{\mathbb{V}} \subset \mathbb{V}$ can be in the best case. Speaking in mathematical terms, the *maximal reduction error*

$$e_{\text{red,max}} := \sup_{(t;\boldsymbol{\mu}) \in I_t \times P} \|x(t;\boldsymbol{\mu}) - \tilde{x}(t;\boldsymbol{\mu})\|_g, \qquad e_{\text{red,max}} \overset{(i)}{\geq} d(S, \tilde{\mathbb{V}}) \overset{(ii)}{\geq} d_n(S),$$

for the FOM solution $x(t; \boldsymbol{\mu}) \in S$ and a reconstructed ROM solution $\tilde{x}(t; \mu) = V(\check{x}(t; \mu)) \in \tilde{\mathbb{V}}$ is bounded from below by the Kolmogorov n-width as (i) the worst best-approximation error $d(S, \tilde{\mathbb{V}})$ minimizes over all elements in $\tilde{\mathbb{V}}$ and (ii) the Kolmogorov n-width $d_n(S)$ minimizes over all possible n-dimensional subspaces of $\mathbb{V}$. In this chapter, we assume that the Kolmogorov n-widths decay sufficiently fast, so efficient MOR on subspaces is possible. More details on this assumption are discussed in Section 6.1.

2.2.3 Snapshot-based Basis Generation

It is yet left open, how to choose the ROB. One class of basis generation techniques are *data-based basis generation techniques*, which determine the reduced basis from given data. A data-based approach for basis generation are *snapshot-based* techniques. Remember that the central object of interest is the set of all solutions (2.7). The idea of snapshot-based basis generation is to (approximately) sample the set of all solutions. Typically, a *training dataset* $P_{\mathrm{train}} \subset P$ with $|P_{\mathrm{train}}| < \infty$ is selected and the according numerical solutions $x_k(\boldsymbol{\mu})$ (see Remark 2.3) are computed to construct the *(training-)set of snapshots*

$$X^{\mathrm{s}} := \left\{ x_k(\boldsymbol{\mu}) \in \mathbb{V} \mid \boldsymbol{\mu} \in P_{\mathrm{train}}, \ 0 \le k \le K \right\} \approx S, \tag{2.13}$$

where each element $x_i^{\mathrm{s}} \in X^{\mathrm{s}}$ for $1 \le i \le n_{\mathrm{s}} := |X^{\mathrm{s}}|$ is called a *snapshot*. For computations, it is helpful to define the *snapshot matrix* $\boldsymbol{X}_{\mathrm{s}} := [\boldsymbol{x}_i^{\mathrm{s}}]_{i=1}^{n_{\mathrm{s}}} \in \mathbb{R}^{N \times n_{\mathrm{s}}}$, which stacks the coordinate vectors of the snapshots in its columns.

2.2.3.1 (Time-Discrete) Proper Orthogonal Decomposition

The most prominent snapshot-based basis generation technique for a Galerkin ROM is the Proper Orthogonal Decomposition (POD). It goes back to works analyzing structures in turbulent flows [79, 111] and can nowadays be found in many textbooks on MOR, e.g. [11, 115]. In other fields the underlying principle of the method is also referred to as principal component analysis [61], Karhunen–Loeve decomposition [63, 78], or Hotelling transformation [57].

We consider an inner-product space $(\mathbb{V}, g)$ with the induced norm $\|v\|_g^2 = \|\boldsymbol{v}\|_{\boldsymbol{g}}^2 = \boldsymbol{v}^\top \boldsymbol{g} \boldsymbol{v}$. The idea of POD is to choose an optimal subspace which reduces the g-based projection error in the mean over all snapshots.

Definition 2.17 (Proper Orthogonal Decomposion (POD), e.g. [115]): *Given an inner product space* $(\mathbb{V}, g)$ *and a snapshot set* $X^s \subset \mathbb{V}$, *the Proper Orthogonal Decomposition (POD) computes a subspace* $\tilde{\mathbb{V}}^{\text{POD}} := \text{span}\left\{\tilde{v}_i^{\text{POD}}\right\}_{i=1}^n$ *by identifying an orthonormal basis via the POD (optimization) problem*

$$\tilde{\mathbb{V}}^{\text{POD}} := \text{span}\left\{\tilde{v}_i^{\text{POD}}\right\}_{i=1}^n = \underset{\substack{\tilde{\mathbb{V}}=\text{span}\{\tilde{v}_i\}_{i=1}^n\subset\mathbb{V}, \\ g(\tilde{v}_i,\tilde{v}_j)=\delta_{ij} \text{ for } 1\leq i,j\leq n}}{\text{argmin}} \sum_{i=1}^{n_s} \left\|x_i^s - \Pi_{g,\tilde{\mathbb{V}}}(x_i^s)\right\|_g^2. \tag{2.14}$$

For the ROB matrix $\boldsymbol{V}^{\text{POD}} = \left[\tilde{\boldsymbol{v}}_i^{\text{POD}}\right]_{i=1}^n \in \mathbb{R}^{N\times n}$, *the POD problem in coordinates reads*

$$\boldsymbol{V}^{\text{POD}} = \underset{\substack{\boldsymbol{V}\in\mathbb{R}^{N\times n} \\ \boldsymbol{V}^\top\boldsymbol{g}\boldsymbol{V}=\boldsymbol{I}_n}}{\text{argmin}} \sum_{i=1}^{n_s} \left\|(\boldsymbol{I}_N - \boldsymbol{V}\boldsymbol{V}^\top\boldsymbol{g})\boldsymbol{x}_i^s\right\|_{\boldsymbol{g}}^2. \tag{2.15}$$

As discussed in the following lemma, each POD problem (2.14) with an inner product matrix $\boldsymbol{g} \neq \boldsymbol{I}_N$ can be transformed with a change of basis to obtain a transformed inner product matrix $\hat{\boldsymbol{g}} = \boldsymbol{I}_N$.

Lemma 2.18 (POD problem in canonical coordinates): *Consider a POD problem (2.14) with an inner product matrix* $\boldsymbol{g} \neq \boldsymbol{I}_N$. *A coordinate transformation with the change-of-basis matrix* $\boldsymbol{g}^{1/2}$ *such that* $\hat{\boldsymbol{x}} = \boldsymbol{g}^{1/2}\boldsymbol{x}$ *yields by the transformation formula for bilinear forms (2.3) that* $\hat{\boldsymbol{g}} = \left(\boldsymbol{g}^{-1/2}\right)^\top \boldsymbol{g}\boldsymbol{g}^{-1/2} = \boldsymbol{I}_N$. *Then, the POD problem in canonical coordinates reads*

$$\hat{\boldsymbol{V}}^{\text{POD}} = \underset{\substack{\hat{\boldsymbol{V}}\in\mathbb{R}^{N\times n} \\ \hat{\boldsymbol{V}}^\top\hat{\boldsymbol{V}}=\boldsymbol{I}_n}}{\text{argmin}} \underbrace{\sum_{i=1}^{n_s} \left\|(\boldsymbol{I}_N - \hat{\boldsymbol{V}}\,\hat{\boldsymbol{V}}^\top)\hat{\boldsymbol{x}}_i^s\right\|_2^2}_{=\left\|(\boldsymbol{I}_N-\hat{\boldsymbol{V}}\,\hat{\boldsymbol{V}}^\top)\hat{\boldsymbol{X}}^s\right\|_{\text{F}}^2} \tag{2.16}$$

with the snapshot matrix in canonical coordinates $\hat{\boldsymbol{X}}^s = \boldsymbol{g}^{1/2}\boldsymbol{X}_s$. *Solving (2.16) is equivalent to solving (2.15) with* $\hat{\boldsymbol{V}}^{\text{POD}} = \boldsymbol{g}^{1/2}\boldsymbol{V}^{\text{POD}}$.

Proof. The equivalence of the POD problems (2.15) and (2.16) follows from transforming all quantities with the coordinate transformation and using $\|\boldsymbol{x}\|_2 = \left\|\boldsymbol{g}^{-1/2}\boldsymbol{x}\right\|_{\boldsymbol{g}}$

$$\left\|(\boldsymbol{I}_N - \hat{\boldsymbol{V}}\,\hat{\boldsymbol{V}}^\top)\hat{\boldsymbol{x}}_i^s\right\|_2 = \left\|\boldsymbol{g}^{-1/2}(\boldsymbol{I}_N - \boldsymbol{g}^{1/2}\boldsymbol{V}\boldsymbol{V}^\top\boldsymbol{g}^{1/2})\boldsymbol{g}^{1/2}\boldsymbol{x}_i^s\right\|_{\boldsymbol{g}} = \left\|(\boldsymbol{I}_N - \boldsymbol{V}\boldsymbol{V}^\top\boldsymbol{g})\boldsymbol{x}_i^s\right\|_{\boldsymbol{g}},$$

$$\boldsymbol{I}_n = \hat{\boldsymbol{V}}^\top\hat{\boldsymbol{V}} = \boldsymbol{V}^\top\boldsymbol{g}\boldsymbol{V}. \qquad \square$$

Remark 2.19 (POD naming convention in literature): *In literature, a slightly different naming convention for the POD problems (2.15) and (2.16) is often used. What we refer to as "POD problem in canonical coordinates" (2.16) is sometimes called "the POD (problem)" and the "POD problem in coordinates" (2.15) is called the "weighted POD (problem)" (e.g. [115]).*

The POD problem in canonical coordinates (2.16) can be solved with the so-called truncated singular value decomposition (truncated SVD) of the snapshot matrix in canonical coordinates.

Theorem 2.20 (Solution to POD, e.g. [115]): *Consider a singular value decomposition (SVD) of the snapshot matrix in canonical coordinates*

$$\hat{\boldsymbol{X}}^{\mathrm{s}} = \boldsymbol{U}_{\hat{\boldsymbol{X}}^{\mathrm{s}}} \boldsymbol{\Sigma}_{\hat{\boldsymbol{X}}^{\mathrm{s}}} \boldsymbol{V}_{\hat{\boldsymbol{X}}^{\mathrm{s}}}^{\top} \qquad \text{with} \qquad \begin{aligned} \boldsymbol{U}_{\hat{\boldsymbol{X}}^{\mathrm{s}}}^{\top} \boldsymbol{U}_{\hat{\boldsymbol{X}}^{\mathrm{s}}} &= \boldsymbol{I}_{N}, \\ \boldsymbol{V}_{\hat{\boldsymbol{X}}^{\mathrm{s}}}^{\top} \boldsymbol{V}_{\hat{\boldsymbol{X}}^{\mathrm{s}}} &= \boldsymbol{I}_{n_{\mathrm{s}}}, \end{aligned} \qquad [\boldsymbol{\Sigma}_{\hat{\boldsymbol{X}}^{\mathrm{s}}}]_{ij} = \begin{cases} \sigma_i, & i = j \\ 0, & else \end{cases}$$

with the matrices $\boldsymbol{U}_{\hat{\boldsymbol{X}}^{\mathrm{s}}} \in \mathbb{R}^{N \times N}$, $\boldsymbol{V}_{\hat{\boldsymbol{X}}^{\mathrm{s}}} \in \mathbb{R}^{n_{\mathrm{s}} \times n_{\mathrm{s}}}$ stacking the left- and right-singular vectors in their columns and the matrix $\boldsymbol{\Sigma}_{\hat{\boldsymbol{X}}^{\mathrm{s}}} \in \mathbb{R}^{N \times n_{\mathrm{s}}}$ with the singular values $\sigma_1 \geq \cdots \geq \sigma_{\min(N, n_{\mathrm{s}})} \geq 0$ in descending order on its diagonal. A solution of the POD problems (2.16) and (2.15) can be derived by truncating the first n left-singular vectors of an SVD, i.e.

$$\hat{\boldsymbol{V}}^{\mathrm{POD}} := \boldsymbol{V}_{\hat{\boldsymbol{X}}^{\mathrm{s}}}[:, : n] \qquad \text{and thus} \qquad \boldsymbol{V}^{\mathrm{POD}} = \boldsymbol{g}^{-1/2} \hat{\boldsymbol{V}}^{\mathrm{POD}} = \boldsymbol{g}^{-1/2} \boldsymbol{V}_{\hat{\boldsymbol{X}}^{\mathrm{s}}}[:, : n].$$

Proof. See e.g. [115, Rem. 3.2.4]. □

Remark 2.21 (POD functional in terms of singular values): *Consider a snapshot matrix in canonical coordinates $\hat{\boldsymbol{X}}^{\mathrm{s}} \in \mathbb{R}^{N \times n_{\mathrm{s}}}$ with an SVD $\hat{\boldsymbol{X}}^{\mathrm{s}} = \boldsymbol{V}_{\hat{\boldsymbol{X}}^{\mathrm{s}}} \boldsymbol{\Sigma}_{\hat{\boldsymbol{X}}^{\mathrm{s}}} \boldsymbol{U}_{\hat{\boldsymbol{X}}^{\mathrm{s}}}^{\top}$. From Theorem 2.20, we know that $\hat{\boldsymbol{V}}^{\mathrm{POD}} := \boldsymbol{V}_{\hat{\boldsymbol{X}}^{\mathrm{s}}}[:, : n]$ is an optimal solution to the POD problem in canonical coordinates. In this case, the POD functional can be expressed in terms of the singular values with*

$$\left\| \left(\boldsymbol{I}_N - \hat{\boldsymbol{V}}^{\mathrm{POD}} \left(\hat{\boldsymbol{V}}^{\mathrm{POD}} \right)^{\top} \right) \hat{\boldsymbol{X}}^{\mathrm{s}} \right\|_{\mathrm{F}}^2 = \sum_{i=n+1}^{\min(N, n_{\mathrm{s}})} \sigma_i^2$$

as the sum over the squared neglected singular values.

Remark 2.22 (Greedy basis generation): *Yet, we did not discuss how to choose the training parameters P_{train} to define the snapshot set (2.13). The straightforward approach would be sampling the parameter domain $P \subset \mathbb{R}^{n_{\mathrm{p}}}$ equidistantly. For high-dimensional parameter spaces,*

however, this leads typically to a computationally expensive offline phase, as the number of total sampling points grows exponentially with the dimension of the parameter space n_{p} if each dimension of the parameter space is sampled with the same number of points. The state-of-the-art solution for this problem is the use of so-called greedy basis generation procedures (see e.g. [35, 36]). These techniques build the ROB iteratively and adapt the snapshot set in each iteration based on a given error measure or error indicator. Most prominent for time-dependent problems is the POD-greedy algorithm [49], which uses the POD in each greedy iteration to compress a trajectory and to extend the ROB. It can be shown that an algebraic (or exponential) decay in the Kolmogorov n-widths induces an algebraic (or exponential) decay of the approximation error in the POD-greedy procedure [47]. We will discuss a greedy procedure in Chapter 4.

2.2.3.2 Time-Continuous Proper Orthogonal Decomposition

Later in this work, it will be helpful for a theoretical analysis to consider a time-continuous formulation of the POD. We reproduce the method from [115, Sec. 3.2] in a non-parametric setting.

Definition 2.23 (Time-continuous POD, e.g. [115, Sec. 3.2])**:** *Given an inner product space* $(\mathbb{V}, g)$ *and a solution trajectory* $x(\cdot) \in C^1(I_t, \mathbb{V})$ *to the FOM (2.6), the time-continuous POD computes a subspace* $\tilde{\mathbb{V}}^{\mathrm{tcPOD}} := \mathrm{span}\left\{\tilde{v}_i^{\mathrm{tcPOD}}\right\}_{i=1}^n$ *by identifying an orthonormal basis via the time-continuous POD (optimization) problem*

$$\tilde{\mathbb{V}}^{\mathrm{tcPOD}} := \mathrm{span}\left\{\tilde{v}_i^{\mathrm{tcPOD}}\right\}_{i=1}^n = \underset{\substack{\tilde{\mathbb{V}}=\mathrm{span}\{\tilde{v}_i\}_{i=1}^n \subset \mathbb{V}, \\ g(\tilde{v}_i, \tilde{v}_j)=\delta_{ij}\ for\ 1\leq i,j\leq n}}{\mathrm{argmin}} \int_{t_0}^{T_{\mathrm{POD}}} \left\|x(t) - \Pi_{g,\tilde{\mathbb{V}}}(x(t))\right\|_g^2 \mathrm{d}t \quad (2.17)$$

with an integration time $T_{\mathrm{POD}} \in (t_0, t_{\mathrm{end}}]$*. For the ROB matrix* $\boldsymbol{V}^{\mathrm{tcPOD}} \in \mathbb{R}^{N\times n}$*, the time-continuous POD problem in coordinates reads*

$$\boldsymbol{V}^{\mathrm{tcPOD}} = \underset{\substack{\boldsymbol{V}\in\mathbb{R}^{N\times n} \\ \boldsymbol{V}^\top \boldsymbol{g}\boldsymbol{V}=\boldsymbol{I}_n}}{\mathrm{argmin}} \underbrace{\int_{t_0}^{T_{\mathrm{POD}}} \left\|(\boldsymbol{I}_N - \boldsymbol{V}\boldsymbol{V}^\top \boldsymbol{g})\boldsymbol{x}(t)\right\|_{\boldsymbol{g}}^2 \mathrm{d}t}_{=:\mathcal{F}_{\mathrm{POD}}(\boldsymbol{V};T_{\mathrm{POD}})} . \quad (2.18)$$

Similarly to the time-discrete POD, an optimal basis can be derived via an eigenvalue problem. To this end, we recall the following theorem, which is formulated in [115] for semi-linear initial value problems with $t_0 = 0$.

Theorem 2.24 (Solution of the time-Continuous POD, [115, Thm. 1.4.3])**:** *Consider the unique FOM solution* $x(\cdot) \in C^1(I_t, \mathbb{V})$ *of* (2.6). *Then a time-continuous POD basis of rank* n *solving the time-continuous POD problem* (2.17) *is given by the eigenvectors of the operator*

$$\mathcal{R} : \mathbb{V} \to \mathbb{V}, \qquad v \mapsto \int_{t_0}^{T_{\mathrm{POD}}} x(t) g\left(x(t), \ v\right) \mathrm{d}t, \tag{2.19}$$

corresponding to the n *largest eigenvalues* $\lambda_1 \geq \cdots \geq \lambda_n$.

2.3 Hamiltonian Models

In the following, we want to consider FOMs (2.6) where the right-hand side has more structure and describes a so-called Hamiltonian system. To this end, we give a brief introduction in symplectic spaces and Hamiltonian systems (Section 2.3.1) and symplectic time integration (Section 2.3.2).

2.3.1 Symplecticity and Hamiltonian Systems

In the scope of this work, we restrict to autonomous, canonical Hamiltonian systems. More general cases are briefly discussed in Remark 2.31 and Remark 2.32. We introduce the concept of a symplectic vector space and parametric Hamiltonian systems in the following.

Definition 2.25 (Symplectic form and symplectic vector space, e.g. [28])**:** *Let* $\mathbb{V}$ *be a finite-dimensional vector space over* $\mathbb{R}$. *A symplectic form (on* $\mathbb{V}$*)* $\omega \in \mathrm{Bil}(\mathbb{V})$ *is a nondegenerate bilinear form (see* (2.2)*) which is skew-symmetric* $(\forall u, v \in \mathbb{V} : \omega(u, v) = -\omega(v, u))$. *The tuple* $(\mathbb{V}, \omega)$ *is then called a symplectic vector space.*

It can be shown that a symplectic vector space is necessarily even-dimensional [28] and thus $\dim(\mathbb{V}) = N = 2\bar{N}$ for some $\bar{N} \in \mathbb{N}$. The coefficient matrix $\boldsymbol{\omega} \in \mathbb{R}^{2\bar{N} \times 2\bar{N}}$ of the bilinear form ω is typically called a *Poisson matrix*. This matrix is skew-symmetric $(-\boldsymbol{\omega}^\top = \boldsymbol{\omega})$ and invertible $(\boldsymbol{\omega} \in \mathrm{GL}(2\bar{N}, \mathbb{R}))$.

Theorem 2.26 (Canonical basis, e.g. [28, Sec. 1.1])**:** *For each* $2\bar{N}$*-dimensional symplectic vector space* $(\mathbb{V}, \omega)$, *we can find a canonical basis* $\{e_i, f_i\}_{i=1}^{\bar{N}}$ *such that for all* $1 \leq i, j \leq \bar{N}$

$$\omega(e_i, f_j) = -\delta_{ij}, \qquad\qquad 0 = \omega(e_i, e_j) = \omega(f_i, f_j).$$

For the canonical basis, the Poisson matrix is the canonical Poisson matrix[2] $\boldsymbol{\omega} = \mathbb{J}_{2\bar{N}}^{\top}$ with

$$\mathbb{J}_{2\bar{N}} := \begin{bmatrix} \mathbf{0}_{\bar{N}\times\bar{N}} & \boldsymbol{I}_{\bar{N}} \\ -\boldsymbol{I}_{\bar{N}} & \mathbf{0}_{\bar{N}\times\bar{N}} \end{bmatrix} \in \mathbb{R}^{2\bar{N}\times 2\bar{N}} \qquad \textit{with} \qquad \begin{aligned} \mathbb{J}_{2\bar{N}}^{\top}\mathbb{J}_{2\bar{N}} &= \boldsymbol{I}_{2\bar{N}}, \\ \mathbb{J}_{2\bar{N}}\mathbb{J}_{2\bar{N}} &= -\boldsymbol{I}_{2\bar{N}}. \end{aligned} \tag{2.20}$$

Proof. See [28, Thm. 1.1]. □

As described in Section 2.1, a linear map which conserves the inner products of the source and target space is called orthogonal. Similarly, we call a function which conserves the symplectic forms a symplectic mapping (or symplectomorphism) as described by the following definition.

Definition 2.27 (Symplectic map and symplectic matrix): *We consider two symplectic vector spaces $(\mathbb{V}, \omega)$ and $(\check{\mathbb{V}}, \check{\omega})$ of dimension $2\bar{N}$ and $2\bar{n}$ with $2\bar{n} \leq 2\bar{N}$ and with Poisson matrices $\boldsymbol{\omega} \in \mathbb{R}^{2\bar{N}\times 2\bar{N}}$ and $\check{\boldsymbol{\omega}} \in \mathbb{R}^{2\bar{n}\times 2\bar{n}}$, respectively. Let $A \in L(\check{\mathbb{V}}; \mathbb{V})$ be a linear map. The map A is called a symplectic map and the coordinate matrix $\boldsymbol{A} \in \mathbb{R}^{2\bar{N}\times 2\bar{n}}$ is called a symplectic matrix if the symplectic structure is preserved, i.e.,*

$$\forall \check{u}, \check{v} \in \check{\mathbb{V}} : \check{\omega}(\check{u}, \check{v}) = \omega(A(\check{u}), A(\check{v})), \qquad \textit{or equivalently} \qquad \boldsymbol{A}^{\top}\boldsymbol{\omega}\boldsymbol{A} = \check{\boldsymbol{\omega}}. \tag{2.21}$$

A differentiable map $f \in C^1(\check{U}, \mathbb{V})$ on an open subset $\check{U} \subset \check{\mathbb{V}}$ is called symplectic if the Jacobian matrix $\mathbf{D}\boldsymbol{\varphi}|_{\check{u}} \in \mathbb{R}^{2\bar{N}\times 2\bar{n}}$ is a symplectic matrix for every $\check{u} \in \check{U}$.

Definition 2.28 (Hamiltonian FOM): *Given a symplectic vector space $(\mathbb{V}, \omega)$, a parameter domain $P \subset \mathbb{R}^{n_{\mathrm{p}}}$, a time interval $\emptyset \neq I_t := [t_0, t_{\mathrm{end}}] \subset \mathbb{R}$ and a function $\mathcal{H}(\cdot; \boldsymbol{\mu}) \in C^1(I_t)$. The task of a (possibly parametric) Hamiltonian FOM is: for an arbitrary, but fixed, parameter vector $\boldsymbol{\mu} \in P$ and a given initial value $x_0(\boldsymbol{\mu}) \in \mathbb{V}$, find $x(\cdot; \boldsymbol{\mu}) \in C^1(I_t, \mathbb{V})$ such that*

$$\frac{\mathrm{d}}{\mathrm{d}t}x(t; \boldsymbol{\mu}) = \sharp_\omega\left(\nabla\mathcal{H}|_{(x(t;\boldsymbol{\mu});\boldsymbol{\mu})}\right) \in \mathbb{V} \quad \forall t \in I_t, \qquad x(t_0; \boldsymbol{\mu}) = x_0(\boldsymbol{\mu}). \tag{2.22}$$

We refer to $\mathbb{V}$ as the phase space, to $\mathcal{H}(\cdot; \boldsymbol{\mu})$ as the Hamiltonian (function), to the right-hand side $X_{\mathcal{H}}(x; \boldsymbol{\mu}) := \sharp_\omega(\nabla\mathcal{H}|_{(x;\boldsymbol{\mu})})$ as the Hamiltonian vector field and to the IVP (2.22) as Hamiltonian system, which we denote as the triple $(\mathbb{V}, \omega, \mathcal{H})$.

---

[2]Contrary to existing works in structure-preserving MOR of Hamiltonian systems, we speak of the symplectic form $\boldsymbol{\omega} = \mathbb{J}_{2\bar{N}}^{\top}$ instead of $\mathbb{J}_{2\bar{N}}$. In the following, this yields the same FOM and ROM as in the existing works, but it helps to understand the more general case of noncanonical coordinates $\boldsymbol{\omega} \neq \mathbb{J}_{2\bar{N}}^{\top}$.

The Hamiltonian vector field in coordinates is $\boldsymbol{X}_{\mathscr{H}}(\boldsymbol{x}; \boldsymbol{\mu}) := \boldsymbol{\omega}^{-1} \nabla \mathscr{H}|_{\boldsymbol{x}; \boldsymbol{\mu}}$, which reads in the special case of a canonical basis (see Theorem 2.26) $\boldsymbol{X}_{\mathscr{H}}(\boldsymbol{x}; \boldsymbol{\mu}) := \mathbb{J}_{2\bar{N}} \nabla \mathscr{H}|_{\boldsymbol{x}; \boldsymbol{\mu}}$. In the context of classical mechanics, the phase space $\mathbb{V} = \mathcal{Q} \times \mathcal{P}$ consists of position states $q \in \mathcal{Q}$ of the configuration space and momentum states $p \in \mathcal{P}$ which form together the state $x = (q, p) \in \mathcal{Q} \times \mathcal{P}$. In the following, we may perform this splitting without explicitly referring to it.

Lemma 2.29 (Important properties of a Hamiltonian FOM): *For a Hamiltonian FOM, it holds:*

1. *the solution preserves the Hamiltonian over time, i.e.*

$$\mathscr{H}(x(t; \boldsymbol{\mu}); \boldsymbol{\mu}) = \mathscr{H}(x_0(\boldsymbol{\mu}); \boldsymbol{\mu}) \qquad \text{for all } (t, \boldsymbol{\mu}) \in I_t \times P,$$

2. *the flow of a Hamiltonian system is a symplectic map.*

Proof. See e.g. [51, Thm. VI.2.4]. □

Typically, the Hamiltonian $\mathscr{H}(\cdot; \boldsymbol{\mu})$ is the energy of the system. Since this function is preserved with Lemma 2.29, the class of Hamiltonian systems is favorable to model energy-preserving systems. Such systems are present e.g. in classical mechanics [1, Sec. 3.8] or quantum dynamics. Similarly, action principles might give rise to partial differential equations which includes the wave equation, the Schrödinger equation, the Korteweg–de Vries equation, the Euler equations, Maxwell's equations [1, Sec. 5.5], the Vlasov–Poisson equations and Vlasov–Maxwell equations [88]. With structure-preserving discretization methods like [17], such systems can turn into a Hamiltonian FOM (2.22).

Definition 2.30 (Special Hamiltonian systems): *We call the Hamiltonian*

1. *quadratic if it is defined via a symmetric bilinear form $H(\cdot, \cdot; \boldsymbol{\mu}) \in \mathrm{Bil}(\mathbb{V})$ and a vector $h(\boldsymbol{\mu}) \in \mathbb{V}$ with*

$$\mathscr{H}(x; \boldsymbol{\mu}) = \frac{1}{2} H(x, x; \boldsymbol{\mu}) + h(\boldsymbol{\mu}), \qquad \mathscr{H}(\boldsymbol{x}; \boldsymbol{\mu}) = \frac{1}{2} \boldsymbol{x}^\top \boldsymbol{H}(\boldsymbol{\mu}) \boldsymbol{x} + \boldsymbol{h}(\boldsymbol{\mu}) \qquad (2.23)$$

and the resulting Hamiltonian system will be linear,

2. *separable if the phase space is $\mathbb{V} = \mathcal{Q} \times \mathcal{P}$ and the Hamiltonian can be split in two terms $\mathscr{H}_q(\cdot, \boldsymbol{\mu}) \in C^1(\mathcal{Q}), \mathscr{H}_p(\cdot, \boldsymbol{\mu}) \in C^1(\mathcal{P})$ with*

$$\mathscr{H}((q, p); \boldsymbol{\mu}) = \mathscr{H}_q(q; \boldsymbol{\mu}) + \mathscr{H}_p(p; \boldsymbol{\mu}),$$

where the functions $\mathcal{H}_q(\cdot, \boldsymbol{\mu}), \mathcal{H}_p(\cdot, \boldsymbol{\mu})$ are typically referred to as the *potential energy* and the *kinetic energy*.

For a quadratic and separable Hamiltonian in coordinates (2.23), it holds

$$\boldsymbol{H}(\boldsymbol{\mu}) = \mathrm{blkdiag}(\boldsymbol{H}_q(\boldsymbol{\mu}), \boldsymbol{H}_p(\boldsymbol{\mu})) \in \mathbb{R}^{2\bar{N} \times 2\bar{N}} \qquad \boldsymbol{H}_q(\boldsymbol{\mu}), \boldsymbol{H}_p(\boldsymbol{\mu}) \in \mathbb{R}^{\bar{N} \times \bar{N}} \text{ symmetric.}$$

We consider autonomous Hamiltonian systems in canonical coordinates. The following two remarks discuss how more general cases can be treated.

Remark 2.31 (Non-canonical systems)**:** *By Theorem 2.26, we can find a canonical basis for every symplectic space, i.e., for a symplectic space $(\mathbb{V}, \omega)$ with a basis for which $\hat{\boldsymbol{\omega}} \neq \mathbb{J}_{2\bar{N}}^{\top}$, we can find a change of basis such that $\boldsymbol{\omega} = \mathbb{J}_{2\bar{N}}^{\top}$. Thus, the Hamiltonian system (2.22) is in literature often w.l.o.g. considered only for $\boldsymbol{\omega} = \mathbb{J}_{2\bar{N}}^{\top}$, $\boldsymbol{X}_{\mathcal{H}}(\boldsymbol{x}; \boldsymbol{\mu}) = \mathbb{J}_{2\bar{N}} \nabla \mathcal{H}|_{\boldsymbol{x}; \boldsymbol{\mu}}$. A corresponding change-of-basis matrix can be derived via the real Schur form, see e.g. [99, Rem. 3.8].*

Remark 2.32 (Non-autonomous Hamiltonian systems, e.g. [82, Sec. 4.3])**:** *The Hamiltonian FOM (2.22) is autonomous since the Hamiltonian vector field does not depend on time. In a more general setting of a time-dependent Hamiltonian $\mathcal{H}(\cdot, \cdot; \boldsymbol{\mu}) : I_t \times \mathbb{V} \to \mathbb{R}$, the corresponding IVP is called a non-autonomous Hamiltonian system. If the dependence on the time is continuously differentiable, this case can be redirected to an autonomous Hamiltonian system (2.22) by considering an extended phase space [70, Cha. VI, Sec. 10]. The construction in the framework of structure-preserving MOR is discussed in [20, Sec. 2.4 and 2.5].*

2.3.2 Symplectic Time Integration

As discussed in Remark 2.3, IVPs are solved with numerical time integration schemes in practice. In order to preserve some of the special properties from Lemma 2.29 during the time discretization, so-called symplectic time integration schemes can be used. A monograph on this topic is the book [51]. We reproduce in the following a small excerpt on symplectic one-step methods and in specific the symplectic Runge–Kutta methods. For the sake of brevity, we suppress the parameter-dependence of the FOM (2.22).

Definition 2.33 ((Symplectic) one-step method)**:** *A one-step method (formulated for the autonomous Hamiltonian systems (2.22)) is a numerical time integration scheme, which is based on a one-step map $\theta_{\Delta t} \in C^1(\mathbb{V}, \mathbb{V})$ such that $x_k = \theta_{\Delta t}(x_{k-1})$. A one-step method is called symplectic if the one-step map is a symplectic mapping in the sense of Definition 2.27.*

Definition 2.34 (*s*-stage Runge–Kutta method)**:** *An s-stage Runge–Kutta method with $s \in \mathbb{N}$ (formulated for the autonomous Hamiltonian system (2.22)) is a one-step method given by the coefficients $\beta_i, \alpha_{ij} \in \mathbb{R}, 1 \leq i, j \leq s$, with the one-step map for $x \in \mathbb{V}$*

$$\theta_{\Delta t, \mathrm{RK}}(x) := x + \Delta t \sum_{i=1}^{s} \beta_i w_i \tag{2.24}$$

where $w_i \in \mathbb{V}$ solve the system of nonlinear equations for each $i \in \{1, \dots, s\}$

$$0 = w_i - X_{\mathscr{H}}\left(x + \Delta t \sum_{j=1}^{s} \alpha_{ij} w_j\right) \in \mathbb{V}.$$

Definition 2.35 (Symplectic Runge–Kutte method, e.g. [51, Thm. VI.4.3])**:** *An s-state Runge–Kutta method is symplectic if the coefficients satisfy*

$$\beta_i \alpha_{ij} + \beta_j \alpha_{ji} = \beta_i \beta_j, \qquad \text{for all } 1 \leq i, j \leq s.$$

Example 2.36 (Implicit midpoint)**:** *A classical example for an implicit symplectic Runge–Kutta method is the implicit midpoint rule with $s = 1$ and coefficients $\alpha_{11} = 1/2, \beta_1 = 1$ such that*

$$\theta_{\Delta t, \mathrm{RK}}(x) = x + \Delta t w_1, \qquad 0 = w_1 - X_{\mathscr{H}}\left(x + \frac{\Delta t}{2} w_1\right). \tag{2.25}$$

Remark 2.37 (Modified Hamiltonian)**:** *Although symplectic integrators preserve the symplectic structure, the Hamiltonian in the time-discrete model might be modified compared to the original Hamiltonian. For a quadratic Hamiltonian in combination with a symplectic Runge–Kutta integrator, however, it can be shown that the modified Hamiltonian equals the original Hamiltonian. Further details can be found in [76, Sec. 5.1.2 and 5.2] or [51, Cha. IX.].*

2.4 Symplectic Model Order Reduction on Subspaces

Applying a classical *g*-ROM to a Hamiltonian system (2.22) will in general not yield a Hamiltonian system of reduced order (which is sometimes referred to as "losing the Hamiltonian structure"). Consequently, this ROM will in general lose all interesting properties of Hamiltonian systems from Lemma 2.29. In [81, 99], *symplectic MOR* is introduced which is a reduction technique that does yield a reduced Hamiltonian system. In this section, we briefly discuss

special subspaces of symplectic vector spaces (Section 2.4.1), introduce the reduced Hamiltonian system (Section 2.4.2) and review symplectic basis generation techniques existing in the literature (Section 2.4.3).

2.4.1 Special Subspaces

For inner product spaces $(\mathbb{V}, g)$, every subspace $\tilde{\mathbb{V}} \subset \mathbb{V}$ is compatible with g. For a symplectic space $(\mathbb{V}, \omega)$, however, not every subspace is compatible with ω. Thus, we will discuss different subspaces of a symplectic space in the following.

Definition 2.38 (Symplectic complement, e.g. [28, Sec. 1.3]): *Let $(\mathbb{V}, \omega)$ be a symplectic vector space. For an n-dimensional subspace $\tilde{\mathbb{V}} \subset \mathbb{V}$, its symplectic complement is*

$$\tilde{\mathbb{V}}^\omega := \{u \in \mathbb{V} \,|\, \omega(u, v) = 0 \ \forall v \in \tilde{\mathbb{V}}\}.$$

Remark 2.39 (Comparison of orthogonal and symplectic complement): *Note that the definition of the symplectic complement is reminiscent of the classical orthogonal complement. However, the two objects behave differently. For orthogonal complements, we know $\tilde{\mathbb{V}}^\perp \cap \tilde{\mathbb{V}} = \{0\}$. For the symplectic complement, however, this may not be case as we will see in the following.*

Definition 2.40 (Special subspaces, e.g. [28, Sec. 1.3]): *Let $(\mathbb{V}, \omega)$ be a symplectic vector space with an n-dimensional subspace $\tilde{\mathbb{V}} \subset \mathbb{V}$ (characterized by a reduced space $\check{\mathbb{V}}$ and an embedding $V \in L(\check{\mathbb{V}}; \mathbb{V})$). We refer to the subspace*

- *as a symplectic subspace, if $\tilde{\mathbb{V}}^\omega \cap \tilde{\mathbb{V}} = \{0\}$ or, equivalently, if $\omega(V(\cdot), V(\cdot)) \in \mathrm{Bil}(\check{\mathbb{V}})$ is nondegenerate, which is exactly our definition of ω being compatible with $\tilde{\mathbb{V}}$,*

- *as an isotropic subspace, if $\tilde{\mathbb{V}} \subset \tilde{\mathbb{V}}^\omega$ or, equivalently, if $\omega(V(\cdot), V(\cdot)) \in \mathrm{Bil}(\check{\mathbb{V}}) \equiv 0$,*

- *as a coisotropic subspace, if $\tilde{\mathbb{V}}^\omega \subset \tilde{\mathbb{V}}$ or, equivalently, if $\tilde{\mathbb{V}}^\omega$ is an isotropic subspace.*

Example 2.41 (Special subspaces from canonical basis, e.g. [28, Sec. 1.3]): *Let $(\mathbb{V}, \omega)$ be a $2\bar{N}$-dimensional symplectic vector space with a canonical basis $\{e_i, f_i\}_{i=1}^{\bar{N}}$. Then,*

- *$\mathrm{span}\,\{e_i, f_i\}_{i=1}^{\bar{n}}$ is a symplectic subspace for all $1 \leq \bar{n} \leq \bar{N}$,*

- *$\mathrm{span}\,\{e_i\}_{i=1}^{\bar{n}}$ is an isotropic subspace for all $1 \leq \bar{n} \leq \bar{N}$,*

- *$\mathrm{span}\,\{e_i\}_{i=1}^{\bar{N}} \oplus \mathrm{span}\,\{f_1\}$ is a coisotropic subspace.*

Proposition 2.42: *Consider a $2\bar{N}$-dimensional symplectic vector space $(\mathbb{V}, \omega)$ and a subspace $\tilde{\mathbb{V}} \subset \mathbb{V}$ (characterized by a reduced space $\check{\mathbb{V}}$ and an embedding $V \in L(\check{\mathbb{V}}; \mathbb{V})$). If $\tilde{\mathbb{V}}$ is a symplectic subspace, then $(\check{\mathbb{V}}, \check{\omega})$ is a symplectic vector space with the reduced symplectic form $\check{\omega} := \omega(V(\cdot), V(\cdot)) \in \mathrm{Bil}(\check{\mathbb{V}})$. It holds $\dim(\tilde{\mathbb{V}}) = \dim(\check{\mathbb{V}}) = 2\bar{n}$ for some $\bar{n}$.*

Proof. Skew-symmetry of $\check{\omega} = \omega(V(\cdot), V(\cdot)) \in \mathrm{Bil}(\check{\mathbb{V}})$ is inherited from ω. Nondegeneracy of $\check{\omega}$ is the definition of the symplectic subspace. $\qquad\square$

(Co)isotropic subspaces are examples for subspaces of $\mathbb{V}$ for which the symplectic form ω is not compatible with $\tilde{\mathbb{V}}$. The compatibility has to be assumed during the basis generation. In coordinates, the compatibility condition "$\omega(V(\cdot), V(\cdot)) \in \mathrm{Bil}(\check{\mathbb{V}})$ nondegenerate" is equivalent to the condition that the representing matrix is invertible, i.e., $\boldsymbol{V}^\top \boldsymbol{\omega} \boldsymbol{V} \in \mathrm{GL}(n, \mathbb{R})$. Since there exists a canonical basis for every symplectic basis, this is equivalent to find a basis such that $\boldsymbol{V}^\top \boldsymbol{\omega} \boldsymbol{V} = \mathbb{J}_{2\bar{n}}^\top$. We will see this condition later on in the basis generation. For $\boldsymbol{\omega} = \mathbb{J}_{2\bar{N}}^\top$, the *symplectic Stiefel manifold* $\mathrm{Sp}(2\bar{n}, \mathbb{R}^{2\bar{N}}) := \{ \boldsymbol{V} \in \mathbb{R}^{2\bar{N} \times 2\bar{n}} \mid \boldsymbol{V}^\top \mathbb{J}_{2\bar{N}}^\top \boldsymbol{V} = \mathbb{J}_{2\bar{n}}^\top \}$ is defined in parallel to the Stiefel manifold from Section 2.1.

2.4.2 Symplectic MOR

By Section 2.4.1, a symplectic subspace $\tilde{\mathbb{V}} \subset \mathbb{V}$ is compatible with ω. This allows us to use the a-based projection (2.4) for $a = \omega$ and define the corresponding projection error and ROM.

Definition 2.43 (Symplectic projection (error)): *Let $(\mathbb{V}, \omega)$ be a symplectic vector space of dimension $2\bar{N}$ and $\tilde{\mathbb{V}} \subset \mathbb{V}$ a symplectic subspace of dimension $2\bar{n}$ with the reduced symplectic form $\check{\omega}$. The a-based projection (2.4) with $a = \omega$ defines the symplectic projection*

$$\Pi_{\omega, \tilde{\mathbb{V}}} = V \circ \sharp_{\check{\omega}} \circ V^* \circ \flat_\omega \in L(\mathbb{V}; \tilde{\mathbb{V}}) \qquad \text{with} \qquad \boldsymbol{\Pi}_{\omega, \tilde{\mathbb{V}}} = \boldsymbol{V} \check{\boldsymbol{\omega}}^{-1} \boldsymbol{V}^\top \boldsymbol{\omega} \in \mathbb{R}^{2\bar{N} \times 2\bar{N}}.$$

We refer to the a-based projection error with $a = \omega$ as the symplectic projection error.

Theorem 2.44 (Symplectic Galerkin ROM (ω-ROM), [81, 99]): *Consider a $2\bar{N}$-dimensional symplectic vector space $(\mathbb{V}, \omega)$ with a $2\bar{n}$-dimensional symplectic subspace $\tilde{\mathbb{V}} \subset \mathbb{V}$ (characterized by a reduced space $\check{\mathbb{V}}$ and an embedding $V \in L(\check{\mathbb{V}}; \mathbb{V})$). By Proposition 2.42, $\tilde{\mathbb{V}}$ and ω are compatible. An a-ROM (see Definition 2.9) with the nondegenerate bilinear form chosen as $a = \omega$ applied to a Hamiltonian FOM (2.22), results in a reduced Hamiltonian system $(\check{\mathbb{V}}, \check{\omega}, \check{\mathcal{H}})$ with the reduced Hamiltonian $\check{\mathcal{H}}(\cdot; \boldsymbol{\mu}) := \mathcal{H}(V(\cdot); \boldsymbol{\mu})$ or in coordinates $\check{\mathcal{H}}(\check{x}; \boldsymbol{\mu}) = \mathcal{H}(\boldsymbol{V}\check{x}; \boldsymbol{\mu})$. If the basis of $\tilde{\mathbb{V}}$ is canonical then $\boldsymbol{V}^\top \boldsymbol{\omega} \boldsymbol{V} = \mathbb{J}_{2\bar{n}}^\top$. We refer to this as the symplectic Galerkin ROM.*

Proof. For the sake of a better overview, we skip the parameter-dependence in this proof. Since $\tilde{\mathbb{V}}$ is a symplectic vector space, ω is compatible with $\tilde{\mathbb{V}}$ (and thus $\tilde{\omega}$ is nondegenerate, and we can use $\flat_{\tilde{\omega}}$ and $\sharp_{\tilde{\omega}}$). Due to linearity of the embedding $V \in L(\check{\mathbb{V}}; \mathbb{V})$, it holds for its derivative $\mathrm{d}V|_{\check{u}}(\check{v}) = V(\check{v})$. Then, it holds with the chain rule (2.5) for all $\check{u}, \check{v} \in \check{\mathbb{V}}$

$$\nabla \check{\mathscr{H}}\Big|_{\check{u}}(\check{v}) = \mathrm{d}(\mathscr{H} \circ V)|_{\check{u}}(\check{v}) \overset{(2.5)}{=} \underbrace{\mathrm{d}\mathscr{H}|_{V(\check{u})}}_{=\nabla\mathscr{H}|_{V(\check{u})}}\left(\underbrace{\mathrm{d}V|_{\check{u}}(\check{v})}_{=V(\check{v})}\right) = \left(V^*\left(\nabla\mathscr{H}|_{V(\check{u})}\right)\right)(\check{v}) \quad (2.26)$$

Thus, the reduced right-hand side

$$\check{f}(\check{x}) \overset{(2.10)}{=} (\sharp_{\check{\omega}} \circ V^*)(\underbrace{\flat_{\omega}\left(X_{\mathscr{H}}(V(\check{x}))\right)}_{=\nabla\mathscr{H}|_{V(\check{x})}}) = \sharp_{\check{\omega}}\left(V^*\left(\nabla\mathscr{H}|_{V(\check{x})}\right)\right) \overset{(2.26)}{=} \sharp_{\check{\omega}}\left(\nabla\check{\mathscr{H}}\Big|_{\check{x}}\right)$$

is the Hamiltonian vector field $X_{\check{\mathscr{H}}}$ of the reduced Hamiltonian system $(\check{\mathbb{V}}, \check{\omega}, \check{\mathscr{H}})$. $\qquad\square$

The ω-ROM uses $V^{-1} \circ \Pi_{\omega,\tilde{\mathbb{V}}} : \mathbb{V} \to \check{\mathbb{V}}$ to project the right-hand side to the reduced space $\check{\mathbb{V}}$ (see Definition 2.9). In coordinates, this operation is $\check{\boldsymbol{\omega}}^{-1}\boldsymbol{V}^{\top}\boldsymbol{\omega}$, which is for $\check{\boldsymbol{\omega}} = \mathbb{J}_{2\bar{n}}^{\top}$ and $\boldsymbol{\omega} = \mathbb{J}_{2\bar{N}}^{\top}$ known as the *symplectic inverse* $\boldsymbol{V}^{+} := \mathbb{J}_{2\bar{n}}\boldsymbol{V}^{\top}\mathbb{J}_{2\bar{N}}^{\top}$.[3]

Remark 2.45 (ω-ROM for noncanonical Hamiltonian system)**:** *The original formulation of symplectic MOR [81, 99] is formulated in canonical coordinates for both the FOM and the ROM. The presented formalism directly extends this idea to noncanonical coordinates. A similar approach has been discussed in [80]. However, our formulation directly relates to the idea of the POD in canonical coordinates from Lemma 2.18 that the canonical coordinates are just a coordinate transformation as we will see in the subsequent section.*

Remark 2.46 (Preservation of stability)**:** *An ω-ROM preserves stability in the following sense:*

- *In [99, Sec. 3.9], the authors prove that if the initial value $x_0 \in \mathbb{V}$ is contained within a neighborhood $U \subset \mathbb{V}$ for which for all points $x \in \partial U$ on the boundary the energy is strictly lower $\mathscr{H}(x) < \mathscr{H}(x_0)$ or strictly higher $\mathscr{H}(x) > \mathscr{H}(x_0)$ than the energy of the initial value, then the FOM and ROM are both uniformly bounded for all times t.*

- *In [99, Thm. 3.10] and [81, Thm. 7], it is proven that Lyapunov stable points $x_{\mathrm{e}} \in \mathbb{V}$ are preserved, if these are included in the reduced space $x_{\mathrm{e}} \in \tilde{\mathbb{V}}$. We comment on such stability result in Section 7.1 in the more general case of MOR on manifolds.*

---

[3]Note however that the symplectic inverse $(\cdot)^{+}$ should not be confused with the Moore–Penrose pseudo inverse which we will later denote with $(\cdot)^{\dagger}$.

Remark 2.47 (Non-intrusive symplectic MOR via Hamiltonian operator inference): *An approach for non-intrusive (see Remark 2.14) symplectic MOR has been introduced in [109]. In that work, the additional structure of a Hamiltonian system helps (a) to give the equations more interpretability, and (b) to guarantee stability (especially for long-time prediction).*

2.4.3 Snapshot-based Symplectic Basis Generation

As discussed in Section 2.2.3 with the classical MOR, we use a snapshot-based basis generation technique to determine a basis spanning the subspace $\tilde{\mathbb{V}} \subset \mathbb{V}$. Symplectic MOR, however, requires a symplectic subspace for the compatibility of $\tilde{\mathbb{V}}$ and ω. Thus, the POD can in general not be used for basis generation and an alternative approach is required.

2.4.3.1 (Time-Discrete) Proper Symplectic Decomposition

For the generation of a symplectic basis, the Proper Symplectic Decomposition (PSD) was proposed in [99]. The PSD chooses the basis to minimize the symplectic projection error (see Definition 2.43) in the mean over all snapshots.

Definition 2.48 (Proper Symplectic Decomposition (PSD)): *Consider a symplectic space* $(\mathbb{V}, \omega)$ *with an inner product* $g \in \mathrm{Bil}(\mathbb{V})$ *and an induced norm* $\|\cdot\|_g : \mathbb{V} \to \mathbb{R}_{\geq 0}$. *Given a snapshot set* $X^{\mathrm{s}} \subset \mathbb{V}$, *the Proper Symplectic Decomposition (PSD) computes a symplectic subspace* $\tilde{\mathbb{V}}^{\mathrm{PSD}} := \mathrm{span}\left\{\tilde{e}_i^{\mathrm{PSD}}, \tilde{f}_i^{\mathrm{PSD}}\right\}_{i=1}^{\bar{n}}$ *by identifying a canonical basis via the PSD (optimization) problem*

$$\tilde{\mathbb{V}}^{\mathrm{PSD}} := \mathrm{span}\left\{\tilde{e}_i^{\mathrm{PSD}}, \tilde{f}_i^{\mathrm{PSD}}\right\}_{i=1}^{\bar{n}} = \underset{\substack{\tilde{\mathbb{V}}:=\mathrm{span}\left\{\tilde{e}_i, \tilde{f}_i\right\}_{i=1}^{\bar{n}} \subset \mathbb{V}, \\ \text{for } 1 \leq i,j \leq \bar{n}: \, \omega\left(\tilde{e}_i, \tilde{f}_j\right) = -\delta_{ij} \text{ and} \\ \omega(\tilde{e}_i, \tilde{e}_j) = \omega(\tilde{f}_i, \tilde{f}_j) = 0}}{\mathrm{argmin}} \sum_{i=1}^{n_{\mathrm{s}}} \left\| x_i^{\mathrm{s}} - \Pi_{\omega, \tilde{\mathbb{V}}}(x_i^{\mathrm{s}}) \right\|_g^2. \quad (2.27)$$

For the ROB matrix $\boldsymbol{V}^{\mathrm{PSD}} = \left[[\tilde{e}_i^{\mathrm{PSD}}]_{i=1}^{\bar{n}}, [\tilde{f}_i^{\mathrm{PSD}}]_{i=1}^{\bar{n}} \right] \in \mathbb{R}^{2\bar{N} \times 2\bar{n}}$, *the reduced symplectic form in coordinates is* $\check{\boldsymbol{\omega}} = \mathbb{J}_{2\bar{n}}^{\top}$ *due to the construction of a canonical basis and thus the PSD problem in coordinates reads*

$$\boldsymbol{V}^{\mathrm{PSD}} = \underset{\substack{\boldsymbol{V} \in \mathbb{R}^{2\bar{N} \times 2\bar{n}} \\ \boldsymbol{V}^{\top} \boldsymbol{\omega} \boldsymbol{V} = \mathbb{J}_{2\bar{n}}^{\top}}}{\mathrm{argmin}} \sum_{i=1}^{n_{\mathrm{s}}} \left\| (\boldsymbol{I}_N - \boldsymbol{V} \mathbb{J}_{2\bar{n}} \boldsymbol{V}^{\top} \boldsymbol{\omega}) \boldsymbol{x}_i^{\mathrm{s}} \right\|_{\boldsymbol{g}}^2. \quad (2.28)$$

As indicated in Theorem 2.26, a canonical basis may be chosen for all symplectic vector spaces. The next lemma shows how the PSD problem looks in canonical coordinates.

Lemma 2.49 (PSD problem in canonical coordinates)**:** *Consider a PSD problem (2.27) for a symplectic vector space $(\mathbb{V}, \omega)$ with a noncanonical Poisson matrix $\boldsymbol{\omega} \neq \mathbb{J}_{2\bar{N}}^{\top}$. A coordinate transformation with the change-of-basis matrix $\boldsymbol{Q}$ exists by Theorem 2.26 with $\hat{\boldsymbol{x}} = \boldsymbol{Q}\boldsymbol{x}$ such that the Poisson matrix $\hat{\boldsymbol{\omega}} \overset{(2.3)}{=} \boldsymbol{Q}^{-\top}\boldsymbol{\omega}\boldsymbol{Q}^{-1} = \mathbb{J}_{2\bar{N}}^{\top}$ in the new coordinates is canonical. In the transformed coordinates the PSD (problem) in canonical coordinates, reads*

$$\hat{\boldsymbol{V}}^{\text{PSD}} = \underset{\substack{\hat{\boldsymbol{V}} \in \mathbb{R}^{N \times n} \\ \hat{\boldsymbol{V}}^{\top}\mathbb{J}_{2\bar{N}}^{\top}\hat{\boldsymbol{V}} = \mathbb{J}_{2\bar{n}}^{\top}}}{\text{argmin}} \sum_{i=1}^{n_{\text{s}}} \left\| (\boldsymbol{I}_N - \hat{\boldsymbol{V}} \underbrace{\mathbb{J}_{2\bar{n}}\hat{\boldsymbol{V}}^{\top}\mathbb{J}_{2\bar{N}}^{\top}}_{=\hat{\boldsymbol{V}}^{+}})\hat{\boldsymbol{x}}_i^{\text{s}} \right\|_{\hat{\boldsymbol{g}}}^2 \tag{2.29}$$

with the snapshots in canonical coordinates $\hat{\boldsymbol{x}}_i^{\text{s}} = \boldsymbol{Q}\boldsymbol{x}_i^{\text{s}}$ for $1 \leq i \leq n_{\text{s}}$ and the inner product matrix $\hat{\boldsymbol{g}} = \boldsymbol{Q}^{-\top}\boldsymbol{g}\boldsymbol{Q}^{-1}$. Solving (2.29) is equivalent to solving (2.28) with $\hat{\boldsymbol{V}}^{\text{PSD}} = \boldsymbol{Q}\boldsymbol{V}^{\text{PSD}}$.

Proof. The equivalence of the PSD problems (2.28) and (2.29) follows from transforming all quantities with the coordinate transformation and using $\|\boldsymbol{x}\|_{\hat{\boldsymbol{g}}} = \|\boldsymbol{Q}^{-1}\boldsymbol{x}\|_{\boldsymbol{g}}$

$$\left\| (\boldsymbol{I}_{2\bar{N}} - \hat{\boldsymbol{V}} \mathbb{J}_{2\bar{n}}\hat{\boldsymbol{V}}^{\top}\mathbb{J}_{2\bar{N}}^{\top})\hat{\boldsymbol{x}}_i^{\text{s}} \right\|_{\hat{\boldsymbol{g}}} = \left\| \boldsymbol{Q}^{-1}(\boldsymbol{I}_{2\bar{N}} - \boldsymbol{Q}\boldsymbol{V}\mathbb{J}_{2\bar{n}}\boldsymbol{V}^{\top}\boldsymbol{Q}^{\top}\mathbb{J}_{2\bar{N}}^{\top})\boldsymbol{Q}\boldsymbol{x}_i^{\text{s}} \right\|_{\boldsymbol{g}}$$

$$= \left\| (\boldsymbol{I}_{2\bar{N}} - \boldsymbol{V}\mathbb{J}_{2\bar{n}}\boldsymbol{V}^{\top}\boldsymbol{\omega})\boldsymbol{x}_i^{\text{s}} \right\|_{\boldsymbol{g}}$$

$$\mathbb{J}_{2\bar{n}}^{\top} = \hat{\boldsymbol{V}}^{\top}\mathbb{J}_{2\bar{N}}^{\top}\hat{\boldsymbol{V}} = \boldsymbol{V}^{\top}\boldsymbol{Q}^{\top}\mathbb{J}_{2\bar{N}}^{\top}\boldsymbol{Q}\boldsymbol{V} = \boldsymbol{V}^{\top}\boldsymbol{\omega}\boldsymbol{V}. \qquad \square$$

Remark 2.50 (Standard formulation of PSD)**:** *Both, Definition 2.48 and Lemma 2.49, are already extended formulations compared to the approaches presented in literature. The standard formulation of the PSD is formulated in canonical coordinates (2.29), while it is additionally assumed $\hat{\boldsymbol{g}} = \boldsymbol{I}_{2\bar{N}}$. This case is also considered in the remainder of the thesis.*

In contrast to the POD problem, however, no general solution procedure is known to the PSD problem. In the following, we present symplectic basis generation techniques known in literature.

Definition 2.51 (Solving PSD in canonical coordinates in restricted sets, [99])**:** *Alongside the PSD (in canonical coordinates for $\hat{\boldsymbol{g}} = \boldsymbol{I}_{2\bar{N}}$), [99] introduces two symplectic basis generation techniques, which optimize the PSD problem on restricted sets:*

- *PSD cotangent lift (PSD CL)*

$$\mathcal{M}_{\mathrm{CL}} := \left\{ \begin{bmatrix} \boldsymbol{\Phi} & \mathbf{0}_{\bar{N} \times \bar{n}} \\ \mathbf{0}_{\bar{N} \times \bar{n}} & \boldsymbol{\Phi} \end{bmatrix} \in \mathbb{R}^{2\bar{N} \times 2\bar{n}} \,\middle|\, \boldsymbol{\Phi} \in \mathbb{R}^{\bar{N} \times \bar{n}}, \ \boldsymbol{\Phi}^{\top} \boldsymbol{\Phi} = \boldsymbol{I}_{\bar{n}} \right\},$$

- *PSD complex SVD (PSD cSVD)*

$$\mathcal{M}_{\mathrm{cSVD}} := \left\{ \begin{bmatrix} \boldsymbol{\Phi} & -\boldsymbol{\Psi} \\ \boldsymbol{\Psi} & \boldsymbol{\Phi} \end{bmatrix} \in \mathbb{R}^{2\bar{N} \times 2\bar{n}} \,\middle|\, \boldsymbol{\Phi}, \boldsymbol{\Psi} \in \mathbb{R}^{\bar{N} \times \bar{n}}, \ \begin{aligned} \boldsymbol{\Phi}^{\top} \boldsymbol{\Psi} &= \boldsymbol{\Psi}^{\top} \boldsymbol{\Phi}, \\ \boldsymbol{\Phi}^{\top} \boldsymbol{\Phi} + \boldsymbol{\Psi}^{\top} \boldsymbol{\Psi} &= \boldsymbol{I}_{\bar{n}} \end{aligned} \right\}.$$

Optimal bases for PSD CL and PSD cSVD can be derived with the (complex) SVD of modified snapshot matrices [99]. Concluding this section, the following two remarks each introduces a further strategy for symplectic basis generation.

Remark 2.52 (Greedy procedure based on symplectic Gram–Schmidt, [81])**:** *A greedy symplectic basis generation procedure was introduced in [81]. It chooses in each greedy iteration the vector with maximal projection error and applies a symplectic Gram–Schmidt procedure to obtain a pair $\boldsymbol{z}_i, \mathbb{J}_{2\bar{N}}^{\top} \boldsymbol{z}_i \in \mathbb{R}^{2\bar{N}}$ to enrich the ROB. After $\bar{n}$ greedy iterations, this results in the symplectic ROB matrix $\boldsymbol{V} = [[\boldsymbol{z}_i]_{i=1}^{\bar{n}}, [\mathbb{J}_{2\bar{N}}^{\top} \boldsymbol{z}_i]_{i=1}^{\bar{n}}]$. We discuss more details on symplectic greedy basis generation in [Chapter 4](#).*

Remark 2.53 (Basis generation via optimization on manifolds)**:** *A series of work [8, 9, 38–40] considers generating a symplectic ROB by optimizing the PSD functional (with $\hat{\boldsymbol{g}} = \boldsymbol{I}_{2\bar{N}}$) iteratively with techniques from optimization on manifolds with gradient-descent methods. The advantage of these techniques is (i) that the constrained optimization problem (2.29) on $\mathbb{R}^{2\bar{N} \times 2\bar{n}}$ becomes an unconstrained optimization problem by confining the solution to the symplectic Stiefel manifold $\mathrm{Sp}(2\bar{n}, \mathbb{R}^{2\bar{N}})$, and (ii) that they do not restrict to a subset of $\mathrm{Sp}(2\bar{n}, \mathbb{R}^{2\bar{N}})$, which enables them to potentially find a global optimum. All these methods are based on geometric formulations that determine an optimization algorithm based on different metrics and different retractions. Roughly speaking, the metric determines how elements are projected, while the retraction updates the iterates with a computed search direction. The work [39] lays the foundation by analyzing the geometry of the symplectic Stiefel manifold and uses the so-called canonical like metric. In contrast, [38] uses the standard Euclidean metric (which is the Frobenius inner product $\langle \cdot, \ \cdot \rangle_{\mathrm{F}}$ on the ambient space $\mathbb{R}^{2\bar{N} \times 2\bar{n}}$). With this choice, the underlying optimization problem is naturally linked to the nearest symplectic matrix problem: Given $\boldsymbol{A} \in \mathbb{R}^{2\bar{N} \times 2\bar{n}}$, find $\boldsymbol{X} \in \mathrm{Sp}(2\bar{n}, \mathbb{R}^{2\bar{N}})$*

such that $\|\boldsymbol{X} - \boldsymbol{A}\|_{\mathrm{F}}$ is minimized. In [9], the optimization is carried out on the so-called symplectic Grassmann manifold (based on work in [8, 39]), which respects that different ROBs might yield the same symplectic subspace. Lastly, in [40], the authors use a modified retraction that is based on the so-called SR-decomposition.

Non-Orthonormal, Symplectic Bases Generation

3

We investigate a new symplectic basis generation technique. Firstly, we identify the classical symplectic basis generation techniques from Definition 2.51 and Remark 2.52 to generate a symplectic orthonormal basis. Secondly, we introduce the PSD SVD-like decomposition, a basis generation technique which, in general, generates a symplectic, non-orthonormal basis. In numerical experiments, we compare the basis generation techniques and show that the newly introduced method produces more accurate ROMs. This is an adaptation of [20].

3.1 Orthosymplectic Basis Generation

In this section, we characterize orthosymplectic basis generation techniques and show that the techniques from Definition 2.51 and Remark 2.52 are of this type.

Definition 3.1 (Orthosymplectic ROB (matrix), [81])**:** *An ROB and the respective ROB matrix* $\boldsymbol{V} \in \mathbb{R}^{2\bar{N} \times 2\bar{n}}$ *are called* orthosymplectic *if the ROB is symplectic and orthonormal, i.e. the ROB matrix* $\boldsymbol{V}$ *is (i) symplectic and (ii) has orthonormal columns*

$$(i)\ \boldsymbol{V}^\top \mathbb{J}_{2\bar{N}} \boldsymbol{V} = \mathbb{J}_{2\bar{n}} \qquad and \qquad (ii)\ \boldsymbol{V}^\top \boldsymbol{V} = \boldsymbol{I}_{2\bar{n}}.$$

In order to get a better understanding of orthosymplectic ROB matrices, we give the following characterization. It shows that orthosymplectic ROB matrices are of a special structure and that orthosymplectic ROB matrices are exactly the ROB matrices for which the symplectic inverse equals the transposed. This characterization extends the results given e.g. in [95] for square matrices $\boldsymbol{Q} \in \mathbb{R}^{2\bar{N} \times 2\bar{N}}$ to the case of rectangular matrices $\boldsymbol{V} \in \mathbb{R}^{2\bar{N} \times 2\bar{n}}$. Partially, this was also addressed in [99, Lem. 4.3.].

Lemma 3.2 (Characterization of a symplectic matrix with orthonormal columns): *The following statements are equivalent for any matrix* $V \in \mathbb{R}^{2\bar{N} \times 2\bar{n}}$

  (i) V *is orthosymplectic,*

  (ii) there exists $E \in \mathbb{R}^{2\bar{N} \times \bar{n}}$ *such that*

$$V = \begin{bmatrix} E & \mathbb{J}_{2\bar{N}}^{\top} E \end{bmatrix} =: V_E \in \mathbb{R}^{2\bar{N} \times 2\bar{n}}, \quad E^{\top} E = I_{\bar{n}}, \quad E^{\top} \mathbb{J}_{2\bar{N}} E = 0_{\bar{n} \times \bar{n}}, \quad (3.1)$$

  (iii) V *is symplectic, and it holds* $V^{\top} = V^{+}$.

Proof. "(i) $\implies$ (ii)": Let $V \in \mathbb{R}^{2\bar{N} \times 2\bar{n}}$ be an orthosymplectic matrix, which we split in two blocks $E, F \in \mathbb{R}^{2\bar{N} \times \bar{n}}$ with $E = [e_1, \dots, e_{\bar{n}}]$ and $F = [f_1, \dots, f_{\bar{n}}]$ such that $V = [E \quad F]$. The condition of symplecticity of the matrix reads in terms of E and F and their columns for all $1 \leq i, j \leq \bar{n}$

$$V^{\top} \mathbb{J}_{2\bar{N}} V = \begin{bmatrix} E^{\top} \mathbb{J}_{2\bar{N}} E & E^{\top} \mathbb{J}_{2\bar{N}} F \\ F^{\top} \mathbb{J}_{2\bar{N}} E & F^{\top} \mathbb{J}_{2\bar{N}} F \end{bmatrix} = \mathbb{J}_{2\bar{n}} \iff \begin{array}{l} e_i^{\top} \mathbb{J}_{2\bar{N}} e_j = f_i^{\top} \mathbb{J}_{2\bar{N}} f_j = 0, \\ -f_i^{\top} \mathbb{J}_{2\bar{N}} e_j = e_i^{\top} \mathbb{J}_{2\bar{N}} f_j = \delta_{ij}. \end{array} \quad (3.2)$$

The orthonormality of the columns of V is characterized by

$$e_i^{\top} e_j = \delta_{ij}, \qquad\qquad f_i^{\top} f_j = \delta_{ij}.$$

For a fixed $i \in \{1, \dots, \bar{n}\}$, we can show with $\mathbb{J}_{2\bar{N}}^{\top} \mathbb{J}_{2\bar{N}} = I_{2\bar{N}}$ that $\mathbb{J}_{2\bar{N}} f_i$ is of unit length

$$1 = \delta_{ii} = f_i^{\top} f_i = f_i^{\top} \mathbb{J}_{2\bar{N}}^{\top} \mathbb{J}_{2\bar{N}} f_i = \| \mathbb{J}_{2\bar{N}} f_i \|_2^2.$$

Both vectors e_i and $\mathbb{J}_{2\bar{N}} f_i$ are of unit length while $1 \stackrel{(3.2)}{=} e_i^{\top} \mathbb{J}_{2\bar{N}} f_i$. In the Cauchy–Bunyakovsky–Schwarz inequality holds as an equality, $e_i^{\top} \mathbb{J}_{2\bar{N}} f_i = \| e_i \|_2 \| \mathbb{J}_{2\bar{N}} f_i \|_2$, if and only if the vectors are parallel or one vector is zero. With $e_i^{\top} \mathbb{J}_{2\bar{N}} f_i = 1$, we thus infer $e_i = \mathbb{J}_{2\bar{N}} f_i$, which is equivalent to $f_i = \mathbb{J}_{2\bar{N}}^{\top} e_i$. Since this holds for all $i \in \{1, \dots, \bar{n}\}$, we conclude that $F = \mathbb{J}_{2\bar{N}}^{\top} E$ and thus V is of the form proposed in (3.1).

  "(ii) $\implies$ (iii)": Let V be of the form (3.1). Direct calculation shows that V is symplectic

$$V^{\top} \mathbb{J}_{2\bar{N}} V = \begin{bmatrix} E^{\top} \mathbb{J}_{2\bar{N}} E & E^{\top} E \\ -E^{\top} E & E^{\top} \mathbb{J}_{2\bar{N}} E \end{bmatrix} \stackrel{(3.1)}{=} \begin{bmatrix} 0_{\bar{n} \times \bar{n}} & I_{\bar{n}} \\ -I_{\bar{n}} & 0_{\bar{n} \times \bar{n}} \end{bmatrix} = \mathbb{J}_{2\bar{n}}.$$

Thus, the symplectic inverse $\boldsymbol{V}^+$ exists. Moreover, direct calculation shows that it equals the transposed $\boldsymbol{V}^\top$

$$\boldsymbol{V}^+ = \mathbb{J}_{2\bar{n}}^\top \boldsymbol{V}^\top \mathbb{J}_{2\bar{N}} = \mathbb{J}_{2\bar{n}}^\top \begin{bmatrix} \boldsymbol{E}^\top \\ \boldsymbol{E}^\top \mathbb{J}_{2\bar{N}} \end{bmatrix} \mathbb{J}_{2\bar{N}} = \begin{bmatrix} -\boldsymbol{E}^\top \mathbb{J}_{2\bar{N}} \mathbb{J}_{2\bar{N}} \\ \boldsymbol{E}^\top \mathbb{J}_{2\bar{N}} \end{bmatrix} = \begin{bmatrix} \boldsymbol{E}^\top \\ \boldsymbol{E}^\top \mathbb{J}_{2\bar{N}} \end{bmatrix} = \boldsymbol{V}^\top.$$

"(iii) $\implies$ (i)": Let $\boldsymbol{V}$ be symplectic with $\boldsymbol{V}^+ = \boldsymbol{V}^\top$. Then, we can show that $\boldsymbol{V}$ has orthonormal columns with

$$\boldsymbol{I}_{\bar{n}} = \boldsymbol{V}^+ \boldsymbol{V} = \boldsymbol{V}^\top \boldsymbol{V}. \qquad\qquad \square$$

We proceed by showing that the classical symplectic basis generation techniques from Definition 2.51 and Remark 2.52 exclusively restrict to the class of orthosymplectic ROBs.

Lemma 3.3 (Orthosymplectic basis generation)**:** *The Cotangent Lift (CT), Complex SVD (cSVD) and the symplectic greedy procedure all determine an orthosymplectic ROB matrix since the ROB matrices of those methods can be rewritten as $\boldsymbol{V}_{\boldsymbol{E}} = [\boldsymbol{E} \quad \mathbb{J}_{2\bar{N}}^\top \boldsymbol{E}]$, with different choices for $\boldsymbol{E}$:*

$$\boldsymbol{E}_{\mathrm{CT}} = \begin{bmatrix} \boldsymbol{\Phi}_{\mathrm{CT}} \\ \boldsymbol{0}_{\bar{N}\times\bar{n}} \end{bmatrix} \qquad \boldsymbol{E}_{\mathrm{cSVD}} = \begin{bmatrix} \boldsymbol{\Phi}_{\mathrm{cSVD}} \\ \boldsymbol{\Psi}_{\mathrm{cSVD}} \end{bmatrix}, \qquad \boldsymbol{E}_{\mathrm{greedy}} = [\boldsymbol{z}_1, \dots, \boldsymbol{z}_{\bar{n}}],$$

where

(i) $\boldsymbol{\Phi}_{\mathrm{CT}}, \boldsymbol{\Phi}_{\mathrm{cSVD}}, \boldsymbol{\Psi}_{\mathrm{cSVD}} \in \mathbb{R}^{\bar{N}\times\bar{n}}$ are matrices that fulfil

$$\boldsymbol{\Phi}_{\mathrm{CT}}^\top \boldsymbol{\Phi}_{\mathrm{CT}} = \boldsymbol{I}_{\bar{n}}, \quad \boldsymbol{\Phi}_{\mathrm{cSVD}}^\top \boldsymbol{\Phi}_{\mathrm{cSVD}} + \boldsymbol{\Psi}_{\mathrm{cSVD}}^\top \boldsymbol{\Psi}_{\mathrm{cSVD}} = \boldsymbol{I}_{\bar{n}}, \quad \boldsymbol{\Phi}_{\mathrm{cSVD}}^\top \boldsymbol{\Psi}_{\mathrm{cSVD}} = \boldsymbol{\Psi}_{\mathrm{cSVD}}^\top \boldsymbol{\Phi}_{\mathrm{cSVD}},$$

which is equivalent to $\boldsymbol{E}^\top \boldsymbol{E} = \boldsymbol{I}_{\bar{n}}$ and $\boldsymbol{E}^\top \mathbb{J}_{2\bar{N}} \boldsymbol{E} = \boldsymbol{0}_{\bar{n}\times\bar{n}}$ for $\boldsymbol{E}_{\mathrm{CT}}$ and $\boldsymbol{E}_{\mathrm{cSVD}}$,

(ii) $\boldsymbol{z}_1, \dots, \boldsymbol{z}_{\bar{n}} \in \mathbb{R}^{2\bar{N}}$ are the basis vectors selected by the greedy algorithm.

Proof. All the listed methods determine a symplectic ROB of the form $\boldsymbol{V}_{\boldsymbol{E}} = [\boldsymbol{E} \quad \mathbb{J}_{2\bar{N}}^\top \boldsymbol{E}]$ which satisfies (3.1) with the respective $\boldsymbol{E}$ from the list above. By Lemma 3.2, these ROBs are all orthosymplectic. $\qquad\square$

Remark 3.4 (Optimal orthosymplectic ROB)**:** *It can be shown that the PSD complex SVD computes an optimal solution of the PSD in the set of orthosymplectic ROBs (see [20, 99]).*

From the perspective of classical MOR, the restriction to an orthonormal basis is not restricting since we can find an orthonormal basis for every subspace $\tilde{\mathbb{V}} \subset \mathbb{V}$. For a symplectic subspace however this is not true as the following lemma shows.

Lemma 3.5 (Orthonormalizing a symplectic basis): *Consider the symplectic vector space* $(\mathbb{V}, \omega)$ *and inner product* g. *For a symplectic subspace* $\tilde{\mathbb{V}} \subset \mathbb{V}$ *(characterized by a reduced space* $\check{\mathbb{V}}$ *and a symplectic embedding* $V \in L(\check{\mathbb{V}}; \mathbb{V})$*) with a canonical basis* $\{e_i, f_i\}_{i=1}^{\bar{n}}$, *we can in general not find a change of basis for* $\check{\mathbb{V}}$ *to obtain an orthosymplectic basis.*

Proof. It holds $\boldsymbol{V}^\top \mathbb{J}_{2\bar{N}}^\top \boldsymbol{V} = \mathbb{J}_{2\bar{n}}^\top$ due to canonical symplecticity of the basis. Assume there exists a change-of-basis matrix $\boldsymbol{B} \in \mathbb{R}^{2\bar{n} \times 2\bar{n}}$ such that $\hat{\boldsymbol{V}} = \boldsymbol{V}\boldsymbol{B}$ is orthosymplectic, i.e.

$$\mathbb{J}_{2\bar{n}}^\top = \hat{\boldsymbol{V}}^\top \mathbb{J}_{2\bar{N}}^\top \hat{\boldsymbol{V}} = \boldsymbol{B}^\top \underbrace{\boldsymbol{V}^\top \mathbb{J}_{2\bar{N}}^\top \boldsymbol{V}}_{=\mathbb{J}_{2\bar{n}}^\top} \boldsymbol{B} = \boldsymbol{B}^\top \mathbb{J}_{2\bar{n}}^\top \boldsymbol{B}, \tag{3.3}$$

$$\boldsymbol{I}_{2\bar{n}} = \hat{\boldsymbol{V}}^\top g \hat{\boldsymbol{V}} = \boldsymbol{B}^\top \boldsymbol{V}^\top g \boldsymbol{V} \boldsymbol{B}. \tag{3.4}$$

The first equation shows that the change-of-basis matrix $\boldsymbol{B}$ is necessarily symplectic. With $\det\left(\mathbb{J}_{2\bar{n}}^\top\right) = 1$, we conclude

$$1 = \det\left(\mathbb{J}_{2\bar{n}}^\top\right) \overset{(3.3)}{=} \det\left(\boldsymbol{B}^\top \mathbb{J}_{2\bar{n}}^\top \boldsymbol{B}\right) = \det\left(\boldsymbol{B}^\top\right) \underbrace{\det\left(\mathbb{J}_{2\bar{n}}^\top\right)}_{=1} \det\left(\boldsymbol{B}\right) = \det\left(\boldsymbol{B}^\top\right) \det\left(\boldsymbol{B}\right)$$

and thus

$$1 = \det(\boldsymbol{I}_{2\bar{n}}) \overset{(3.4)}{=} \det(\boldsymbol{B}^\top \boldsymbol{V}^\top g \boldsymbol{V} \boldsymbol{B}) = \underbrace{\det(\boldsymbol{B}^\top)\det(\boldsymbol{B})}_{=1} \det(\boldsymbol{V}^\top g \boldsymbol{V}) = \det(\boldsymbol{V}^\top g \boldsymbol{V}).$$

However, we can find a symplectic basis with $\det(\boldsymbol{V}^\top g \boldsymbol{V}) \neq 1$, e.g. for $g = \boldsymbol{I}_{2\bar{N}}, \gamma \in \mathbb{R} \setminus 0$

$$\boldsymbol{V} = \begin{bmatrix} 1 & 0 \\ 0 & 0 \\ 0 & 1 \\ 0 & \gamma \end{bmatrix}, \quad \boldsymbol{V}^\top \boldsymbol{V} = \begin{bmatrix} 1 & 0 \\ 0 & 1 + \gamma^2 \end{bmatrix}, \quad \det\left(\boldsymbol{V}^\top \boldsymbol{V}\right) = 1 + \gamma^2 \neq 1.$$

This is a contradiction and thus not every symplectic basis is orthonormalizable. $\square$

3.2 Symplectic, Non-Orthonormal Basis Generation

Essentially, Lemma 3.2 limits an orthosymplectic ROB matrix $\boldsymbol{V}$ to be of the form (3.1) which leaves only half of the basis for optimization in the PSD functional. This sparks the research question, if there are basis generation techniques which are able to generate symplectic, non-orthonormal ROBs. We refer to such techniques as a *symplectic, non-orthonormal basis generation technique*. In the present section, we present a new non-orthonormal basis generation technique that is based on the SVD-like decomposition from [117]. Firstly, we reproduce this decomposition from [117]. Secondly, we present theoretical results which link the value of the PSD functional with the "singular values" of the SVD-like decomposition, which we call symplectic singular values.

Theorem 3.6 (SVD-like decomposition [117])**:** *Each real matrix $\boldsymbol{B} \in \mathbb{R}^{2\bar{N} \times l}$ can be decomposed as the product $\boldsymbol{B} = \boldsymbol{S}\boldsymbol{D}\boldsymbol{Q}$ of a symplectic matrix $\boldsymbol{S} \in \mathbb{R}^{2\bar{N} \times 2\bar{N}}$, a sparse (potentially non-diagonal) matrix $\boldsymbol{D} \in \mathbb{R}^{2\bar{N} \times l}$ and an orthogonal matrix $\boldsymbol{Q} \in \mathbb{R}^{l \times l}$ with*

$$
\boldsymbol{D} = \begin{array}{c} \\ \end{array} \begin{array}{cccc} {\scriptstyle p} & {\scriptstyle q} & {\scriptstyle p} & {\scriptstyle l-2p-q} \\ \left[\begin{array}{cccc} \boldsymbol{\Sigma}_\mathrm{s} & \boldsymbol{0} & \boldsymbol{0} & \boldsymbol{0} \\ \boldsymbol{0} & \boldsymbol{I} & \boldsymbol{0} & \boldsymbol{0} \\ \boldsymbol{0} & \boldsymbol{0} & \boldsymbol{0} & \boldsymbol{0} \\ \boldsymbol{0} & \boldsymbol{0} & \boldsymbol{\Sigma}_\mathrm{s} & \boldsymbol{0} \\ \boldsymbol{0} & \boldsymbol{0} & \boldsymbol{0} & \boldsymbol{0} \\ \boldsymbol{0} & \boldsymbol{0} & \boldsymbol{0} & \boldsymbol{0} \end{array}\right] & \begin{array}{c} {\scriptstyle p} \\ {\scriptstyle q} \\ {\scriptstyle \bar{N}-p-q} \\ {\scriptstyle p} \\ {\scriptstyle q} \\ {\scriptstyle \bar{N}-p-q} \end{array} \end{array} , \qquad \begin{array}{c} \boldsymbol{\Sigma}_\mathrm{s} = \mathrm{diag}(\sigma_1^\mathrm{s}, \dots, \sigma_p^\mathrm{s}) \in \mathbb{R}^{p \times p}, \\ \sigma_i^\mathrm{s} > 0 \quad \text{for } 1 \le i \le p, \end{array} \tag{3.5}
$$

with $p, q \in \mathbb{N}$ and $\mathrm{rank}(\boldsymbol{B}) = 2p + q$, where the dimensions of the blocks in $\boldsymbol{D}$ are denoted by small letters. This decomposition is referred to as SVD-like decomposition. We call the diagonal entries $\sigma_i^\mathrm{s}, 1 \le i \le p$, of the matrix $\boldsymbol{\Sigma}_\mathrm{s}$ symplectic singular values.

The idea is to define a symplectic basis generation technique based on the SVD-like decomposition of the snapshot matrix by selecting $\bar{n} \in \mathbb{N}$ pairs of columns of $\boldsymbol{S}$ to obtain a symplectic ROB matrix $\boldsymbol{V} \in \mathbb{R}^{2\bar{N} \times 2\bar{n}}$. In order to decide which columns should be selected, the following lemma links so-called weighted symplectic singular values to the Frobenius norm of a matrix.

Proposition 3.7: *Let $\boldsymbol{B} \in \mathbb{R}^{2\bar{N} \times l}$ with an SVD-like decomposition $\boldsymbol{B} = \boldsymbol{S}\boldsymbol{D}\boldsymbol{Q}$ with $p, q \in \mathbb{N}$ from Theorem 3.6. The Frobenius norm of $\boldsymbol{B}$ can be rewritten as*

$$\|\boldsymbol{B}\|_{\mathrm{F}}^2 = \sum_{i=1}^{p+q}(w_i^{\mathrm{s}})^2, \qquad w_i^{\mathrm{s}} := \begin{cases} \sigma_i^{\mathrm{s}}\sqrt{\|\boldsymbol{s}_i\|_2^2 + \|\boldsymbol{s}_{\bar{N}+i}\|_2^2}, & 1 \le i \le p, \\ \|\boldsymbol{s}_i\|_2, & p+1 \le i \le p+q, \end{cases} \tag{3.6}$$

where $\boldsymbol{s}_i \in \mathbb{R}^{2\bar{N}}$ is the i-th column of $\boldsymbol{S}$ for $1 \le i \le 2\bar{N}$. In the following, we refer to $\{w_i^{\mathrm{s}}\}_{1 \le i \le p+q}$ as the weighted symplectic singular values.

Proof. With the SVD-like decomposition $\boldsymbol{B} = \boldsymbol{S}\boldsymbol{D}\boldsymbol{Q}$, the Frobenius norm reads

$$\begin{aligned}
\|\boldsymbol{B}\|_{\mathrm{F}}^2 = \|\boldsymbol{S}\boldsymbol{D}\boldsymbol{Q}\|_{\mathrm{F}}^2 &= \|\boldsymbol{S}\boldsymbol{D}\|_{\mathrm{F}}^2 = \operatorname{trace}(\boldsymbol{D}^\top \boldsymbol{S}^\top \boldsymbol{S}\boldsymbol{D}) \\
&= \sum_{i=1}^{p}(\sigma_i^{\mathrm{s}})^2 \boldsymbol{s}_i^\top \boldsymbol{s}_i + \sum_{i=1}^{q}\boldsymbol{s}_{p+i}^\top \boldsymbol{s}_{p+i} + \sum_{i=1}^{p}(\sigma_i^{\mathrm{s}})^2 \boldsymbol{s}_{\bar{N}+i}^\top \boldsymbol{s}_{\bar{N}+i} \\
&= \sum_{i=1}^{p}(\sigma_i^{\mathrm{s}})^2 \left(\|\boldsymbol{s}_i\|_2^2 + \|\boldsymbol{s}_{\bar{N}+i}\|_2^2\right) + \sum_{i=1}^{q}\|\boldsymbol{s}_{p+i}\|_2^2,
\end{aligned}$$

where we use that $\boldsymbol{Q}$ is orthogonal. $\qquad\square$

Definition 3.8 (PSD SVD-like decomposition)**:** *For a given snapshot matrix $\boldsymbol{X}_{\mathrm{s}} \in \mathbb{R}^{2\bar{N} \times n_{\mathrm{s}}}$, consider an SVD-like decomposition $\boldsymbol{X}_{\mathrm{s}} = \boldsymbol{S}\boldsymbol{D}\boldsymbol{Q}$ with $p, q \in \mathbb{N}$ as in Theorem 3.6. The PSD SVD-like decomposition chooses the ROB matrix*

$$\boldsymbol{V} = [\boldsymbol{s}_{i_1}, \dots, \boldsymbol{s}_{i_{\bar{n}}}, \boldsymbol{s}_{\bar{N}+i_1}, \dots, \boldsymbol{s}_{\bar{N}+i_{\bar{n}}}] \in \mathbb{R}^{2\bar{N} \times 2\bar{n}}$$

to stack the $\bar{n}$ pairs of columns of $\boldsymbol{S} = [\boldsymbol{s}_1, \dots \boldsymbol{s}_{2\bar{N}}]$ based on $\bar{n}$ indices

$$\mathcal{I}_{\mathrm{PSD}} := \{i_1, \dots, i_{\bar{n}}\} := \operatorname*{argmax}_{\substack{\mathcal{I} \subset \{1, \dots, p+q\} \\ |\mathcal{I}| = \bar{n}}} \left(\sum_{i \in \mathcal{I}}(w_i^{\mathrm{s}})^2\right) \tag{3.7}$$

with the largest weighted symplectic singular values w_i^{s} from (3.6).

The specific choice of the ROB matrix in the PSD SVD-like decomposition is motivated by the following lemma which is very analogous to the result in Remark 2.21 known for the classical POD in the framework of orthogonal projections.

Theorem 3.9 (PSD functional): *Let $\boldsymbol{V} \in \mathbb{R}^{2\bar{N} \times 2\bar{n}}$ be an ROB matrix constructed with the PSD SVD-like decomposition with the index set $\mathcal{I}_{\text{PSD}} \subset \{1, \dots, p+q\}$. Then, the PSD functional*

$$\left\|(\boldsymbol{I}_{2\bar{N}} - \boldsymbol{V}\boldsymbol{V}^+)\boldsymbol{X}_{\text{s}}\right\|_{\text{F}}^2 = \sum_{i \in \{1,\dots,p+q\}\setminus\mathcal{I}_{\text{PSD}}} (w_i^{\text{s}})^2, \tag{3.8}$$

equals the cumulative sum of the squares of the neglected weighted symplectic singular values.

Proof. For a snapshot matrix $\boldsymbol{X}_{\text{s}} \in \mathbb{R}^{2\bar{N} \times n_{\text{s}}}$ with an SVD-like decomposition $\boldsymbol{X}_{\text{s}} = \boldsymbol{SDQ}$, let $\boldsymbol{V} \in \mathbb{R}^{2\bar{N} \times 2\bar{n}}$ be an ROB matrix from the PSD SVD-like decomposition with the index set $\mathcal{I}_{\text{PSD}} = \{i_1, \dots, i_{\bar{n}}\} \subset \{1, \dots, p+q\}$ from (3.7). For a cleaner notation, we define two selection matrices $\boldsymbol{I}_{\mathcal{I}_{\text{PSD}}} \in \mathbb{R}^{2\bar{N} \times \bar{n}}$, $\boldsymbol{I}_{\mathcal{I}_{\text{PSD}}^{2\bar{n}}} \in \mathbb{R}^{2\bar{N} \times 2\bar{n}}$ such that for $1 \le \alpha \le 2\bar{N}, 1 \le \beta \le \bar{n}$,

$$\left(\boldsymbol{I}_{\mathcal{I}_{\text{PSD}}}\right)_{\alpha,\beta} := \begin{cases} 1, & \alpha = i_\beta \in \mathcal{I}_{\text{PSD}}, \\ 0, & \text{else}, \end{cases} \qquad \boldsymbol{I}_{\mathcal{I}_{\text{PSD}}^{2\bar{n}}} := [\boldsymbol{I}_{\mathcal{I}_{\text{PSD}}}, \ \mathbb{J}_{2\bar{N}}^\top \boldsymbol{I}_{\mathcal{I}_{\text{PSD}}}],$$

which allows writing the ROB matrix with $\boldsymbol{V} = \boldsymbol{S}\boldsymbol{I}_{\mathcal{I}_{\text{PSD}}^{2\bar{n}}}$. Moreover, it holds

$$\boldsymbol{I}_{\mathcal{I}_{\text{PSD}}^{2\bar{n}}}^+ = \mathbb{J}_{2\bar{n}}^\top \boldsymbol{I}_{\mathcal{I}_{\text{PSD}}^{2\bar{n}}}^\top \mathbb{J}_{2\bar{N}} = \mathbb{J}_{2\bar{n}}^\top \begin{bmatrix} \boldsymbol{I}_{\mathcal{I}_{\text{PSD}}}^\top \\ \boldsymbol{I}_{\mathcal{I}_{\text{PSD}}}^\top \mathbb{J}_{2\bar{N}} \end{bmatrix} \mathbb{J}_{2\bar{N}} = \begin{bmatrix} \boldsymbol{0}_{\bar{n}\times\bar{n}} & -\boldsymbol{I}_{\bar{n}} \\ \boldsymbol{I}_{\bar{n}} & \boldsymbol{0}_{\bar{n}\times\bar{n}} \end{bmatrix} \begin{bmatrix} \boldsymbol{I}_{\mathcal{I}_{\text{PSD}}}^\top \mathbb{J}_{2\bar{N}} \\ -\boldsymbol{I}_{\mathcal{I}_{\text{PSD}}}^\top \end{bmatrix} = \boldsymbol{I}_{\mathcal{I}_{\text{PSD}}^{2\bar{n}}}^\top.$$

Using the orthogonality of $\boldsymbol{Q}$, symplecticity of $\boldsymbol{S}$, the weighted symplectic singular values w_i^{s} from (3.6), and, in the last step, that the term in the braces sets all rows of $\boldsymbol{D}$ with indices i and $\bar{N} + i$ to zero for all $i \in \mathcal{I}_{\text{PSD}}$, the PSD functional reads

$$\left\|(\boldsymbol{I}_{2\bar{N}} - \boldsymbol{V}\boldsymbol{V}^+)\boldsymbol{X}_{\text{s}}\right\|_{\text{F}}^2 = \left\|(\boldsymbol{I}_{2\bar{N}} - \boldsymbol{S}\boldsymbol{I}_{\mathcal{I}_{\text{PSD}}^{2\bar{n}}} \mathbb{J}_{2\bar{n}}^\top \boldsymbol{I}_{\mathcal{I}_{\text{PSD}}^{2\bar{n}}}^\top \boldsymbol{S}^\top \mathbb{J}_{2\bar{N}})\boldsymbol{SDQ}\right\|_{\text{F}}^2$$

$$= \left\|\boldsymbol{S}(\boldsymbol{I}_{2\bar{N}} - \boldsymbol{I}_{\mathcal{I}_{\text{PSD}}^{2\bar{n}}} \underbrace{\mathbb{J}_{2\bar{n}}^\top \boldsymbol{I}_{\mathcal{I}_{\text{PSD}}^{2\bar{n}}}^\top \overbrace{\boldsymbol{S}^\top \mathbb{J}_{2\bar{N}} \boldsymbol{S}}^{=\mathbb{J}_{2\bar{N}}})\boldsymbol{D}\right\|_{\text{F}}^2}_{=\boldsymbol{I}_{\mathcal{I}_{\text{PSD}}^{2\bar{n}}}^+ = \boldsymbol{I}_{\mathcal{I}_{\text{PSD}}^{2\bar{n}}}^\top}$$

$$= \left\|\boldsymbol{S}\left(\boldsymbol{I}_{2\bar{N}} - \boldsymbol{I}_{\mathcal{I}_{\text{PSD}}^{2\bar{n}}} \boldsymbol{I}_{\mathcal{I}_{\text{PSD}}^{2\bar{n}}}^\top\right)\boldsymbol{D}\right\|_{\text{F}}^2 = \sum_{i \in \{1,\dots,p+q\}\setminus\mathcal{I}_{\text{PSD}}} (w_i^{\text{s}})^2. \qquad \square$$

The computational steps of the new method are concluded in Algorithm 3.1, which is in the notation of MATLAB®. The function $[\boldsymbol{S}, \boldsymbol{D}, \boldsymbol{Q}, p, q] = \text{SVD\_like\_decomp}(\boldsymbol{X}_{\text{s}})$ computes an SVD-like decomposition (3.5), while the unused matrix $\boldsymbol{Q}$ is replaced with $\sim$.

> **Algorithm 3.1: PSD SVD-like decomposition in MATLAB® notation.**[1]
>
> **Input:** Snapshot matrix $\boldsymbol{X}_\mathrm{s} \in \mathbb{R}^{2\bar{N} \times n_\mathrm{s}}$, size $2\bar{n}$ of the ROB
> **Output:** Symplectic ROB matrix $\boldsymbol{V} \in \mathbb{R}^{2\bar{N} \times 2\bar{n}}$
> 1 $[\boldsymbol{S}, \boldsymbol{D}, \sim, p, q] \leftarrow \texttt{SVD\_like\_decomp}(\boldsymbol{X}_\mathrm{s})$ ▷ compute SVD-like decomposition
> 2 $\boldsymbol{\sigma}^\mathrm{s} \leftarrow \texttt{diag}(\boldsymbol{D}(1:p,\ 1:p))$ ▷ extract symplectic singular values
> 3 $\boldsymbol{r} \leftarrow \texttt{sum}(\texttt{power}(\boldsymbol{S},\ 2),\ 1)$ ▷ squares of the 2-norm of each column of $\boldsymbol{S}$
> 4 $\boldsymbol{w}^\mathrm{s} \leftarrow \texttt{times}(\boldsymbol{\sigma}^\mathrm{s},\ \texttt{sqrt}(\boldsymbol{r}(1:p) + \boldsymbol{r}(\bar{N} + (1:p))))$ ▷ $w_1^\mathrm{s}, \dots, w_p^\mathrm{s}$
> 5 $\boldsymbol{w}^\mathrm{s} \leftarrow [\boldsymbol{w}^\mathrm{s},\ \boldsymbol{r}(p + (1:q))]$ ▷ append w. sympl. sing. val. $w_{p+1}^\mathrm{s}, \dots, w_{p+q}^\mathrm{s}$
> 6 $[\sim, \mathcal{I}_\mathrm{PSD}] \leftarrow \texttt{maxk}(\boldsymbol{w}^\mathrm{s},\ \bar{n})$ ▷ find indices of $\bar{n}$ highest w. sympl. sing. val.
> 7 $\boldsymbol{V} \leftarrow \boldsymbol{S}(:, [\mathcal{I}_\mathrm{PSD}, \bar{N} + \mathcal{I}_\mathrm{PSD}])$ ▷ select columns with indices $\mathcal{I}_\mathrm{PSD}$ and $\bar{N} + \mathcal{I}_\mathrm{PSD}$

Remark 3.10 (Computation of SVD-like decomposition): *The literature offers multiple methods to compute an SVD-like decomposition of $\boldsymbol{B}$: In [117], a factorization of $\boldsymbol{B}^\top \mathbb{J}_{2\bar{N}} \boldsymbol{B}$ is used, in [116] an implicit version is formulated which avoids the computation of the full product $\boldsymbol{B}^\top \mathbb{J}_{2\bar{N}} \boldsymbol{B}$, and [2] is based on a block-power iterative method. Here, we use the implicit approach [116].*

3.2.1 Interplay of Non-Orthonormal and Orthonormal ROBs

To compare the PSD SVD-like decomposition with the orthosymplectic basis generation techniques, we present two bounds on the respective PSD functional. In both cases, we require the basis size to satisfy $\bar{n} \leq \bar{N}$ or $2\bar{n} \leq \bar{N}$, respectively. This restriction is not limiting in the context of symplectic MOR as in all application cases $\bar{n} \ll \bar{N}$. The fundamental theorem in these bounds is the Orthogonal SR decomposition, which is introduced first.

Theorem 3.11 (Orthogonal SR decomposition e.g. [27, 117]): *For each matrix $\boldsymbol{B} \in \mathbb{R}^{2\bar{N} \times l}$ with $l \leq \bar{N}$, there exists an orthosymplectic matrix $\boldsymbol{S}_\mathrm{SR} \in \mathbb{R}^{2\bar{N} \times 2\bar{N}}$, an upper triangular matrix $\boldsymbol{R}_{11} \in \mathbb{R}^{l \times l}$ and a strictly upper triangular matrix $\boldsymbol{R}_{21} \in \mathbb{R}^{l \times l}$ which characterize the orthogonal SR decomposition*

$$
\boldsymbol{B} = \boldsymbol{S}_\mathrm{SR} \begin{bmatrix} \boldsymbol{R}_{11} \\ \boldsymbol{0}_{(\bar{N}-l) \times l} \\ \boldsymbol{R}_{21} \\ \boldsymbol{0}_{(\bar{N}-l) \times l} \end{bmatrix} = [\boldsymbol{S}_l \quad \mathbb{J}_{2\bar{N}}^\top \boldsymbol{S}_l] \begin{bmatrix} \boldsymbol{R}_{11} \\ \boldsymbol{R}_{21} \end{bmatrix}, \qquad \begin{aligned} \boldsymbol{S}_\mathrm{SR} &= [\boldsymbol{s}_1, \dots, \boldsymbol{s}_{\bar{N}}, \mathbb{J}_{2\bar{N}}^\top \boldsymbol{s}_1, \dots, \mathbb{J}_{2\bar{N}}^\top \boldsymbol{s}_{\bar{N}}], \\ \boldsymbol{S}_l &= [\boldsymbol{s}_1, \dots, \boldsymbol{s}_l]. \end{aligned}
$$

---

[1]The algorithm is adapted from [20].

The first bound relates an orthosymplectic basis with the POD by proving that there exists an orthosymplectic basis which requires at most twice the number of basis vectors to obtain an orthogonal projection error smaller or equal to the classical POD. A similar result has been presented in [100, Prop. 3.11]. In comparison, we are able to improve it by a factor of $1/2$.

Proposition 3.12 (Estimate POD with orthosymplectic PSD): *Let $\boldsymbol{V} \in \mathbb{R}^{2\bar{N} \times \bar{n}}$ be a minimizer of POD with $\bar{n} \leq \bar{N}$ basis vectors and let $\boldsymbol{V_E} \in \mathbb{R}^{2\bar{N} \times 2\bar{n}}$ be a minimizer of the PSD in the class of orthosymplectic ROBs with $2\bar{n}$ basis vectors, i.e. twice as many basis vectors as $\boldsymbol{V}$. Then, the orthogonal projection errors of $\boldsymbol{V_E}$ and $\boldsymbol{V}$ satisfy*

$$\left\|(\boldsymbol{I}_{2\bar{N}} - \boldsymbol{V_E}\boldsymbol{V_E}^{\top})\boldsymbol{X}_{\mathrm{s}}\right\|_{\mathrm{F}}^2 \leq \left\|(\boldsymbol{I}_{2\bar{N}} - \boldsymbol{V}\boldsymbol{V}^{\top})\boldsymbol{X}_{\mathrm{s}}\right\|_{\mathrm{F}}^2 .$$

Proof. Let $\boldsymbol{V} \in \mathbb{R}^{2\bar{N} \times \bar{n}}$ be a minimizer of POD and $\boldsymbol{V} = \boldsymbol{S}_{\mathrm{SR},\bar{n}}\boldsymbol{R}_{\mathrm{SR}}$ an SR decomposition of it with $\boldsymbol{S}_{\mathrm{SR},\bar{n}} := [\boldsymbol{S}_{\bar{n}}, \mathbb{J}_{2\bar{N}}^{\top}\boldsymbol{S}_{\bar{n}}] \in \mathbb{R}^{2\bar{N} \times 2\bar{n}}$ and $\boldsymbol{R}_{\mathrm{SR}} := \left([\boldsymbol{R}_{11}^{\top}, \boldsymbol{R}_{21}^{\top}]\right)^{\top} \in \mathbb{R}^{2\bar{n} \times \bar{n}}$. Since both matrices $\boldsymbol{V}$ and $\boldsymbol{S}_{\mathrm{SR},\bar{n}}$ have orthonormal columns and $\mathrm{colspan}(\boldsymbol{V}) \subset \mathrm{colspan}(\boldsymbol{S}_{\mathrm{SR},\bar{n}})$, we can show that $\boldsymbol{S}_{\mathrm{SR},\bar{n}}$ yields a lower orthogonal projection error than $\boldsymbol{V}$ with

$$\begin{aligned}
\left\|\left(\boldsymbol{I}_{2\bar{N}} - \boldsymbol{S}_{\mathrm{SR},\bar{n}}\boldsymbol{S}_{\mathrm{SR},\bar{n}}^{\top}\right)\boldsymbol{X}_{\mathrm{s}}\right\|_{\mathrm{F}}^2 &= \left\|\left(\boldsymbol{I}_{2\bar{N}} - \boldsymbol{S}_{\mathrm{SR},\bar{n}}\boldsymbol{S}_{\mathrm{SR},\bar{n}}^{\top}\right)\left(\boldsymbol{I}_{2\bar{N}} - \boldsymbol{V}\boldsymbol{V}^{\top}\right)\boldsymbol{X}_{\mathrm{s}}\right\|_{\mathrm{F}}^2 \\
&\leq \underbrace{\left\|\boldsymbol{I}_{2\bar{N}} - \boldsymbol{S}_{\mathrm{SR},\bar{n}}\boldsymbol{S}_{\mathrm{SR},\bar{n}}^{\top}\right\|_2^2}_{\leq 1} \left\|\left(\boldsymbol{I}_{2\bar{N}} - \boldsymbol{V}\boldsymbol{V}^{\top}\right)\boldsymbol{X}_{\mathrm{s}}\right\|_{\mathrm{F}}^2 \\
&\leq \left\|\left(\boldsymbol{I}_{2\bar{N}} - \boldsymbol{V}\boldsymbol{V}^{\top}\right)\boldsymbol{X}_{\mathrm{s}}\right\|_{\mathrm{F}}^2 .
\end{aligned}$$

Let $\boldsymbol{V_E} \in \mathbb{R}^{2\bar{N} \times 2\bar{n}}$ be a minimizer of the PSD in the class of orthosymplectic ROBs. Since both ROBs are orthosymplectic and $\boldsymbol{V_E}$ is assumed to be optimal, it yields a lower projection error than $\boldsymbol{S}_{\mathrm{SR},\bar{n}}$ and thus

$$\left\|\left(\boldsymbol{I}_{2\bar{N}} - \boldsymbol{V}\boldsymbol{V}^{\top}\right)\boldsymbol{X}_{\mathrm{s}}\right\|_{\mathrm{F}}^2 \geq \left\|\left(\boldsymbol{I}_{2\bar{N}} - \boldsymbol{S}_{\mathrm{SR},\bar{n}}\boldsymbol{S}_{\mathrm{SR},\bar{n}}^{\top}\right)\boldsymbol{X}_{\mathrm{s}}\right\|_{\mathrm{F}}^2 \geq \left\|\left(\boldsymbol{I}_{2\bar{N}} - \boldsymbol{V_E}\boldsymbol{V_E}^{\top}\right)\boldsymbol{X}_{\mathrm{s}}\right\|_{\mathrm{F}}^2 . \qquad \square$$

The second bound shows that for a given (potentially non-orthonormal) minimizer of PSD, an orthosymplectic ROB requires at most twice the number of basis vectors to achieve the same or lower symplectic projection error.

Proposition 3.13 (Estimate PSD with orthosymplectic PSD): *We assume that there exists a minimizer $\boldsymbol{V} \in \mathbb{R}^{2\bar{N} \times 2\bar{n}}$ of the PSD for a basis size $2\bar{n} \leq \bar{N}$ with potentially non-orthonormal columns. Let $\boldsymbol{V_E} \in \mathbb{R}^{2\bar{N} \times 4\bar{n}}$ be a minimizer of the PSD in the class of orthosymplectic bases of*

size $4\bar{n}$, i.e. twice as many basis vectors as $\boldsymbol{V}$. Then, we know that the symplectic projection error of $\boldsymbol{V_E}$ is less than or equal to the one of $\boldsymbol{V}$, i.e.

$$\left\|(\boldsymbol{I}_{2\bar{N}} - \boldsymbol{V_E}\boldsymbol{V_E^+})\boldsymbol{X}_{\mathrm{s}}\right\|_{\mathrm{F}}^2 \leq \left\|(\boldsymbol{I}_{2\bar{N}} - \boldsymbol{V}\boldsymbol{V^+})\boldsymbol{X}_{\mathrm{s}}\right\|_{\mathrm{F}}^2 .$$

Proof. The proof works analogously to Proposition 3.12.   □

3.3 Numerical Experiments

The numerical experiment investigates the performance of different (structure-preserving) MOR techniques for a parametric Hamiltonian equation obtained from semi-discretization of a PDE for linear elastodynamics.

3.3.1 Full-Order Model

Linear elasticity, in general, can be described by a Lamé–Navier equation (sometimes also described as Navier–Cauchy equation)

$$\rho_0 \frac{\partial^2}{\partial^2 t^2} q(\xi, t, \boldsymbol{\mu}) - \mu_{\mathrm{L}} \, \varDelta_\xi q(\xi, t, \boldsymbol{\mu}) + (\lambda_{\mathrm{L}} + \mu_{\mathrm{L}})\nabla_\xi \left(\mathrm{div}_\xi \left(q(\xi, t, \boldsymbol{\mu})\right)\right) = \rho_0 \, g(\xi, t)$$

complemented by appropriate boundary conditions, where $\xi \in \varOmega$ denotes the spatial variable in the domain $\varOmega \subset \mathbb{R}^2$, $t \in [t_0, t_{\mathrm{end}}]$ the time, $\rho_0 \in \mathbb{R}_{>0}$ the density, $\boldsymbol{\mu} = (\lambda_{\mathrm{L}}, \mu_{\mathrm{L}}) \in \mathbb{R}_{>0}^2$ the so-called Lamé parameters, ∇_ξ the gradient, $\varDelta_\xi$ the Laplacian, div_ξ the divergence, and $g : \varOmega \times [t_0, t_{\mathrm{end}}] \to \mathbb{R}^2$ an external body force. We use non-dimensionalization (see e.g. [72, Cha. 4.1], [18, Sec. 2.2 and 5.1.3]) to obtain a dimensionless formulation. Without external body forces, i.e. $g(\xi, t) = \boldsymbol{0}_{2\times 1}$, the system can be understood as a parametric Hamiltonian PDE [85, Ex. 3.2] with

$$\partial_t q(t, \xi; \mu) = \left(\frac{\delta \mathscr{H}_{\mathrm{PDE}}}{\delta p}[q, p; \mu]\right)(t, \xi; \mu),$$

$$\partial_t p(t, \xi; \mu) = -\left(\frac{\delta \mathscr{H}_{\mathrm{PDE}}}{\delta q}[q, p; \mu]\right)(t, \xi; \mu),$$

$$\mathscr{H}_{\mathrm{PDE}}[q, p; \boldsymbol{\mu}] = \frac{1}{2}\int_\varOmega \rho_0 \|p\|_2^2 + \langle \sigma[q; \boldsymbol{\mu}], \, \varepsilon[q]\rangle_{\mathrm{F}} \, \mathrm{d}\xi,$$
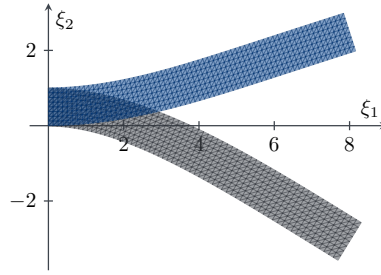
Figure 3.1: The beam model with exaggerated displacements at the time with maximum displacement (gray) and at the final time t_{end} (blue). This figure is taken from [20].

with the stress and the strain tensor

$$\sigma[q; \boldsymbol{\mu}] = \lambda_{\mathrm{L}} \operatorname{trace}\left(\varepsilon[q]\right) \boldsymbol{I}_2 + 2\mu_{\mathrm{L}}\varepsilon[q] \in \mathbb{R}^{2 \times 2}, \quad \varepsilon[q] = \frac{1}{2}\left(\nabla_\xi q + \left(\nabla_\xi q\right)^\top\right) \in \mathbb{R}^{2 \times 2}.$$

In particular, we model a cantilever beam clamped on the left side with a time-dependent force applied to the right boundary (see Figure 3.1) by choosing a rectangular domain Ω together with zero Dirichlet boundary conditions on the left boundary, forced Neumann condition on the right boundary, and otherwise zero Neumann conditions. We inspect the model for different material parameters

$$\boldsymbol{\mu} = (\lambda_{\mathrm{L}}, \mu_{\mathrm{L}}) \in P = [35 \cdot 10^9, 125 \cdot 10^9] \, \mathrm{N/m^2} \times [35 \cdot 10^9, 83 \cdot 10^9] \, \mathrm{N/m^2},$$

which vary between cast iron and steel with approx. 12% chromium ([90], App. E 1 Table 1). Fixed model parameters are $\rho_0 = 7856 \, \mathrm{kg/m^3}, t_0 = 0\,\mathrm{s}, t_{\mathrm{end}} = 7.2 \cdot 10^{-2} \, \mathrm{s}$.

For discretization in space, we use a triangular mesh and the Finite Element Method (FEM) with piecewise linear Lagrangian ansatz functions (see e.g. [37]). This results in a non-autonomous Hamiltonian system with a quadratic separable Hamiltonian (2.23)

$$\boldsymbol{x}(t, \boldsymbol{\mu}) = \begin{bmatrix} \boldsymbol{q}(t, \boldsymbol{\mu}) \\ \boldsymbol{p}(t, \boldsymbol{\mu}) \end{bmatrix}, \quad \boldsymbol{H}(\boldsymbol{\mu}) = \begin{bmatrix} \boldsymbol{K}(\boldsymbol{\mu}) & \boldsymbol{0}_{\bar{N} \times \bar{N}} \\ \boldsymbol{0}_{\bar{N} \times \bar{N}} & \boldsymbol{M}^{-1} \end{bmatrix}, \quad \boldsymbol{h}(t, \boldsymbol{\mu}) = \begin{bmatrix} -\boldsymbol{f}(t, \boldsymbol{\mu}) \\ \boldsymbol{0}_{\bar{N} \times 1} \end{bmatrix}, \quad (3.9)$$

with the displacements $\boldsymbol{q}(t, \boldsymbol{\mu}) \in \mathbb{R}^{\bar{N}}$, the conjugated momenta $\boldsymbol{p}(t, \boldsymbol{\mu}) \in \mathbb{R}^{\bar{N}}$, the stiffness and mass matrix $\boldsymbol{K}(\boldsymbol{\mu}), \boldsymbol{M} \in \mathbb{R}^{\bar{N} \times \bar{N}}$, and the vector of external forces $\boldsymbol{f}(t, \boldsymbol{\mu}) \in \mathbb{R}^{\bar{N}}$. For time integration, we use the implicit midpoint rule with $n_t = 151$ time steps.

method	reduced-order basis (ROB) matrix	orthonorm.	sympl.
POD full	$V = U(:, 1 : 2\bar{n})$	✓	✗
	$U = \texttt{left-SVD}(X_\mathrm{s})$		
POD separate	$V = \begin{bmatrix} U_q(:, 1 : \bar{n}) & \mathbf{0}_{\bar{N} \times \bar{n}} \\ \mathbf{0}_{\bar{N} \times \bar{n}} & U_p(:, 1 : \bar{n}) \end{bmatrix}$	✓	✗
	$U_q = \texttt{left-SVD}\left([q_1, \dots, q_{n_\mathrm{s}}]\right)$		
	$U_p = \texttt{left-SVD}\left([p_1, \dots, p_{n_\mathrm{s}}]\right)$		
PSD cSVD	$V = [E(:, 1 : \bar{n}) \quad \mathbb{J}_{2\bar{N}}^\top E(:, 1 : \bar{n})]$	✓	✓
	$E = \begin{bmatrix} \Phi \\ \Psi \end{bmatrix}, \quad \Phi + \mathrm{i}\Psi = \texttt{left-cSVD}\left(C_\mathrm{s}\right)$		
	$C_\mathrm{s} = [q_1 + \mathrm{i}p_1, \dots, q_{n_\mathrm{s}} + \mathrm{i}p_{n_\mathrm{s}}]$		
sympl. greedy	$V = [E(:, 1 : \bar{n}) \quad \mathbb{J}_{2\bar{N}}^\top E(:, 1 : \bar{n})]$	✓	✓
	E from greedy algorithm (Remark 2.52)		
PSD SVD-like	$V = [s_{i_1}, \dots, s_{i_{\bar{n}}}, s_{\bar{N}+i_1}, \dots, s_{\bar{N}+i_{\bar{n}}}]$	✗	✓
	$S = [s_1, \dots, s_{2\bar{N}}]$ from (3.5)		
	$\mathcal{I}_\mathrm{PSD} = \{i_1, \dots, i_{\bar{n}}\}$ from (3.7)		

Table 3.1: Basis generation techniques relevant in the numerical experiments of Chapter 3, where MATLAB® notation is used to denote the selection of columns and `left-SVD`(·) and `left-cSVD`(·) denote obtaining the left-singular-vectors from SVD and the complex SVD, respectively. This table is adapted from [20].

3.3.2 Experiments

In four experiments, we investigate (i) the preservation of the Hamiltonian (Section 3.3.2.1), (ii) the ROB quality on the training data (Section 3.3.2.2), (iii) the symplecticity and orthonormality of the ROB (Section 3.3.2.3), and (iv) the ROM quality on test data (Section 3.3.2.4).

The considered MOR techniques are summarized in Table 3.1. Two different POD methods are considered: *POD full state* applies the POD applied to the full state $x(t, \mu)$, while *POD separate states* builds a POD basis for the displacement $q(t, \mu)$ and linear momentum states $p(t, \mu)$ separately. The symplectic greedy uses the modified symplectic Gram–Schmidt procedure with re-orthogonalization [3] to obtain an orthosymplectic ROB in each iteration.

In order to compute snapshots for the basis generation, we choose nine different training parameter vectors $\mu \in P_\mathrm{train} \subset P$ on a regular grid. Thus, the number of snapshots is $n_\mathrm{s} = 9 \cdot 151 = 1359$. The resultant ROMs are evaluated for 16 random parameter vectors
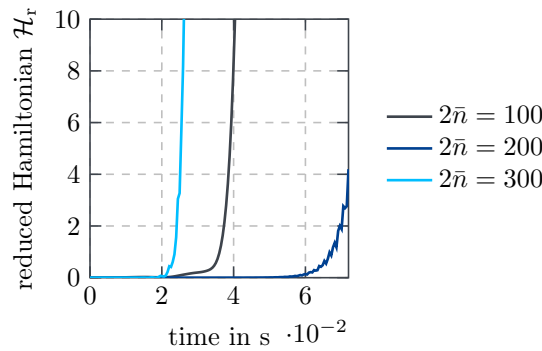
Figure 3.2: Evolution of the reduced Hamiltonian for POD separate states for a selected parameter vector $(\lambda, \mu) \in P$. This figure is adapted from [20].

that are distinct from the nine training parameter vectors as a generalization experiment. The size $2\bar{n}$ of the ROB $\boldsymbol{V}$ is varied in steps of 20 with $2\bar{n} \in \{20, 40, \ldots, 280, 300\}$. In total, this results in 15 different basis sizes, which are investigated for each of the 16 random parameter vectors $\boldsymbol{\mu} \in P_{\text{test}} \subset P$, which results in 240 reduced simulations for each MOR technique.

The numerical experiments are implemented in RBmatlab[1], which is an open-source library based on the proprietary software package MATLAB®. The experiments can be reproduced with the add-on for RBmatlab 1.16.09 provided in [19].

3.3.2.1 Preservation of Hamiltonian over Time

The ROMs obtained from symplectic MOR are Hamiltonian systems and thus preserve the quadratic Hamiltonian over time (see Lemma 2.29 and Remark 2.37), which is one big advantage of this MOR technique. In the present experiment, we briefly validate this preservation of the Hamiltonian numerically for a beam model with external forces $\boldsymbol{f}(t; \boldsymbol{\mu})$, which are constant in time. We observe that all PSD methods from Table 3.1 preserve the Hamiltonian over time, while the POD methods show a non-constant Hamiltonian. We exemplify this non-constant evolution in Figure 3.2 for one selected test parameter vector $(\lambda, \mu) \in P$ and three selected basis sizes $2\bar{n}$ with a basis generated with POD separate states. This shows that PSD methods are energy-preserving while the POD methods not necessarily do so.

In what follows, we consider a more complex system with a time-dependent forcing $\boldsymbol{f}(t, \boldsymbol{\mu})$, which results in a non-autonomous beam model.

---

[1]https://www.morepas.org/software/rbmatlab/
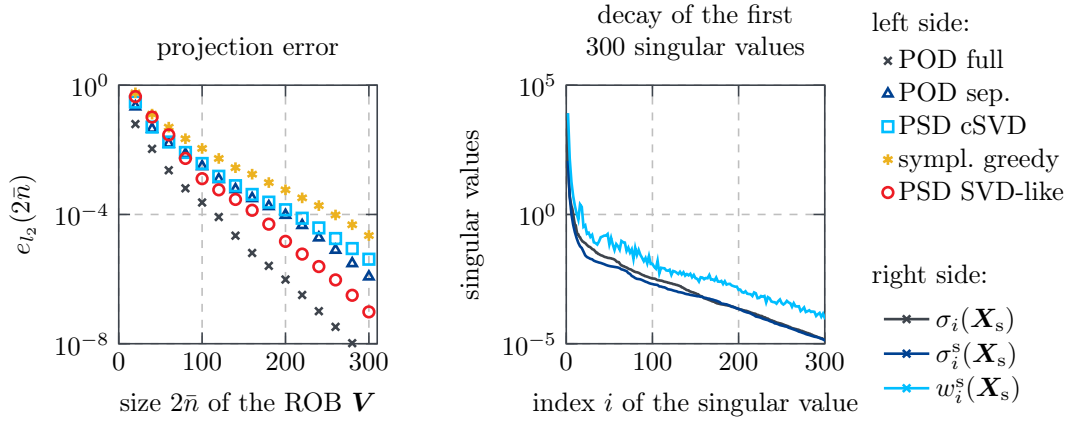
Figure 3.3: Left: Projection error (3.10). Right: Decay of the (symplectic) singular values (2.20), (3.5), and (3.6). This figure is adapted from [20].

3.3.2.2 ROB Quality Based on Training Data

In order to quantify the approximation quality based on the training data, we compare the projection error and the respective singular values. As projection error, we consider the error on the training data collected in the snapshot matrix $\boldsymbol{X}_{\mathrm{s}}$, i.e.

$$
e_{l_2}(2\bar{n}) = \left\| (\boldsymbol{I}_{2\bar{N}} - \boldsymbol{V}\boldsymbol{W}^\top)\boldsymbol{X}_{\mathrm{s}} \right\|_{\mathrm{F}}^2, \qquad
\begin{aligned}
&\text{POD} : \boldsymbol{W}^\top = \boldsymbol{V}^\top, \\
&\text{PSD} : \boldsymbol{W}^\top = \boldsymbol{V}^+ (= \boldsymbol{V}^\top \text{for orthosympl.}).
\end{aligned}
\tag{3.10}
$$

Figure 3.3 (left) shows the projection error (3.10). For all basis generation techniques, we observe an exponential decay of the projection error for an increasing ROB size, which is an indicator that MOR can be applied to this model. As expected from theory, POD full state yields the lowest projection error. The newly introduced PSD SVD-like shows a lower projection error than the other symplectic methods for $2\bar{n} \geq 80$ and yields a similar projection error for $2\bar{n} \leq 60$. This supports the assumption that the PSD SVD-like has more freedom to adapt to the data than the other symplectic basis generation techniques. Based on the projection error solely, the full-state POD is expected to yield the best approximation of the FOM data. Figure 3.3 (right) displays the difference between the singular values σ_i from (2.20), the symplectic singular values σ_i^{s} from (3.5), and the weighted symplectic singular values w_i^{s} from (3.6). The weighted symplectic singular values are sorted by the magnitude of the non-weighted symplectic singular values. The non-monotonic, zigzagging behavior of w_i^{s} shows that the weighting, indeed, influences the order in which the modes are selected.
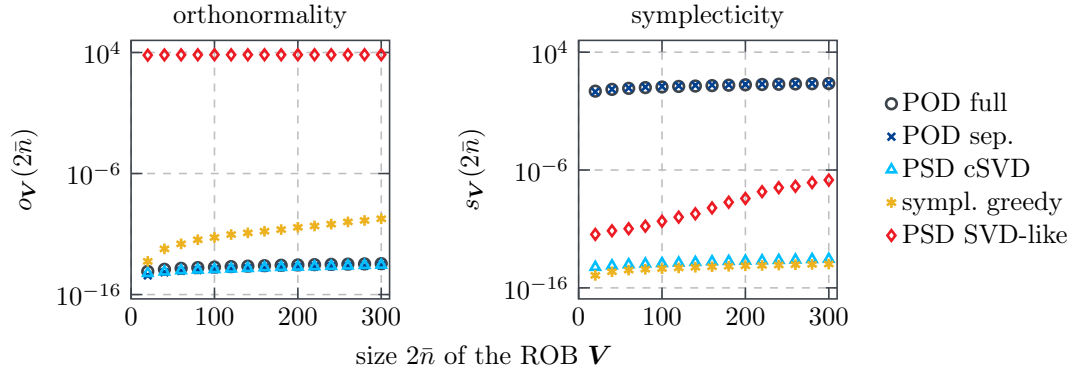
Figure 3.4: The orthonormality (left) and the symplecticity (right) from (3.11). This figure is adapted from [20].

3.3.2.3 ROB Quality in Terms of Structure

Next, we investigate the structural properties of the ROBs. We check the orthonormality and the symplecticity of the respective ROBs numerically with

$$o_{\boldsymbol{V}}(2\bar{n}) = \left\|\boldsymbol{V}^{\top}\boldsymbol{V} - \boldsymbol{I}_{2\bar{n}}\right\|_{\mathrm{F}}, \qquad s_{\boldsymbol{V}}(2\bar{n}) = \left\|\mathbb{J}_{2\bar{n}}^{\top}\boldsymbol{V}^{\top}\mathbb{J}_{2N}\boldsymbol{V} - \boldsymbol{I}_{2\bar{n}}\right\|_{\mathrm{F}}. \qquad (3.11)$$

In Figure 3.4, we show both these values for the considered basis generation techniques and sizes $2\bar{n}$ of the ROB. The orthonormality of the ROBs (Figure 3.4, left) is as expected from theory: All MOR techniques compute an orthonormal ROB except for the PSD SVD-like. For the symplectic greedy, a minor loss in the orthonormality is observed for an increasing ROB size which, however, is known as an issue of the modified symplectic Gram–Schmidt procedure with re-orthogonalization [3]. The results for the symplecticity of the ROBs (Figure 3.4, right) are also in accordance with the theory. All PSD methods generate a symplectic ROB, while the POD methods do not. The symplecticity slightly degenerates for PSD SVD-like with higher reduced dimensions $2\bar{n}$, which is assumed to stem from the algorithm used to compute an SVD-like decomposition. However, in the following experiments, no major impact on the reduction quality is observed.

3.3.2.4 ROM Quality

Finally, we investigate how the different ROMs perform on test data by examining 16 test parameter vectors $\boldsymbol{\mu} \in P_{\text{test}}$, which are distinct from the training parameter vectors (general-
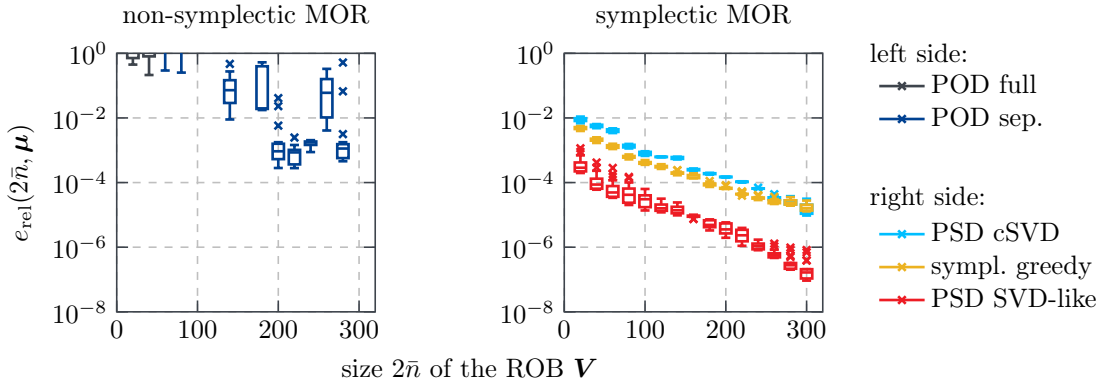
Figure 3.5: Statistics of the reduction error (3.12) over 16 test parameter vectors $\boldsymbol{\mu} \in P_{\text{test}}$ for different sizes $2\bar{n}$ of the ROB and different MOR techniques.

ization experiment). We investigate the *relative reduction error*

$$e_{\text{rel}}(2\bar{n}, \boldsymbol{\mu}) := \sqrt{\frac{\sum_{k=1}^{n_t} \|\boldsymbol{x}_k(\boldsymbol{\mu}) - \boldsymbol{V}\check{\boldsymbol{x}}_k(\boldsymbol{\mu})\|_2^2}{\sum_{k=1}^{n_t} \|\boldsymbol{x}_k(\boldsymbol{\mu})\|_2^2}} \tag{3.12}$$

with the FOM solution $\boldsymbol{x}_k(\boldsymbol{\mu}) \in \mathbb{R}^{2\bar{N}}$, the ROM solution $\check{\boldsymbol{x}}_k(\boldsymbol{\mu}) \in \mathbb{R}^{2\bar{n}}$, and a test parameter vector $\boldsymbol{\mu} \in P_{\text{train}}$. The statistics of the relative reduction error e_{rel} over all 16 test parameter vectors are displayed in Figure 3.5 with box plots. The visual elements of a box plot are: The box (25%- and 75%-quantile), a dash in the box (median), whiskers (denoting the range of data points which lay within 1.5 times the interquartile range (IQR)), and crosses (outliers that are outside the IQR). Errors above $10^0 = 100\%$ are truncated. Figure 3.5 (left) shows that the non-symplectic MOR techniques yield high errors and strongly non-monotonic behavior. For nearly each basis size $2\bar{n}$, one of the 16 test parameter vectors produces a ROM with a relative error above 100%. Overall, none of these methods is able to produce a reliable ROM. Figure 3.5 (right) displays the same error for the symplectic MOR techniques. In contrast to the non-symplectic methods, all symplectic methods show an exponentially decreasing error. Moreover, the IQR of the box plots is remarkably small, which indicates that these methods generalize very well to unseen parameters and yield a reliable ROM. The highest error observed for the orthosymplectic methods is 1.11% and for PSD SVD-like 0.11%. The PSD SVD-like shows a reduction error approximately one order lower consistently for all considered ROB sizes. This again supports the claim that the PSD SVD-like adapts better to the data than the orthosymplectic methods.

PSD-Greedy Symplectic Basis Generation

4

As discussed in Remark 2.22, greedy basis generation methods are standard for parametric, time-dependent problems with high-dimensional parameter spaces. This motivates to derive a symplectic greedy technique, which is the subject of this chapter. We call the new method the PSD-greedy. It is based on the ideas of the POD-greedy algorithm (Remark 2.22) and complements the existing symplectic greedy approach (Remark 2.52): Like the POD-greedy, we compress whole trajectories in each iteration of the greedy algorithm. In order to preserve the symplectic structure, however, we use a symplectic instead of an orthogonal projection. The advantages of our formulation in comparison to the existing symplectic greedy approach [81] are twofold: (i) It is known for the non-structure-preserving case [45, 49] that stagnation issues may appear if single snapshots of maximum projection error are selected in each greedy iteration (as in the existing symplectic greedy) instead of considering whole trajectories in each greedy iteration (as in our formulation). Moreover, (ii) our approach works in combination with any symplectic basis generation technique, while the existing symplectic greedy relies on an orthosymplectic basis generation. Thus, we are able to use the PSD SVD-like from the previous chapter with the new PSD-greedy formulation, which leads to improved accuracy in the numerical experiments. The following is adapted from [26].

4.1 Formulation of PSD-Greedy

In this section, we introduce the new PSD-greedy. The PSD-greedy is an iterative algorithm. In each iteration i of the algorithm, the current ROB matrix $\boldsymbol{V}_i$ is extended greedily with basis vectors from the worst-approximated parameter. As a first step, we characterize how to extend a symplectic basis with additional basis vectors in a structure-preserving way.

Lemma 4.1 (Symplectic extension)**:** *For two given symplectic matrices $V \in \mathbb{R}^{2\bar{N} \times 2\bar{n}_V}$ and $W \in \mathbb{R}^{2\bar{N} \times 2\bar{n}_W}$, the matrix stacking the $2\bar{n}_U := 2\bar{n}_V + 2\bar{n}_W$ columns of V and W with*

$$U := [V, W]P \in \mathbb{R}^{2\bar{N} \times 2\bar{n}_U}, \qquad P = \begin{bmatrix} I_{\bar{n}_V} & 0 & 0 & 0 \\ 0 & 0 & I_{\bar{n}_V} & 0 \\ 0 & I_{\bar{n}_W} & 0 & 0 \\ 0 & 0 & 0 & I_{\bar{n}_W} \end{bmatrix} \in \mathbb{R}^{2\bar{n}_U \times 2\bar{n}_U}, \qquad (4.1)$$

is a symplectic matrix if and only if the symplectic projection of V on W vanishes or vice versa,

$$W^+ V = 0_{2\bar{n}_W \times 2\bar{n}_V} \qquad\qquad \text{or} \qquad\qquad V^+ W = 0_{2\bar{n}_V \times 2\bar{n}_W}. \qquad (4.2)$$

Proof. Since P is of full rank, symplecticity of U is equivalent to

$$P U^\top \mathbb{J}_{2\bar{N}} U P^\top = P \mathbb{J}_{2\bar{n}_U} P^\top$$

by multiplying with P and $P^\top$ from left and right. Both of these terms can be rewritten to

$$\begin{aligned} P U^\top \mathbb{J}_{2\bar{N}} U P^\top &= \begin{bmatrix} V^\top \\ W^\top \end{bmatrix} \mathbb{J}_{2\bar{N}} \begin{bmatrix} V & W \end{bmatrix} = \begin{bmatrix} V^\top \mathbb{J}_{2\bar{N}} V & V^\top \mathbb{J}_{2\bar{N}} W \\ W^\top \mathbb{J}_{2\bar{N}} V & W^\top \mathbb{J}_{2\bar{N}} W \end{bmatrix} \\ P \mathbb{J}_{2\bar{n}_U} P^\top &= \begin{bmatrix} \mathbb{J}_{2\bar{n}_V} & 0_{2\bar{n}_V \times 2\bar{n}_W} \\ 0_{2\bar{n}_W \times 2\bar{n}_V} & \mathbb{J}_{2\bar{n}_W} \end{bmatrix} \end{aligned} \qquad (4.3)$$

If symplecticity of V and W is assumed, then the terms for the two parts in (4.3) on the diagonal are equal. Thus, symplecticity of U is equivalent to

$$W^\top \mathbb{J}_{2\bar{N}} V = 0_{2\bar{n}_W \times 2\bar{n}_V}. \qquad (4.4)$$

Multiplying (4.4) (or the transposed of it) with $\mathbb{J}_{2\bar{n}}^\top$ from the left is equivalent to the symplectic projections (4.2). $\qquad \square$

Note that the construction of U in Lemma 4.1 relies on gluing two matrices V and W. In general, linearly dependent columns may occur in this step. However, under the assumptions of Lemma 4.1, the resulting matrix U is guaranteed to be symplectic and thus the columns of the glued matrix U are linearly independent.

We continue to introduce the new symplectic basis generation technique, the PSD-greedy. We assume to be given the following building blocks (BB):

(BB1): An error indicator $\Delta\left(\cdot,\,\cdot\right) : \mathbb{R}^{2\bar{N}\times2\bar{n}} \times P,\, (\boldsymbol{V},\boldsymbol{\mu}) \mapsto \Delta\left(\boldsymbol{V},\,\boldsymbol{\mu}\right)$ that estimates the approximation quality of a given ROB matrix $\boldsymbol{V}$ and a given parameter vector $\boldsymbol{\mu}$. Possible choices are the projection error of the snapshots, the actual reduction error (which requires running ROMs during the greedy procedure), or an error estimator.

(BB2): A symplectic basis generation technique $\boldsymbol{V} = \text{PSD}\left(\boldsymbol{R}\right)$ which generates ROB matrices from $\boldsymbol{R} \in \mathbb{R}^{2\bar{N}\times n_{\mathrm{s}}}$ such that

   a) $\boldsymbol{V}$ is a symplectic matrix,

   b) $\text{colspan}\left(\boldsymbol{V}\right) \subset \text{colspan}\left(\boldsymbol{R}\right)$, i.e. $\boldsymbol{V}$ is in the range of the given data matrix $\boldsymbol{R}$.

(BB3): The permutation matrix $\boldsymbol{P} \in \mathbb{R}^{2\bar{n}_U\times2\bar{n}_U}$ from Lemma 4.1 for different sizes $2\bar{n}_U$, which is why we denote the different sizes as a subscript with $\boldsymbol{P}_{2\bar{n}_U}$.

Based on these building blocks, the PSD-greedy is presented in Algorithm 4.1 as Python pseudocode. The goal of the algorithm is to compute a symplectic ROB matrix $\boldsymbol{V}_{i_{\max}}$ with a maximum of $i_{\max}$ greedy iterations. The inputs are (a) a finite parameter set $M \subset P$, (b) a target error tolerance $r_{\mathrm{tol}} > 0$ and (c) a snapshot generation algorithm $\boldsymbol{X}_{\mathrm{s}} : M \to \mathbb{R}^{2\bar{N}\times n_{\mathrm{s}}(\boldsymbol{\mu})}$, which generates a snapshot matrix $\boldsymbol{X}_{\mathrm{s}}(\boldsymbol{\mu})$ for a given parameter $\boldsymbol{\mu}$ where the number of snapshots $n_{\mathrm{s}}(\boldsymbol{\mu})$ might vary with $\boldsymbol{\mu}$. In each greedy iteration i, the PSD-greedy determines "greedily" the parameter vector $\boldsymbol{\mu}_i \in M$ with maximum error via the error indicator from **(BB1)**. The symplectic basis generation technique from **(BB2)** is then applied to the residual $\boldsymbol{R}_i$ from Line 5, which projects the snapshot matrix $\boldsymbol{X}_{\mathrm{s}}(\boldsymbol{\mu}_i)$ such that contributions from the previous ROB matrix $\boldsymbol{V}_{i-1}$ are eliminated. Finally, the output of the PSD is then concatenated with the basis of the previous iteration with the symplectic extension matrix from **(BB3)**. In the first iteration of the algorithm, the ROB matrix $\boldsymbol{V}_0 \in \mathbb{R}^{2\bar{N}\times0}$ is empty. All terms linked to $\boldsymbol{V}_0$ are neglected, i.e. set to zero, when the error indicator in Lines 2 and 4 is evaluated and the residual in Line 5 is computed. We do not restrict how many basis vectors are added in each iteration. The simplest choice is to add a fixed number $\Delta\bar{n}_1 = \cdots = \Delta\bar{n}_{i_{\max}}, \Delta\bar{n}_i := \bar{n}_i - \bar{n}_{i-1}$, of basis vectors in each iteration. More adaptivity is obtained if the module $\text{PSD}\left(\cdot\right)$ chooses the number of basis vectors in each iteration based on the given residual.

Algorithm 4.1: PSD-greedy[1]

Input: Finite parameter set $M \subset P$, error tolerance $r_{\text{tol}} > 0$, snapshot-generation
algorithm $\boldsymbol{X}_{\text{s}} : M \to \mathbb{R}^{2\bar{N} \times n_{\text{s}}}$

Output: Symplectic ROB matrix $\boldsymbol{V}_{i_{\max}} \in \mathbb{R}^{2\bar{N} \times 2\bar{n}_{i_{\max}}}$, number of iterations $i_{\max}$

1   $\boldsymbol{V}_0 \leftarrow [\,]; \; i \leftarrow 0; \; \bar{n}_0 = 0$ ▷ `start with empty ROB matrix`

2 **while** $\exists \boldsymbol{\mu} \in M : \Delta\,(\boldsymbol{V}_i, \, \boldsymbol{\mu}) > r_{\text{tol}}$ **do**

3      $i \leftarrow i + 1$

4      $\boldsymbol{\mu}_i \leftarrow \operatorname{argmax}_{\boldsymbol{\mu} \in M} \Delta\,(\boldsymbol{V}_{i-1}, \, \boldsymbol{\mu})$

5      $\boldsymbol{R}_i \leftarrow (\boldsymbol{I}_{2\bar{N}} - \boldsymbol{V}_{i-1}\boldsymbol{V}_{i-1}^+)\boldsymbol{X}_{\text{s}}(\boldsymbol{\mu}_i)$ ▷ `compute residual w.r.t. previous basis`

6      $\boldsymbol{V}_i^{\text{ext}} \leftarrow \text{PSD}\,(\boldsymbol{R}_i)$ ▷ `compute extension`

7      $\bar{n}_i \leftarrow \bar{n}_{i-1} + \text{size}(\boldsymbol{V}_i^{\text{ext}}, -1)/2$ ▷ `update basis size`

8      $\boldsymbol{V}_i \leftarrow [\boldsymbol{V}_{i-1} \;\; \boldsymbol{V}_i^{\text{ext}}]\boldsymbol{P}_{2\bar{n}_i}$ ▷ `extend ROB matrix 'symplectically', see (4.1)`

9 **end**

10 $i_{\max} \leftarrow i$

In the remainder of this section, we prove that Algorithm 4.1 indeed computes a symplectic ROB matrix.

Lemma 4.2 (Symplecticity of one iteration)**:** *For a given matrix $\boldsymbol{X} \in \mathbb{R}^{2\bar{N} \times n_{\boldsymbol{X}}}$ and a given symplectic matrix $\boldsymbol{W} \in \mathbb{R}^{2\bar{N} \times 2\bar{n}_{\boldsymbol{W}}}$, the extended matrix*

$$\boldsymbol{U} := [\boldsymbol{W} \;\; \boldsymbol{V}^{\text{ext}}]\boldsymbol{P} \quad \textit{with} \quad \boldsymbol{V}^{\text{ext}} = \textit{PSD}\,(\boldsymbol{R}) \in \mathbb{R}^{2\bar{N} \times 2\bar{n}_{\boldsymbol{V}^{\text{ext}}}}, \quad \boldsymbol{R} = (\boldsymbol{I}_{2\bar{N}} - \boldsymbol{W}\boldsymbol{W}^+)\boldsymbol{X},$$

is a symplectic matrix.

Proof. With Lemma 4.1, it is sufficient to show $\boldsymbol{W}^\top \mathbb{J}_{2\bar{N}} \boldsymbol{V}^{\text{ext}} = \boldsymbol{0}_{2\bar{n}_{\boldsymbol{W}} \times 2\bar{n}_{\boldsymbol{V}^{\text{ext}}}}$ since $\boldsymbol{W}$ and $\boldsymbol{V}^{\text{ext}}$ are symplectic matrices by assumption. Due to assumption (b) from **(BB2)**, there exists a matrix $\boldsymbol{C} \in \mathbb{R}^{n_{\boldsymbol{X}} \times 2\bar{n}_{\boldsymbol{V}^{\text{ext}}}}$ such that we can express $\boldsymbol{V}^{\text{ext}} = \boldsymbol{R}\boldsymbol{C}$. With the identity

$$\boldsymbol{W}^\top \mathbb{J}_{2\bar{N}} \boldsymbol{W}\boldsymbol{W}^+ = \boldsymbol{W}^\top \mathbb{J}_{2\bar{N}} \boldsymbol{W} \mathbb{J}_{2\bar{n}_{\boldsymbol{W}}}^\top \boldsymbol{W}^\top \mathbb{J}_{2\bar{N}} \overset{(2.21)}{=} \mathbb{J}_{2\bar{n}_{\boldsymbol{W}}} \mathbb{J}_{2\bar{n}_{\boldsymbol{W}}}^\top \boldsymbol{W}^\top \mathbb{J}_{2\bar{N}} \overset{(2.20)}{=} \boldsymbol{W}^\top \mathbb{J}_{2\bar{N}},$$

it indeed holds

$$\boldsymbol{W}^\top \mathbb{J}_{2\bar{N}} \boldsymbol{V}^{\text{ext}} = \boldsymbol{W}^\top \mathbb{J}_{2\bar{N}}(\boldsymbol{I}_{2\bar{N}} - \boldsymbol{W}\boldsymbol{W}^+)\boldsymbol{X}\boldsymbol{C} = \boldsymbol{0}_{2\bar{n}_{\boldsymbol{W}} \times 2\bar{n}_{\boldsymbol{V}^{\text{ext}}}}. \qquad \square$$

---

[1]The algorithm is adapted from [26].
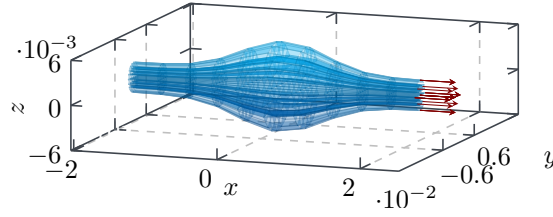
Figure 4.1: Discretized fusiform-muscle-shaped domain Ω in blue and boundary traction (Neumann values) as dark red arrows. This figure is taken from [26].

Theorem 4.3 (Symplecticity of ROB matrix generated by PSD-greedy): *The ROB matrix computed by the PSD-greedy (Algorithm 4.1) is a symplectic ROB matrix.*

Proof. We prove the statement by induction over the greedy iteration i. The induction basis holds for $i = 1$ since the ROB matrix $\boldsymbol{V}_1 = \boldsymbol{V}_1^{\text{ext}}$ is symplectic by assumption (a) of **(BB2)**. The induction step is proven by Lemma 4.2: It shows that all ROB matrices $\boldsymbol{V}_i$ in Algorithm 4.1 are symplectic matrices (with $\boldsymbol{X} = \boldsymbol{X}_{\text{s}}(\boldsymbol{\mu}_i)$, $\boldsymbol{W} = \boldsymbol{V}_{i-1}$, $\boldsymbol{V}^{\text{ext}} = \boldsymbol{V}_i^{\text{ext}}$, $\boldsymbol{P} = \boldsymbol{P}_{2\bar{n}_i}$, $\boldsymbol{U} = \boldsymbol{V}_i$).   □

4.2 Numerical Experiments

4.2.1 Full-Order Model

As FOM, we consider linear elasticity (see Section 3.3.1) with a three-dimensional physical domain $\Omega \subset \mathbb{R}^3$ that is shaped like a so-called fusiform muscle (see Figure 4.1). An external force is applied in axial direction on the right boundary of the muscle. The parameter vector $\boldsymbol{\mu} := [\lambda_{\text{L}}, \mu_{\text{L}}, F_{\text{max}}] \in \mathbb{R}^3_{>0}$ varies the Lamé parameters $(\lambda_{\text{L}}, \mu_{\text{L}})$ and a parameter for external forces F_{max}, while the parameter domain is based on the parameters given in [62] with $\lambda_{\text{L}} \in [6\text{e}4, 1.2\text{e}5] \, \text{N/m}^2$, $\mu_{\text{L}} \in [6\text{e}3, 1.22\text{e}4] \, \text{N/m}^2$, $F_{\text{max}} \in [0.49, 5.89] \, \text{N}$. The density $\rho_0 = 1059.7 \, \text{kg/m}^3$ is fixed and the considered time interval is $I_t := [0, 0.5]s$. For spatial discretization, we use FEM with 1920 first-order Lagrangian elements, which results in a non-autonomous Hamiltonian system of the same structure as (3.9). For symplectic integration, we use the implicit midpoint rule (see Section 2.3.2) with $n_t = 1000$ time steps. The experiments are implemented in the MOR framework pyMOR [87] in combination with the FEM library FEnics [71].

Greedy MOR technique	abbreviation	ortho.	sympl.	ref.
POD-greedy with $\boldsymbol{H}_{\mathrm{fix}}$ as inner product matrix	$\mathrm{POD_G}$	✓	✗	[49]
Based on symplectic Gram–Schmidt	$\mathrm{sGS_G}$	✓	✓	[81]
PSD-greedy with PSD $(\cdot)$ submodule:				
PSD Complex SVD	$\mathrm{PSD_G}$ cSVD	✓	✓	[99]
PSD SVD-like decomposition	$\mathrm{PSD_G}$ SVD-like	✗	✓	[20]

Table 4.1: Greedy MOR techniques used in the experiments classified by orthogonality and symplecticity. This table is taken from [26].

4.2.2 Experiments

The approximation quality of four different greedy basis generation techniques is compared:

- the POD-greedy ($\mathrm{POD_G}$) with $\boldsymbol{H}_{\mathrm{fix}}$ as inner product matrix,
- the newly introduced PSD-greedy from Algorithm 4.1 based on two different symplectic basis generation techniques as **(BB2)**:

  - the PSD Complex SVD ($\mathrm{PSD_G}$ cSVD) from Definition 2.51 and
  - the PSD SVD-like decomposition ($\mathrm{PSD_G}$ SVD-like) from Definition 3.8

- the existing symplectic greedy approach ($\mathrm{sGS_G}$) from [81] (see Table 4.1 for a summary).

A $4 \times 4 \times 4$ Cartesian grid on P is used as training set $M \subset P$. In each greedy iteration $2\Delta\bar{n}_i = 2$ vectors are added. The termination condition is set to leave the greedy algorithm after $i_{\max} = 30$ greedy iterations, which results in a maximal ROB dimension of $2\bar{n}_{i_{\max}} = 60$.

In order to compare the approximation quality of these four techniques, we use the $L_2(I_t, \mathbb{R}^{2\bar{N}})$ norm with a $\boldsymbol{H}_{\mathrm{fix}}$-weighted norm in space

$$\|\boldsymbol{x}(\cdot)\|_{L_2, \boldsymbol{H}_{\mathrm{fix}}}^2 := \int_{I_t} \|\boldsymbol{x}(t)\|_{\boldsymbol{H}_{\mathrm{fix}}}^2 \, \mathrm{d}t, \qquad \|\boldsymbol{x}(t)\|_{\boldsymbol{H}_{\mathrm{fix}}}^2 := (\boldsymbol{x}(t))^\top \boldsymbol{H}_{\mathrm{fix}} \boldsymbol{x}(t),$$

where the integral over time is approximated with the composite trapezoidal rule and the weighting matrix $\boldsymbol{H}_{\mathrm{fix}} := \boldsymbol{H}(\boldsymbol{\mu}_{\mathrm{fix}})$ is fixed with $\boldsymbol{\mu}_{\mathrm{fix}} := (80\,690, 8\,966, 3.83) \in P$.
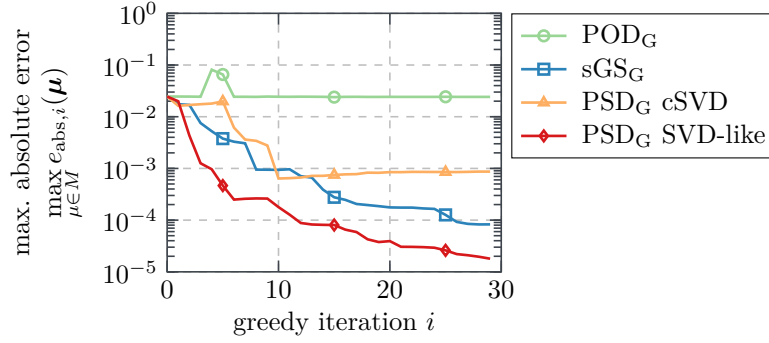
Figure 4.2: Maximum absolute reduction error over 64 parameter vectors in M used for the greedy training in dependence on the greedy iteration i. This figure is taken from [26].

We compare the absolute and the relative reduction error

$$e_{\mathrm{abs},i}(\boldsymbol{\mu}) := \|\boldsymbol{x}(\cdot,\boldsymbol{\mu}) - \boldsymbol{V}_i \check{\boldsymbol{x}}_i(\cdot,\boldsymbol{\mu})\|_{L_2,\boldsymbol{H}_{\mathrm{fix}}}, \qquad e_{\mathrm{rel},i}(\boldsymbol{\mu}) := \frac{e_{\mathrm{abs},i}(\boldsymbol{\mu})}{\|\boldsymbol{x}(\cdot,\boldsymbol{\mu})\|_{L_2,\boldsymbol{H}_{\mathrm{fix}}}}, \qquad (4.5)$$

with the FOM solution $\boldsymbol{x}(t,\boldsymbol{\mu}) \in \mathbb{R}^{2\bar{N}}$, the ROB matrix $\boldsymbol{V}_i \in \mathbb{R}^{2\bar{N} \times 2\bar{n}_i}$, and the ROM solution $\check{\boldsymbol{x}}_i(t,\boldsymbol{\mu}) \in \mathbb{R}^{2\bar{n}_i}$ at the i-th greedy iteration. As error indicator (required in **(BB1)**), the absolute reduction error $\Delta(\boldsymbol{\mu}, \boldsymbol{V}_i) = e_{\mathrm{abs},i}(\boldsymbol{\mu})$ is used for all investigated greedy basis generation methods. We present two experiments which investigate (a) the training and (b) how well the trained models generalize to parameter vectors that are not included in the training set.

4.2.2.1 ROB Quality Based on Training Data

The results of the training are shown in Figure 4.2 with the maximum absolute reduction error (4.5) over all 64 training parameter vectors $\boldsymbol{\mu} \in M$ in dependence on the greedy iteration i. This is exactly the error that is computed in Line 4 of Algorithm 4.1 (and comparably for the other greedy methods) to decide which parameter is used to enrich the basis. Note that this is an error which uses ROMs with the current ROB matrix $\boldsymbol{V}_i$ already during the training phase. We observe for the $\mathrm{POD_G}$ that it is not able to produce meaningful ROMs and thus the absolute reduction error does not decay. The symplectic greedy methods all construct ROMs for which the absolute reduction error decreases below 10^{-3}. The $\mathrm{PSD_G}$ cSVD seems to stagnate at 10^{-3}. The best method is the $\mathrm{PSD_G}$ SVD-like, which yields errors below 10^{-4}. This matches the observations from the previous sections that the PSD SVD-like decomposition does not constrain the basis to be orthogonal which allows it to adapt to the data faster.
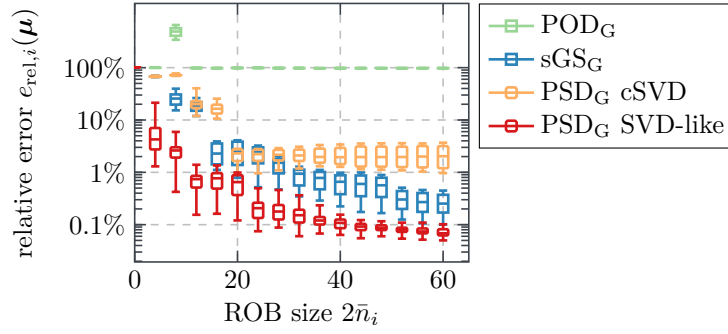
Figure 4.3: Statistics of the relative error over 100 random test parameter vectors for different ROB sizes $2\bar{n}_i$. This figure is taken from [26].

4.2.2.2 ROM Quality

Now, we investigate how well the ROBs constructed by the greedy algorithms generalize to 100 random parameter vectors $\boldsymbol{\mu} \in P \setminus M$ that are not included in the training set. Figure 4.3 visualizes for each considered MOR technique the statistics of the relative reduction error (4.5) of ROBs trained with $i_{\max} \in \{2, 4, \ldots, 30\}$ greedy iterations resulting in an ROB size $2\bar{n}_i = 2i_{\max} \in \{4, 8, \ldots, 60\}$. Box plots are used for the visualization, where the whiskers indicate the minimum and maximum relative error. The results are as expected from training: Firstly, the POD does not produce meaningful ROMs and yields high errors. Secondly, the symplectic methods are able to reduce the error below 100%, where the PSD_{G} cSVD stagnates between a relative reduction error of 10% and 1% and the PSD_{G} SVD-like yields the best models. Especially for low ROM sizes $2\bar{n}_i \in \{8, 12, 16\}$, the PSD_{G} SVD-like has a notable advantage over the other methods. For example with ROB sizes $2\bar{n}_i \geq 12$, the median of the relative error of PSD_{G} SVD-like is always below 1% relative error which occurs for sGS_{G} with $2\bar{n}_i \geq 32$. This means, the new PSD_{G} SVD-like is able to reduce the ROB size by a factor of 2.6 compared to sGS_{G} while achieving the same relative error. This supports the claim that the PSD SVD-like decomposition produces ROBs which can better adapt to the data.

Optimal Symplectic Basis Generation for Canonizable Systems

5

As a last symplectic basis generation technique, we discuss a provably optimal basis in the special case of a so-called canonizable linear Hamiltonian system with a periodic solution. To this end, we derive for this specific case the eigenvectors of the time-continuous POD from Section 2.2.3.2 and show that these build automatically a symplectic basis for a specific choice of the integration time T_{POD}. With this result, we are able to show that this basis is also an optimal solution of a time-continuous PSD functional. A numerical experiment for the linear wave equation validates the theoretical findings numerically by investigating the symplecticity of the constructed basis. The following is adapted from [21].

5.1 Canonizable Linear Hamiltonian Systems

In this section, we introduce canonizable (linear Hamiltonian) systems. Furthermore, we present a transformation from linear Hamiltonian systems to a canonizable system which we refer to as energy coordinates. For the sake of brevity, we consider a parameter-independent formulation.

Definition 5.1 (Hamiltonian(-positive) matrix [10])**:** *A matrix $\boldsymbol{A} \in \mathbb{R}^{2\bar{N} \times 2\bar{N}}$ is called Hamiltonian, if there exists a symmetric matrix $\boldsymbol{G} \in \mathbb{R}^{2\bar{N} \times 2\bar{N}}$ with $\boldsymbol{A} = \mathbb{J}_{2\bar{N}}\boldsymbol{G}$. The matrix is called Hamiltonian-positive, if additionally $\boldsymbol{G}$ is positive-definite.*

Definition 5.2 (Canonizable matrix)**:** *We call a matrix $\boldsymbol{A} \in \mathbb{R}^{2\bar{N} \times 2\bar{N}}$ that is Hamiltonian-positive and skew-symmetric a canonizable matrix.*

Definition 5.3 (Canonizable system)**:** *We call a Hamiltonian system $(\mathbb{V}, \omega, \mathcal{H})$ with quadratic Hamiltonian (2.23) a linear Hamiltonian system in canonizable coordinates (or canonizable*

system in short) *if there exists a canonizable matrix* $\boldsymbol{A} = \mathbb{J}_{2\bar{N}}\boldsymbol{G} \in \mathbb{R}^{2\bar{N}\times 2\bar{N}}$ *which defines the Hamiltonian vector field in coordinates with* $\boldsymbol{X}_{\mathscr{H}}(\boldsymbol{x}) = \boldsymbol{\omega}^{-1}\nabla\mathscr{H}|_{\boldsymbol{x}} = \boldsymbol{A}\boldsymbol{x}$. *The dynamical system of a canonizable system thus reads*

$$\frac{\mathrm{d}}{\mathrm{d}t}\boldsymbol{x}(t) = \boldsymbol{A}\boldsymbol{x}(t) = \mathbb{J}_{2\bar{N}}\boldsymbol{G}\boldsymbol{x}(t), \qquad\qquad \boldsymbol{x}(0) = \boldsymbol{x}_0. \qquad (5.1)$$

Theorem 5.4 (Energy coordinates): *We assume to be given a Hamiltonian system* $(\mathbb{V}, \omega, \mathscr{H})$ *with a quadratic Hamiltonian* (2.23) *with* $\boldsymbol{h} = \boldsymbol{0}_{2\bar{N}\times 1}$ *and* $\boldsymbol{H} = \boldsymbol{C}^{\top}\boldsymbol{C}$ *for an invertible matrix* $\boldsymbol{C} \in \mathbb{R}^{2\bar{N}\times 2\bar{N}}$ *such that*

$$\hat{\boldsymbol{\omega}}^{-1} := \boldsymbol{C}\boldsymbol{\omega}^{-1}\boldsymbol{C}^{\top} \text{ is Hamiltonian-positive.} \qquad (5.2)$$

Then, the linear Hamiltonian system can be transformed to a canonizable system with the coordinate transformation $\hat{\boldsymbol{x}}(t) = \boldsymbol{C}\boldsymbol{x}(t)$ *which we call* *energy coordinates.*

One possible choice for $\boldsymbol{C}$ in Theorem 5.4 is $\boldsymbol{C} = \boldsymbol{H}^{1/2}$ if $\boldsymbol{H}$ is positive-definite, which we will consider in the remainder of this chapter.

Proof. Applying the proposed state transformation $\hat{\boldsymbol{x}}(t) = \boldsymbol{C}\boldsymbol{x}(t)$ and using the Hamiltonian system (2.22) with quadratic Hamiltonian (2.23) yields

$$\frac{\mathrm{d}}{\mathrm{d}t}\hat{\boldsymbol{x}}(t) = \boldsymbol{C}\frac{\mathrm{d}}{\mathrm{d}t}\boldsymbol{x}(t) \overset{(2.22)}{=} \boldsymbol{C}\boldsymbol{\omega}^{-1}\underbrace{\boldsymbol{H}}_{=\boldsymbol{C}^{\top}\boldsymbol{C}}\boldsymbol{x}(t) = \hat{\boldsymbol{\omega}}^{-1}\hat{\boldsymbol{x}}(t).$$

The matrix $\hat{\boldsymbol{\omega}}^{-1}$ is by construction skew-symmetric and by assumption (5.2), this matrix is Hamiltonian-positive, which makes the transformed system a canonizable system. $\square$

We give a characterization of the assumption (5.2) for systems with a separable, quadratic Hamiltonian with positive-definite blocks.

Lemma 5.5 (Transformation to energy coordinates for a separable, quadratic Hamiltonian in canonical coordinates): *Consider a linear canonical Hamiltonian system with a separable, quadratic Hamiltonian (see* Definition 2.30*) and positive define blocks* $\boldsymbol{H}_q$ *and* $\boldsymbol{H}_p$ *in canonical coordinates (i.e.* $\omega = \mathbb{J}_{2\bar{N}}^{\top}$*). Then, assumption* (5.2) *is fulfilled for* $\boldsymbol{C} = \boldsymbol{H}^{1/2}$ *if and only if the two matrices* $\boldsymbol{H}_q, \boldsymbol{H}_p \in \mathbb{R}^{\bar{N}\times\bar{N}}$ *commute.*

Proof. By assumption, the blocks $\boldsymbol{H}_q$ and $\boldsymbol{H}_p$ are symmetric and positive-definite and thus, so are $\boldsymbol{H}_q^{1/2}$ and $\boldsymbol{H}_p^{1/2}$. Then, $\boldsymbol{H} = \mathrm{blkdiag}(\boldsymbol{H}_q, \boldsymbol{H}_p)$ is also symmetric and positive-definite

and $C = H^{1/2}$ is well-defined. We need to show that $\widehat{\omega}^{-1} = C\mathbb{J}_{2\bar{N}}C^\top$ is Hamiltonian-positive if and only if H_q and H_p commute. By Definition 5.1, "$\widehat{\omega}^{-1}$ Hamiltonian-positive" is equivalent to "$\mathbb{J}_{2\bar{N}}^\top \widehat{\omega}^{-1}$ symmetric and positive-definite". Moreover, it holds for this matrix

$$
\mathbb{J}_{2\bar{N}}^\top \widehat{\omega}^{-1} = \begin{bmatrix} \mathbf{0}_{\bar{N}\times\bar{N}} & -I_{\bar{N}} \\ I_{\bar{N}} & \mathbf{0}_{\bar{N}\times\bar{N}} \end{bmatrix} \begin{bmatrix} H_q^{1/2} & \mathbf{0}_{\bar{N}\times\bar{N}} \\ \mathbf{0}_{\bar{N}\times\bar{N}} & H_p^{1/2} \end{bmatrix} \begin{bmatrix} \mathbf{0}_{\bar{N}\times\bar{N}} & I_{\bar{N}} \\ -I_{\bar{N}} & \mathbf{0}_{\bar{N}\times\bar{N}} \end{bmatrix} \begin{bmatrix} H_q^{1/2} & \mathbf{0}_{\bar{N}\times\bar{N}} \\ \mathbf{0}_{\bar{N}\times\bar{N}} & H_p^{1/2} \end{bmatrix}
$$

$$
= \begin{bmatrix} H_p^{1/2}H_q^{1/2} & \mathbf{0}_{\bar{N}\times\bar{N}} \\ \mathbf{0}_{\bar{N}\times\bar{N}} & H_q^{1/2}H_p^{1/2} \end{bmatrix}.
$$

Due to the block-diagonal structure, $\mathbb{J}_{2\bar{N}}^\top \widehat{\omega}^{-1}$ is symmetric and positive-definite if and only if $H_p^{1/2}H_q^{1/2}$ and $H_q^{1/2}H_p^{1/2}$ are symmetric and positive-definite. We prove that this is equivalent to the fact "H_p and H_p commute" separately for each direction:

" $\Longrightarrow$ ": By assumption $H_q^{1/2}$, $H_p^{1/2}$, $H_p^{1/2}H_q^{1/2}$, and $H_q^{1/2}H_p^{1/2}$ are symmetric. Then, H_q and H_p commute since

$$
H_p^{1/2}H_q^{1/2} = \left(H_p^{1/2}H_q^{1/2}\right)^\top = \left(H_q^{1/2}\right)^\top \left(H_p^{1/2}\right)^\top = H_q^{1/2}H_p^{1/2},
$$

$$
H_pH_q = H_p^{1/2}H_p^{1/2}H_q^{1/2}H_q^{1/2} = H_q^{1/2}H_q^{1/2}H_p^{1/2}H_p^{1/2} = H_qH_p.
$$

" $\Longleftarrow$ ": By assumption H_p and H_q are symmetric, positive-definite and commute. The same holds for the respective matrix square roots. Then (a) the products $H_p^{1/2}H_q^{1/2}$ and $H_q^{1/2}H_p^{1/2}$ are symmetric, and, thus, (b) those products are positive-definite (see e.g. [56, p. 469]). $\qquad\square$

A notable property of a canonizable matrix $A = \mathbb{J}_{2\bar{N}}G$ is that $\mathbb{J}_{2\bar{N}}$ commutes with G.

Lemma 5.6: *Consider a canonizable matrix $A = \mathbb{J}_{2\bar{N}}G \in \mathbb{R}^{2\bar{N}\times 2\bar{N}}$. Then, $\mathbb{J}_{2\bar{N}}$ commutes with A.*

Proof. Since A is skew-symmetric, G is symmetric and $\mathbb{J}_{2\bar{N}}$ skew-symmetric, it holds

$$
\mathbf{0}_{2\bar{N}\times 2\bar{N}} = A + (A)^\top = \mathbb{J}_{2\bar{N}}G + G^\top \mathbb{J}_{2\bar{N}}^\top = \mathbb{J}_{2\bar{N}}G - G\mathbb{J}_{2\bar{N}}.
$$

$\qquad\square$

5.2 Optimal Bases for Symplectic MOR

We show in the time-continuous setting of basis generation (see Section 2.2.3.2) with $\boldsymbol{g} = \boldsymbol{I}_{2\bar{N}}$ that the POD computes an optimal basis for the time-continuous analogue of the PSD under the assumptions that: (i) the solution is from a canonizable system (5.1), (ii) the solution is periodic with period $T > 0$, and (iii) the integration time in the time-continuous POD T_{POD} is an l-multiple, $l \in \mathbb{N}$, of $T/2$, i.e. $T_{\mathrm{POD}} = lT/2$. The workflow is the following: (a) we introduce the time-continuous PSD (below), (b) characterize solutions of a canonizable system via the solution formula for autonomous linear systems (Section 5.2.1), (c) compute the eigenpairs of the time-continuous POD operator (Section 5.2.2), (d) show that the time-continuous POD admits a symplectic basis that is optimal in the sense of the time-continuous PSD (Section 5.2.3).

Definition 5.7 (Time-continuous PSD): *Given a solution $x(\cdot) \in C^1(I_t, \mathbb{V})$ to a Hamiltonian FOM (2.22), the time-continuous PSD computes a subspace $\tilde{\mathbb{V}}^{\mathrm{tcPSD}} := \mathrm{span}\left\{ \tilde{e}_i^{\mathrm{tcPSD}}, \tilde{f}_i^{\mathrm{tcPSD}} \right\}_{i=1}^{\bar{n}}$ by identifying a canonical basis via the time-continuous PSD problem*

$$\tilde{\mathbb{V}}^{\mathrm{tcPSD}} := \mathrm{span}\left\{ \tilde{e}_i^{\mathrm{tcPSD}}, \tilde{f}_i^{\mathrm{tcPSD}} \right\}_{i=1}^{\bar{n}} = \underset{\substack{\tilde{\mathbb{V}} = \mathrm{span}\left\{ \tilde{e}_i, \tilde{f}_i \right\}_{i=1}^{\bar{n}} \subset \mathbb{V}, \\ \omega(\tilde{e}_i, \tilde{f}_j) = -\delta_{ij} \text{ for } 1 \le i,j \le \bar{n}}}{\mathrm{argmin}} \int_{t_0}^{T_{\mathrm{PSD}}} \left\| x(t) - \Pi_{\omega, \tilde{\mathbb{V}}}(x(t)) \right\|_g^2 \, \mathrm{d}t$$

(5.3)

with an integration time $T_{\mathrm{PSD}} \in (t_0, t_{\mathrm{end}}]$. For the ROB matrix $\boldsymbol{V}^{\mathrm{tcPSD}}$, the time-continuous PSD problem in coordinates reads

$$\boldsymbol{V}^{\mathrm{tcPSD}} = \underset{\substack{\boldsymbol{V} \in \mathbb{R}^{2\bar{N} \times 2\bar{n}} \\ \boldsymbol{V}^\top \boldsymbol{\omega} \boldsymbol{V} = \mathbb{J}_{2\bar{n}}^\top}}{\mathrm{argmin}} \underbrace{\int_{t_0}^{T_{\mathrm{PSD}}} \left\| (\boldsymbol{I}_{2\bar{N}} - \boldsymbol{V} \mathbb{J}_{2\bar{n}} \boldsymbol{V}^\top \boldsymbol{\omega}) \boldsymbol{x}(t) \right\|_g^2 \, \mathrm{d}t}_{=: \mathcal{F}_{\mathrm{PSD}}(\boldsymbol{V}; T_{\mathrm{PSD}})} . \tag{5.4}$$

5.2.1 Solutions of a Canonizable System

In the following, we consider a canonizable matrix $\boldsymbol{A} = \mathbb{J}_{2\bar{N}} \boldsymbol{G} \in \mathbb{R}^{2\bar{N} \times 2\bar{N}}$ (see Definition 5.3). We characterize its eigendecomposition to formulate the solutions of a canonizable system via the solution formula for autonomous linear systems.

Assumption 5.8: *In order to simplify the analysis, we assume that the pairs of eigenvalues of $\boldsymbol{G}$ are pairwise distinct, i.e. $\gamma_i \ne \gamma_j$ for $i \ne j$ for all $1 \le i, j \le \bar{N}$.*

Lemma 5.9 (Eigendecomposition of G): *If (γ, v) is an eigenpair of G, then $(\gamma, \mathbb{J}_{2\bar{N}} v)$ is another eigenpair of G. Thus,*

$$G = Z \begin{bmatrix} \Gamma & \\ & \Gamma \end{bmatrix} Z^\top \tag{5.5}$$

is an eigendecomposition of G with the diagonal matrix of eigenvalues $\Gamma := \mathrm{diag}\,(\gamma_1, \dots, \gamma_{\bar{N}})$, $\gamma_i > 0$ for $1 \le i \le \bar{N}$ and an orthosymplectic matrix $Z := \left[Q, \; \mathbb{J}_{2\bar{N}}^\top Q \right] \in \mathbb{R}^{2\bar{N} \times 2\bar{N}}$ of eigenvectors with $Q \in \mathbb{R}^{2\bar{N} \times \bar{N}}$.

Proof. G has eigenpairs (γ_i, q_i) with real eigenvalues $\gamma_i > 0$ and real eigenvectors $q_i \in \mathbb{R}^{2\bar{N}}$ since it is symmetric and positive-definite. By Lemma 5.6, G commutes with $\mathbb{J}_{2\bar{N}}$. Thus, $(\gamma_i, \mathbb{J}_{2\bar{N}} q_i)$ is another eigenpair of G with $q_i \perp \mathbb{J}_{2\bar{N}} q_i$ and (5.5) is an eigendecomposition of G with $Q := [q_i]_{i=1}^{\bar{N}}$. By construction of Q, it holds $Q^\top Q = I_{\bar{N}}$ and $Q^\top \mathbb{J}_{2\bar{N}} Q = 0_{\bar{N} \times \bar{N}}$, which is why Z is an orthosymplectic matrix by Lemma 3.2 point (ii). $\qquad\square$

Lemma 5.10 (Decomposition of A): *With Z and Γ from Lemma 5.9, it holds*

$$A = Z \begin{bmatrix} & \Gamma \\ -\Gamma & \end{bmatrix} Z^\top. \tag{5.6}$$

Proof. Left-multiply (5.5) with $\mathbb{J}_{2\bar{N}}$ and use that Z commutes with $\mathbb{J}_{2\bar{N}}$ since, by Lemma 5.9, $Z = \left[Q, \; \mathbb{J}_{2\bar{N}}^\top Q \right]$ and thus $\mathbb{J}_{2\bar{N}} Z = [\mathbb{J}_{2\bar{N}} Q, \; Q] = [Q, \; -\mathbb{J}_{2\bar{N}} Q] \, \mathbb{J}_{2\bar{N}} = Z \mathbb{J}_{2\bar{N}}$. $\qquad\square$

In the following, we use the 2-by-2 rotation matrix and a few selected properties.

Lemma 5.11: *For the 2-by-2 rotation matrix*

$$R_2(\theta) := \begin{bmatrix} \cos(\theta) & \sin(\theta) \\ -\sin(\theta) & \cos(\theta) \end{bmatrix} \in \mathbb{R}^{2 \times 2},$$

it holds with the notation $\sigma\,(\cdot)$ for the spectrum of a matrix that for all $\theta \in \mathbb{R}$

1. $R_2(\theta) = \exp(\mathbb{J}_2 \theta)$,

2. $\frac{\mathrm{d}}{\mathrm{d}\theta} R_2 \big|_\theta = R_2(\theta + \pi/2)$,

3. $\int R_2(\theta) \mathrm{d}\theta = R_2(\theta - \pi/2)$,

4. $R_2(\theta + \pi) = -R_2(\theta)$,

5. $(R_2(\varphi))^\top R_2(\theta) = R_2(\theta - \varphi)$,

6. $\sigma\,(R_2(\theta)) = \{\exp(\mathrm{i}\theta), \exp(-\mathrm{i}\theta)\}$.

Proposition 5.12 (Solution of canonizable system and important properties): *The solution of a canonizable system* (5.1) *can be written as*

$$\boldsymbol{x}(t) = \boldsymbol{Z}\boldsymbol{R}(\boldsymbol{\gamma}t)\boldsymbol{y}_0, \qquad \boldsymbol{y}_0 := \boldsymbol{Z}^\top \boldsymbol{x}_0, \qquad \boldsymbol{R}(\boldsymbol{\gamma}t) := \sum_{j=1}^{\bar{N}} \boldsymbol{P}_j \boldsymbol{R}_2(\gamma_j t)\boldsymbol{P}_j^\top, \qquad (5.7)$$

with $\boldsymbol{\gamma} := (\gamma_1, \dots, \gamma_{\bar{N}}) \in \mathbb{R}^{\bar{N}}$, $\boldsymbol{P}_i := [\boldsymbol{e}_i, \boldsymbol{e}_{\bar{N}+i}] \in \mathbb{R}^{2\bar{N}\times 2}$, *and* $\boldsymbol{e}_i \in \mathbb{R}^{2\bar{N}}$ *the i-th standard basis vector. For a periodic solution* $\boldsymbol{x}(T+t) = \boldsymbol{x}(t)$ *of* (5.1) *with period $T > 0$, either of the two cases holds true for each* $1 \le i \le \bar{N}$:

1. $\boldsymbol{P}_i^\top \boldsymbol{y}_0 = [\boldsymbol{z}_i, \ \mathbb{J}_{2\bar{N}}\boldsymbol{z}_i]^\top \boldsymbol{x}_0 = \boldsymbol{0}_{2\times 1}$ *(i.e. the $\boldsymbol{x}_0$ is orthogonal to $\boldsymbol{z}_i$ and $\mathbb{J}_{2\bar{N}}\boldsymbol{z}_i$),*

2. *there exists an* $l_i \in \mathbb{N}$ *such that* $T = l_i T_i$ *for* $T_i := 2\pi/\gamma_i$ *(i.e. the l_i-multiple of the period T_i is contained within the whole period T).*

Proof. According to the solution formula for autonomous linear systems, the solution $\boldsymbol{x}(t)$ of a canonizable system (5.1) can be expressed with the matrix exponential as $\boldsymbol{x}(t) = \exp(\boldsymbol{A}t)\boldsymbol{x}_0$. We define $\boldsymbol{P} := [\boldsymbol{P}_i]_{i=1}^{\bar{N}} \in \mathbb{R}^{2\bar{N}\times 2\bar{N}}$ to stack all $\boldsymbol{P}_i$ in its columns. Due to $\boldsymbol{P}_i^\top \boldsymbol{P}_j = \delta_{ij}\boldsymbol{I}_2$, it holds $\boldsymbol{P}^\top \boldsymbol{P} = \boldsymbol{I}_{2\bar{N}}$. With $\boldsymbol{Z}, \boldsymbol{\Gamma}$ from Lemma 5.10, it holds

$$\begin{bmatrix} & \boldsymbol{\Gamma}t \\ -\boldsymbol{\Gamma}t & \end{bmatrix} = \sum_{i=1}^{\bar{N}} \boldsymbol{P}_i \mathbb{J}_2 \gamma_i t \boldsymbol{P}_i^\top = \boldsymbol{P}\,\mathrm{blkdiag}\,(\mathbb{J}_2\gamma_1 t, \dots, \mathbb{J}_2\gamma_{\bar{N}}t)\boldsymbol{P}^\top$$

and with properties of the matrix exponential due to $\boldsymbol{Z}^\top \boldsymbol{Z} = \boldsymbol{I}_{2\bar{N}}$, $\boldsymbol{P}^\top \boldsymbol{P} = \boldsymbol{I}_{2\bar{N}}$, and with Lemma 5.11 item 1

$$
\begin{aligned}
\exp(\boldsymbol{A}t) &= \boldsymbol{Z}\exp\left(\begin{bmatrix} & \boldsymbol{\Gamma} \\ -\boldsymbol{\Gamma} & \end{bmatrix}t\right)\boldsymbol{Z}^\top \\
&= \boldsymbol{Z}\boldsymbol{P}\exp(\mathrm{blkdiag}\,(\mathbb{J}_2\gamma_1 t, \dots, \mathbb{J}_2\gamma_{\bar{N}}t))\boldsymbol{P}^\top \boldsymbol{Z}^\top \\
&= \boldsymbol{Z}\boldsymbol{P}\,\mathrm{blkdiag}\,(\exp(\mathbb{J}_2\gamma_1 t), \dots, \exp(\mathbb{J}_2\gamma_{\bar{N}}t))\boldsymbol{P}^\top \boldsymbol{Z}^\top \\
&= \boldsymbol{Z}\boldsymbol{P}\,\mathrm{blkdiag}\,(\boldsymbol{R}_2(\gamma_1 t), \dots, \boldsymbol{R}_2(\mathbb{J}_2\gamma_{\bar{N}}t))\boldsymbol{P}^\top \boldsymbol{Z}^\top \\
&= \boldsymbol{Z}\sum_{i=1}^{\bar{N}} \boldsymbol{P}_i \boldsymbol{R}_2(\gamma_i t)\boldsymbol{P}_i^\top \boldsymbol{Z}^\top
\end{aligned}
$$

from which (5.7) follows. In the case of a periodic solution $\boldsymbol{x}(t)$ with period $T > 0$, it holds

with $\boldsymbol{P}_i^\top \boldsymbol{P}_j = \delta_{ij}\boldsymbol{I}_2$ for each $1 \leq i \leq \bar{N}$,

$$\boldsymbol{P}_i^\top \boldsymbol{Z}^\top \boldsymbol{x}(t) = \boldsymbol{R}_2(\gamma_i t)\boldsymbol{P}_i^\top \boldsymbol{y}_0 \overset{!}{=} \boldsymbol{R}_2(\gamma_i(t+T))\boldsymbol{P}_i^\top \boldsymbol{y}_0 = \boldsymbol{P}_i^\top \boldsymbol{Z}^\top \boldsymbol{x}(t+T).$$

Multiplication with $(\boldsymbol{R}_2(\gamma_i t))^\top$ from the left implies with Lemma 5.11 item 5

$$\boldsymbol{P}_i^\top \boldsymbol{y}_0 \overset{!}{=} (\boldsymbol{R}_2(\gamma_i t))^\top \boldsymbol{R}_2(\gamma_i(t+T))\boldsymbol{P}_i^\top \boldsymbol{y}_0 = \boldsymbol{R}_2(\gamma_i T)\boldsymbol{P}_i^\top \boldsymbol{y}_0.$$

So necessarily either $\boldsymbol{P}_i^\top \boldsymbol{y}_0 = \boldsymbol{0}_{\bar{N}\times 1}$ or $\boldsymbol{P}_i^\top \boldsymbol{y}_0$ is an eigenvector with eigenvalue 1 of $\boldsymbol{R}_2(\gamma_i T)$, where the latter is by Lemma 5.11 item 6 only possible for $\gamma_i T = 2\pi l_i$ for some $l_i \in \mathbb{N}$. $\square$

5.2.2 Eigenpairs of Time-Continuous POD Operator

In the remainder, we assume that $\boldsymbol{x}(t)$ is a periodic solution. To evaluate the time-continuous POD functional, we have to analyze integrals over products $\boldsymbol{x}(t)\,(\boldsymbol{x}(t))^\top$ of the solution. The following lemma computes the relevant integrals by hand.

Lemma 5.13 (Relevant integrals of quadratic products of the solution): *Consider* T, $\boldsymbol{P}_i$, $\boldsymbol{R}_2(t)$, $\boldsymbol{y}_0$ *and* γ_i *from Proposition 5.12,* $l \in \mathbb{N}$, *and* $1 \leq i, j \leq \bar{N}$ *with* $i \neq j$. *Then*

$$\begin{aligned}
\boldsymbol{M}_{ij}(l) &:= \int_0^{lT/2} \boldsymbol{R}_2(\gamma_i t)\boldsymbol{P}_i^\top \boldsymbol{y}_0 \left(\boldsymbol{R}_2(\gamma_j t)\boldsymbol{P}_j^\top \boldsymbol{y}_0\right)^\top \mathrm{d}t = \boldsymbol{0}_{2\times 2}, \\
\boldsymbol{M}_{ii}(l) &:= \int_0^{lT/2} \boldsymbol{R}_2(\gamma_i t)\boldsymbol{P}_i^\top \boldsymbol{y}_0 \left(\boldsymbol{R}_2(\gamma_i t)\boldsymbol{P}_i^\top \boldsymbol{y}_0\right)^\top \mathrm{d}t = \lambda_i(l)\boldsymbol{I}_2
\end{aligned} \tag{5.8}$$

with $\lambda_i(l) = lT/4\,\|\boldsymbol{P}_i^\top \boldsymbol{y}_0\|_2^2$.

Proof. If $\boldsymbol{P}_i^\top \boldsymbol{y}_0 = \boldsymbol{0}_{2\times 1}$ (or $\boldsymbol{P}_j^\top \boldsymbol{y}_0 = \boldsymbol{0}_{2\times 1}$), the identity for $\boldsymbol{M}_{ii}(l)$ (for $\boldsymbol{M}_{ij}(l)$, respectively) is fulfilled trivially. Thus, we consider the case $\boldsymbol{P}_i^\top \boldsymbol{y}_0 \neq \boldsymbol{0}_{2\times 1}$, $\boldsymbol{P}_j^\top \boldsymbol{y}_0 \neq \boldsymbol{0}_{2\times 1}$ for the rest of the proof. In this case, it holds by Proposition 5.12 $\gamma_i T = 2\pi l_i$ and $\gamma_j T = 2\pi l_j$. Moreover, we start with the case $l = 1$. Applying partial integration in $\boldsymbol{M}_{ij}(1)$ twice leads with the properties from Lemma 5.11 for $\boldsymbol{R}_2(\theta)$ to

$$\boldsymbol{M}_{ij}(1) = \underbrace{\frac{1}{\gamma_i}\boldsymbol{R}_2(\gamma_i t - \pi/2)\boldsymbol{P}_i^\top \boldsymbol{y}_0 \left(\boldsymbol{R}_2(\gamma_j t)\boldsymbol{P}_j^\top \boldsymbol{y}_0\right)^\top \Big|_0^{T/2}}_{=\boldsymbol{0}_{2\times 2}}$$
$$- \frac{\gamma_j}{\gamma_i}\int_0^{T/2} \boldsymbol{R}_2(\gamma_i t - \pi/2)\boldsymbol{P}_i^\top \boldsymbol{y}_0 \left(\boldsymbol{R}_2(\gamma_j t + \pi/2)\boldsymbol{P}_j^\top \boldsymbol{y}_0\right)^\top \mathrm{d}t$$

$$= -\frac{\gamma_j}{\gamma_i^2} \underbrace{\boldsymbol{R}_2(\gamma_i t - \pi/2) \boldsymbol{P}_i^\top \boldsymbol{y}_0 \left(\boldsymbol{R}_2(\gamma_j t) \boldsymbol{P}_j^\top \boldsymbol{y}_0\right)^\top \Big|_0^{T/2}}_{=\boldsymbol{0}_{2\times 2}}$$

$$+ \frac{\gamma_j^2}{\gamma_i^2} \int_0^{T/2} \underbrace{\boldsymbol{R}_2(\gamma_i t - \pi)}_{=-\boldsymbol{R}_2(\gamma_i t)} \boldsymbol{P}_i^\top \boldsymbol{y}_0 \big(\underbrace{\boldsymbol{R}_2(\gamma_j t + \pi)}_{=-\boldsymbol{R}_2(\gamma_j t)} \boldsymbol{P}_j^\top \boldsymbol{y}_0\big)^\top \mathrm{d}t = \frac{\gamma_j^2}{\gamma_i^2} \boldsymbol{M}_{ij}(1),$$

where the terms for $t = 0$ and $t = T/2$ cancel out each other in both boundary terms since $\gamma_i T/2 = \pi l_i$ and $\gamma_j T/2 = \pi l_j$, and using Lemma 5.11 item 4. Thus, it holds that $(1 - (\gamma_j/\gamma_i)^2)\boldsymbol{M}_{ij}(1) = \boldsymbol{0}_{2\times 2}$, which shows with Assumption 5.8 that $\boldsymbol{M}_{ij}(1) = \boldsymbol{0}_{2\times 2}$ if $i \neq j$. For $\boldsymbol{M}_{ii}(1)$, direct computation shows $\boldsymbol{M}_{ii}(1) = \lambda_i(1)\boldsymbol{I}_2$ with $\lambda_i(1) = T/4\|\boldsymbol{P}_i^\top \boldsymbol{y}_0\|_2^2$ due to the identities

$$\int_0^{T/2} \sin^2(\gamma_i t)\mathrm{d}t = \int_0^{T/2} \cos^2(\gamma_i t)\mathrm{d}t = T/4, \qquad \int_0^{T/2} \cos(\gamma_i t)\sin(\gamma_i t)\mathrm{d}t = 0.$$

The case $l > 1$ can be redirected to $l = 1$ (exemplified for $l = 2$): The integral in $\boldsymbol{M}_{ij}(2)$ can be split in (a) $t \in [0, T/2]$ and (b) $t \in [T/2, T]$. The integral (a) is treated as above, while for (b), we use that $\gamma_i T/2 = \pi l_i$ and $\gamma_j T/2 = \pi l_j$, from which it follows with Lemma 5.11 item 4 that $\boldsymbol{R}_2(\gamma_i(t + T/2)) = \pm\boldsymbol{R}_2(\gamma_i t)$ and $\boldsymbol{R}_2(\gamma_j(t + T/2)) = \pm\boldsymbol{R}_2(\gamma_j t)$. Thus, $\boldsymbol{M}_{ij}(2) = \boldsymbol{M}_{ij}(1) \pm \boldsymbol{M}_{ij}(1) = \boldsymbol{0}_{2\times 2}$ and, in general, $\boldsymbol{M}_{ij}(l) = \boldsymbol{0}_{2\times 2}$. Similarly, it holds $\boldsymbol{M}_{ii}(l) = l\boldsymbol{M}_{ii}(1)$. $\qquad\square$

Proposition 5.14 (Eigenpairs of time-continuous POD operator): *Consider a periodic solution of a canonizable system* (5.1) *with* $\boldsymbol{x}(t) = \boldsymbol{Z}\boldsymbol{R}(\boldsymbol{\gamma}t)\boldsymbol{y}_0$ *in the notation of Proposition 5.12. Then, the columns* $\boldsymbol{z}_i$ *and* $\boldsymbol{z}_{\bar{N}+1}$ *of* $\boldsymbol{Z}$ *are eigenvectors of the POD operator* $\mathcal{R}$ *from* (2.19) *for* $T_{\mathrm{POD}} = lT/2$ *with eigenvalue* $\lambda_i(l) = T/4\|\boldsymbol{P}_i^\top \boldsymbol{y}_0\|_2^2$ *for all* $1 \leq i \leq \bar{N}$.

Proof. Consider an arbitrary but fixed $i \in \{1, \ldots, \bar{N}\}$ and a pair $[\boldsymbol{z}_i, \boldsymbol{z}_{\bar{N}+i}] = \boldsymbol{Z}\boldsymbol{P}_i$ of columns of $\boldsymbol{Z}$. It holds with Proposition 5.12

$$(\boldsymbol{x}(t))^\top \boldsymbol{Z}\boldsymbol{P}_i = \boldsymbol{y}_0^\top (\boldsymbol{R}(\boldsymbol{\gamma}t))^\top \boldsymbol{Z}^\top \boldsymbol{Z}\boldsymbol{P}_i = \boldsymbol{y}_0^\top (\boldsymbol{R}(\boldsymbol{\gamma}t))^\top \boldsymbol{P}_i.$$

Due to the pairwise orthogonality $\boldsymbol{P}_j^\top \boldsymbol{P}_i = \delta_{ij}\boldsymbol{I}_2$ with the Kronecker delta δ_{ij}, it holds

$$(\boldsymbol{x}(t))^\top \boldsymbol{Z}\boldsymbol{P}_i = \boldsymbol{y}_0^\top \left(\sum_{j=1}^{\bar{N}} \boldsymbol{P}_j (\boldsymbol{R}_2(\gamma_j t))^\top \boldsymbol{P}_j^\top\right) \boldsymbol{P}_i = \boldsymbol{y}_0^\top \boldsymbol{P}_i (\boldsymbol{R}_2(\gamma_i t))^\top. \qquad (5.9)$$

Applying $\mathcal{R}$ to z_i and $z_{\bar{N}+1}$ yields with $ZP_i = [z_i,\ z_{\bar{N}+i}]$

$$[\mathcal{R}(z_i),\ \mathcal{R}(z_{\bar{N}+i})] = \int_0^{lT/2} x(t)\underbrace{(x(t))^\top ZP_i}_{\overset{(5.9)}{=}y_0^\top P_i(R_2(\gamma_i t))^\top}\ \mathrm{d}t = Z\int_0^{lT/2} R(\gamma t)y_0\left(R_2(\gamma_i t)P_i^\top y_0\right)^\top \mathrm{d}t.$$

Inserting the definition of $R(\gamma t)$ from (5.7) yields

$$[\mathcal{R}(z_i),\ \mathcal{R}(z_{\bar{N}+i})] = Z\sum_{j=1}^{\bar{N}} P_j \underbrace{\int_0^{lT/2} R_2(\gamma_j t)P_j^\top y_0\left(R_2(\gamma_i t)P_i^\top y_0\right)^\top \mathrm{d}t}_{=M_{ij}(l)\overset{(5.8)}{=}\delta_{ij}\lambda_i(l)I_2} = \lambda_i(l)ZP_i,$$

which shows that z_i and $z_{\bar{N}+1}$ are eigenvectors of $\mathcal{R}$ with eigenvalue $\lambda_i(l)$. $\square$

5.2.3 Optimal Solution of the Time-Continuous PSD

Based on the previous lemmas, the following theorem shows that the POD computes an orthosymplectic ROB for $T_{\mathrm{PSD}} = T_{\mathrm{POD}} = lT/2$ with $l \in \mathbb{N}$ and moreover that this is an optimal ROB for the PSD functional.

Theorem 5.15 (Optimality of PSD): *Consider a canonizable Hamiltonian system* (5.1) *for which G fulfills Assumption 5.8 and which has a periodic solution $x(t) = x(t + T)$. Then, an optimal solution of the time-continuous PSD with $T_{\mathrm{PSD}} = lT/2$ can be computed with the time-continuous POD with $T_{\mathrm{POD}} = lT/2$ for $l \in \mathbb{N}$.*

Proof. Assume $\tilde{\mathbb{V}}^{\mathrm{tcPSD}}$ is an optimal subspace resulting from the time-continuous PSD (2.27) with ROB matrix $V^{\mathrm{tcPSD}} \in \mathbb{R}^{2\bar{N}\times 2\bar{n}}$. Our goal is to construct an orthosymplectic ROB matrix from the time-continuous POD $V^{\mathrm{tcPOD}} \in \mathbb{R}^{2\bar{N}\times 2\bar{n}}$ such that this basis is optimal in the PSD functional, i.e. $\mathcal{F}_{\mathrm{PSD}}(V^{\mathrm{tcPSD}}; lT/2) = \mathcal{F}_{\mathrm{PSD}}(V^{\mathrm{tcPOD}}; lT/2)$.

Consider $x(t) = ZR(\gamma t)y_0$ in the notation of Proposition 5.12. The matrix Z is orthosymplectic by Lemma 5.9. The columns of this matrix are eigenvectors of the time-continuous POD operator $\mathcal{R}$ (2.19) with $T_{\mathrm{POD}} = lT/2$ by Proposition 5.14. With Theorem 2.24, we conclude that these eigenvectors build an optimal basis in the time-continuous POD $V^{\mathrm{tcPOD}} := \left[z_1, \ldots, z_{\bar{n}}, \mathbb{J}_{2\bar{N}}^\top z_1, \ldots, \mathbb{J}_{2\bar{N}}^\top z_{\bar{n}}\right]$, which is orthosymplectic. From Lemma 3.2 point (iii), we know that $(V^{\mathrm{tcPOD}})^\top = (V^{\mathrm{tcPOD}})^+$ since the ROB matrix is orthosymplectic. This allows us to replace the symplectic projection $V^{\mathrm{tcPOD}}(V^{\mathrm{tcPOD}})^+$ with the orthogonal projection $V^{\mathrm{tcPOD}}(V^{\mathrm{tcPOD}})^\top$ and thus $\mathcal{F}_{\mathrm{PSD}}(V^{\mathrm{tcPOD}}; lT/2) = \mathcal{F}_{\mathrm{POD}}(V^{\mathrm{tcPOD}}; lT/2)$. Since $\mathcal{F}_{\mathrm{PSD}}$

optimizes over all possible symplectic matrices and $\boldsymbol{V}^{\mathrm{tcPSD}}$ is an optimal solution, we know $\mathcal{F}_{\mathrm{PSD}}(\boldsymbol{V}^{\mathrm{tcPSD}}; lT/2) \le \mathcal{F}_{\mathrm{PSD}}(\boldsymbol{V}^{\mathrm{tcPOD}}; lT/2)$ and, thus,

$$\mathcal{F}_{\mathrm{PSD}}(\boldsymbol{V}^{\mathrm{tcPSD}}; lT/2) \le \mathcal{F}_{\mathrm{PSD}}(\boldsymbol{V}^{\mathrm{tcPOD}}; lT/2) = \mathcal{F}_{\mathrm{POD}}(\boldsymbol{V}^{\mathrm{tcPOD}}; lT/2). \tag{5.10}$$

Moreover, there exists an ROB matrix $\boldsymbol{U}^{\mathrm{tcPSD}} \in \mathbb{R}^{2\bar{N} \times 2\bar{n}}$ for $\tilde{\mathbb{V}}^{\mathrm{tcPSD}}$, which has pairwise orthogonal columns (but is not necessarily symplectic). We deduce for all $\boldsymbol{x} \in \mathbb{R}^{2\bar{N}}$

$$\left\| (\boldsymbol{I}_{2\bar{N}} - \boldsymbol{V}^{\mathrm{tcPSD}}(\boldsymbol{V}^{\mathrm{tcPSD}})^{+})\boldsymbol{x} \right\|_2 \ge \left\| (\boldsymbol{I}_{2\bar{N}} - \boldsymbol{U}^{\mathrm{tcPSD}}(\boldsymbol{U}^{\mathrm{tcPSD}})^{\top})\boldsymbol{x} \right\|_2$$

since $\boldsymbol{U}^{\mathrm{tcPSD}}(\boldsymbol{U}^{\mathrm{tcPSD}})^{\top}\boldsymbol{x}$ is the best approximation in $\tilde{\mathbb{V}}^{\mathrm{tcPSD}}$ by orthogonal projection. Using (a) the previous inequality and (b) the optimality of the POD basis $\boldsymbol{V}^{\mathrm{tcPOD}}$, it holds

$$\mathcal{F}_{\mathrm{PSD}}(\boldsymbol{V}^{\mathrm{tcPSD}}; lT/2) \overset{(a)}{\ge} \mathcal{F}_{\mathrm{POD}}(\boldsymbol{U}^{\mathrm{tcPSD}}; lT/2) \overset{(b)}{\ge} \mathcal{F}_{\mathrm{POD}}(\boldsymbol{V}^{\mathrm{tcPOD}}; lT/2). \tag{5.11}$$

Combining (5.10) and (5.11), we conclude $\mathcal{F}_{\mathrm{PSD}}(\boldsymbol{V}^{\mathrm{tcPSD}}; lT/2) = \mathcal{F}_{\mathrm{POD}}(\boldsymbol{V}^{\mathrm{tcPOD}}; lT/2)$. $\qquad\square$

5.3 Numerical Experiments

We validate our theoretical findings numerically with a FOM from a discretized linear wave equation. The main focus is to verify Theorem 5.15, i.e. that the POD of a canonizable system with $T_{\mathrm{POD}} = lT/2$ for a periodic solution yields a symplectic ROB.

5.3.1 Full-Order Model

The FOM considered here is adapted from [99] and is based on the linear wave equation with homogeneous Dirichlet boundary conditions and zero initial velocity

$$\begin{aligned}
\partial_{tt}^2 u(t,\xi) &= c^2 \partial_{\xi\xi}^2 u(t,\xi), &&\text{for } (t,\xi) \in I \times \Omega, \\
u(0,\xi) &= u_0(\xi), \quad \partial_t u(0,\xi) = 0, &&\text{for } \xi \in \Omega, \\
u(t,\xi) &= 0, &&\text{for } t \in I, \xi \in \partial\Omega,
\end{aligned}$$

with a physical domain $\Omega = (-0.5, 0.5)$, time interval $I = (0, 50)$, wave speed $c = 0.1$, initial value $u_0(\xi) := h(10\,|\xi|)$ for $\xi \in \Omega$ and the spline function

$$h(s) := \begin{cases} 1 - 3/2s^2 + 3/4s^3, & 0 \le s \le 1, \\ (2 - s)^3/4, & 1 < s \le 2, \\ 0, & \text{otherwise.} \end{cases}$$

The solution of this initial-boundary-value problem is a periodic solution $u(t) = u(t + T)$ with period $T = 20$ that resembles two waves that travel in opposite directions and which are reflected at the boundary. Finite differences are used to discretize the PDE in space with a spatial step width $\Delta\xi = 1/499$ resulting in $\bar{N} = 500$ equidistant discretization points $\xi_i = -1/2 + (i-1)\Delta\xi$, $1 \le i \le \bar{N}$. This yields a canonical Hamiltonian system with a separable, quadratic Hamiltonian (2.23) with

$$\boldsymbol{H} := \begin{bmatrix} -c^2 \boldsymbol{D}_{\xi\xi} & \boldsymbol{0}_{\bar{N}\times\bar{N}} \\ \boldsymbol{0}_{\bar{N}\times\bar{N}} & \boldsymbol{I}_{\bar{N}} \end{bmatrix}, \qquad \begin{aligned} \boldsymbol{q}(t) &:= [u(t, \xi_i)]_{i=1}^{\bar{N}}, \\ \boldsymbol{p}(t) &:= [\partial u(t, \xi_i)]_{i=1}^{\bar{N}}, \end{aligned} \qquad \boldsymbol{x}(t) := \begin{bmatrix} \boldsymbol{q}(t) \\ \boldsymbol{p}(t) \end{bmatrix},$$

where $\boldsymbol{D}_{\xi\xi} \in \mathbb{R}^{\bar{N}\times\bar{N}}$ is an approximation of the second-order derivative. For time integration, the implicit midpoint rule (2.25) is used with $K = 5000$ steps and $\Delta t = 0.01$. To obtain a canonizable system, the transformation via energy coordinates (Theorem 5.4) is used with $\boldsymbol{C} = \boldsymbol{H}^{1/2}$. This transformation can be implicitly carried out by using a MOR technique with an inner-product matrix $\boldsymbol{g} = \boldsymbol{H}$. Note that this also changes the norm $\|\cdot\|_{\boldsymbol{g}}$, which is why the following results are presented for $\|\cdot\|_2$ (for $\boldsymbol{g} = \boldsymbol{I}_{2\bar{N}}$) and $\|\cdot\|_{\boldsymbol{H}}$ (for $\boldsymbol{g} = \boldsymbol{H}$).

5.3.2 Experiments

We compare the performance of four different MOR techniques (see Table 5.1) for the reproduction of the solution. The investigated methods are the (time-discrete) POD, the PSD complex SVD (PSD cSVD) for a non-canonizable system $(\boldsymbol{g} = \boldsymbol{I}_{2\bar{N}})$ and as a canonizable system $(\boldsymbol{g} = \boldsymbol{H})$. Different basis sizes $2\bar{n} \in \{10, 20, \dots, 80\}$ are considered. The ROB matrices are computed with all $K = 5000$ time steps as snapshots such that exactly 2.5 periods of the system are included in the basis generation.

MOR technique	ROB matrix	
POD ($\boldsymbol{g} = \boldsymbol{I}_{2\bar{N}}$)	$\boldsymbol{V} = \texttt{left-SVD}(\boldsymbol{X}_{\mathrm{s}})[:,:2\bar{n}]$	$\boldsymbol{W} = \boldsymbol{V}$
POD ($\boldsymbol{g} = \boldsymbol{H}$)	$\boldsymbol{V} = \boldsymbol{H}^{-1/2}\texttt{left-SVD}(\boldsymbol{H}^{1/2}\boldsymbol{X}_{\mathrm{s}})[:,:2\bar{n}]$	$\boldsymbol{W} = \boldsymbol{H}\boldsymbol{V}$
PSD cSVD ($\boldsymbol{g} = \boldsymbol{I}_{2\bar{N}}$)	$\boldsymbol{V} = [\boldsymbol{E},\ \mathbb{J}_{2\bar{N}}^{\top}\boldsymbol{E}],\ \boldsymbol{E} = [\boldsymbol{\Phi}^{\top},\ \boldsymbol{\Psi}^{\top}]^{\top}$	$\boldsymbol{W} = \boldsymbol{V}$
	$\boldsymbol{\Phi} + \mathrm{i}\boldsymbol{\Psi} = \texttt{left-cSVD}(\boldsymbol{Q}_{\mathrm{s}} + \mathrm{i}\boldsymbol{P}_{\mathrm{s}})[:,:\bar{n}]$	
PSD cSVD ($\boldsymbol{g} = \boldsymbol{H}$)	$\boldsymbol{V} = \boldsymbol{H}^{-1/2}[\boldsymbol{E},\ \mathbb{J}_{2\bar{N}}^{\top}\boldsymbol{E}],\ \boldsymbol{E} = [\boldsymbol{\Phi}^{\top},\ \boldsymbol{\Psi}^{\top}]^{\top}$	$\boldsymbol{W} = \boldsymbol{H}\boldsymbol{V}$
	$\boldsymbol{\Phi} + \mathrm{i}\boldsymbol{\Psi} = \texttt{left-cSVD}(\boldsymbol{H}_q^{1/2}\boldsymbol{Q}_{\mathrm{s}} + \mathrm{i}\boldsymbol{H}_p^{1/2}\boldsymbol{P}_{\mathrm{s}})[:,:\bar{n}]$	

Table 5.1: Summary of MOR techniques used in this section. Python notation is used to select columns. $\boldsymbol{X}_{\mathrm{s}} = [\boldsymbol{Q}_{\mathrm{s}}^{\top},\ \boldsymbol{P}_{\mathrm{s}}^{\top}]^{\top}$ denotes the snapshot matrix which is separated in parts for $\boldsymbol{q}$ and $\boldsymbol{p}$. $\texttt{left-SVD}(\cdot)$ and $\texttt{left-cSVD}(\cdot)$ denote obtaining the left-singular-vectors from SVD and the complex SVD. This table is adapted from [21].

5.3.2.1 ROB and ROM Quality

The considered error measures to evaluate the quality of the reduction are (a) the relative projection error e_{proj} and (b) the relative reduction error e_{red},

$$e_{\mathrm{proj}} := \sqrt{\frac{\sum_{k=0}^{K} \|(\boldsymbol{I}_{2\bar{N}} - \boldsymbol{V}\boldsymbol{W}^{\top})\boldsymbol{x}_k\|_{\boldsymbol{g}}^2}{\sum_{k=0}^{K} \|\boldsymbol{x}_k\|_{\boldsymbol{g}}^2}} \quad \text{and} \quad e_{\mathrm{red}} := \sqrt{\frac{\sum_{k=0}^{K} \|\boldsymbol{V}\check{\boldsymbol{x}}_k - \boldsymbol{x}_k\|_{\boldsymbol{g}}^2}{\sum_{k=0}^{K} \|\boldsymbol{x}_k\|_{\boldsymbol{g}}^2}}, \quad (5.12)$$

where $\boldsymbol{x}_k \in \mathbb{R}^{2\bar{N}}$ is the FOM solution and $\check{\boldsymbol{x}}_k \in \mathbb{R}^{2\bar{n}}$ the ROM solution for all time instances $0 \le k \le K$ and $\boldsymbol{W} \in \mathbb{R}^{2\bar{N} \times 2\bar{n}}$ is the respective matrix from Table 5.1 for the different MOR techniques.

Both error measures from (5.12) are displayed in Figure 5.1 for two different norms with inner-product matrix $\boldsymbol{g} = \boldsymbol{I}_{2\bar{N}}$ and $\boldsymbol{g} = \boldsymbol{H}$. Similarly to the numerical examples from the previous chapters, we observe that the structure-preserving methods (PSD cSVD ($\boldsymbol{g} = \boldsymbol{I}_{2\bar{N}}$), PSD cSVD ($\boldsymbol{g} = \boldsymbol{H}$) and POD ($\boldsymbol{g} = \boldsymbol{H}$)) give a reduction error comparable to what is promised by the projection error. In contrast, the POD ($\boldsymbol{g} = \boldsymbol{I}_{2\bar{N}}$) yields the best projection error for $\boldsymbol{g} = \boldsymbol{I}_{2\bar{N}}$, but fails to reproduce the same level of quality in the reduction error (up to two orders).
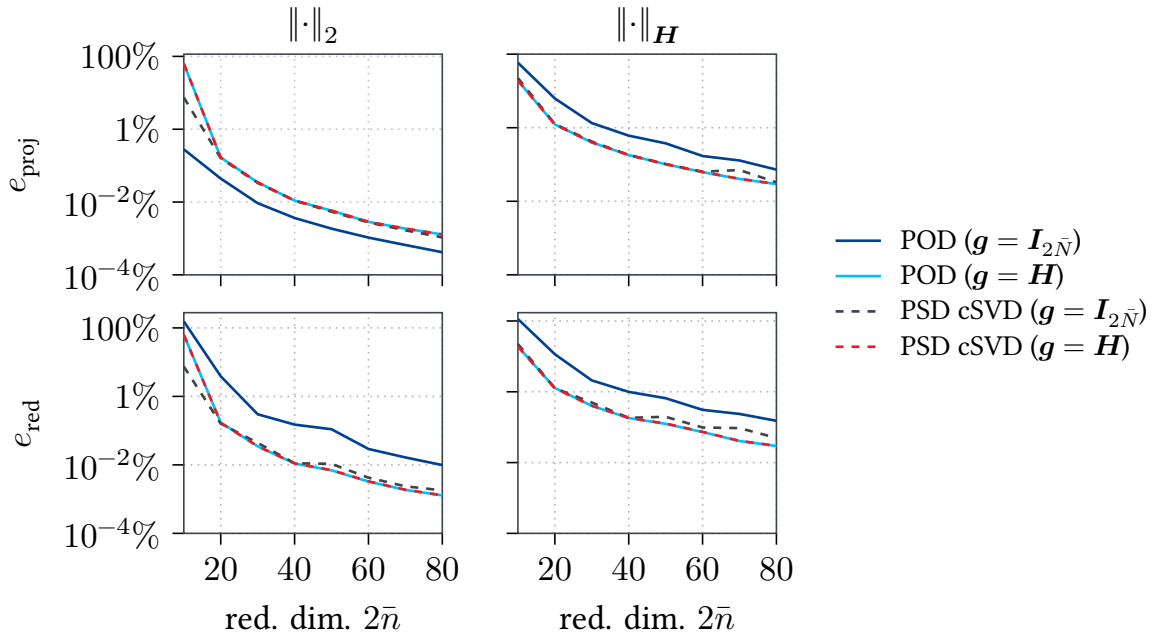
Figure 5.1: Comparison of MOR techniques from Table 5.1 for different reduced dimensions $2\bar{n} \in \{10, 20, \ldots, 80\}$. Top: relative projection error (5.12); bottom: relative reduction error (5.12); left: two-norm $\|\cdot\|_2$; right: $\|\cdot\|_H$. This figure is adapted from [21].

5.3.2.2 ROB Quality in Terms of Structure

In order to validate numerically that the POD computes a symplectic ROB matrix for a canonizable system with a periodic solution and $T_{\text{POD}} = lT/2$ with $l \in \mathbb{N}$, we investigate the error in symplecticity[1]

$$e_{\text{sympl}} := \left\| \boldsymbol{V}^\top \mathbb{J}_{2\bar{N}} \boldsymbol{V} - \mathbb{J}_{2\bar{n}} \right\|_{\text{F}}. \tag{5.13}$$

The error is analyzed for the POD ($\boldsymbol{g} = \boldsymbol{H}$) with a fixed ROB size $2\bar{n} = 10$ varying the number of (consecutive) snapshots that are used to generate the basis

$$\boldsymbol{V} = \boldsymbol{H}^{-1/2} \text{svd}(\boldsymbol{H}^{1/2} \boldsymbol{X}_{\text{s}}[:, :k])$$

with $k \in \{250, 500, \ldots, 5000\}$, which relates to increasing the integration time T_{POD} in the time-continuous formulation of the POD.

---

[1]As a technical remark: In order to group pairs of vectors for the symplecticity, we pair the singular vector with the highest singular value iteratively with the singular vector with the closest singular value while respecting that basis vectors are not selected twice.
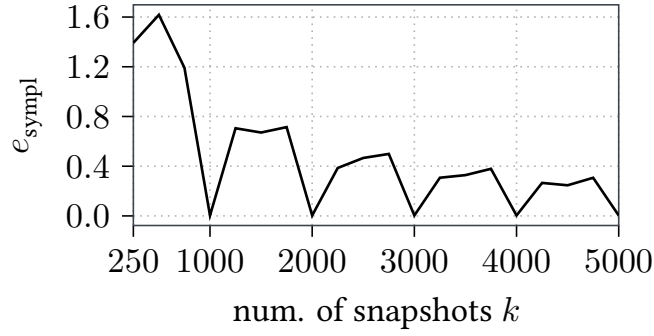
Figure 5.2: Error in symplecticity (5.13) for POD ($\boldsymbol{g} = \boldsymbol{H}$) of size $2\bar{n} = 10$ generated from a varying number of snapshots k. This figure is taken from [21].

The results for e_{sympl} are shown in Figure 5.2. One period of the solution corresponds to 2000 time steps. We see that e_{sympl} drops to zero for multiples of $k = 1000$ time steps which relates to multiples of the half period $T/2$. This strongly indicates that the symplecticity of the POD ($\boldsymbol{g} = \boldsymbol{H}$) for $T_{\text{POD}} = lT/2$ proven in Theorem 5.15 for the time-continuous POD also holds for the time-discrete counterpart. Secondly, this figure supports the assumption that the requirement of $T_{\text{POD}} = lT/2$ is indeed necessary as the error in symplecticity is non-zero for $k \neq 1000l$. Thus, it suggests that Theorem 5.15 can in general not be further generalized over the current case $T_{\text{POD}} = lT/2$. However, judging from the decreasing trend from $k = 250$ to $k = 5000$, the error in the symplecticity decreases if multiple periods are included in the snapshots which suggests that the theorem holds in the limit $T_{\text{POD}} \to \infty$.

Part II
Structure-preserving MOR on Manifolds

Model Reduction on Manifolds: A Differential Geometric Framework

6

In this chapter, we build a framework based on differential geometry to generalize the projection-based MOR introduced in Section 2.2.2 for (linear) subspaces to MOR on manifolds. The chapter is subdivided in the following steps: We

- *motivate MOR on manifolds* by revisiting Kolmogorov n-widths (Section 6.1),
- establish a *general framework for MOR on manifolds* by

  - giving a brief *introduction to differential geometry* (Section 6.2),
  - and *establishing the framework* and introducing the *manifold Petrov–Galerkin (MPG)* as a special reduction map (Section 6.3),

- extend the framework to *structure-preserving MOR on manifolds* by

  - revisiting differential geometry to introduce tensor fields as relevant *structures on manifolds* and *Lagrangian and Hamiltonian systems* (Section 6.4),
  - and introducing the *generalized manifold Galerkin (GMG)* as an alternative reduction map, which is then used for *structure-preserving MOR on manifolds* for Lagrangian and Hamiltonian systems (Section 6.4),

- and, finally, discuss how to *generate nonlinear embeddings from snapshot data* and relate the framework to different MOR techniques existing in the literature (Section 6.6).

Note that some concepts may feel repetitive to Chapter 2. However, in the present chapter, the more general case of a manifold (instead of an $\mathbb{R}$-vector-space) is discussed. The following is adapted from [24].

6.1 Limitations of MOR on Subspaces

As discussed in Section 2.2.2, the accuracy of MOR on subspaces is limited by the Kolmogorov n-widths $d_n(S)$ of the set of all solutions S. Let us emphasize at this point that MOR on subspaces has proven valuable in practice. We refer to [14, Sec. 1.1] for a comprehensive overview of applications in design, control, optimization, and uncertainty quantification. Moreover, in the case of linear coercive elliptic PDEs, it can be shown that the Kolmogorov n-widths of the set of all solutions decay (a) exponentially for problems with one parameter $d_n(S) \leq C \exp^{-\gamma n}$ for $C, \gamma > 0$ [83, 84], or (b) for multiple parameters, at least with a rate $d_n(S) \leq C \exp^{-cn^\gamma}$ for $C, c, \gamma > 0$ if the problem is affinely decomposable [4, 92]. Theoretical insight for the decay of the Kolmogorov n-widths has also been found in combination with the so-called Hankel singular values [113].

However, it has been shown that the Kolmogorov n-widths decay slowly for FOMs with transport-dominated solutions like the advection equation ($d_n(S) \geq 1/2 \cdot n^{-1/2}$, [92]) or wave equation ($d_n(S) \geq 1/4 \cdot n^{-1/2}$, [44]) with special initial values. In such cases, MOR on subspaces cannot determine an efficient ROM, as the maximum reduction error is bounded from below by the Kolmogorov n-widths (see Section 2.2.2). In order to broaden the applicability of MOR to such problems, nonlinear embeddings are recently considered. In the scope of the present thesis, we refer to such techniques as *MOR on manifolds*.

6.2 A Primer on Differential Geometry

In this section, we recall several important definitions and results from the theory of smooth manifolds to render this manuscript self-contained. Our presentation is largely based on the monograph [74]. In particular, all material within this section that is not explicitly referenced is adopted from [74]. To motivate the forthcoming definitions, we briefly discuss the tools required (i) to formulate a differential equation on a manifold, and (ii) to define a submanifold. We start by fixing some notation (Section 6.2.1). For the differential geometric formulation of the FOM, we stepwise introduce the structure of a *smooth manifold* starting from *topological spaces*. The topology allows us to characterize *continuous functions* and *smooth manifolds* (Section 6.2.2). We continue to define *continuously differentiable functions* on smooth manifolds (Section 6.2.3). Subsequently, we introduce the *tangent space* at a point on the manifold (Section 6.2.4) to be able to formulate the *differential of a function*

IVP on a vector space		IVP on a manifold	
$\mathbb{V}$	N-dim. $\mathbb{R}$-vector-space	$\mathcal{M}$	N-dim. smooth manifold
		$T_m\mathcal{M}, T\mathcal{M}$	tangent space, tangent bundle
$f\colon \mathbb{V} \to \mathbb{V}$	right-hand side	$X\colon \mathcal{M} \to T\mathcal{M}$	vector field
$x\colon \mathcal{I} \to \mathbb{V}$	solution curve	$\gamma\colon \mathcal{I} \to \mathcal{M}$	solution curve
$\frac{\mathrm{d}}{\mathrm{d}t}x(t) \in \mathbb{V}$	time-derivative	$\frac{\mathrm{d}}{\mathrm{d}t}\gamma\big|_t \in T_{\gamma(t)}\mathcal{M}$	velocity
$\begin{cases} \frac{\mathrm{d}}{\mathrm{d}t}x(t) = f(x(t)) \in \mathbb{V} \\ x(t_0) = x_0 \in \mathbb{V} \end{cases}$		$\begin{cases} \frac{\mathrm{d}}{\mathrm{d}t}\gamma\big|_t = X\big|_{\gamma(t)} \in T_{\gamma(t)}\mathcal{M} \\ \gamma(t_0) = \gamma_0 \in \mathcal{M} \end{cases}$	

Table 6.1: Formulation of an initial value problem (IVP) with time interval $\mathcal{I}$ on a vector space (left) and on a manifold (right). This table is adapted from [24].

(Section 6.2.5), which is used to generalize the time-derivative of the state to the manifold setting. In order to describe the evolution of an initial value problem, we set the right-hand side to be a *vector field* (Section 6.2.6). With these preparations, an initial value problem on a manifold can be formulated (Section 6.2.7). We refer to Table 6.1 for a comparison of a dynamical system on a vector space and on a smooth manifold. Furthermore, for the model reduction framework, we discuss embedded submanifolds (Section 6.2.9).

6.2.1 Notation

The notation of this part will be guided by the notation which is common in the differential geometric community. Thus, the notation will only be partially compatible with the notation of the first part of this thesis. A translation between Part I and Part II is offered in Table 6.1. Moreover, we use the *index notation*, which differentiates between upper indices $v^{\underline{i}}$ and lower indices $\lambda_{\underline{i}}$. Let us emphasize that indices that concern the index notation are underlined. The position of the index indicates the type of the geometric object. Furthermore, we utilize the *Einstein summation convention*, which implies the summation over an index if the index appears twice (once as a lower index and once as an upper index). For an N-dimensional vector space $\mathbb{V}$, this notation is used to abbreviate (i) the linear combination of a basis $\{E_{\underline{i}}\}_{i=1}^{N} \subset \mathbb{V}$ with coefficients $\{v^{\underline{i}}\}_{i=1}^{N} \subset \mathbb{R}$, (ii) the linear combination of a dual basis $\{F^{\underline{i}}\}_{i=1}^{N} \subset \mathbb{V}^*$ with coefficients $\{\lambda_{\underline{i}}\}_{i=1}^{N} \subset \mathbb{R}$, or (iii) the dual product of the respective coefficients,

$$\text{(i) } v^{\underline{i}}E_{\underline{i}} := \sum_{i=1}^{N} v^{\underline{i}}E_{\underline{i}} \in \mathbb{V}, \quad \text{(ii) } \lambda_{\underline{i}}F^{\underline{i}} := \sum_{i=1}^{N} \lambda_{\underline{i}}F^{\underline{i}} \in \mathbb{V}^*, \quad \text{(iii) } v^{\underline{i}}\lambda_{\underline{i}} := \sum_{i=1}^{N} v^{\underline{i}}\lambda_{\underline{i}} \in \mathbb{R}. \quad (6.1)$$

Moreover, we use $\left[v^{\underline{i}}\right]_{1 \leq i \leq N} \in \mathbb{R}^N$ to stack scalars $v^{\underline{i}} \in \mathbb{R}$ as a vector in $\mathbb{R}^N$. Further notation is introduced in Section 6.2.8.

6.2.2 Chart and Smooth Manifold

For two topological spaces $\mathcal{M}$ and $\mathcal{Q}$ (Appendix A.1.1), a map $F \colon \mathcal{M} \to \mathcal{Q}$ is called a *homeo-morphism* if (i) it is bijective (and thus the inverse $F^{-1} \colon \mathcal{Q} \to \mathcal{M}$ exists) and (ii) both F and F^{-1} are continuous. Moreover, $\mathcal{M}$ is called *locally homeomorphic to* $\mathbb{R}^N$ for $N \in \mathbb{N}$ if for every point $m \in \mathcal{M}$ there exists an open set $U \subset \mathcal{M}$ with $m \in U$ and a homeomorphism $F \colon U \to F(U) \subset \mathbb{R}^N$. A topological space $\mathcal{M}$ is called a *topological manifold* of *dimension* N if it is locally homeomorphic to $\mathbb{R}^N$ (and additionally Hausdorff and second-countable, see e.g. [74, Cha. 1 and App. A]). We denote the dimension with $\dim(\mathcal{M}) = N$.

Let $\mathcal{M}$ be a topological manifold of dimension N. A *chart* is a tuple (U, x) where the *chart domain* $U \subset \mathcal{M}$ is an open set and the *chart mapping* $x \colon U \to x\,(U) \subset \mathbb{R}^N$ is a homeomorphism. For two charts (U, x) and (V, y) with $U \cap V \neq \emptyset$, we can define the *transition mappings*

$$x \circ y^{-1} \colon y\,(U \cap V) \to x\,(U \cap V) \qquad \text{and} \qquad y \circ x^{-1} \colon x\,(U \cap V) \to y\,(U \cap V)\,,$$

which are homeomorphisms as composition of homeomorphisms (Figure 6.1). The charts (U, x) and (V, y) are called C^k-*compatible* for $k \in \mathbb{N}$ or $k = \infty$ if either $U \cap V = \emptyset$ or

$$x \circ y^{-1} \in C^k(y\,(U \cap V)\,, x\,(U \cap V)) \qquad \text{and} \qquad y \circ x^{-1} \in C^k(x\,(U \cap V)\,, y\,(U \cap V)),$$

where differentiability is defined in the classical sense since $x\,(U \cap V)\,, y\,(U \cap V) \subset \mathbb{R}^N$. A collection of charts $\mathcal{A} = \{(U_i, x_i) \mid i \in I\}$ with some index set I is called an *atlas for* $\mathcal{M}$ if $\mathcal{M} = \bigcup_{i \in I} U_i$. The atlas is called *of class* C^k (or a C^k-*atlas*) if all charts in $\mathcal{A}$ are mutually C^k-compatible. We call a C^k-atlas $\mathcal{A}$ *maximal* if all charts that are C^k-compatible with any chart in $\mathcal{A}$ are already elements of $\mathcal{A}$. If $\mathcal{A}$ is a maximal C^k-atlas for $\mathcal{M}$, then the tuple $(\mathcal{M}, \mathcal{A})$ is called a C^k-*manifold* and, in particular, a *smooth manifold* if $k = \infty$. As common in the literature, we omit the explicit mentioning of the maximal atlas whenever possible and say that $\mathcal{M}$ is a C^k-manifold, implicitly assuming a maximal C^k-atlas to be available.
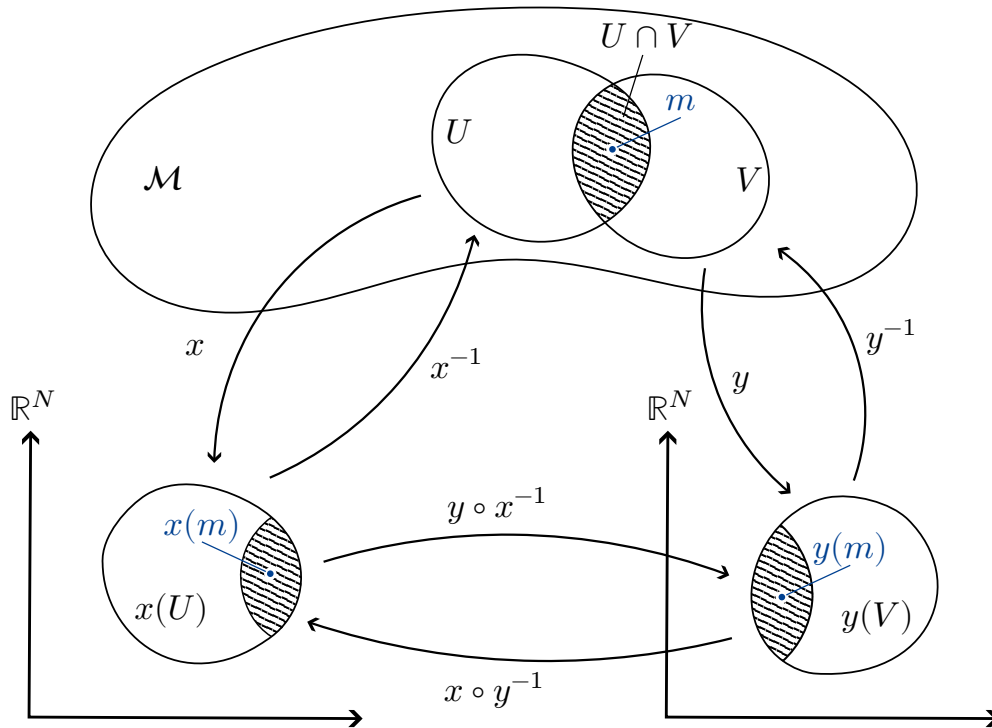
Figure 6.1: Two intersecting chart domains $U, V \subset \mathcal{M}$ with respective chart mappings x, y and transitions $x \circ y^{-1}, y \circ x^{-1}$ on $x\,(U \cap V)\,, y\,(U \cap V) \subset \mathbb{R}^N$. This figure is taken from [24].

6.2.3 Diffeomorphism and Partial Derivative

Assume now that we have smooth manifolds $\mathcal{M}$ and $\mathcal{Q}$ of dimension N and Q. A mapping $F\colon \mathcal{M} \to \mathcal{Q}$ is called *of class C^k*, or in short notation $F \in C^k(\mathcal{M}, \mathcal{Q})$, if for every $m \in \mathcal{M}$, there exist charts (U, x) and (V, y) for $\mathcal{M}$ and $\mathcal{Q}$ with $m \in U$ and $F(m) \in V$ such that $y \circ F \circ x^{-1} \in C^k(x\,(U)\,, y\,(V))$ in the classical sense since $x\,(U) \subset \mathbb{R}^N$ and $y\,(V) \subset \mathbb{R}^Q$. Note that due to the C^k-compatibility of the charts, this definition of differentiability does not depend on the choice of the chart. Throughout the document, a *smooth* mapping is synonymous with mappings of the class C^∞. We restrict ourselves in this work to smooth manifolds and smooth mappings to simplify the presentation. A *smooth diffeomorphism (from $\mathcal{M}$ to $\mathcal{Q}$)* is a smooth bijective map $F \in C^\infty(\mathcal{M}, \mathcal{Q})$ which has a smooth inverse.

For calculations, we formulate the derivative in the index notation (Section 6.2.1). In more detail, we denote for $1 \leq i \leq Q$ the *i-th component function of the chart mapping* as $x^{\underline{i}}\colon U \to \mathbb{R}$ and the *i-th component function (of F)* with $F^{\underline{i}} := y^i \circ F\colon U \to \mathbb{R}$. Then, the *$i$-th partial derivative of the j-th component of $F \in C^1(\mathcal{M}, \mathcal{Q})$ at $m \in \mathcal{M}$ (in (U, x)*

and $(V, y))$ is defined by

$$\left.\frac{\partial F^{\underline{j}}}{\partial x^{\underline{i}}}\right|_m := \left(\partial_i (F^{\underline{j}} \circ x^{-1})\right)(x(m)) \qquad \text{for } 1 \le i \le N, \tag{6.2}$$

where $\partial_i(\cdot)$ describes the i-th partial derivative of functions mapping between Euclidean vector spaces. For scalar-valued functions $f \in C^1(\mathcal{M}, \mathbb{R})$, we omit the index, i.e., $f^{\underline{1}} \equiv f$ and thus $\left.\frac{\partial f^{\underline{1}}}{\partial x^{\underline{i}}}\right|_m = \left.\frac{\partial f}{\partial x^{\underline{i}}}\right|_m$. For the derivative of the chart mapping, we obtain

$$x \in C^\infty(\mathcal{M}, \mathbb{R}^N) \quad \text{with} \quad \left.\frac{\partial x^{\underline{j}}}{\partial x^{\underline{i}}}\right|_m = \partial_i(x^{\underline{j}} \circ x^{-1})(x(m)) = \delta^{\underline{j}}_{\underline{i}} := \begin{cases} 1, & i = j, \\ 0, & i \neq j, \end{cases} \tag{6.3}$$

due to $(x^{\underline{j}} \circ x^{-1}) = (x \circ x^{-1})^{\underline{j}} = (\mathrm{id}_{\mathbb{R}^N})^{\underline{j}}$. The function $\delta^{\underline{j}}_{\underline{i}}$ is known as the *Kronecker delta*.

6.2.4 Tangent and Tangent Space

Consider a smooth manifold $\mathcal{M}$ of dimension N. The tangent space of $\mathcal{M}$ can be defined in multiple alternative ways (see, e.g., [1, Sec. 1.6] for an overview). In the present work, we present the *derivation approach* and closely follow [15, Sec. 1.7]. For an arbitrary but fixed point $m \in \mathcal{M}$, we consider the set

$$F_m^\infty := \{f \in C^\infty(U, \mathbb{R}) \,|\, U \subset \mathcal{M} \text{ open with } m \in U\}.$$

Then, a *tangent at $m \in \mathcal{M}$* is a function on this set $v \colon F_m^\infty \to \mathbb{R}$ which is (i) linear and (ii) fulfills the product rule, i.e., for every $f, g \in F_m^\infty$ and $a, b \in \mathbb{R}$, it holds[1]

(i) $v(af + bg) = av(f) + bv(g) \in \mathbb{R}$, (ii) $v(f \cdot g) = v(f) \cdot g(m) + f(m) \cdot v(g) \in \mathbb{R}$.

In a broader context, the properties (i) and (ii) define a *derivation*. The set of all tangents at $m \in \mathcal{M}$

$$T_m\mathcal{M} := \{v \colon F_m^\infty \to \mathbb{R} \,|\, v \text{ is a tangent at } m\} \tag{6.4}$$

---

[1]Note that for the sum/product of functions $f \colon U_f \to \mathbb{R}$ and $g \colon U_g \to R$ from F_m^∞, the domain of the products/sums is shrinked to the intersection $U_f \cap U_g$, which is still open and $m \in U_f \cap U_g$ and thus $(f + g), (f \cdot g) \in F_m^\infty$.

defines the *tangent space at* m, which can be shown to be an N-dimensional vector space. Thus, we also refer to elements $v \in T_m\mathcal{M}$ as *tangent vectors* at m. The i-th partial derivative (6.2) of a scalar-valued function $f \in F_m^\infty$ can be used to define elements in $T_m\mathcal{M}$,

$$\left.\frac{\partial}{\partial x^i}\right|_m \in T_m\mathcal{M} \qquad \text{with} \qquad \left.\frac{\partial}{\partial x^i}\right|_m : F_m^\infty \to \mathbb{R}, \ f \mapsto \left.\frac{\partial f}{\partial x^i}\right|_m.$$

Moreover, $\left(\left.\frac{\partial}{\partial x^1}\right|_m, \dots, \left.\frac{\partial}{\partial x^N}\right|_m\right)$ is an ordered basis of $T_m\mathcal{M}$, and, thus, we can represent each tangent vector

$$v \in T_m\mathcal{M} \qquad \text{with} \qquad v = v^i \left.\frac{\partial}{\partial x^i}\right|_m,$$

where we refer to $v^i \in \mathbb{R}$, $1 \leq i \leq N$, as the *components (of v)* and where we implicitly sum over $1 \leq i \leq N$ by the Einstein summation convention (6.1). Note that for this formalism to work, the index i in the denominator of $\left.\frac{\partial}{\partial x^i}\right|_m$ counts as a lower index. In the case of a vector space $\mathbb{V}$, the tangent space $T_m\mathbb{V}$ can be identified with the vector space $T_m\mathbb{V} \cong \mathbb{V}$ for all $m \in \mathbb{V}$ [74, p. 59], in particular $T_m\mathbb{R}^k \cong \mathbb{R}^k$ for $k \in \mathbb{N}$.

6.2.5 Differential and Chain Rule

Consider smooth manifolds $\mathcal{M}, \mathcal{Q}$, and $\mathcal{L}$ of dimension N, Q, and L with charts $(U, x), (V, y)$, and (W, z) and a point $m \in U$. The *differential of a smooth map $F \in C^\infty(\mathcal{M}, \mathcal{Q})$ at m* is a linear map

$$\left.\mathrm{d}F\right|_m \in C^\infty(T_m\mathcal{M}, T_{F(m)}\mathcal{Q}), \quad v^i \left.\frac{\partial}{\partial x^i}\right|_m \mapsto v^i \left.\frac{\partial F^j}{\partial x^i}\right|_m \left.\frac{\partial}{\partial y^j}\right|_{F(m)}, \tag{6.5}$$

which maps between the respective tangent spaces using the i-th partial derivative (6.2) of the j-th component function F^j of F, where we sum over $1 \leq i \leq N$ and $1 \leq j \leq Q$ by the Einstein summation convention (6.1). The *chain rule* is an important property of the differential: For two smooth mappings $F \in C^\infty(\mathcal{M}, \mathcal{Q}), G \in C^\infty(\mathcal{Q}, \mathcal{L})$, it holds

$$\left.\mathrm{d}(G \circ F)\right|_m = \left.\mathrm{d}G\right|_{F(m)} \circ \left.\mathrm{d}F\right|_m : T_m\mathcal{M} \to T_{(G \circ F)(m)}\mathcal{L}. \tag{6.6}$$

In respective charts (U, x), (V, y), (W, z) with $m \in U$, $F(m) \in V$ and $(G \circ F)(m) \in W$, the chain rule reads

$$
\left. \frac{\partial (G \circ F)^i}{\partial x^j} \right|_m = \left. \frac{\partial G^i}{\partial y^k} \right|_{F(m)} \left. \frac{\partial F^k}{\partial x^j} \right|_m \qquad \text{for all} \quad \begin{cases} 1 \leq j \leq N, \\ 1 \leq i \leq L, \end{cases}
$$

where the right-hand side sums over $1 \leq k \leq Q$ by the Einstein summation convention (6.1).

6.2.6 Tangent Bundle and Vector Field

The *tangent bundle* is the disjoint union of all tangent spaces

$$
T\mathcal{M} := \dot{\bigcup}_{m \in \mathcal{M}} T_m \mathcal{M} := \{(m, v) \mid m \in \mathcal{M},\ v \in T_m \mathcal{M}\}, \tag{6.7}
$$

which bundles all points $m \in \mathcal{M}$ and corresponding tangent vectors $v \in T_m \mathcal{M}$ in one set. The *tangent bundle* itself is a smooth manifold of dimension $2N$. We typically use $(m, v) \in T\mathcal{M}$ to denote elements in $T\mathcal{M}$. Whenever we have a mapping into a tangent bundle, then we use the notation $(\cdot)|_m$ to denote the second part of the mapping. For a given smooth mapping $F \in C^\infty(\mathcal{M}, \mathcal{Q})$, the *differential (on the tangent bundle)*

$$
\mathrm{d}F \in C^\infty(T\mathcal{M}, T\mathcal{Q}),\ (m, v) \mapsto (F(m), \mathrm{d}F|_m(v)) \tag{6.8}
$$

collects the differentials $\mathrm{d}F|_m \in C^\infty(T_m\mathcal{M}, T_{F(m)}\mathcal{Q})$ at m for all points $m \in \mathcal{M}$. For a given chart (U, x) of $\mathcal{M}$, the differential of the chart mapping $\mathrm{d}x \in C^\infty(TU, T\mathbb{R}^N)$ defines a *natural chart* of TU by identifying $T\mathbb{R}^N$ with $\mathbb{R}^{2N}$. It maps

$$
\mathrm{d}x \left(\left(m, v^i \left. \frac{\partial}{\partial x^i} \right|_m \right) \right) = \left(x(m), \left[v^i \right]_{1 \leq i \leq N} \right) \in \mathbb{R}^{2N} \tag{6.9}
$$

since for a chart mapping[2] $y \in C^\infty(\mathbb{R}^N, \mathbb{R}^N)$ of $\mathbb{R}^N$, it holds with (6.3) and (6.5) that

$$
\mathrm{d}x|_m \left(v^i \left. \frac{\partial}{\partial x^i} \right|_m \right) = v^i \left. \frac{\partial x^j}{\partial x^i} \right|_m \left. \frac{\partial}{\partial y^j} \right|_{x(m)} = v^i \delta^j_i \left. \frac{\partial}{\partial y^j} \right|_{x(m)} = v^i \left. \frac{\partial}{\partial y^i} \right|_{x(m)} \in T_{x(m)} \mathbb{R}^N,
$$

which we identify with $\left[v^i \right]_{1 \leq i \leq N} \in \mathbb{R}^N$.

---

[2] This chart mapping may seem redundant as $y \equiv \mathrm{id}_{\mathbb{R}^N}$. However, we use it to illustrate how $T_{x(m)} \mathbb{R}^N$ is identified with $\mathbb{R}^N$ by using y to denote the basis vectors $\left. \frac{\partial}{\partial y^j} \right|_{x(m)} \in T_{x(m)} \mathbb{R}^N$.

Since $\mathcal{M}$ and $T\mathcal{M}$ are both smooth manifolds, we are able to define smooth mappings from $\mathcal{M}$ to $T\mathcal{M}$ based on Section 6.2.3. A *smooth vector field* is a mapping $X \in C^\infty(\mathcal{M}, T\mathcal{M})$ with $\pi \circ X = \mathrm{id}_\mathcal{M}$ with $\pi\colon T\mathcal{M} \to \mathcal{M}$, $(m, v) \mapsto m$. It assigns each point $m \in \mathcal{M}$ an element $X(m) := (m, X|_m) \in T\mathcal{M}$ in the tangent bundle, where we denote the *vector field at $m \in \mathcal{M}$* with $X|_m \in T_m\mathcal{M}$. The *set of all smooth vector fields on $\mathcal{M}$* is denoted with $\mathfrak{X}_\mathcal{M}$.

6.2.7 Curve and Initial Value Problem

For a given smooth manifold $\mathcal{M}$ and an interval $\mathcal{I} := (t_0, t_\mathrm{f})$ with $t_0 < t_\mathrm{f} < \infty$, we call $\gamma \in C^\infty(\mathcal{I}, \mathcal{M})$ a *smooth curve*. We refer to elements $t \in \mathcal{I}$ as *time points*. By custom, we use for the derivative w.r.t. time the notation $\frac{\mathrm{d}}{\mathrm{d}t}(\cdot)$. The *velocity of a curve γ at $t \in \mathcal{I}$* is

$$\frac{\mathrm{d}}{\mathrm{d}t}\gamma\Big|_t := \left(\frac{\mathrm{d}}{\mathrm{d}t}\gamma^i\Big|_t\right)\frac{\partial}{\partial x^i}\Big|_{\gamma(t)} \in T_{\gamma(t)}\mathcal{M},$$

i.e., an element in the tangent space based on the (classical) derivative of the component functions $\gamma^i\colon \mathbb{R} \supset \mathcal{I} \to \mathbb{R}$ of the curve.[3] For a smooth vector field $X \in \mathfrak{X}_\mathcal{M}$, we call $\gamma \in C^\infty(\mathcal{I}, \mathcal{M})$ an *integral curve of X* with *initial value $\gamma_0 \in \mathcal{M}$*, if

$$\begin{cases} \frac{\mathrm{d}}{\mathrm{d}t}\gamma\big|_t = X|_{\gamma(t)} \in T_{\gamma(t)}\mathcal{M}, & t \in \mathcal{I} \\ \gamma(t_0) = \gamma_0 \in \mathcal{M}. \end{cases} \tag{6.10}$$

We refer to (6.10) as an *initial value problem (on $\mathcal{M}$)*. For a given chart (U, x), the system (6.10) can be solved via an N-dimensional initial value problem on $\mathbb{R}^N$

$$\frac{\mathrm{d}}{\mathrm{d}t}\gamma^i\Big|_t = (X|_{\gamma(t)})^i \in \mathbb{R} \qquad \text{for } 1 \leq i \leq N, \qquad \gamma^i(t_0) = x^i(\gamma_0) \in \mathbb{R}. \tag{6.11}$$

Due to the assumption of a smooth vector field, there exists a unique integral curve by the fundamental theorem on flows [74, Thm. 9.12], if the time interval $|t_\mathrm{f} - t_0|$ is small enough. If we assume that there exists a time interval such that all integral curves exist for a set $M_0 \subset \mathcal{M}$ with the starting points $\gamma_0 \in M_0$, the *flow of X* can be defined as $\theta_t\colon M_0 \to \mathcal{M}$, $\gamma_0 \mapsto \gamma(t; \gamma_0)$.

---

[3]Alternatively, the velocity of a curve can be understood in terms of the derivative introduced in Section 6.2.5 with $\frac{\mathrm{d}}{\mathrm{d}t}\gamma\big|_t = \mathrm{d}\gamma|_t$. In the presented notation, this would require understanding $\mathcal{I}$ as a smooth manifold with the chart $(\mathcal{I}, x_\mathcal{I})$, chart mapping $x_\mathcal{I} \equiv \mathrm{id}_\mathcal{I}\colon \mathcal{I} \to \mathbb{R}$ and the derivative $\frac{\mathrm{d}}{\mathrm{d}t}\gamma^i\big|_t = \frac{\partial \gamma^i}{\partial x_\mathcal{I}^1}\big|_t$.

type	element	bold notation
point	$m \in U \subset \mathcal{M}$	$\boldsymbol{m} := x\,(m) \in \mathbb{R}^N$
mapping	$F \in C^\infty(U, V)$	$\boldsymbol{F} := y \circ F \circ x^{-1} : \mathbb{R}^N \supset x(U) \to y(V) \subset \mathbb{R}^Q$
tangent vector	$v = v^i \frac{\partial}{\partial x^i}\big|_m \in T_m U$	$\boldsymbol{v} := \left[v^i\right]_{1 \leq i \leq N} \in \mathbb{R}^N$
Jacobian matrix	$\mathrm{d}F\vert_m \in C^\infty(T_m U, T_{F(m)} V)$	$\boldsymbol{DF}\vert_{\boldsymbol{m}} := \left[\frac{\partial F^i}{\partial x^j}\big|_m\right]_{\substack{1 \leq i \leq Q, \\ 1 \leq j \leq N}} \in \mathbb{R}^{Q \times N}$
dynamical system	$\begin{cases} \frac{\mathrm{d}}{\mathrm{d}t}\gamma\big|_t = X\vert_{\gamma(t)} \in T_{\gamma(t)} U, \\ \gamma(t_0) = \gamma_0 \in \mathcal{M} \end{cases}$	$\begin{cases} \frac{\mathrm{d}}{\mathrm{d}t}\boldsymbol{\gamma}\big|_t = \boldsymbol{X}\vert_{\boldsymbol{\gamma}(t)} \in \mathbb{R}^N, \\ \boldsymbol{\gamma}(t_0) = \boldsymbol{\gamma}_0 \in \mathbb{R}^N \end{cases}$

Table 6.2: Bold notation for two smooth manifolds $\mathcal{M}, \mathcal{Q}$ of dimension N, Q with charts $(U, x), (V, y)$. This table is taken from [24].

6.2.8 Bold Notation

We introduce a notation that collects all previously introduced types of differential geometric objects (like points, functions, tangent vectors) in a fixed chart and thereby reduces to computations in $\mathbb{R}$-vector-spaces. We refer to this notation as the *bold notation*.[4] For a given smooth manifold $\mathcal{M}$ with a chart (U, x), we use

$$x \in C^\infty(U, \mathbb{R}^N), \quad \mathrm{d}x\vert_m \in C^\infty(T_m U, \mathbb{R}^N) \quad \text{with } m \in U, \quad \mathrm{d}x \in C^\infty(TU, \mathbb{R}^{2N})$$

to map the different types of objects accordingly, where we identify $T_{x(m)}\mathbb{R}^N$ with $\mathbb{R}^N$ for $\mathrm{d}x\vert_m$ and $T\mathbb{R}^N$ with $\mathbb{R}^{2N}$ for $\mathrm{d}x$. Let us state clearly that (i) this formulation loses geometrical information (as it treats different types of objects as a vector in $\mathbb{R}^N$) and (ii) it only works for one fixed chart (since the explicit dependence on the chart is neglected). However, this formulation can be helpful for readers new to the field of differential geometry with more background in classical numerical analysis and engineering. The notation for the different types of differential geometric objects (points, mappings, tangent vectors, differentials (via the Jacobian matrix[5]), and dynamical systems) for two smooth manifolds $\mathcal{M}, \mathcal{Q}$ with charts $(U, x), (V, y)$, respectively, are summarized in Table 6.2.

---

[4] Be aware that bold symbols may be used for other purposes in other scripts on differential geometry.
[5] The Jacobian matrix is the coordinate matrix of the linear mapping described by the differential in coordinates $\mathrm{d}y\vert_{F(m)} \circ \mathrm{d}F\vert_m \circ \mathrm{d}x\vert_m^{-1} : \mathbb{R}^N \to \mathbb{R}^Q$.

6.2.9 Embedding and Embedded Submanifold

Consider two smooth manifolds $\breve{\mathcal{M}}$ and $\mathcal{M}$ of dimension n and N, respectively. A smooth mapping $F \in C^\infty(\breve{\mathcal{M}}, \mathcal{M})$ is called an *immersion* if the differential $\mathrm{d}F|_{\breve{m}} \colon T_{\breve{m}}\breve{\mathcal{M}} \to T_{F(\breve{m})}\mathcal{M}$ is injective at each point $\breve{m} \in \breve{\mathcal{M}}$. Moreover, F is called a *smooth embedding* if it is a smooth immersion and a homeomorphism onto its image $F(\breve{\mathcal{M}}) \subset \mathcal{M}$. For a given smooth embedding $\varphi \in C^\infty(\breve{\mathcal{M}}, \mathcal{M})$, the image $\varphi(\breve{\mathcal{M}})$ is an n-dimensional smooth manifold, which is called an *embedded (or regular) submanifold* of $\mathcal{M}$. We denote the tangent space of $\varphi(\breve{\mathcal{M}})$ at $\varphi(\breve{m})$ with $T_{\varphi(\breve{m})}(\varphi(\breve{\mathcal{M}})) := \mathrm{d}\varphi|_{\breve{m}}(T_{\breve{m}}\breve{\mathcal{M}})$. From the assumptions, it follows automatically that the embedding φ is a smooth diffeomorphism onto its image [74, Prop. 5.2].

Lemma 6.1: *Consider smooth manifolds $\breve{\mathcal{M}}, \mathcal{M}$ and smooth mappings $\varphi \in C^\infty(\breve{\mathcal{M}}, \mathcal{M})$ and $\varrho \in C^\infty(\mathcal{M}, \breve{\mathcal{M}})$ with $\varrho \circ \varphi \equiv \mathrm{id}_{\breve{\mathcal{M}}}$. Then, φ is a smooth embedding and $\varphi(\breve{\mathcal{M}}) \subset \mathcal{M}$ is an embedded submanifold.*

Proof. (Appendix A.1.2).   □

6.3 Model Order Reduction on Manifolds

With the geometric fundamentals at hand, we can now introduce *model order reduction on manifolds*. We start with the general framework for model order reduction (Section 6.3.1). Then, we detail conditions such that exact reproduction can be achieved (Section 6.3.2). Finally, we present the so-called manifold Petrov–Galerkin as a reduction map (Section 6.3.3).

6.3.1 General Framework

This section sits at the heart of this paper and introduces the general framework upon which the remainder is built. We start this section by defining the FOM on manifolds (Section 6.3.1.1). We then focus on the goal that MOR strives to achieve and what assumptions are required to reach this goal (Section 6.3.1.2). Subsequently, we define the reduction map and the reduced-order model (Section 6.3.1.3). We conclude the general framework with a workflow for MOR on manifolds (Section 6.3.1.4).

6.3.1.1 Full-Order Model

In the scope of the present work, we consider high-dimensional parametric initial value problems. More precisely, assume that we are given a time interval $\mathcal{I} := (t_0, t_f)$ with initial time t_0 and final time $t_f > t_0$, a parameter set $P \subset \mathbb{R}^p$, an N-dimensional smooth manifold $\mathcal{M}$ with large N, a (possibly parametric) smooth vector field $X \colon P \to \mathfrak{X}_{\mathcal{M}}$, and a (possibly parametric) initial value $\gamma_0 \colon P \to \mathcal{M}$. We consider for $\mu \in P$ the initial value problem

$$\begin{cases} \left.\frac{\mathrm{d}}{\mathrm{d}t}\gamma\right|_{t;\mu} = X(\mu)|_{\gamma(t;\mu)} \in T_{\gamma(t;\mu)}\mathcal{M}, \quad t \in \mathcal{I} \\ \gamma(t_0;\mu) = \gamma_0(\mu) \in \mathcal{M}, \end{cases} \tag{6.12}$$

which we want to solve for the integral curve $\gamma(\cdot\,;\mu) \in C^\infty(\mathcal{I}, \mathcal{M})$. We refer to (6.12) as the FOM and to $X(\mu)$ as the *FOM vector field*.

Remark 6.2 (Parameter dependency): *In the following, we may suppress the explicit notation of the parameter dependence for the sake of brevity. This is possible since the parameter is fixed for each FOM evaluation. We indicate the parameter dependence only if it is relevant in a specific context.*

6.3.1.2 Goal of Model Order Reduction

The goal of MOR can be formulated as to be able to well-approximate the *set of all solutions*

$$S := \{\gamma(t;\mu) \in \mathcal{M} \mid (t, \mu) \in \mathcal{I} \times P\} \subset \mathcal{M} \tag{6.13}$$

computationally efficiently. As discussed in Remark 2.8, the set of all solutions is sometimes referred to as the *solution manifold*, which may be misleading since S is in general not a manifold. The crucial assumption for MOR to be reasonable is the following.

Assumption 6.3: *Given a metric $d_{\mathcal{M}} \colon \mathcal{M} \times \mathcal{M} \to \mathbb{R}_{\geq 0}$, we assume that there exists a low-dimensional embedded submanifold $\varphi(\check{\mathcal{M}}) \subset \mathcal{M}$ defined by an n-dimensional manifold $\check{\mathcal{M}}$ and a smooth embedding $\varphi \in C^\infty(\check{\mathcal{M}}, \mathcal{M})$ with $\dim(\check{\mathcal{M}}) = n \ll N = \dim(\mathcal{M})$ such that the set of solutions S can be approximated well, i.e., the worst best-approximation error of S in $\varphi(\check{\mathcal{M}})$*

$$d_{\mathcal{M}}(S, \varphi(\check{\mathcal{M}})) := \sup_{m \in S} \inf_{\check{m} \in \check{\mathcal{M}}} d_{\mathcal{M}}(m, \varphi(\check{m}))$$

is small.
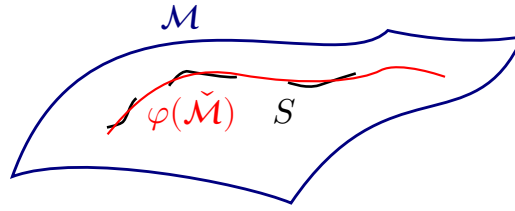
Figure 6.2: Schematic illustration of the full manifold $\mathcal{M}$ (dark blue), the set of all solutions S (black), and the approximating embedded submanifold $\varphi(\check{\mathcal{M}})$ (red). The set of solutions is schematically depicted as three separate trajectories that may occur due to a possible discontinuous behavior in the parameter μ. This figure is taken from [24].

We refer to $\mathcal{M}$ as the *full(-order) manifold* and to $\check{\mathcal{M}}$ as the *reduced(-order) manifold*. Let us emphasize that the goal is to approximate the set $S \subset \mathcal{M}$, not the full manifold $\mathcal{M}$. We refer to Figure 6.2 for a schematic illustration of the relation between the full manifold $\mathcal{M}$, the set of all solutions S, and the approximating embedded submanifold $\varphi(\check{\mathcal{M}})$.

6.3.1.3 Reduction Map and Reduced-Order Model

Assume that we have identified an n-dimensional embedded submanifold $\varphi(\check{\mathcal{M}}) \subset \mathcal{M}$ with smooth embedding $\varphi \in C^\infty(\check{\mathcal{M}}, \mathcal{M})$ and that Assumption 6.3 is satisfied. To find an ROM, we want to replace $\gamma(t)$ in (6.12) with the approximation $\varphi(\check{\gamma}(t))$ based on a reduced integral curve $\check{\gamma} \in C^\infty(\mathcal{I}, \check{\mathcal{M}})$. Note that, even if we would have an exact reproduction, i.e., $\gamma(t) = \varphi(\check{\gamma}(t))$ for all $t \in \mathcal{I}$, the initial value problem (6.12) in the reduced integral curve $\check{\gamma}$ would be overdetermined, in the sense that we have (locally in each chart) N equations for n unknowns. Thus, we must also reduce the initial value problem and give the following definition.

Definition 6.4 (Reduction map): *A map $R \in C^\infty(T\mathcal{M}, T\check{\mathcal{M}})$ is called reduction map for a smooth embedding $\varphi \in C^\infty(\check{\mathcal{M}}, \mathcal{M})$ if it satisfies the projection property*

$$R \circ \mathrm{d}\varphi = \mathrm{id}_{T\check{\mathcal{M}}} . \tag{6.14}$$

As in Section 6.2.6, we split the reduction map

$$R \in C^\infty(T\mathcal{M}, T\check{\mathcal{M}}), \qquad (m, v) \mapsto (\varrho(m), R|_m(v))$$

with $\varrho \in C^\infty(\mathcal{M}, \check{\mathcal{M}})$ and $R|_m \in C^\infty(T_m\mathcal{M}, T_{\varrho(m)}\check{\mathcal{M}})$ for $m \in \mathcal{M}$. We refer to ϱ as a point reduction for φ and to $R|_m$ as a tangent reduction for φ.

(a) Schematic illustration of the relation of the embedding φ and the point reduction ϱ.

(b) Schematic illustration of the relation of the tangent spaces involved in MOR on manifolds. The reduced tangent space $T_{\breve{m}}\breve{\mathcal{M}}$ is displayed orthogonally to $\breve{\mathcal{M}}$ for a better visualization.
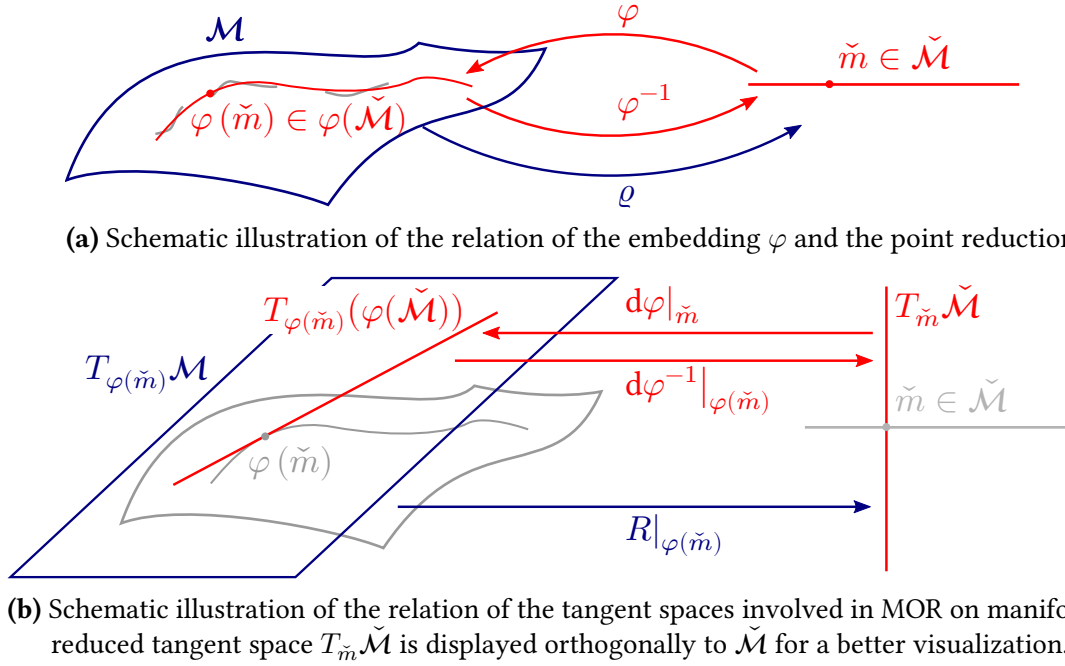
Figure 6.3: Schematic illustration of the relation between the embedding φ and the reduction map $R\left(m,v\right) = \left(\varrho\left(m\right), R|_m\left(v\right)\right)$ with $m \in \mathcal{M}$. This figure is taken from [24].

Note that (6.14) immediately implies that $\mathrm{d}\varphi \circ R \in C^\infty(T\mathcal{M}, T\varphi(\breve{\mathcal{M}}))$ is idempotent and thus a projection. Moreover, (6.14) implies that a point reduction and a tangent reduction for φ satisfy

$$\varrho \circ \varphi = \mathrm{id}_{\breve{\mathcal{M}}}, \tag{6.15a}$$

$$R|_{\varphi(\breve{m})} \circ \mathrm{d}\varphi|_{\breve{m}} = \mathrm{id}_{T_{\breve{m}}\breve{\mathcal{M}}} \qquad \text{for all } \breve{m} \in \breve{\mathcal{M}}, \tag{6.15b}$$

which we refer to as the *point projection property* and the *tangent projection property*, respectively. The relation between the embedding φ and the reduction map R is illustrated in Figure 6.3.

Example 6.5 (MOR on subspaces): *Projection-based MOR on subspaces from Section 2.2.2 is included in MOR on manifolds as a special case: For an N-dimensional $\mathbb{R}$-vector-space $\mathbb{V}$ with a coordinate mapping $\varphi_{\mathbb{V}} : \mathbb{V} \to \mathbb{R}^N$ with a n-dimensional subspace $\tilde{\mathbb{V}} \subset \mathbb{V}$ characterized by an n-dimensional reduced space $\breve{\mathbb{V}}$ and an embedding $V \in L(\breve{\mathbb{V}}; \mathbb{V})$, the two approaches relate with $\mathcal{M} = U = \mathbb{V}$, $x = \varphi_{\mathbb{V}}$, and $\breve{\mathcal{M}} = \breve{U} = \breve{\mathbb{V}}$, $\breve{x} = \breve{\varphi}_{\breve{\mathbb{V}}}$ (where $\breve{\varphi}_{\breve{\mathbb{V}}} : \breve{\mathbb{V}} \to \mathbb{R}^n$ denotes a coordinate mapping of $\breve{\mathbb{V}}$). The embedding is $\varphi \equiv V$. The point reduction was not clearly labelled in Chapter 2. In the most general case, it can be characterized by a projection matrix*

$W \in \mathbb{R}^{N \times n}$ such that

$$\varrho\,(m) := W^\top m, \qquad\qquad R|_m(v) := W^\top v, \qquad\qquad \varphi\,(\check{m}) := V\check{m}.$$

This exactly covers the case where φ and ϱ are linear. The projection property (6.14) then relates to the *biorthogonality* of W and V

$$\varrho \circ \varphi \equiv \mathrm{id}_{\mathbb{R}^n} \qquad\qquad \Longleftrightarrow \qquad\qquad W^\top V = I_n \in \mathbb{R}^{n \times n},$$
$$R|_{\varphi(\check{m})} \circ \mathrm{d}\varphi|_{\check{m}} \equiv \mathrm{id}_{\mathbb{R}^n} \qquad\qquad \Longleftrightarrow \qquad\qquad W^\top V = I_n \in \mathbb{R}^{n \times n},$$

which is often assumed in MOR on subspaces.

Definition 6.6 (Reduced-order model): *Assume to be given a FOM* (6.12), *a smooth embedding* $\varphi \in C^\infty(\check{\mathcal{M}}, \mathcal{M})$, *and a reduction map* $R \in C^\infty(T\mathcal{M}, T\check{\mathcal{M}})$ *for* φ *with point and tangent reduction given by* $R\,(m, v) = \left(\varrho\,(m)\,, R|_m\,(v)\right)$. *We define the ROM vector field* $\check{X}\colon P \to \mathfrak{X}_{\check{\mathcal{M}}}$ *with*

$$\check{X}(\mu)\big|_{\check{m}} := R|_{\varphi(\check{m})}\left(X(\mu)\big|_{\varphi(\check{m})}\right) \in T_{\check{m}}\check{\mathcal{M}}.$$

Then, for $\mu \in P$, *we call the initial value problem on* $\check{\mathcal{M}}$

$$\begin{cases} \frac{\mathrm{d}}{\mathrm{d}t}\check{\gamma}\big|_{t;\mu} = \check{X}(\mu)\big|_{\check{\gamma}(t;\mu)} \in T_{\check{\gamma}(t;\mu)}\check{\mathcal{M}} \\[2mm] \check{\gamma}\,(t_0; \mu) = \check{\gamma}_0(\mu) := \varrho\,(\gamma_0\,(\mu)) \in \check{\mathcal{M}} \end{cases} \qquad (6.16)$$

the ROM for (6.12) *under the reduction map* R *with solution* $\check{\gamma}(\cdot; \mu) \in C^\infty(\mathcal{I}, \check{\mathcal{M}})$.

We emphasize that both the point and the tangent reduction are relevant for the ROM, since the point reduction is used to map the initial value γ_0, while the tangent reduction maps the FOM vector field to the tangent space of the reduced manifold $\check{\mathcal{M}}$. Moreover, we see that it is not sufficient to define ϱ and $R|_{\varphi(\check{m})}$ only in the image of φ and $\mathrm{d}\varphi|_{\check{m}}$, respectively, since the initial value and the evaluated FOM vector field may be elements of $\mathcal{M} \setminus \varphi\,(\check{\mathcal{M}})$ and $T_{\varphi(\check{m})}\mathcal{M} \setminus T_{\varphi(\check{m})}(\varphi(\check{\mathcal{M}}))$, respectively.

6.3.1.4 MOR Workflow

With Assumption 6.3 at hand, MOR (in the scope of this work) can be summarized in three steps:

1. APPROXIMATION: Given the FOM (6.12), find a reduced manifold $\check{\mathcal{M}}$ and a smooth embedding $\varphi \in C^\infty(\check{\mathcal{M}}, \mathcal{M})$ such that $d_{\mathcal{M}}(S, \varphi(\check{\mathcal{M}}))$ is small.
2. REDUCTION: Identify a reduction map $R \in C^\infty(T\mathcal{M}, T\check{\mathcal{M}})$ for φ and construct the ROM (6.16).
3. RECONSTRUCTION: Solve the ROM (6.16) for $\check{\gamma}$ and approximate the FOM solution curve γ with

$$\gamma(t; \mu) \approx \varphi(\check{\gamma}(t; \mu)) \qquad \text{for } (t, \mu) \in \mathcal{I} \times P. \tag{6.17}$$

In the remainder of the manuscript, we discuss all three steps, starting with the RE-CONSTRUCTION step in the subsequent subsection. Possible constructions of the reduction map in the REDUCTION step are discussed in Sections 6.3.3 and 6.5. The construction of the embedding φ in the APPROXIMATION step is analyzed in a data-driven framework in Section 6.6.

6.3.2 Exact Reproduction

A desirable property in the RECONSTRUCTION step is to answer the question when the approximation in (6.17) is exact, which we refer to as *exact reproduction*. Clearly, if for a given parameter $\mu \in P$, the FOM solution γ evolves on $\varphi(\check{\mathcal{M}})$, i.e., $\gamma(t; \mu) \in \varphi(\check{\mathcal{M}})$ for all $t \in \mathcal{I}$, then we can define the smooth curve

$$\check{\beta} := \varphi^{-1}(\gamma(\cdot; \mu)) \in C^\infty(\mathcal{I}, \check{\mathcal{M}}), \tag{6.18}$$

since, by assumption, φ is a diffeomorphism onto its image. With this choice, we immediately obtain

$$X(\mu)|_{\varphi(\check{\beta}(t;\mu))} = X(\mu)|_{\gamma(t;\mu)} = \frac{\mathrm{d}}{\mathrm{d}t}\gamma\Big|_{t;\mu} = \frac{\mathrm{d}}{\mathrm{d}t}(\varphi \circ \check{\beta})\Big|_{t;\mu} = \mathrm{d}\varphi|_{\check{\beta}(t;\mu)}\left(\frac{\mathrm{d}}{\mathrm{d}t}\check{\beta}\Big|_{t;\mu}\right), \tag{6.19}$$

where the last equality follows from the chain rule (6.6). It remains to prove that the ROM (6.16) is able to recover the reduced curve $\check{\beta}$, which we show in the following.

Theorem 6.7 (Exact reproduction of a solution)**:** *Assume that the FOM* (6.12) *is uniquely solvable for a parameter* $\mu \in P$ *and consider a smooth embedding* $\varphi \in C^\infty(\check{\mathcal{M}}, \mathcal{M})$ *with reduction map* $R \in C^\infty(T\mathcal{M}, T\check{\mathcal{M}})$. *Assume that the ROM* (6.16) *is uniquely solvable and* $\gamma(t; \mu) \in \varphi(\check{\mathcal{M}})$ *for all* $t \in \mathcal{I}$. *Then the ROM solution* $\check{\gamma}(\cdot; \mu)$ *exactly recovers the FOM solution* $\gamma(\cdot; \mu)$ *for this parameter, i.e.,*

$$\varphi\left(\check{\gamma}(t; \mu)\right) = \gamma(t; \mu) \qquad\qquad \text{for all } t \in \mathcal{I}. \qquad (6.20)$$

Proof. Since $\gamma(t; \mu) \in \varphi(\check{\mathcal{M}})$ for all $t \in \mathcal{I}$, we can construct $\check{\beta}$ as in (6.18). It remains to show that $\check{\beta}$ satisfies the ROM (6.16). First, we obtain

$$\check{\gamma}_0(\mu) = \varrho\left(\gamma_0(\mu)\right) = \varrho\left(\gamma(t_0; \mu)\right) = (\varrho \circ \varphi)\left(\check{\beta}(t_0; \mu)\right) = \check{\beta}(t_0; \mu),$$

where the last equality is due to the projection property (6.15) for the point reduction. Second, $\check{\beta}$ satisfies the initial value problem of the ROM since the tangent projection property (6.15b) implies with (6.19)

$$R\big|_{\varphi(\check{\beta}(t;\mu))}\left(X(\mu)\big|_{\varphi(\check{\beta}(t;\mu))}\right) = \left(R\big|_{\varphi(\check{\beta}(t;\mu))} \circ \mathrm{d}\varphi\big|_{\check{\beta}(t;\mu)}\right)\left(\tfrac{\mathrm{d}}{\mathrm{d}t}\check{\beta}\big|_{t;\mu}\right) = \tfrac{\mathrm{d}}{\mathrm{d}t}\check{\beta}\big|_{t;\mu}. \qquad \square$$

In the following, we give an example for which the exact reproduction can be achieved for a specific choice of $\check{\mathcal{M}}$ and φ.

Corollary 6.8 (Special case $\varphi \equiv \gamma$)**:** *For a given FOM* (6.12) *on* $\mathcal{M}$, *assume that* $\check{\mathcal{M}} := \mathcal{I} \times P$ *is an* $(n_p + 1)$-*dimensional smooth manifold, that the FOM is uniquely solvable, that the FOM solution* $\gamma\colon \mathcal{I} \times P = \check{\mathcal{M}} \to \mathcal{M}$ *is a smooth embedding, and that there exists a respective reduction map* $R \in C^\infty(T\mathcal{M}, T\check{\mathcal{M}})$ *for the smooth embedding* $\varphi \equiv \gamma$. *Then, the ROM* (6.16) *reproduces the FOM solution exactly with the reduced integral curve* $\check{\gamma}(t; \mu) = (t, \mu)$ *such that the flow of the ROM is* $\check{\theta}_s(t, \mu) = (t + s, \mu)$. *Moreover, the ROM in bold notation reads*

$$\tfrac{\mathrm{d}}{\mathrm{d}t}\check{\boldsymbol{\gamma}}\big|_{t;\mu} = \boldsymbol{e}_1 \in \mathbb{R}^{n_p+1}, \qquad\qquad \check{\boldsymbol{\gamma}}_0(\mu) = (t_0, \mu),$$

where $\boldsymbol{e}_1 \in \mathbb{R}^{n_p+1}$ *denotes the first unit vector.*

Proof. With the assumptions of Corollary 6.8, the choice $\varphi \equiv \gamma$ guarantees that the assumptions of Theorem 6.7 are fulfilled and that $\check{\beta}(t; \mu) = (t, \mu)$ is a valid choice for the curve in (6.18), which was used in the proof of Theorem 6.7 as the ROM solution candidate. For the

remaining statement, we observe

$$\frac{\mathrm{d}}{\mathrm{d}t}\check{\beta}^{\underline{1}}\Big|_{t;\mu} = 1, \qquad\qquad \frac{\mathrm{d}}{\mathrm{d}t}\check{\beta}^{\underline{i}}\Big|_{t;\mu} = 0 \qquad \text{for } 1 < i \le n_p + 1,$$

and $\check{\gamma}_0(\mu) = \check{\beta}(t_0;\mu) = (t_0,\mu)$, which completes the proof. $\qquad\square$

6.3.3 Manifold Petrov–Galerkin (MPG)

Now we want to address one example of how to construct a reduction map (Definition 6.4), i.e., how to do the REDUCTION step from the general MOR workflow described in Section 6.3.1.4. Note that this specific choice of reduction map has been independently developed in [93]. Moreover, we emphasize that the specific choice of the reduction map is crucial for the approximation quality of the ROM; see, for instance, [94]. Nevertheless, our goal here is not to present an optimal choice but rather an example of leveraging the point reduction ϱ to construct a reduction map using the previously introduced framework in Section 6.3.1.

Assume that we have completed the APPROXIMATION step from the general MOR workflow, i.e., we have already identified a reduced manifold $\check{\mathcal{M}}$ together with a smooth embedding φ. Since φ is a homeomorphism onto its image, we know that $\varphi^{-1}\colon \varphi(\check{\mathcal{M}}) \to \check{\mathcal{M}}$ exists. Under for MOR reasonable assumptions, the extension lemma for smooth functions (see for instance [74, Lem. 2.26]) guarantees that we can find a smooth extension ϱ of φ^{-1}, which by construction satisfies the point projection property (6.15a). We refer to Figure 6.3a for an illustration of the relation between φ^{-1} and ϱ. Differentiating the point projection property (6.15a) with the chain rule (6.6) implies

$$\mathrm{d}\varrho|_{\varphi(\check{m})} \circ \mathrm{d}\varphi|_{\check{m}} = \mathrm{d}(\mathrm{id}_{\check{\mathcal{M}}})|_{\check{m}} = \mathrm{id}_{T_{\check{m}}\check{\mathcal{M}}}\colon T_{\check{m}}\check{\mathcal{M}} \to T_{\check{m}}\check{\mathcal{M}}, \tag{6.21}$$

i.e., $\mathrm{d}\varrho|_{\varphi(\check{m})}$ is a left-inverse to $\mathrm{d}\varphi|_{\check{m}}$. In particular, we have proven the following result.

Theorem 6.9 (MPG reduction map): *Consider a smooth embedding φ and a point reduction ϱ for φ. Then, the differential of the point reduction ϱ is a left inverse to the differential of the embedding φ. Consequently,*

$$R_{MPG}\colon T\mathcal{M} \to T\check{\mathcal{M}} \qquad (m,v) \mapsto (\varrho(m), \mathrm{d}\varrho|_m(v)) \tag{6.22}$$

is a smooth reduction map for φ, which we call the MPG reduction map for (ϱ,φ).

We refer to the ROM (6.16) obtained with the MPG reduction map from Theorem 6.9 as the *MPG-ROM* for (ϱ, φ). In index and bold notation, the tangent projection property (6.21) reads

$$\left.\frac{\partial \varrho^i}{\partial x^k}\right|_{\varphi(\check{m})} \left.\frac{\partial \varphi^k}{\partial \check{x}^j}\right|_{\check{m}} = \delta^i_{\underline{j}}, \qquad\qquad \left.\boldsymbol{D\varrho}\right|_{\boldsymbol{\varphi}(\check{\boldsymbol{m}})} \left.\boldsymbol{D\varphi}\right|_{\check{\boldsymbol{m}}} = \boldsymbol{I}_n \in \mathbb{R}^{n \times n}. \qquad (6.23)$$

It can be interpreted as that the columns of $\boldsymbol{D\varphi}|_{\check{\boldsymbol{m}}}$ span an n-dimensional reduced vector space that changes with the reduced coordinates $\check{\boldsymbol{m}} \in \mathbb{R}^n$, whereas the rows of $\boldsymbol{D\varrho}|_{\boldsymbol{\varphi}(\check{\boldsymbol{m}})}$ span an n-dimensional vector space dual to the reduced vector space.

Example 6.10 (MOR on subspaces)**:** *If φ and ϱ are linear as in Example 6.5, then the MPG-ROM (6.16) with the MPG reduction map from Theorem 6.9 is the ROM obtained in classical MOR on subspaces via Petrov–Galerkin projection*

$$\left.\boldsymbol{R}_{MPG}\right|_{\boldsymbol{\varphi}(\check{\boldsymbol{m}})} = \left.\boldsymbol{D\varrho}\right|_{\boldsymbol{\varphi}(\check{\boldsymbol{m}})} = \boldsymbol{W}^\top, \qquad\qquad \left.\frac{\mathrm{d}}{\mathrm{d}t}\check{\boldsymbol{\gamma}}\right|_t = \boldsymbol{W}^\top \boldsymbol{X}|_{\check{\boldsymbol{\gamma}}(t)},$$

which is the motivation for the terminology MPG.

6.4 Manifolds with Structure

As a next step, we want to discuss structure-preserving MOR on manifolds (Section 6.5). Beforehand, we specify the relevant structures on the FOM level in the present section. The idea is to equip the underlying full manifold $\mathcal{M}$ with additional structure to formulate a FOM vector field X, which guarantees physical properties, e.g., that the FOM solutions preserve energy over time. We introduce additional structure on $\mathcal{M}$ (Section 6.4.1), which allows us to formulate Lagrangian systems (Section 6.4.2) and Hamiltonian systems (Section 6.4.3) on manifolds. Both systems admit a FOM vector field, which guarantees that the FOM solutions preserve the corresponding energy over time.

6.4.1 Additional Structure on $\mathcal{M}$

To keep this work self-contained, we proceed by detailing more concepts of differential geometry. We discuss the cotangent space and covectors (Section 6.4.1.1), tensors (Section 6.4.1.2), tensor fields (Section 6.4.1.3), structured tensor fields (Section 6.4.1.4), and pullbacks of covectors, tensor fields, and functions (Section 6.4.1.5).

6.4.1.1 Cotangent Space, Covectors, and Cotangent Bundle

The dual of the tangent space at $m \in \mathcal{M}$ (6.4) is the *cotangent space at $m \in \mathcal{M}$*

$$T_m^*\mathcal{M} := \{\lambda \mid \lambda\colon T_m\mathcal{M} \to \mathbb{R} \text{ linear}\},$$

which is again an N-dimensional vector space. Elements in the cotangent space are called *cotangent vectors* or simply *covectors*. Covectors can be constructed from scalar-valued functions $f \in C^\infty(\mathcal{M}, \mathbb{R})$, as its differential at m, $\mathrm{d}f|_m \in C^\infty(T_m\mathcal{M}, T_{f(m)}\mathbb{R})$, defines a linear functional on $T_m\mathcal{M}$ if we identify $T_{f(m)}\mathbb{R}$ with $\mathbb{R}$. Thus, the differential at m of a scalar-valued function is a covector $\mathrm{d}f|_m \in T_m^*\mathcal{M}$. For a given chart (U, x) of $\mathcal{M}$, this construction can be used to define a basis of $T_m^*\mathcal{M}$: For each $i \in \{1, \dots, N\}$, the i-th component function of the chart mapping $x^i \in C^\infty(U, \mathbb{R})$ is a scalar-valued function and thus $\mathrm{d}x^i|_m \in T_m^*\mathcal{M}$. Moreover, with (6.3), (6.5), and identifying $T_{x(m)}\mathbb{R} \cong \mathbb{R}$, it holds for all basis vectors of the tangent space $\frac{\partial}{\partial x^j}|_m \in T_m\mathcal{M}$, $1 \leq j \leq N$ the dual relationship

$$\mathrm{d}x^i|_m \left(\frac{\partial}{\partial x^j}\Big|_m\right) = \frac{\partial x^i}{\partial x^j}\Big|_m = \delta^i_j \in \mathbb{R} \cong T_{x(m)}\mathbb{R}.$$

The differentials $\{\mathrm{d}x^i|_m\}_{1 \leq i \leq N}$ define a basis of $T_m^*\mathcal{M}$ and we can represent each covector $\lambda \in T_m^*\mathcal{M}$ as

$$\lambda = \lambda_i\, \mathrm{d}x^i|_m \in T_m^*\mathcal{M},$$

with *(covector) components* $\lambda_i \in \mathbb{R}$, where the right-hand side sums over $1 \leq i \leq N$ by Einstein summation convention (6.1). By the duality of the bases of $T_m\mathcal{M}$ and $T_m^*\mathcal{M}$, it holds for each covector $\lambda \in T_m^*\mathcal{M}$ and vector $v \in T_m\mathcal{M}$ that

$$\lambda(v) = \left(\lambda_j\, \mathrm{d}x^j\right)\left(v^i \frac{\partial}{\partial x^i}\Big|_m\right) = \lambda_j\, v^i\, \mathrm{d}x^j|_m \left(\frac{\partial}{\partial x^i}\Big|_m\right) = \lambda_i\, v^i \in \mathbb{R}.$$

Analogously to the tangent bundle (6.7), a *cotangent bundle $T^*\mathcal{M}$* can be formulated as the disjoint union of $T_m^*\mathcal{M}$, which can be shown to be a smooth manifold of dimension $2N$.

6.4.1.2 Tensors

A generalization of vectors and covectors are the so-called *tensors*. For a vector space $\mathbb{V}$ and its dual $\mathbb{V}^*$, the *space of (r, s)-tensors* given by

$$T^{(r,s)}(\mathbb{V}) := \underbrace{\mathbb{V} \otimes \cdots \otimes \mathbb{V}}_{r \text{ times}} \otimes \underbrace{\mathbb{V}^* \otimes \cdots \otimes \mathbb{V}^*}_{s \text{ times}}.$$

In the present work we consider tensors on the tangent and cotangent space, i.e., $\mathbb{V} = T_m\mathcal{M}$ and $\mathbb{V}^* = T_m^*\mathcal{M}$. Special cases are $T^{(1,0)}(T_m\mathcal{M}) = T_m\mathcal{M}$ and $T^{(0,1)}(T_m\mathcal{M}) = T_m^*\mathcal{M}$. An element $\sigma \in T^{(r,s)}(T_m\mathcal{M})$ of a general (r, s)-tensor space is called an *r-times contravariant s-times covariant tensor*. This element can be represented by

$$\sigma = \sigma^{\underline{i_1 \dots i_r}}_{\underline{j_1 \dots j_s}} \left.\frac{\partial}{\partial x^{\underline{i_1}}}\right|_m \otimes \cdots \otimes \left.\frac{\partial}{\partial x^{\underline{i_r}}}\right|_m \otimes \mathrm{d}x^{\underline{j_1}}\Big|_m \otimes \cdots \otimes \mathrm{d}x^{\underline{j_s}}\Big|_m$$

with *components* $\sigma^{\underline{i_1 \dots i_r}}_{\underline{j_1 \dots j_s}} \in \mathbb{R}$ for $1 \leq i_1, \dots, i_r, j_1, \dots, j_s \leq N$, where the right-hand side sums over each index $1 \leq \underline{i}_1, \dots, i_r, j_1, \dots, j_s \leq N$ by the Einstein summation convention (6.1). The position of the index (upper or lower index) indicates which type (co- or contravariant) the respective index belongs to. To extend the bold notation from Section 6.2.8 for tensors, we stack the components with

$$\boldsymbol{\sigma} := \left[\sigma^{\underline{i_1 \dots i_r}}_{\underline{j_1 \dots j_s}}\right]_{1 \leq i_1, \dots, i_r, j_1, \dots, j_s \leq N} \in \mathbb{R}^{\overbrace{N \times N \times \cdots \times N}^{r+s \text{ times}}}.$$

6.4.1.3 Tensor Field and Bundle of (r, s)-Tensors

A so-called *tensor field* is a mapping which assigns each point $m \in \mathcal{M}$ a tensor in the corresponding (r, s)-tensor space $T^{(r,s)}(T_m\mathcal{M})$ analogous to the smooth vector field introduced in Section 6.2.6. To this end we define the *bundle of (r, s)-tensors* as the disjoint union of all (r, s)-tensor spaces

$$T^{(r,s)}(T\mathcal{M}) := \dot{\bigcup}_{m \in \mathcal{M}} T^{(r,s)}(T_m\mathcal{M}) := \{(m, \sigma) \mid m \in \mathcal{M}, \ \sigma \in T^{(r,s)}(T_m\mathcal{M})\}.$$

Similarly as before, we obtain the special cases $T^{(1,0)}(T\mathcal{M}) = T\mathcal{M}$ and $T^{(0,1)}(T\mathcal{M}) = T^*\mathcal{M}$. An *$(r, s)$-tensor field* is defined as a map

$$\tau \colon \mathcal{M} \to T^{(r,s)}(T\mathcal{M}), \ m \mapsto (m, \tau|_m) \qquad \text{such that } \tau|_m \in T^{(r,s)}(T_m\mathcal{M}).$$

For a given chart (U, x) of $\mathcal{M}$, we denote the $((r + s) \cdot N)$ functions $\tau_{\underline{j_1 \cdots j_s}}^{\underline{i_1 \cdots i_r}} \colon U \to \mathbb{R}$ for $1 \leq i_1, \ldots, i_r, j_1, \ldots, j_s \leq N$ with $\tau_{\underline{j_1 \cdots j_s}}^{\underline{i_1 \cdots i_r}}(m) := (\tau|_m)_{\underline{j_1 \cdots j_s}}^{\underline{i_1 \cdots i_r}}$ as the *component functions* to stress the dependence on the point m. To extend the bold notation from Section 6.2.8 for tensor fields, we stack the component functions with

$$\boldsymbol{\tau} := \left[\tau_{\underline{j_1 \cdots j_s}}^{\underline{i_1 \cdots i_r}} \circ x^{-1}\right]_{1 \leq i_1, \ldots, i_r, j_1, \ldots, j_s \leq N} \colon \mathbb{R}^N \supset x\,(U) \to \mathbb{R}^{\overbrace{N \times N \times \cdots \times N}^{r+s \text{ times}}}.$$

An (r, s)-tensor field τ is called *smooth* if all of its component functions are smooth, i.e., $\tau_{\underline{j_1 \cdots j_s}}^{\underline{i_1 \cdots i_r}} \in C^\infty(U, \mathbb{R})$. The set of all smooth (r, s)-tensor fields is the so-called *smooth section of the (r, s)-tensor bundle* $\Gamma(T^{(r,s)}(T\mathcal{M}))$. A special case are the smooth vector fields $\mathfrak{X}_{\mathcal{M}} = \Gamma(T^{(1,0)}(T\mathcal{M}))$.

6.4.1.4 Structured Tensor Fields and Musical Isomorphisms

Tensor fields may possess additional properties, which we refer to as *structure*. In the following, we introduce two important examples of tensor fields with special structures, namely Riemannian metrics and symplectic forms.

Consider a smooth manifold $\mathcal{M}$ with a chart (U, x). Then, the smooth $(0, 2)$-tensor field $\tau \in \Gamma(T^{(0,2)}(T\mathcal{M}))$ with its component functions $\tau_{\underline{ij}} \in C^\infty(U, \mathbb{R})$, $1 \leq i, j \leq N$, is called

- *symmetric*, if $(\tau|_m)_{\underline{ij}} = (\tau|_m)_{\underline{ji}}$ for each $m \in U$ and for all $1 \leq i, j \leq N$;
- *skew-symmetric* or *2-form*, if $(\tau|_m)_{\underline{ij}} = -(\tau|_m)_{\underline{ji}}$ for each $m \in U$ and all $1 \leq i, j \leq N$;
- *nondegenerate*, if $[(\tau|_m)_{\underline{ij}}]_{1 \leq i,j \leq N} \in \mathbb{R}^{N \times N}$ is nondegenerate for each $m \in U$;
- *positive definite*, if $[(\tau|_m)_{\underline{ij}}]_{1 \leq i,j \leq N} \in \mathbb{R}^{N \times N}$ is positive definite for all $m \in U$;
- a *closed 2-form*, if τ is a 2-form and for each $m \in U$

$$\left.\frac{\partial \tau_{jk}}{\partial x^{\underline{i}}}\right|_m + \left.\frac{\partial \tau_{ki}}{\partial x^{\underline{j}}}\right|_m + \left.\frac{\partial \tau_{ij}}{\partial x^{\underline{k}}}\right|_m = 0 \qquad \text{for all } 1 \leq i \leq j \leq k \leq N. \qquad (6.24)$$

Combining some of the previous properties, we obtain the following concepts. A smooth $(0, 2)$-tensor field $\tau \in \Gamma(T^{(0,2)}(T\mathcal{M}))$ on $\mathcal{M}$ is called

- a *Riemannian metric on $\mathcal{M}$* if τ is symmetric and positive definite;
- a *symplectic form on $\mathcal{M}$* if τ is skew-symmetric, nondegenerate, and closed.

If $\tau, \omega \in \Gamma(T^{(0,2)}(T\mathcal{M}))$ are a Riemannian metric and a symplectic form on $\mathcal{M}$, respectively, then we call $(\mathcal{M}, \tau)$ and $(\mathcal{M}, \omega)$ a *Riemannian manifold* and *symplectic manifold*, respectively. Note that the nondegeneracy of a symplectic form implies that a symplectic manifold has even dimension, i.e., $\dim(\mathcal{M}) = N =: 2\bar{N}$.

Both the Riemannian metric and the symplectic form are nondegenerate tensor fields. This allows to formulate the inverse $(2,0)$-tensor field $\tau^{-1} \in \Gamma(T^{(2,0)}(T\mathcal{M}))$ such that $(\tau|_m^{-1})^{ik}(\tau|_m)_{kj} = \delta^i_j$, where, for the sake of brevity, the components of the inverse tensor are typically denoted with $(\tau|_m)^{ik} := (\tau|_m^{-1})^{ik}$, i.e., the classical notation of the inverse $(\cdot)^{-1}$ is not explicitly denoted since this is clear from the position of the indices. Moreover, the nondegeneracy allows to formulate an isomorphism between the tangent and the cotangent bundle. Loosely speaking, this means that the indices in the index notation can be switched from covariant (superindices) to contravariant (subindices) and vice versa. This is typically referred to as *musical isomorphisms*

$$\flat_\tau \in C^\infty(T\mathcal{M}, T^*\mathcal{M}), \quad \left(m, v^i \frac{\partial}{\partial x^i}\Big|_m\right) \mapsto \left(m, (\tau|_m)_{ij}\, v^j \, \mathrm{d}x^i\Big|_m\right), \tag{6.25}$$

$$\sharp_\tau \in C^\infty(T^*\mathcal{M}, T\mathcal{M}), \quad \left(m, \lambda_i \, \mathrm{d}x^i\Big|_m\right) \mapsto \left(m, (\tau|_m)^{ij} \lambda_j \frac{\partial}{\partial x^i}\Big|_m\right). \tag{6.26}$$

Due to the nondegeneracy of τ, the two mappings are inverses of each other, i.e.,

$$\sharp_\tau \circ \flat_\tau \equiv \mathrm{id}_{T\mathcal{M}}. \tag{6.27}$$

By a slight abuse of notation, we use the same symbols from (6.25) and (6.26) also to map between (co)tangent spaces $\flat_\tau \colon T_m\mathcal{M} \to T_m^*\mathcal{M}$ and $\sharp_\tau \colon T_m^*\mathcal{M} \to T_m\mathcal{M}$ (instead of the respective bundles).

6.4.1.5 Pullback of Covectors, Tensor Fields, and Functions

Consider two smooth manifolds $\mathcal{M}, \mathcal{Q}$ and a smooth map $F \in C^\infty(\mathcal{M}, \mathcal{Q})$. Let (U, x) and (V, y) be charts of $\mathcal{M}$ and $\mathcal{Q}$ respectively such that $m \in U$ and $F(m) \in V$. The differential (6.5) of F can be used to define the *pointwise pullback (of covectors) by F at m* via

$$\mathrm{d}F^*|_m \in C^\infty\left(T_{F(m)}^*\mathcal{Q}, T_m^*\mathcal{M}\right), \quad \lambda_i \, \mathrm{d}y^i\Big|_{F(m)} \mapsto \frac{\partial F^i}{\partial x^j}\Big|_m \lambda_i \, \mathrm{d}x^j\Big|_m. \tag{6.28}$$

For a smooth $(0, s)$-tensor field $\tau \in \Gamma(T^{(0,s)}(T\mathcal{Q}))$, the *pullback of τ by F*, denoted by

$F^*\tau \in \Gamma(T^{(0,s)}(T\mathcal{M}))$, is a smooth tensor field (see [74, Prop. 11.26]) with component functions[6]

$$\left(F^*\tau|_m\right)_{\underline{j_1 \dots j_s}} := \left(\tau|_{F(m)}\right)_{\underline{\ell_1 \dots \ell_s}} \cdot \frac{\partial F^{\underline{\ell_1}}}{\partial x^{\underline{j_1}}}\bigg|_m \cdots \frac{\partial F^{\underline{\ell_s}}}{\partial x^{\underline{j_s}}}\bigg|_m. \tag{6.29}$$

A scalar-valued smooth function $h \in C^\infty(\mathcal{Q}, \mathbb{R})$ can be interpreted as a $(0,0)$-tensor field. Then, as a special case of (6.29), the *pullback of (a function) h by F* is a smooth function $F^*h \in C^\infty(\mathcal{M}, \mathbb{R})$ with

$$\left(F^*h\right)(m) = h\left(F(m)\right) = \left(h \circ F\right)(m). \tag{6.30}$$

By Section 6.4.1.1, the differential of a smooth scalar-valued function $G \in C^\infty(\mathcal{Q}, \mathbb{R})$ defines a covector $dG|_{F(m)} \in T_m^*\mathcal{Q}$. Then an analogue to the chain rule (6.6) is

$$d(F^*G)|_m = dF^*|_m dG|_{F(m)} \in T_m^*\mathcal{M}, \tag{6.31}$$

which uses the pullback of a function (6.30) on the left-hand side and applies the pointwise pullback $dF^*|_m \in C^\infty(T_m^*\mathcal{Q}, T_m^*\mathcal{M})$ to the covector $dG|_{F(m)} \in T_m^*\mathcal{Q}$ on the right-hand side of the equation.

6.4.2 Lagrangian Systems

This subsection defines Lagrangian systems formulated on a manifold and additionally introduces further structure required for the MOR part discussed in the forthcoming Section 6.5.2. Consider a Q-dimensional smooth manifold $\mathcal{Q}$ with chart (V, y). As mentioned in Section 6.2.6, the tangent bundle $T\mathcal{Q}$ is a $2Q$-dimensional smooth manifold and the differential $dy \in C^\infty(TV, \mathbb{R}^{2Q})$ defines a natural chart (6.9). We abbreviate this chart with $\xi := dy$ for brevity. By (6.9), it holds

$$\xi \colon TV \to \mathbb{R}^{2Q}, \quad \left(q, v^{\underline{i}} \frac{\partial}{\partial y^{\underline{i}}}\bigg|_q\right) \mapsto \left(y(q), [v^{\underline{i}}]_{1 \le i \le Q}\right).$$

---

[6]The pullbacks from (6.28) and (6.29) can be related in the case of smooth covector fields $\alpha \in \Gamma(T^{(0,1)}(T\mathcal{Q}))$, i.e., $s = 1$, with $(F^*\alpha)|_m = dF^*|_m \alpha|_{F(m)} \in T_m^*\mathcal{M}$.

It will be relevant to differentiate between the first Q and the latter Q entries of ξ for a point $Y_{\mathcal{Q}} = (q, v) \in T\mathcal{Q}$, which will be denoted with

$$\xi^{\underline{i}}(Y_{\mathcal{Q}}) = y^{\underline{i}}(q), \qquad \qquad \xi^{\underline{Q+i}}(Y_{\mathcal{Q}}) = v^{\underline{i}}, \qquad \qquad \text{for } 1 \le i \le Q.$$

To lift a smooth curve $\gamma_{\mathcal{Q}} \in C^{\infty}(\mathcal{I}, \mathcal{Q})$ to its tangent bundle, we define

$$\Gamma_{\gamma_{\mathcal{Q}}} \in C^{\infty}(\mathcal{I}, T\mathcal{Q}), \; t \mapsto \left(\gamma_{\mathcal{Q}}(t), \tfrac{\mathrm{d}}{\mathrm{d}t}\gamma_{\mathcal{Q}}\big|_t\right).$$

We denote a *Lagrangian system* as the tuple $(\mathcal{Q}, \mathscr{L})$ of a smooth manifold $\mathcal{Q}$ and a smooth function $\mathscr{L} \in C^{\infty}(T\mathcal{Q}, \mathbb{R})$, which we refer to as the *Lagrangian function*. The associated second-order differential equation on the manifold is given by the *Euler–Lagrange equation*

$$\frac{\partial\mathscr{L}}{\partial\xi^{\underline{i}}}\bigg|_{\Gamma_{\gamma_{\mathcal{Q}}}(t)} - \frac{\mathrm{d}}{\mathrm{d}t}\left(\frac{\partial\mathscr{L}}{\partial\xi^{\underline{Q+i}}}\bigg|_{\Gamma_{\gamma_{\mathcal{Q}}}(\cdot)}\right)\bigg|_t = 0 \qquad \text{for } 1 \le i \le Q, \qquad \Gamma_{\gamma_{\mathcal{Q}}}(t_0) = \begin{bmatrix} q_0 \\ v_0 \end{bmatrix}, \qquad (6.32)$$

with *initial value* $(q_0, v_0) \in T\mathcal{Q}$, which has to be solved for $\gamma_{\mathcal{Q}} \in C^{\infty}(\mathcal{I}, \mathcal{Q})$. In bold notation, the equation reads for the Lagrangian $\boldsymbol{\mathscr{L}} := \mathscr{L} \circ \xi^{-1} \colon \mathbb{R}^{2Q} \supset \xi(TV) \to \mathbb{R}$, $(\boldsymbol{q}, \boldsymbol{v}) \mapsto \boldsymbol{\mathscr{L}}(\boldsymbol{q}, \boldsymbol{v})$

$$\boldsymbol{D_q\mathscr{L}}\big|_{\left(\boldsymbol{\gamma_{\mathcal{Q}}}(t), \frac{\mathrm{d}}{\mathrm{d}t}\boldsymbol{\gamma_{\mathcal{Q}}}(t)\right)} - \frac{\mathrm{d}}{\mathrm{d}t}\left(\boldsymbol{D_v\mathscr{L}}\big|_{\left(\boldsymbol{\gamma_{\mathcal{Q}}}(\cdot), \frac{\mathrm{d}}{\mathrm{d}t}\boldsymbol{\gamma_{\mathcal{Q}}}(\cdot)\right)}\right)\bigg|_t = \boldsymbol{0}_{Q\times 1} \in \mathbb{R}^Q,$$

where $\boldsymbol{D_q}(\cdot)$ denotes the derivative with respect to the first Q coordinates (named $\boldsymbol{q}$ here) and $\boldsymbol{D_v}(\cdot)$ the derivative for the last Q coordinates (named $\boldsymbol{v}$ here).

Since the Euler–Lagrange equations are obtained from a variation of an action functional, it is well-known that the solution curve is guaranteed to conserve a scalar-valued function (see, e.g., [1, Sec. 3.5] and [85, Prop. 7.3.1]):

Theorem 6.11 (Preservation of energy): *The* *energy*

$$\mathcal{E} \colon T\mathcal{Q} \to \mathbb{R}, \qquad Y_{\mathcal{Q}} = \left(q, v^{\underline{i}}\frac{\partial}{\partial y^{\underline{i}}}\bigg|_q\right) \mapsto v^{\underline{j}}\frac{\partial\mathscr{L}}{\partial\xi^{\underline{Q+j}}}\bigg|_{Y_{\mathcal{Q}}} - \mathscr{L}(Y_{\mathcal{Q}})$$

is conserved along the lift of the solution curve $\gamma_{\mathcal{Q}}$ of the Euler–Lagrange equations, i.e.,

$$\frac{\mathrm{d}}{\mathrm{d}t}\mathcal{E}\left(\Gamma_{\gamma_{\mathcal{Q}}}(\cdot)\right)\bigg|_t = 0 \qquad \text{for all } t \in \mathcal{I}.$$

The Lagrangian is called *regular* if the smooth $(0, 2)$-tensor field defined by the second-order derivative of the Lagrangian w.r.t. the velocity

$$\tau_v|_{Y_Q} := \left.\frac{\partial^2 \mathscr{L}}{\partial \xi^{Q+j} \partial \xi^{Q+i}}\right|_{Y_Q} \mathrm{d}\xi^{Q+i}\Big|_{Y_Q} \otimes \mathrm{d}\xi^{Q+j}\Big|_{Y_Q} \tag{6.33}$$

at each point $Y_Q \in TQ$ is nondegenerate (Section 6.4.1.4). In this case, we can formulate the *Euler–Lagrangian vector field* $X_{\mathscr{L}} \in \mathfrak{X}_{TQ}$ such that at a point $Y_Q = \left(q, v^i \frac{\partial}{\partial x^i}\Big|_q\right) \in TQ$, it holds

$$X_{\mathscr{L}}|_{Y_Q} := v^i \frac{\partial}{\partial \xi^i}\Big|_{Y_Q} + (\tau_v|_{Y_Q})^{(Q+i)(Q+j)} \left(\frac{\partial \mathscr{L}}{\partial \xi^j}\Big|_{Y_Q} - \frac{\partial^2 \mathscr{L}}{\partial \xi^k \partial \xi^{Q+j}}\Big|_{Y_Q} v^k\right) \frac{\partial}{\partial \xi^{Q+i}}\Big|_{Y_Q}, \tag{6.34}$$

where we use the convention from Section 6.4.1.4 to use upper indices to denote the corresponding inverse tensor field. This vector field can be used to formulate the Lagrangian system: Let $\gamma \in C^\infty(\mathcal{I}, TQ)$ be an integral curve of $X_{\mathscr{L}}$ with starting point $(q_0, v_0) \in TQ$. Then, solving the Euler–Lagrange equations (6.32) for γ_Q is equivalent to finding the integral curve γ of $X_{\mathscr{L}}$ with $\gamma(t) = \Gamma_{\gamma_Q}(t)$. In bold notation, the system for γ reads

$$\frac{\mathrm{d}}{\mathrm{d}t}\boldsymbol{\gamma}\Big|_t = \begin{bmatrix} \boldsymbol{\gamma}_v(t) \\ \boldsymbol{\tau}_v|_{\boldsymbol{\gamma}(t)}^{-1} \left(\boldsymbol{D_q}\mathscr{L}|_{\boldsymbol{\gamma}(t)} - \boldsymbol{D}_{\boldsymbol{vq}}^2 \mathscr{L}|_{\boldsymbol{\gamma}(t)} \boldsymbol{\gamma}_v(t)\right) \end{bmatrix} \in \xi(TV) \subset \mathbb{R}^{2Q}. \tag{6.35}$$

Here we denote by $\boldsymbol{D}_{\boldsymbol{vq}}^2 \mathscr{L}|_{\boldsymbol{Y_Q}} \in \mathbb{R}^{Q \times Q}$ the mixed derivative w.r.t. $\boldsymbol{v}$ and $\boldsymbol{q}$ and the solution curve is split $\boldsymbol{\gamma}(t) = (\boldsymbol{\gamma}_q(t), \boldsymbol{\gamma}_v(t)) \in \xi(TV) \subset \mathbb{R}^{2Q}$ in a part for $\boldsymbol{q}$ and a part for $\boldsymbol{v}$. The system (6.35) is typically referred to as the *first-order formulation* for the Lagrangian system.

6.4.3 Hamiltonian Systems

In this subsection, we derive a formulation of Hamiltonian systems on a manifold,[7] providing the structure to perform MOR in the forthcoming Section 6.5.3. Let us recall from Section 6.4.1.1 that the differential of a smooth function $G \in C^\infty(\mathcal{M}, \mathbb{R})$ at a point $m \in \mathcal{M}$ defines a covector $\mathrm{d}G|_m \in T_m^*\mathcal{M}$. Extending this idea, the differential $\mathrm{d}G \in C^\infty(T\mathcal{M}, T\mathbb{R})$ defines a smooth covector field $\mathrm{d}G \in \Gamma(T^{(0,1)}(T\mathcal{M}))$ with component functions $(\mathrm{d}G|_m)_{\underline{i}} = \frac{\partial G}{\partial x^{\underline{i}}}\Big|_m$.

---

[7]Hamiltonian systems may result from Lagrangian systems via a Legendre transformation, but this is not the subject of the current work, so we refer to [1, Sec. 3.6].

For a given symplectic manifold $(\mathcal{M}, \omega)$ and a smooth function $\mathscr{H} \in C^\infty(\mathcal{M}, \mathbb{R})$ referred to as the *Hamiltonian (function)*, the *Hamiltonian vector field*

$$X_{\mathscr{H}} := \sharp_\omega (\mathrm{d}\mathscr{H}) \in \Gamma(T^{(1,0)}(T\mathcal{M})), \quad \text{or in index notation:} \quad (X_{\mathscr{H}}|_m)^{\underline{i}} = (\omega|_m)^{\underline{ij}} (\mathrm{d}\mathscr{H}|_m)_{\underline{j}}$$

is uniquely defined due to the nondegeneracy of ω. A *Hamiltonian system* $(\mathcal{M}, \omega, \mathscr{H})$ is an initial value problem (6.10) with an integral curve $\gamma \in C^\infty(\mathcal{I}, \mathcal{M})$ of $X_{\mathscr{H}}$ with starting point $\gamma_0 \in \mathcal{M}$, i.e.,

$$\left.\frac{\mathrm{d}}{\mathrm{d}t}\gamma\right|_t = X_{\mathscr{H}}|_{\gamma(t)} \in T_{\gamma(t)}\mathcal{M} \qquad \text{and} \qquad \gamma(t_0) = \gamma_0 \in \mathcal{M}. \qquad (6.36)$$

We denote a Hamiltonian system in bold notation[8] with

$$\left.\frac{\mathrm{d}}{\mathrm{d}t}\boldsymbol{\gamma}\right|_t = \left(\boldsymbol{\omega}|_{\boldsymbol{\gamma}(t)}\right)^{-1} \boldsymbol{D}\boldsymbol{\mathscr{H}}|_{\boldsymbol{\gamma}(t)}^\top \in \mathbb{R}^{2\bar{N}}, \qquad \boldsymbol{\gamma}(t_0) = \boldsymbol{\gamma}_0 \in \mathbb{R}^{2\bar{N}}. \qquad (6.37)$$

This special construction of the vector field guarantees that the Hamiltonian is conserved along the solution curve, since

$$\left.\frac{\mathrm{d}}{\mathrm{d}t}(\mathscr{H} \circ \gamma)\right|_t \overset{(6.6)}{=} \left(\mathrm{d}\mathscr{H}|_{\gamma(t)}\right)_{\underline{i}} \left(\left.\frac{\mathrm{d}}{\mathrm{d}t}\gamma\right|_t\right)^{\underline{i}} \overset{(6.36)}{=} \left(\mathrm{d}\mathscr{H}|_{\gamma(t)}\right)_{\underline{i}} \left(\omega|_{\gamma(t)}\right)^{\underline{ij}} \left(\mathrm{d}\mathscr{H}|_{\gamma(t)}\right)_{\underline{j}} = 0,$$

where the last step uses that for skew-symmetric tensors $\sigma \in T^{(2,0)}(T_m\mathcal{M})$, it holds $\lambda_{\underline{i}} \sigma^{\underline{ij}} \lambda_{\underline{j}} = -\lambda_{\underline{i}} \sigma^{\underline{ij}} \lambda_{\underline{j}} = 0$ for all covectors $\lambda \in T_m^*\mathcal{M}$.

For two given symplectic manifolds $(\mathcal{M}, \omega)$ and $(\mathcal{Q}, \eta)$, we call a smooth diffeomorphism $F \in C^\infty(\mathcal{Q}, \mathcal{M})$ a *symplectomorphism* if $F^*\omega = \eta$. It can be shown that the flow of a Hamiltonian system $\theta_t : \mathcal{M} \supset M \to \mathcal{M}$ is a symplectomorphism.

The theorem of Darboux (see e.g. [1, Thm. 3.2.2]) guarantees that for each point $m \in \mathcal{M}$, there exists a chart (U, x) with $m \in U$ which is *canonical*, i.e., the symplectic form in these coordinates can be represented with $\boldsymbol{\omega}|_m \equiv \mathbb{J}_{2\bar{N}}^\top$ by the *canonical Poisson tensor*

$$\mathbb{J}_{2\bar{N}} = \begin{bmatrix} \mathbf{0}_{\bar{N}\times\bar{N}} & \boldsymbol{I}_{\bar{N}} \\ -\boldsymbol{I}_{\bar{N}} & \mathbf{0}_{\bar{N}\times\bar{N}} \end{bmatrix} \in \mathbb{R}^{2\bar{N}\times2\bar{N}} \qquad \text{for which} \qquad \mathbb{J}_{2\bar{N}}^\top = -\mathbb{J}_{2\bar{N}} = \mathbb{J}_{2\bar{N}}^{-1}, \qquad (6.38)$$

---

[8]As the Jacobian $\boldsymbol{D}\boldsymbol{\mathscr{H}}|_m \in \mathbb{R}^{1\times2\bar{N}}$ is a row vector, we need to transpose it for the multiplication to match dimensions.

In the case of $\mathcal{M} = \mathbb{R}^{2\bar{N}}$ with $\boldsymbol{\omega}|_{\boldsymbol{m}} = \mathbb{J}_{2\bar{N}}^{\top}$ for all $m \in \mathcal{M}$, we call $(\mathbb{R}^{2\bar{N}}, \mathbb{J}_{2\bar{N}}^{\top}, \mathcal{H})$ a *canonical Hamiltonian system*.

6.5 Structure-preserving MOR on Manifolds

With the general model reduction framework presented in Section 6.3 at hand, we now discuss how the general framework can be specialized to preserve important features of the initial value problem on the manifold. In more detail, we first introduce the *generalized manifold Galerkin* (GMG) reduction map in Section 6.5.1 and then use it to discuss the structure-preserving MOR of

- Lagrangian systems in Section 6.5.2, and
- Hamiltonian systems in Section 6.5.3.

6.5.1 Generalized Manifold Galerkin

Assume that the manifold $\mathcal{M}$ of dimension N is endowed with a nondegenerate $(0,2)$-tensor field $\tau \in \Gamma(T^{(0,2)}(T\mathcal{M}))$, as defined in Section 6.4.1.4. As in Section 6.3.3, we assume that we have already constructed an embedded submanifold $\varphi(\check{\mathcal{M}}) \subset \mathcal{M}$ defined by a smooth embedding $\varphi \in C^{\infty}(\check{\mathcal{M}}, \mathcal{M})$, i.e., we have completed the APPROXIMATION step from the general MOR workflow in Section 6.3.1.4. The straightforward way to define a reduced tensor field is to use the pullback from Section 6.4.1.5. Hence, we make the following assumption.

Assumption 6.12: *Given the nondegenerate $(0,2)$-tensor field $\tau \in \Gamma(T^{(0,2)}(T\mathcal{M}))$, the smooth embedding $\varphi \in C^{\infty}(\check{\mathcal{M}}, \mathcal{M})$ is such that the reduced tensor field*

$$\check{\tau} := \varphi^{*}\tau \in \Gamma(T^{(0,2)}(T\check{\mathcal{M}})) \,,$$

is nondegenerate.

Note that the reduced tensor field in bold notation reads

$$\check{\boldsymbol{\tau}}|_{\check{\boldsymbol{m}}} = \boldsymbol{D}\boldsymbol{\varphi}|_{\check{\boldsymbol{m}}}^{\top} \, \boldsymbol{\tau}|_{\boldsymbol{\varphi}(\check{\boldsymbol{m}})} \boldsymbol{D}\boldsymbol{\varphi}|_{\check{\boldsymbol{m}}} \in \mathbb{R}^{n \times n}. \tag{6.39}$$

which immediately illustrates that Assumption 6.12 may not be satisfied, in general. For instance, if we take $\mathcal{M} = \mathbb{R}^2$ and $\check{\mathcal{M}} = \mathbb{R}$, the tensor field to be a constant skew-symmetric

matrix and a linear embedding, then Assumption 6.12 is violated. See also the forthcoming Example 6.26. On the other hand, if the tensor field is a Riemannian metric on $\mathcal{M}$, i.e., symmetric and positive definite, then the reduced tensor field is also a Riemannian metric.

We immediately obtain the following relation between the full and reduced musical isomorphisms discussed in Section 6.4.1.4.

Lemma 6.13: *Under Assumption 6.12, it holds*

$$\mathrm{d}\varphi^*|_{\check{m}} \circ \flat_\tau \circ \mathrm{d}\varphi|_{\check{m}} = \flat_{\check{\tau}} \in C^\infty(T_{\check{m}}\check{\mathcal{M}}, T^*_{\check{m}}\check{\mathcal{M}}). \tag{6.40}$$

Proof. We prove the statement in index notation. Using (6.25), (6.29), (6.5), and (6.28), we obtain for all $\check{m} \in \check{\mathcal{M}}$, all $\check{v} \in T_{\check{m}}\check{\mathcal{M}}$ and all $1 \leq i \leq n$

$$
\begin{aligned}
(\flat_{\check{\tau}}(\check{v}))_{\underline{i}} &= (\check{\tau}|_{\check{m}})_{ij}\,\check{v}^{\underline{j}} = (\tau|_{\varphi(\check{m})})_{\ell_1\ell_2}\left.\frac{\partial\varphi^{\underline{\ell_1}}}{\partial x^{\underline{i}}}\right|_{\check{m}}\left.\frac{\partial\varphi^{\underline{\ell_2}}}{\partial x^{\underline{j}}}\right|_{\check{m}}\check{v}^{\underline{j}} \\
&= \left.\frac{\partial\varphi^{\underline{\ell_1}}}{\partial x^{\underline{i}}}\right|_{\check{m}}(\tau|_{\varphi(\check{m})})_{\underline{\ell_1\ell_2}}\left.\frac{\partial\varphi^{\underline{\ell_2}}}{\partial x^{\underline{j}}}\right|_{\check{m}}\check{v}^{\underline{j}} = \left((\mathrm{d}\varphi^*|_{\check{m}} \circ \flat_\tau \circ \mathrm{d}\varphi|_{\check{m}})\,(\check{v})\right)_{\underline{i}}. \qquad \square
\end{aligned}
$$

The additional structure allows us to construct an alternative reduction mapping to the MPG reduction map (6.22), which we refer to as the *generalized manifold Galerkin* (GMG)

$$R_{\mathrm{GMG}} \colon T\mathcal{M} \supseteq E_{\varphi(\check{\mathcal{M}})} \to T\check{\mathcal{M}}, \qquad (m, v) \mapsto \left(\varrho(m), \left(\sharp_{\check{\tau}} \circ \mathrm{d}\varphi^*|_{\varrho(m)} \circ \flat_\tau\right)(v)\right), \tag{6.41}$$

which is defined on the vector bundle

$$E_{\varphi(\check{\mathcal{M}})} := \dot{\bigcup}_{m\in\varphi(\check{\mathcal{M}})}T_m\mathcal{M}.$$

The domain $E_{\varphi(\check{\mathcal{M}})} \subseteq T\mathcal{M}$ of the GMG reduction map is in general smaller than in the original definition of a reduction map (Definition 6.4). Nevertheless, all previous results are valid for reduction maps $R : E_{\varphi(\check{\mathcal{M}})} \to T\check{\mathcal{M}}$ as the reduction map is only used in the ROM to project $X|_{\varphi(\check{m})} \in T_{\varphi(\check{m})}\mathcal{M}$ which is part of $E_{\varphi(\check{\mathcal{M}})}$. We avoided introducing $E_{\varphi(\check{\mathcal{M}})}$ earlier for a better readability. The restriction of the domain for the GMG is necessary as $\mathrm{d}\varphi^*|_{\check{m}} : T^*_{\varphi(\check{m})}\mathcal{M} \to T^*_{\check{m}}\check{\mathcal{M}}$ is defined on $T^*_{\varphi(\check{m})}\mathcal{M}$ only.

By construction, (6.15a), Lemma 6.13, and (6.27), we obtain

$$R_{\mathrm{GMG}}|_{\varphi(\check{m})} \circ \mathrm{d}\varphi|_{\check{m}} = \sharp_{\tilde{\tau}} \circ \mathrm{d}\varphi^*|_{(\varrho \circ \varphi)(\check{m})} \circ \flat_{\tau} \circ \mathrm{d}\varphi|_{\check{m}} = \sharp_{\tilde{\tau}} \circ \flat_{\tilde{\tau}} = \mathrm{id}_{T_{\check{m}}\check{\mathcal{M}}},$$

which proves the following result.

Theorem 6.14: *The GMG reduction* (6.41) *is a reduction map for* φ.

The corresponding ROM (6.16) obtained with the GMG reduction map is called *GMG-ROM*. In bold notation, the associated reduced vector field for the FOM vector field $X \in \mathfrak{X}_{\mathcal{M}}$ reads with (6.15a)

$$\boldsymbol{R}_{\mathrm{GMG}}|_{\boldsymbol{\varphi}(\check{\boldsymbol{m}})}(\boldsymbol{X}|_{\boldsymbol{\varphi}(\check{\boldsymbol{m}})}) = \left(\boldsymbol{D\varphi}|_{(\varrho \circ \varphi)(\check{\boldsymbol{m}})}^{\top} \boldsymbol{\tau}|_{\boldsymbol{\varphi}(\check{\boldsymbol{m}})} \boldsymbol{D\varphi}|_{(\varrho \circ \varphi)(\check{\boldsymbol{m}})}\right)^{-1} \boldsymbol{D\varphi}|_{(\varrho \circ \varphi)(\check{\boldsymbol{m}})}^{\top} \boldsymbol{\tau}|_{\boldsymbol{\varphi}(\check{\boldsymbol{m}})} \boldsymbol{X}|_{\boldsymbol{\varphi}(\check{\boldsymbol{m}})}$$

$$= \left(\boldsymbol{D\varphi}|_{\check{\boldsymbol{m}}}^{\top} \boldsymbol{\tau}|_{\boldsymbol{\varphi}(\check{\boldsymbol{m}})} \boldsymbol{D\varphi}|_{\check{\boldsymbol{m}}}\right)^{-1} \boldsymbol{D\varphi}|_{\check{\boldsymbol{m}}}^{\top} \boldsymbol{\tau}|_{\boldsymbol{\varphi}(\check{\boldsymbol{m}})} \boldsymbol{X}|_{\boldsymbol{\varphi}(\check{\boldsymbol{m}})} \in \mathbb{R}^n. \qquad (6.42)$$

To motivate the name GMG, we consider the special case that $\mathcal{M} = \mathbb{R}^N$, $\check{\mathcal{M}} = \mathbb{R}^n$ are vector spaces over $\mathbb{R}$ (with identity charts $x \equiv \mathrm{id}_{\mathbb{R}^N}$, $\check{x} \equiv \mathrm{id}_{\mathbb{R}^n}$) and the nondegenerate tensor field τ is a Riemannian metric that is constant in coordinates, i.e., $\boldsymbol{\tau}|_{\boldsymbol{m}} = \boldsymbol{\tau} = \mathrm{const}$. We then obtain with (6.42)

$$\boldsymbol{R}_{\mathrm{GMG}}|_{\boldsymbol{\varphi}(\check{\boldsymbol{m}})}\left(\boldsymbol{X}|_{\boldsymbol{\varphi}(\check{\boldsymbol{m}})}\right) = \left(\left(\boldsymbol{D\varphi}|_{\check{\boldsymbol{m}}}^{\top} \boldsymbol{\tau}^{1/2}\right)\left(\boldsymbol{\tau}^{1/2} \boldsymbol{D\varphi}|_{\check{\boldsymbol{m}}}\right)\right)^{-1} \left(\boldsymbol{D\varphi}|_{\check{\boldsymbol{m}}}^{\top} \boldsymbol{\tau}^{1/2}\right) \boldsymbol{\tau}^{1/2} \boldsymbol{X}|_{\boldsymbol{\varphi}(\check{\boldsymbol{m}})}$$

$$= \left(\boldsymbol{\tau}^{1/2} \boldsymbol{D\varphi}|_{\check{\boldsymbol{m}}}\right)^{\dagger} \boldsymbol{\tau}^{1/2} \boldsymbol{X}|_{\boldsymbol{\varphi}(\check{\boldsymbol{m}})},$$

where $(\cdot)^{\dagger}$ denotes the Moore–Penrose pseudoinverse. In particular, we recover the *manifold Galerkin projection* introduced in [75, Rem 3.4], which allows interpreting the reduced vector field as the optimal projection w.r.t. the Riemannian metric τ; see [75, Sec. 3.2].

Example 6.15 (Special case: MOR on subspaces)**:** *In the case of* ϱ, φ *being linear as in Example 6.5 with* $\boldsymbol{\tau} \equiv \mathrm{const}$, *the GMG reduction*

$$\boldsymbol{R}_{GMG}|_{\boldsymbol{\varphi}(\check{\boldsymbol{m}})}(\boldsymbol{v}) = \left(\boldsymbol{V}^{\top} \boldsymbol{\tau} \boldsymbol{V}\right)^{-1} \boldsymbol{V}^{\top} \boldsymbol{\tau} \boldsymbol{v}, \qquad \frac{\mathrm{d}}{\mathrm{d}t}\check{\boldsymbol{\gamma}}\Big|_t = \left(\boldsymbol{V}^{\top} \boldsymbol{\tau} \boldsymbol{V}\right)^{-1} \boldsymbol{V}^{\top} \boldsymbol{\tau} \boldsymbol{X}|_{\check{\boldsymbol{\gamma}}(t)}$$

is exactly the ROM obtained in Part I via the a-based projection (2.4), *where Assumption 6.12 is exactly the compatibility condition.*

As discussed in Section 6.4, the FOM vector field may possess additional structure in specific applications, such as Lagrangian or Hamiltonian dynamics. In the following, we show that

the GMG reduction can be used to formulate structure-preserving MOR (on manifolds) for Lagrangian and Hamiltonian systems by choosing a specific nondegenerate tensor field.

6.5.2 MOR on Manifolds for Lagrangian Systems

As in Section 6.4.2, consider a Q-dimensional smooth manifold Q with a chart (V, y) and the corresponding natural chart (TV, ξ) of the tangent bundle TQ (Section 6.4.2). The manifold to be reduced in the context of Lagrangian systems is the tangent bundle TQ. To be consistent with the notation introduced before, we thus set $\mathcal{M} := TQ$ with even dimension $N := \dim(\mathcal{M}) := 2Q$. Instead of working directly on $\mathcal{M}$, we still aim for a construction on Q by employing that the differential of a smooth map (Section 6.2.6) is a mapping between the associated tangent spaces.

Definition 6.16 (Lifted embedding and lifted point reduction): *Consider an embedded submanifold $\varphi_Q(\check{Q}) \subset Q$ defined by a $\check{Q}$-dimensional manifold $\check{Q}$ and a smooth embedding $\varphi_Q \colon \check{Q} \to \varphi_Q(\check{Q})$. Then, we call*

$$\varphi := \mathrm{d}\varphi_Q \colon T\check{Q} \to T\big(\varphi_Q(\check{Q})\big), \qquad (\check{q}, \check{v}) \mapsto \Big(\varphi_Q\left(\check{q}\right), \mathrm{d}\varphi_Q\big|_{\check{q}}\left(\check{v}\right)\Big)$$

the lifted embedding for φ_Q. Analogously, for a point reduction $\varrho_Q \colon Q \to \check{Q}$, we define the lifted point reduction

$$\varrho := \mathrm{d}\varrho_Q \colon TQ \to T\check{Q}, \qquad (q, v) \mapsto \Big(\varrho_Q\left(q\right), \mathrm{d}\varrho_Q\big|_q(v)\Big).$$

Let us emphasize that ϱ is indeed a point reduction on $\mathcal{M} = TQ$ for the lifted embedding φ, which is a straightforward consequence of Theorem 6.9. For $\left(\check{q}, \check{v}^k \frac{\partial}{\partial \check{y}^k}\big|_{\check{q}}\right) \in T\check{Q}$ with a chart $(\check{V}, \check{y})$ for $\check{Q}$ and $(T\check{V}, \check{\xi})$ for $T\check{Q}$, we immediately obtain

$$\frac{\partial \varphi^i}{\partial \check{\xi}^j}\bigg|_{\left(\check{q}, \check{v}^k \frac{\partial}{\partial \check{y}^k}\big|_{\check{q}}\right)} = \begin{cases} \dfrac{\partial \varphi_Q{}^i}{\partial \check{y}^j}\bigg|_{\check{q}}, & 1 \le i \le Q,\ 1 \le j \le \check{Q}, \\[2ex] 0, & 1 \le i \le Q,\ 1 \le j - \check{Q} \le \check{Q}, \\[2ex] \dfrac{\partial^2 \varphi_Q{}^{i-Q}}{\partial \check{y}^j \partial \check{y}^k}\bigg|_{\check{q}} \check{v}^k, & 1 \le i - Q \le Q,\ 1 \le j \le \check{Q}, \\[2ex] \dfrac{\partial \varphi_Q{}^{i-Q}}{\partial \check{y}^{j-\check{Q}}}\bigg|_{\check{q}}, & 1 \le i - Q \le Q,\ 1 \le j - \check{Q} \le \check{Q}, \end{cases}$$

which reads in bold notation

$$\boldsymbol{\varphi}\left(\check{\boldsymbol{q}},\check{\boldsymbol{v}}\right)=\begin{bmatrix}\boldsymbol{\varphi}_{\mathcal{Q}}\left(\check{\boldsymbol{q}}\right)\\\boldsymbol{D}\boldsymbol{\varphi}_{\mathcal{Q}}\big|_{\check{\boldsymbol{q}}}\check{\boldsymbol{v}}\end{bmatrix}\in\mathbb{R}^{2Q},\quad\boldsymbol{D}\boldsymbol{\varphi}\big|_{(\check{\boldsymbol{q}},\check{\boldsymbol{v}})}=\begin{bmatrix}\boldsymbol{D}\boldsymbol{\varphi}_{\mathcal{Q}}\big|_{\check{\boldsymbol{q}}}&\boldsymbol{0}_{Q\times\check{Q}}\\\boldsymbol{D}\left(\boldsymbol{D}\boldsymbol{\varphi}_{\mathcal{Q}}\big|_{(\cdot)}\check{\boldsymbol{v}}\right)\big|_{\check{\boldsymbol{q}}}&\boldsymbol{D}\boldsymbol{\varphi}_{\mathcal{Q}}\big|_{\check{\boldsymbol{q}}}\end{bmatrix}\in\mathbb{R}^{2Q\times2\check{Q}}.$$

Example 6.17: *For a linear embedding $\boldsymbol{\varphi}_{\mathcal{Q}}\left(\check{\boldsymbol{q}}\right)=\boldsymbol{V}\check{\boldsymbol{q}}$ as in Example 6.5, the lifted embedding from Definition 6.16 is described by a block-diagonal basis matrix*

$$\boldsymbol{\varphi}\left(\check{\boldsymbol{q}},\check{\boldsymbol{v}}\right)=\begin{bmatrix}\boldsymbol{V}&\boldsymbol{0}_{Q\times\check{Q}}\\\boldsymbol{0}_{Q\times\check{Q}}&\boldsymbol{V}\end{bmatrix}\begin{bmatrix}\check{\boldsymbol{q}}\\\check{\boldsymbol{v}}\end{bmatrix},$$

which is frequently used in MOR for second-order systems (see, e.g., [106]).

With these preparations, let us now assume that we have a Lagrangian system $(\mathcal{Q},\mathscr{L})$ with initial value $(q_0,v_0)\in T\mathcal{Q}$ together with embedded submanifold $\varphi_{\mathcal{Q}}(\check{\mathcal{Q}})\subset\mathcal{Q}$ with the embedding $\varphi_{\mathcal{Q}}$ and a point reduction $\varrho_{\mathcal{Q}}$ available. Let φ and ϱ denote the corresponding lifted embedding and lifted point reduction as in Definition 6.16. To preserve the Lagrangian system structure in the ROM, we do not aim for a projection of the Euler–Lagrange equations (6.32) but rather start by constructing a reduced Lagrangian via

$$\check{\mathscr{L}}:=\varphi^*\mathscr{L}=\mathscr{L}\circ\varphi\in C^\infty(T\check{\mathcal{Q}},\mathbb{R})\tag{6.43}$$

and immediately obtain the reduced Lagrangian system $(\check{\mathcal{Q}},\check{\mathscr{L}})$ with the reduced initial value $(\check{q}_0,\check{v}_0):=\varrho\left(q_0,v_0\right)\in T\check{\mathcal{Q}}=:\check{\mathcal{M}}$. Note that with this strategy, we immediately obtain the ROM that itself is a Lagrangian system, which is not automatically guaranteed if we reduce the vector field (6.34). Straightforward calculations (see Appendix A.2.1) show that the Euler-Lagrange equations of the reduced Lagrangian system read

$$\begin{aligned}0=\frac{\partial\varphi_{\mathcal{Q}}{}^j}{\partial\check{y}^{\check{\imath}}}\bigg|_{\check{\gamma}(t)}&\left(\frac{\partial\mathscr{L}}{\partial\xi^{\underline{j}}}\bigg|_{\varphi(\Gamma_{\check{\gamma}}(t))}-\frac{\partial^2\mathscr{L}}{\partial\xi^{\underline{k}}\,\partial\xi^{\underline{Q+j}}}\bigg|_{\varphi\left(\Gamma_{\check{\gamma}_{\mathcal{Q}}}(t)\right)}\frac{\partial\varphi_{\mathcal{Q}}{}^k}{\partial\check{y}^{\check{\ell}}}\bigg|_{\check{\gamma}_{\mathcal{Q}}(t)}\frac{\mathrm{d}}{\mathrm{d}t}\check{\gamma}_{\mathcal{Q}}{}^{\underline{\ell}}\bigg|_t\right.\\[1em]&-\frac{\partial^2\mathscr{L}}{\partial\xi^{\underline{Q+k}}\,\partial\xi^{\underline{Q+j}}}\bigg|_{\varphi\left(\Gamma_{\check{\gamma}_{\mathcal{Q}}}(t)\right)}\frac{\partial^2\varphi_{\mathcal{Q}}{}^k}{\partial\check{y}^{\check{\ell}}\,\partial\check{y}^{\check{p}}}\bigg|_{\check{\gamma}_{\mathcal{Q}}|_t}\frac{\mathrm{d}}{\mathrm{d}t}\check{\gamma}_{\mathcal{Q}}{}^{\underline{p}}\bigg|_t\frac{\mathrm{d}}{\mathrm{d}t}\check{\gamma}_{\mathcal{Q}}{}^{\underline{\ell}}\bigg|_t\\[1em]&\left.-\frac{\partial^2\mathscr{L}}{\partial\xi^{\underline{Q+k}}\,\partial\xi^{\underline{Q+j}}}\bigg|_{\varphi\left(\Gamma_{\check{\gamma}_{\mathcal{Q}}}(t)\right)}\frac{\partial\varphi_{\mathcal{Q}}{}^k}{\partial\check{y}^{\check{\ell}}}\bigg|_{\check{\gamma}_{\mathcal{Q}}(t)}\frac{\mathrm{d}^2}{\mathrm{d}t^2}\check{\gamma}_{\mathcal{Q}}{}^{\underline{\ell}}\bigg|_t\right)\end{aligned}\tag{6.44}$$

for $1 \leq i \leq n$ where the right-hand side sums over $1 \leq j, k \leq Q$ and $1 \leq \ell, p \leq \check{Q}$ by the Einstein summation convention (6.1). In bold notation, the reduced Euler–Lagrange equations read

$$
\begin{aligned}
\mathbf{0}_{\check{Q}\times 1} = \boldsymbol{D\varphi_Q}\big|_{\check{\gamma}_Q(t)}^{\top} \Bigg(&\boldsymbol{D_q\mathscr{L}}\big|_{\boldsymbol{\varphi}\left(\check{\gamma}_Q(t), \frac{\mathrm{d}}{\mathrm{d}t}\check{\gamma}_Q\big|_t\right)} - \boldsymbol{D_{vq}^2\mathscr{L}}\big|_{\boldsymbol{\varphi}\left(\check{\gamma}_Q(t), \frac{\mathrm{d}}{\mathrm{d}t}\check{\gamma}_Q\big|_t\right)} \boldsymbol{D\varphi_Q}\big|_{\check{\gamma}_Q(t)} \frac{\mathrm{d}}{\mathrm{d}t}\check{\gamma}_Q\big|_t \\
&- \boldsymbol{D_{vv}^2\mathscr{L}}\big|_{\boldsymbol{\varphi}\left(\check{\gamma}_Q(t), \frac{\mathrm{d}}{\mathrm{d}t}\check{\gamma}_Q\big|_t\right)} \boldsymbol{D^2\varphi_Q}\big|_{\check{\gamma}_Q(t)} \left(\frac{\mathrm{d}}{\mathrm{d}t}\check{\gamma}_Q\big|_t \otimes \frac{\mathrm{d}}{\mathrm{d}t}\check{\gamma}_Q\big|_t\right) \\
&- \boldsymbol{D_{vv}^2\mathscr{L}}\big|_{\boldsymbol{\varphi}\left(\check{\gamma}_Q(t), \frac{\mathrm{d}}{\mathrm{d}t}\check{\gamma}_Q\big|_t\right)} \boldsymbol{D\varphi_Q}\big|_{\check{\gamma}_Q(t)} \frac{\mathrm{d}^2}{\mathrm{d}t^2}\check{\gamma}_Q\big|_t \Bigg) \in \mathbb{R}^{\check{Q}}.
\end{aligned}
\tag{6.45}
$$

By construction, the reduced Lagrangian system fulfills the Euler–Lagrange equations for the reduced Lagrangian $\check{\mathscr{L}}$. Thus, Theorem 6.11 guarantees that along the lift of the solution curve $\check{\gamma}_Q$, the *reduced energy*

$$
\check{\mathcal{E}} \colon T\check{\mathcal{Q}} \to \mathbb{R}, \qquad \check{Y}_Q = \left(\check{q}, \check{v}^i \frac{\partial}{\partial \check{y}^i}\Big|_{\check{q}}\right) \mapsto \check{v}^j \frac{\partial \check{\mathscr{L}}}{\partial \check{\xi}^{\check{Q}+j}}\Big|_{\check{Y}_Q} - \check{\mathscr{L}}\left(\check{Y}_Q\right)
$$

is preserved. Moreover, it holds $\check{\mathcal{E}} \equiv \mathcal{E} \circ \varphi$.

Following the construction in Section 6.4.2 and assuming that the reduced Lagrangian $\check{\mathscr{L}}$ is regular, we can formulate a reduced vector field $\check{X}_{\check{\mathscr{L}}} \in \Gamma(T^{(1,0)}(T\check{\mathcal{M}}))$ for the reduced Euler–Lagrange equations (6.45). Indeed, we obtain for a point $\check{Y}_Q = \left(\check{q}, \check{v}^i \frac{\partial}{\partial \check{y}^i}\Big|_{\check{q}}\right) \in T\check{\mathcal{Q}}$ as

$$
\check{X}_{\check{\mathscr{L}}}\big|_{\check{Y}_Q} =: \check{v}^i \frac{\partial}{\partial \check{\xi}^i}\Big|_{\check{Y}_Q} + (\sigma|_{\check{Y}_Q})^i_{\underline{\ell}}\left(\left(X_{\mathscr{L}}\big|_{\varphi(\check{Y}_Q)}\right)^{Q+\ell} - \frac{\partial^2 \varphi_Q{}^\ell}{\partial \check{y}^p \partial \check{y}^r}\Big|_{\check{q}} \check{v}^{\underline{p}}\check{v}^{\underline{r}}\right) \frac{\partial}{\partial \check{\xi}^{\check{Q}+i}}\Big|_{\check{Y}_Q}
\tag{6.46}
$$

with indices $1 \leq k, \ell \leq Q$ and $1 \leq i, j, p, r \leq \check{Q}$ and

$$
(\sigma|_{\check{Y}_Q})^i_{\underline{\ell}} := (\check{\tau}_v|_{\check{Y}_Q})^{ij} \frac{\partial \varphi_Q{}^k}{\partial \check{y}^{\underline{j}}}\Big|_{\check{q}} \left(\tau_v|_{\varphi(\check{Y}_Q)}\right)_{\underline{k\ell}}.
$$

In order to relate this reduction to our framework, we show in the following that the reduced Euler–Lagrangian vector field (6.46) can be interpreted as a GMG reduction (6.41) of the Euler–Lagrangian vector field (6.34) if an appropriate tensor field is selected. We refer to this as the *Lagrangian manifold Galerkin* (LMG). With the nondegenerate tensor field τ_v

from (6.33), we define a tensor field $\tau_{\mathsf{LMG}} \in \Gamma(T^{(0,2)}(T\mathcal{M}))$ on $\mathcal{M} = TQ$ with

$$\tau_{\mathsf{LMG}}\big|_{Y_Q} := \left(\tau_q\big|_{Y_Q}\right)_{\underline{ij}} \, \mathrm{d}\xi^{\underline{Q+i}}\big|_{Y_Q} \otimes \mathrm{d}\xi^{\underline{j}}\big|_{Y_Q} + \left(\tau_v\big|_{Y_Q}\right)_{\underline{ij}} \, \mathrm{d}\xi^{\underline{i}}\big|_{Y_Q} \otimes \mathrm{d}\xi^{\underline{Q+j}}\big|_{Y_Q}, \qquad (6.47)$$

where $\left(\tau_q\big|_{Y_Q}\right)_{\underline{ij}}$ are additional components. A typical choice could be $\left(\tau_q\big|_{Y_Q}\right)_{\underline{ij}} = \left(\tau_v\big|_{Y_Q}\right)_{\underline{ij}}$. In bold notation, the tensor field reads

$$\boldsymbol{\tau}_{\mathsf{LMG}}\big|_{\boldsymbol{Y}_Q} = \begin{bmatrix} \mathbf{0}_{Q \times Q} & \boldsymbol{\tau}_v\big|_{\boldsymbol{Y}_Q} \\ \boldsymbol{\tau}_q\big|_{\boldsymbol{Y}_Q} & \mathbf{0}_{Q \times Q} \end{bmatrix}. \qquad (6.48)$$

The associated reduced tensor field is denoted with $\check{\tau}_{\mathsf{LMG}}$ (as in Section 6.5.1). Assuming that $\check{\tau}_{\mathsf{LMG}}$ is nondegenerate, we define the LMG reduction map

$$R_{\mathsf{LMG}} \colon T\mathcal{M} \supseteq E_{\varphi(\check{\mathcal{M}})} \to T\check{\mathcal{M}}, \quad (m, v) \mapsto \left(\varrho(m), \left(\sharp_{\check{\tau}_{\mathsf{LMG}}} \circ \mathrm{d}\varphi^*\big|_{\varrho(m)} \circ \flat_{\tau_{\mathsf{LMG}}}\right)(v)\right). \quad (6.49)$$

The LMG reduction map (6.49) is a particular case of a GMG reduction map, and thus, we immediately obtain from Theorem 6.14 that R_{LMG} is a reduction map for the lifted embedding φ.

Theorem 6.18: *Consider the ROM obtained by reducing the Euler–Lagrange vector field with R_{LMG}. Then solving this ROM for $\check{\gamma}$ is equivalent to solving the reduced Euler–Lagrange equations (6.44) for $\check{\gamma}_Q$ with $\check{\gamma}(t) = \Gamma_{\check{\gamma}_Q}(t)$.*

Proof. (Appendix A.2.2).   □

We conclude this section with four remarks.

Remark 6.19: *In the special case of classical MOR $Q = \mathbb{R}^Q$, $\check{Q} = \mathbb{R}^{\check{Q}}$ with a linear embedding $\varphi_Q(\check{q}) = V\check{q}$ as in Example 6.17, a linear point reduction map $\varrho_Q(q) = V^\top q$, and a quadratic Lagrangian $\mathscr{L}$, the reduced Euler–Lagrange equations (6.45) recover the ROM from [69]. In our framework that relates to the choice $\mathcal{M} = \mathbb{R}^{2Q}$, $\check{\mathcal{M}} = \mathbb{R}^{2\check{Q}}$, φ as in Example 6.17, and $\boldsymbol{R}_{LMG}(\boldsymbol{v_q}, \boldsymbol{v_v}) = [\boldsymbol{v_q}^\top V^\top, \, \boldsymbol{v_v}^\top V^\top]^\top$.*

Remark 6.20: *In [69], the authors argue that the reduced Euler–Lagrange equations cannot be obtained from a projection with the embedding φ_Q of the first-order system (which is formulated with the Euler–Lagrange vector field (6.34) in the scope of our work). This is no contradiction to our work (where we project the first-order system) since we suggest a projection based on the*

lifted embedding φ from Definition 6.16 to obtain the reduced Euler–Lagrange equations via a reduction of the Euler–Lagrange vector field.

Remark 6.21 (Second-order derivatives of φ_Q)**:** *The reduced Euler–Lagrange equations require the computation of second-order derivatives of φ_Q, which might be computationally intensive. Notably, the formulation of structure-preserving MOR for Hamiltonian systems presented in the following subsection is independent of second-order derivatives of the embedding φ_Q.*

Remark 6.22 (Nonintrusive MOR)**:** *A nonintrusive technique for structure-preserving MOR of Lagrangian systems on subspaces was presented in [107]. It learns a Lagrangian function from snapshot data using knowledge about the governing equations (but not its discretization). So, it does not require access to the FOM operators and is nonintrusive by means of Remark 2.14.*

6.5.3 MOR on Manifolds for Hamiltonian Systems

Lastly, we assume to be given a Hamiltonian system $(\mathcal{M}, \omega, \mathcal{H})$ as FOM and demonstrate how structure-preserving MOR on manifolds can be formulated. The procedure works analogously to the GMG from Section 6.5.1, while choosing the symplectic form ω as the nondegenerate tensor field $\tau = \omega$. First, we assume that the APPROXIMATION step is completed and we are given a reduced manifold $\breve{\mathcal{M}}$ and a smooth embedding $\varphi \in C^\infty(\breve{\mathcal{M}}, \mathcal{M})$ fulfilling Assumption 6.12, i.e., $\varphi^*\omega$ is nondegenerate. We show at the end of this section (Lemma 6.25) that this assumption is sufficient for $\breve{\omega} := \varphi^*\omega$ being a symplectic form and $(\breve{\mathcal{M}}, \breve{\omega})$ being a symplectic manifold. In this case, the embedding $\varphi \colon (\breve{\mathcal{M}}, \breve{\omega}) \to (\varphi(\breve{\mathcal{M}}), \omega|_{\varphi(\breve{\mathcal{M}})})$ is a symplectomorphism. Second, we use the reduction map

$$R_{\mathrm{SMG}} \colon T\mathcal{M} \supseteq E_{\varphi(\breve{\mathcal{M}})} \to T\breve{\mathcal{M}}, \qquad (m, v) \mapsto \left(\varrho(m), \left(\sharp_{\breve{\omega}} \circ \mathrm{d}\varphi^*|_{\varrho(m)} \circ \flat_\omega \right)(v) \right), \qquad (6.50)$$

which we refer to as the *symplectic manifold Galerkin* (SMG) reduction map. The SMG reduction map is a special case of the GMG reduction map (6.41) with $\tau = \omega$ and $\breve{\tau} = \breve{\omega}$, and, thus, we obtain from Theorem 6.14 that R_{SMG} is a reduction map for φ. Hence, the SMG reduction fits in our MOR framework from Section 6.3.1 and it defines a ROM by (6.16), which we refer to as the SMG-ROM. It remains to show that the SMG-ROM indeed is a Hamiltonian system, which was the motivation for preserving the underlying structure.

Theorem 6.23: *The SMG-ROM is a Hamiltonian system $(\breve{\mathcal{M}}, \breve{\omega}, \breve{\mathcal{H}})$ with the reduced Hamiltonian $\breve{\mathcal{H}} := \varphi^*\mathcal{H} = \mathcal{H} \circ \varphi$.*

Proof. The ROM vector field with the SMG reduction (6.50) reads with (a) equations (6.15a) and (6.27), and (b) equation (6.31)

$$
\begin{aligned}
R_{\mathrm{SMG}}|_{\varphi(\tilde{m})}(X_{\mathcal{H}}|_{\varphi(\tilde{m})}) &= \left(\sharp_{\check{\omega}} \circ \mathrm{d}\varphi^*|_{(\varrho\circ\varphi)(\tilde{m})} \circ \flat_{\omega}\right)\left(\sharp_{\omega}\left(\mathrm{d}\mathcal{H}|_{\varphi(\tilde{m})}\right)\right) \\
&\overset{(a)}{=} \sharp_{\check{\omega}}\left(\mathrm{d}\varphi^*|_{\tilde{m}}\left(\mathrm{d}\mathcal{H}|_{\varphi(\tilde{m})}\right)\right) \overset{(b)}{=} \sharp_{\check{\omega}}\left(\mathrm{d}\check{\mathcal{H}}|_{\tilde{m}}\right),
\end{aligned}
\tag{6.51}
$$

which is exactly the Hamiltonian vector field of the Hamiltonian system $(\check{\mathcal{M}}, \check{\omega}, \check{\mathcal{H}})$. $\qquad\square$

Using (6.42), the reduced vector field in the SMG-ROM in bold notation reads

$$
\boldsymbol{R}_{\mathrm{SMG}}|_{\boldsymbol{\varphi}(\check{\boldsymbol{m}})}(\boldsymbol{X}_{\mathcal{H}}|_{\boldsymbol{\varphi}(\check{\boldsymbol{m}})}) = \left(\boldsymbol{D\varphi}|_{\check{\boldsymbol{m}}}^{\top}\boldsymbol{\omega}|_{\boldsymbol{\varphi}(\check{\boldsymbol{m}})}\boldsymbol{D\varphi}|_{\check{\boldsymbol{m}}}\right)^{-1}\underbrace{\boldsymbol{D\varphi}|_{\check{\boldsymbol{m}}}^{\top}\boldsymbol{\omega}|_{\boldsymbol{\varphi}(\check{\boldsymbol{m}})}\boldsymbol{X}_{\mathcal{H}}|_{\boldsymbol{\varphi}(\check{\boldsymbol{m}})}}_{=\boldsymbol{D\varphi}|_{\check{\boldsymbol{m}}}^{\top}\boldsymbol{D\mathcal{H}}|_{\boldsymbol{\varphi}(\check{\boldsymbol{m}})}^{\top}=\boldsymbol{D\check{\mathcal{H}}}|_{\check{\boldsymbol{m}}}^{\top}}.
\tag{6.52}
$$

For a canonical Hamiltonian system, our generalization of the SMG-ROM is consistent with the definitions existing in the literature, which is shown by the following lemma.

Lemma 6.24: *For a canonical Hamiltonian system* $(\mathbb{R}^{2\bar{N}}, \mathbb{J}_{2\bar{N}}^{\top}, \mathcal{H})$ *and reduced symplectic manifold* $(\check{\mathcal{M}}, \check{\omega}) = (\mathbb{R}^{2\bar{n}}, \mathbb{J}_{2\bar{n}}^{\top})$*, it holds that*

1. *the SMG reduction evaluated at the base point* $\boldsymbol{\varphi}(\check{\boldsymbol{m}})$ *equals the symplectic inverse*

$$
\boldsymbol{R}_{SMG}|_{\boldsymbol{\varphi}(\check{\boldsymbol{m}})}(\boldsymbol{v}) = \boldsymbol{D\varphi}|_{\check{\boldsymbol{m}}}^{+}\boldsymbol{v} := \mathbb{J}_{2\bar{n}}\,\boldsymbol{D\varphi}|_{\check{\boldsymbol{m}}}^{\top}\,\mathbb{J}_{2\bar{N}}^{\top}\boldsymbol{v} \qquad \textit{for all } \boldsymbol{v} \in \mathbb{R}^{2\bar{N}},
$$

2. *the SMG-ROM is consistent with [22], and*

3. *if, moreover, the embedding* φ *is linear, the SMG-ROM equals the symplectic Galerkin ROM introduced in [81, 99] and Section 2.4.*

Proof. By assumption, it holds $\mathcal{M} = \mathbb{R}^{2\bar{N}}$, $\boldsymbol{\omega} = \mathbb{J}_{2\bar{N}}^{\top}$, $\check{\mathcal{M}} = \mathbb{R}^{2\bar{n}}$, $\check{\boldsymbol{\omega}} = \mathbb{J}_{2\bar{n}}^{\top}$. (i) Inserting the quantities in (6.52) yields the statement. (ii) For φ to be a symplectomorphism, i.e., $(\varphi^*\omega)|_{\tilde{m}} = \check{\omega}|_{\tilde{m}}$ for all $\tilde{m} \in \check{\mathcal{M}}$, is with (6.39) equivalent to

$$
\boldsymbol{D\varphi}|_{\check{\boldsymbol{m}}}^{\top}\,\mathbb{J}_{2\bar{N}}^{\top}\boldsymbol{D\varphi}|_{\check{\boldsymbol{m}}} = \mathbb{J}_{2\bar{n}}^{\top} \qquad \textit{for all } \check{\boldsymbol{m}} \in \mathbb{R}^{2\bar{n}}.
\tag{6.53}
$$

Considering $\mathbb{J}_{2\bar{N}}^{\top} = -\mathbb{J}_{2\bar{N}}$ and $\mathbb{J}_{2\bar{n}}^{\top} = -\mathbb{J}_{2\bar{n}}$ and multiplying the previous equation on both sides with (-1), gives exactly the definition of a symplectic embedding from [22, Def. 2]. Thus, the assumptions on the embedding are equivalent (up to smoothness requirements). Moreover, the SMG-ROM in [22] is projected with the symplectic inverse which (by point (i))

is equivalent to the SMG reduction map for the case assumed in the present lemma ($\mathcal{M} = \mathbb{R}^{2\bar{N}}$, $\boldsymbol{\omega} = \mathbb{J}_{2\bar{N}}^\top$, $\check{\mathcal{M}} = \mathbb{R}^{2\bar{n}}$, $\check{\boldsymbol{\omega}} = \mathbb{J}_{2\bar{n}}^\top$).

(iii) If the embedding is linear, then there exists $\boldsymbol{V} \in \mathbb{R}^{2\bar{N} \times 2\bar{n}}$ such that $\boldsymbol{\varphi}(\check{\boldsymbol{m}}) = \boldsymbol{V}\check{\boldsymbol{m}}$. Then, the requirement of φ to be a symplectomorphism is equivalent to $\boldsymbol{V}^\top \mathbb{J}_{2\bar{N}} \boldsymbol{V} = \mathbb{J}_{2\bar{n}}$, which is in [99, Eq. 3.2] formulated as the condition that $\boldsymbol{V}$ is a symplectic matrix. Moreover, the symplectic inverse of $\boldsymbol{V}$ is used to obtain the ROM, which is, again, by point (i), equivalent to our approach in this particular case. $\square$

However, our approach extends the existing methods, as it also works (i) on general smooth manifolds (not just $\mathcal{M} = \mathbb{R}^{2\bar{N}}$) and (ii), as in Section 2.4, in the case $\mathcal{M} = \mathbb{R}^{2\bar{N}}$ for noncanonical symplectic forms $\boldsymbol{\omega} \neq \mathbb{J}_{2\bar{N}}^\top$.

It remains to show that assuming nondegeneracy of $\varphi^*\omega$ is sufficient for $\varphi^*\omega$ being a symplectic form, which we show in the following.

Lemma 6.25: *Consider a symplectic manifold $(\mathcal{M}, \omega)$, a smooth manifold $\check{\mathcal{M}}$, and a smooth embedding $\varphi \in C^\infty(\check{\mathcal{M}}, \mathcal{M})$ such that $\check{\omega} := \varphi^*\omega$ is nondegenerate. Then $\check{\omega}$ is a symplectic form, $(\check{\mathcal{M}}, \check{\omega})$ is a symplectic manifold, and φ is a symplectomorphism.*

Proof. It is sufficient to show that $\check{\omega} = \varphi^*\omega$ is a symplectic form, which in this case results in showing that $\check{\omega}$ is skew-symmetric and closed. The skew-symmetry is inherited pointwise for all points $\check{m} \in \check{\mathcal{M}}$. Closedness is inherited as the pullback of a closed form is closed [74, proof of Prop. 17.2]. $\square$

Note that this is a central difference to reduced Riemannian metrics, which are automatically nondegenerate due to positive definiteness. The following example shows that the reduced tensor field can degenerate if arbitrary embeddings φ are considered for symplectic forms.

Example 6.26 (Degenerate $\varphi^*\omega$)**:** *For an arbitrary $\bar{n}$ with $2\bar{n} \leq N$, consider $\mathcal{M} = \mathbb{R}^{2\bar{N}}$, $\boldsymbol{\omega} = \mathbb{J}_{2\bar{N}}^\top$, $\check{\mathcal{M}} = \mathbb{R}^{2\bar{n}}$, and the embedding*

$$\boldsymbol{\varphi}(\check{\boldsymbol{m}}) = \boldsymbol{E}\check{\boldsymbol{m}} \qquad \text{with} \qquad \boldsymbol{E} := \begin{bmatrix} \boldsymbol{I}_{2\bar{n}} \\ \boldsymbol{0}_{(2\bar{N}-2\bar{n}) \times 2\bar{n}} \end{bmatrix} \in \mathbb{R}^{2\bar{N} \times 2\bar{n}}.$$

In this case, $\varphi(\check{\mathcal{M}}) \subset \mathbb{R}^{2\bar{N}}$ is an isotropic subspace (see Section 2.4.1) and, thus, it holds with

name	ref.		details
QPROM	[5, 41, 59]	MPG	ϱ linear, φ quadratic
Galerkin-BQ	[108]	MPG	ϱ linear, φ blockwise-quadratic
EncROM	[93]	MPG	ϱ, φ autoencoders
qmf	[12]	GMG	$\tau \equiv I_N$, ϱ linear, φ quadratic
manifold Galerkin	[75]	GMG	τ independent of m, symmetric, pos. def.
	[31, 69]	LMG	τ as in (6.48), ϱ, φ linear
symplectic Galerkin	[81, 99]	SMG	$\tau \equiv \mathbb{J}_{2\bar{N}}^\top$, ϱ, φ linear
SMG-QMCL	[108]	SMG	$\tau \equiv \mathbb{J}_{2\bar{N}}^\top$, ϱ linear, φ from manifold cotangent lift
SMG	[22]	SMG	$\tau \equiv \mathbb{J}_{2\bar{N}}^\top$, ϱ, φ autoencoders

Table 6.3: MOR techniques from different works that are covered by MPG (6.22), GMG (6.41), LMG (6.49), and SMG (6.50) introduced in our work. This table is adapted from [24].

$D\varphi|_{\check{m}} = E$ *that*

$$\check{\omega}|_{\check{m}} = D\varphi|_{\check{m}}^\top \omega|_{\varphi(\check{m})} D\varphi|_{\check{m}} = \begin{bmatrix} I_{2\bar{n}} & 0_{2\bar{n} \times (2\bar{N} - 2\bar{n})} \end{bmatrix} \begin{bmatrix} 0_{N \times N} & I_N \\ -I_N & 0_{N \times N} \end{bmatrix} \begin{bmatrix} I_{2\bar{n}} \\ 0_{(2\bar{N} - 2\bar{n}) \times 2\bar{n}} \end{bmatrix}$$

$$= 0_{2\bar{n} \times 2\bar{n}},$$

which is clearly degenerate.

6.6 Snapshot-based Generation of Embedding and Point Reduction

Another key task in MOR is the choice of a particular embedding φ (the APPROXIMATION step in Section 6.3.1.4). In this section, we thus consider the construction of the embedding in a data-driven setting, which is directly combined with the construction of a point reduction ϱ. We first introduce the data-driven setting (Section 6.6.1) and then detail four techniques to generate an embedding and a corresponding point reduction. In Table 6.3, we present an overview of selected methods discussed in the literature and how they fit into our general framework. Throughout the section, we assume to be given the N-dimensional smooth manifold $\mathcal{M}$ and a metric $d_{\mathcal{M}} \colon \mathcal{M} \times \mathcal{M} \to \mathbb{R}_{\geq 0}$.

6.6.1 Snapshot-based Generation

In the scope of the present work, we focus on *snapshot-based generation of an embedding and a point reduction*. Consider a finite subset $S_{\text{train}} \subset S$ of the set of all solutions $S \subset \mathcal{M}$ from (6.13), which is referred to as the *(training-)set of snapshots* and its elements $m_{\text{train}} \in S_{\text{train}}$ as *snapshots*. Typically, the embedding and the point reduction are determined by searching in a given family of functions

$$\mathcal{F}_{\varphi,\varrho} := \left\{ (\varphi, \varrho) \in C^\infty(\check{\mathcal{M}}, \mathcal{M}) \times C^\infty(\mathcal{M}, \check{\mathcal{M}}) \,\middle|\, \varrho \text{ is a point reduction for } \varphi \text{ (6.15a)} \right\}$$

by optimizing over a functional $L \colon \mathcal{F}_{\varphi,\varrho} \to \mathbb{R}_{\geq 0}$ that measures the quality of approximation based on the snapshots $m_{\text{train}} \in S_{\text{train}}$, i.e.,

$$(\varphi^\star, \varrho^\star) := \operatorname*{argmin}_{(\varphi,\varrho) \in \mathcal{F}_{\varphi,\varrho}} L(\varphi, \varrho). \tag{6.54}$$

We emphasize that Lemma 6.1 guarantees that searching within $\mathcal{F}_{\varphi,\varrho}$ automatically yields that φ is a smooth embedding and $\varphi(\check{\mathcal{M}})$ is an embedded submanifold. Note that for practical purposes, which we do not further consider, one might want to relax the smoothness assumptions in $\mathcal{F}_{\varphi,\varrho}$.

One well-established functional is the *mean squared error* (MSE)

$$L_{\text{MSE}}(\varphi, \varrho) := \frac{1}{|S_{\text{train}}|} \sum_{m_{\text{train}} \in S_{\text{train}}} \left(d_{\mathcal{M}}(m_{\text{train}}, (\varphi \circ \varrho)(m_{\text{train}})) \right)^2 \in \mathbb{R}_{\geq 0}. \tag{6.55}$$

The motivation of minimizing the MSE is that if $L_{\text{MSE}}(\varphi, \varrho) = 0$, it is guaranteed that all snapshots $m_{\text{train}} \in S_{\text{train}}$ are in the image of the embedding φ and thus directly lay on the embedded submanifold, i.e., $S_{\text{train}} \subset \varphi(\check{\mathcal{M}})$. In general, however, the MSE is not equal to zero. Nevertheless, then we know that for each addend of (6.55) it holds that

$$\left(d_{\mathcal{M}}(m_{\text{train}}, (\varphi \circ \varrho)(m_{\text{train}})) \right)^2 \leq |S_{\text{train}}| \cdot L_{\text{MSE}}(\varphi, \varrho) \tag{6.56}$$

for all snapshots $m_{\text{train}} \in S_{\text{train}}$ due to non-negativity of the respective addends.

In the following we present four examples for snapshot-based generation for the case where $\mathcal{M} = \mathbb{R}^N$, $\check{\mathcal{M}} = \mathbb{R}^n$, $T_m\mathcal{M} = \mathbb{R}^N$, $T_{\check{m}}\check{\mathcal{M}} = \mathbb{R}^n$ are Euclidean vector spaces with chart mappings $x \equiv \operatorname{id}_{\mathbb{R}^N}$, $\check{x} \equiv \operatorname{id}_{\mathbb{R}^n}$ and the metric $d_{\mathcal{M}}$ is defined by a symmetric, positive-definite

matrix $\boldsymbol{g} \in \mathbb{R}^{N \times N}$ with

$$\|\boldsymbol{m}\|_{\boldsymbol{g}} := \sqrt{\boldsymbol{m}^\top \boldsymbol{g} \boldsymbol{m}}, \qquad d_{\mathcal{M}}(\boldsymbol{m}, \boldsymbol{w}) = \|\boldsymbol{m} - \boldsymbol{w}\|_{\boldsymbol{g}}, \qquad \text{for } \boldsymbol{m}, \boldsymbol{w} \in \mathbb{R}^N.$$

With this choice, the MSE (6.55) in coordinates reads

$$\boldsymbol{L}_{\text{MSE}}(\boldsymbol{\varphi}, \boldsymbol{\varrho}) = \frac{1}{|S_{\text{train}}|} \sum_{\boldsymbol{m}_{\text{train}} \in S_{\text{train}}} \|\boldsymbol{m}_{\text{train}} - (\boldsymbol{\varphi} \circ \boldsymbol{\varrho})(\boldsymbol{m}_{\text{train}})\|_{\boldsymbol{g}}^2. \tag{6.57}$$

For each of the four presented approaches, we

1. formulate the respective family of functions as a subset of $\mathcal{F}_{\varphi,\varrho}$,
2. describe how the MSE functional (6.55) is optimized,
3. refer to existing work that uses the respective technique.

6.6.2 Linear Subspaces

As discussed in Example 6.5, MOR on subspaces from Part I is included in our framework if the embedding φ and the point reduction ϱ are linear maps

$$\boldsymbol{\varphi}_{\text{lin}}(\check{\boldsymbol{m}}) := \boldsymbol{V}\check{\boldsymbol{m}}, \qquad\qquad \boldsymbol{\varrho}_{\text{lin}}(\boldsymbol{m}) := \boldsymbol{W}^\top \boldsymbol{m}, \tag{6.58}$$

based on the matrices $\boldsymbol{V}, \boldsymbol{W} \in \mathbb{R}^{N \times n}$ with $n \ll N$. We formulate the respective family of functions by

$$\mathcal{F}_{\varphi,\varrho,\text{lin}} := \left\{ (\boldsymbol{\varphi}_{\text{lin}}, \boldsymbol{\varrho}_{\text{lin}}) \text{ from } (6.58) \,\middle|\, \boldsymbol{V}, \boldsymbol{W} \in \mathbb{R}^{N \times n} \text{ such that } \boldsymbol{W}^\top \boldsymbol{V} = \boldsymbol{I}_n \right\}.$$

Proposition 6.27: *The family of functions $\mathcal{F}_{\varphi,\varrho,\text{lin}}$ is a subset of $\mathcal{F}_{\varphi,\varrho}$.*

Proof. The assumption $\boldsymbol{W}^\top \boldsymbol{V} = \boldsymbol{I}_n$ implies the point projection property (6.15a) with

$$(\boldsymbol{\varrho}_{\text{lin}} \circ \boldsymbol{\varphi}_{\text{lin}})(\check{\boldsymbol{m}}) = \boldsymbol{W}^\top \boldsymbol{V} \check{\boldsymbol{m}} = \check{\boldsymbol{m}}. \qquad\qquad \square$$

In the case of a *Galerkin projection*, i.e., $\boldsymbol{W}^\top = \boldsymbol{V}^\top \boldsymbol{g}$ with $\boldsymbol{V}^\top \boldsymbol{g} \boldsymbol{V} = \boldsymbol{I}_n$, solving (6.54) for $\mathcal{F}_{\varphi,\varrho,\text{lin}}$ simplifies to the POD in coordinates (2.15), which is recited here for the sake of

completeness

$$V^* = \operatorname*{argmin}_{\substack{V \in \mathbb{R}^{N \times n} \\ V^\top g V = I_n}} \sum_{m_{\text{train}} \in S_{\text{train}}} \left\| (I_N - V V^\top g) m_{\text{train}} \right\|_g^2 . \tag{6.59}$$

For structure-preserving MOR on subspaces techniques, $\mathcal{F}_{\varphi, \varrho, \text{lin}}$ may have to be restricted to a class that preserves the respective structure. For structure-preserving MOR for Hamiltonian systems, this structure is the assumption that the ROB matrix V is a symplectic matrix (see Section 2.4) and the projection matrix is the symplectic inverse $W = \mathbb{J}_{2\bar{N}} V \mathbb{J}_{2\bar{n}}^\top$.

6.6.3 Quadratic Manifolds

Recently, so-called *MOR on quadratic manifolds* has become an active field of research [5, 12, 41, 59, 108]. In our terms, the embedding and point reduction are set to

$$\varphi_{\text{quad}}(\check{m}) := A_2 \check{m}^{\otimes^s 2} + A_1 \check{m} + A_0, \qquad \varrho_{\text{quad}}(m) := A_1^\top (m - A_0), \tag{6.60}$$

with matrices $A_2 \in \mathbb{R}^{N \times n(n+1)/2}$, $A_1 \in \mathbb{R}^{N \times n}$, $A_0 \in \mathbb{R}^N$ and where we denote by $(\cdot)^{\otimes^s 2} \colon \mathbb{R}^n \to \mathbb{R}^{n(n+1)/2}$, $\check{m} \mapsto \check{m}^{\otimes^s 2}$ the *symmetric Kronecker product* which produces all pairwise products of components $[\check{m}]^i \in \mathbb{R}$ of $\check{m}$ for $1 \le i \le n$ while neglecting redundant entries, i.e.,

$$\check{m}^{\otimes^s 2} = \left[[\check{m}]^1 \cdot [\check{m}]^1, \ [\check{m}]^1 \cdot [\check{m}]^2, \ [\check{m}]^2 \cdot [\check{m}]^2, \ \dots, \ [\check{m}]^n \cdot [\check{m}]^n \right]^\top \in \mathbb{R}^{n(n+1)/2}.$$

The respective family of functions is

$$\mathcal{F}_{\varphi, \varrho, \text{quad}} := \left\{ (\varphi_{\text{quad}}, \varrho_{\text{quad}}) \text{ from (6.60)} \, \middle| \, A_1^\top A_1 = I_n \text{ and } A_1^\top A_2 = 0_{n \times n(n+1)/2} \right\}. \tag{6.61}$$

Proposition 6.28: *The family $\mathcal{F}_{\varphi, \varrho, \text{quad}}$ is a subset of $\mathcal{F}_{\varphi, \varrho}$.*

Proof. The assumptions (6.61) on A_2 and A_1 imply the point projection property (6.15a),

$$(\varrho_{\text{quad}} \circ \varphi_{\text{quad}})(\check{m}) = A_1^\top \left(A_2 \check{m}^{\otimes^s 2} + A_1 \check{m} + A_0 - A_0 \right) \overset{(6.61)}{=} \check{m}. \qquad \square$$

The matrices A_1 and A_2 are obtained in [5, 12, 41, 59, 108] from the MSE functional (6.57). In this setting, the assumptions in (6.61) allow to determine the matrices A_0, A_1 and A_2

sequentially: First, $\boldsymbol{A}_0$ is chosen, e.g., as the mean of S_{train}. Then, (6.57) is optimized for $\boldsymbol{A}_1$ (similarly to (6.59)). Finally, (6.57) is optimized for $\boldsymbol{A}_2$, which results in a (regularized) linear least squares problem. The preceding papers use different tangent reductions to derive the ROM, which can be classified with the framework introduced in the present paper: [5, 41, 59] use the MPG reduction map (6.22), while [12] relies on the GMG reduction map (6.41) (but neglects a few higher order terms). The major difference between using MPG or GMG in that context is that the MPG projects the FOM vector field with the tangent reduction

$$\boldsymbol{R}_{\text{MPG}}\big|_{\boldsymbol{\varphi}_{\text{quad}}(\check{\boldsymbol{m}})} = \boldsymbol{D}\boldsymbol{\varrho}_{\text{quad}}\big|_{\boldsymbol{\varphi}_{\text{quad}}(\check{\boldsymbol{m}})} = \boldsymbol{A}_1^\top$$

which is constant, while the GMG uses the tangent reduction from (6.42) with $\boldsymbol{\tau}\big|_{\boldsymbol{m}} = \boldsymbol{I}_N$ for all $\boldsymbol{m} \in \mathbb{R}^N$ and $\boldsymbol{D}\boldsymbol{\varphi}\big|_{\check{\boldsymbol{m}}} = \boldsymbol{A}_2\boldsymbol{B}_2(\check{\boldsymbol{m}}) + \boldsymbol{A}_1$ with a linear function $\boldsymbol{B}_2 \colon \mathbb{R}^n \to \mathbb{R}^{n(n+1)/2 \times n}$ describing the derivative of $(\cdot)^{\otimes^s 2}$, resulting in

$$\begin{aligned} \boldsymbol{R}_{\text{GMG}}\big|_{\boldsymbol{\varphi}_{\text{quad}}(\check{\boldsymbol{m}})} &= \left(\boldsymbol{D}\boldsymbol{\varphi}\big|_{\check{\boldsymbol{m}}}^\top \, \boldsymbol{\tau}\big|_{\boldsymbol{\varphi}_{\text{quad}}(\check{\boldsymbol{m}})} \boldsymbol{D}\boldsymbol{\varphi}\big|_{\check{\boldsymbol{m}}} \right)^{-1} \boldsymbol{D}\boldsymbol{\varphi}\big|_{\check{\boldsymbol{m}}}^\top \, \boldsymbol{\tau}\big|_{\boldsymbol{\varphi}_{\text{quad}}(\check{\boldsymbol{m}})} \\ &= \left(\boldsymbol{I}_n + (\boldsymbol{B}_2(\check{\boldsymbol{m}}))^\top \, \boldsymbol{A}_2^\top \boldsymbol{A}_2 \boldsymbol{B}_2(\check{\boldsymbol{m}}) \right)^{-1} (\boldsymbol{A}_2\boldsymbol{B}_2(\check{\boldsymbol{m}}) + \boldsymbol{A}_1)^\top, \end{aligned}$$

which is typically nonlinear in $\check{\boldsymbol{m}}$, and, thus, so is the reduced vector field in general.

In [108], structure-preserving MOR of Hamiltonian systems on quadratic manifolds is investigated. Two approaches are presented and compared: (i) The *blockwise quadratic* approach uses an embedding of a comparable structure as (6.60) in combination with the MPG tangent reduction. In contrast, (ii) the *quadratic manifold cotangent lift* uses the SMG-ROM. In order to construct a symplectomorphism from a quadratic embedding, the PSD cotangent lift from Definition 2.51 (which generates a linear embedding $\boldsymbol{\varphi}$) is generalized to the case of nonlinear embeddings $\boldsymbol{\varphi}$ by introducing the so-called *manifold cotangent lift*. Based on this idea, the authors construct an embedding $\boldsymbol{\varphi} \colon \mathbb{R}^{2\bar{n}} \to \mathbb{R}^{2\bar{N}}$, where the first $\bar{N}$ component functions are of the structure (6.60) and the last $\bar{N}$ component functions are rational functions. The SMG is then used for a structure-preserving tangent reduction of the Hamiltonian vector field.

6.6.4 Nonlinear Compressive Approximation

Following the idea of the previous subsection, the embedding and the point reduction can be defined more generally with

$$\varphi_{\mathrm{NCA}}\left(\check{\boldsymbol{m}}\right) := \boldsymbol{A}_2 \boldsymbol{f}\left(\check{\boldsymbol{m}}\right) + \boldsymbol{A}_1 \check{\boldsymbol{m}} + \boldsymbol{A}_0, \qquad \varrho_{\mathrm{NCA}}\left(\boldsymbol{m}\right) := \boldsymbol{B}^\top\left(\boldsymbol{m} - \boldsymbol{A}_0\right), \qquad (6.62)$$

where $\boldsymbol{A}_2 \in \mathbb{R}^{N \times \tilde{n}}$, $\boldsymbol{A}_1 \in \mathbb{R}^{N \times n}$, $\boldsymbol{A}_0 \in \mathbb{R}^N$, $\boldsymbol{B} \in \mathbb{R}^{N \times n}$ are matrices, and $\boldsymbol{f} \in C^\infty(\mathbb{R}^n, \mathbb{R}^{\tilde{n}})$ is a smooth nonlinear mapping for a given $\tilde{n} \in \mathbb{N}$. Following [33], we refer to this approach as *nonlinear compressive approximation* (NCA). The respective family of functions is

$$\mathcal{F}_{\varphi,\varrho,\mathrm{NCA}} := \left\{ (\varphi_{\mathrm{NCA}}, \varrho_{\mathrm{NCA}}) \text{ from (6.62)} \,\middle|\, \boldsymbol{B}^\top \boldsymbol{A}_1 = \boldsymbol{I}_n, \ \boldsymbol{B}^\top \boldsymbol{A}_2 = \boldsymbol{0}_{n \times \tilde{n}} \right\}. \qquad (6.63)$$

Proposition 6.29: *The family $\mathcal{F}_{\varphi,\varrho,\mathrm{NCA}}$ is a subset of $\mathcal{F}_{\varphi,\varrho}$.*

Proof. The assumptions on $\boldsymbol{A}_1$, $\boldsymbol{A}_2$, and $\boldsymbol{B}$ in (6.63) imply the point projection property (6.15a) with

$$\left(\varrho_{\mathrm{NCA}} \circ \varphi_{\mathrm{NCA}}\right)\left(\check{\boldsymbol{m}}\right) = \boldsymbol{B}^\top\left(\boldsymbol{A}_2 \boldsymbol{f}\left(\check{\boldsymbol{m}}\right) + \boldsymbol{A}_1 \check{\boldsymbol{m}} + \boldsymbol{A}_0 - \boldsymbol{A}_0\right) = \check{\boldsymbol{m}}. \qquad \square$$

The MSE for this approach may be optimized sequentially as in the MOR on quadratic manifolds discussed in the previous section using $\boldsymbol{B} = \boldsymbol{A}_1$. This method is, e.g., used in [6], where $\boldsymbol{f}$ is a neural network.

Multiple works investigate NCA: First, the quadratic embedding (6.60) discussed in the previous subsection is a special case of the NCA when choosing $\boldsymbol{f}(\check{\boldsymbol{m}}) = \check{\boldsymbol{m}}^{\otimes^{\mathrm{s}} 2}$. Similarly, $\boldsymbol{f}$ can be chosen as a higher-order polynomial in $\check{\boldsymbol{m}}$ to obtain a more general approximation. Second, in [6], $\boldsymbol{f}$ is learned with an artificial neural network, while a time-discrete setting is considered for the reduction, which is not covered by our methods. Third, [33] analyzes the approximation of a set of traveling wave solutions with (and without) varying support on the PDE level using decision trees and random forests in their numerical experiments. Interestingly, the authors show that a linear point reduction is enough to reproduce the set of traveling wave solutions. Fourth, in [23], it is shown that the NCA has its limitations in terms of the Kolmogorov $(\tilde{n} + n)$-width since the solution is contained in an $(\tilde{n} + n)$-dimensional linear subspace of $\mathbb{R}^N$.

6.6.5 Autoencoders

Autoencoders are a well-known technique in nonlinear dimension reduction (see, e.g., [43, Cha. 14]). In the understanding of the present work, MOR with autoencoders chooses

$$\boldsymbol{\varphi}_{\mathrm{AE}} \in C^{\infty}(\mathbb{R}^n, \mathbb{R}^N), \qquad\qquad \boldsymbol{\varrho}_{\mathrm{AE}} \in C^{\infty}(\mathbb{R}^N, \mathbb{R}^n), \qquad (6.64)$$

where both functions are artificial neural networks (ANNs) with network parameters $\boldsymbol{\theta} \in \mathbb{R}^{n_\theta}$ (like weights and biases). Since $\boldsymbol{\varrho}_{\mathrm{AE}} \colon \mathbb{R}^N \to \mathbb{R}^n$ and $\boldsymbol{\varphi}_{\mathrm{AE}} \colon \mathbb{R}^n \to \mathbb{R}^N$, the concatenation $\boldsymbol{\varphi}_{\mathrm{AE}} \circ \boldsymbol{\varrho}_{\mathrm{AE}}$ maps from $\mathbb{R}^N$ over $\mathbb{R}^n$ back to $\mathbb{R}^N$. The in-between compression to $\mathbb{R}^n$ is typically referred to as the *bottleneck*, $\boldsymbol{\varrho}_{\mathrm{AE}}$ as the *encoder*, $\boldsymbol{\varphi}_{\mathrm{AE}}$ as the *decoder*, and the concatenation $\boldsymbol{\varphi}_{\mathrm{AE}} \circ \boldsymbol{\varrho}_{\mathrm{AE}}$ as an *autoencoder*. The respective family is

$$\mathcal{F}_{\varphi,\varrho,\mathrm{AE}} := \left\{ (\boldsymbol{\varphi}_{\mathrm{AE}}, \boldsymbol{\varrho}_{\mathrm{AE}}) \text{ from } (6.64) \mid \boldsymbol{\theta} \in \mathbb{R}^{n_\theta} \text{ network parameters} \right\}.$$

Without special assumptions about the architecture of the ANNs, it is generally impossible to show the point projection property (6.15a). However, whenever the minimum of the cost functional (6.54) is small, and the domain of interest is sampled well, then we show in the following that the point projection property (6.15a) holds approximately. We assume to be given a norm $\|\cdot\|_{\check{\boldsymbol{g}}} \colon \mathbb{R}^n \to \mathbb{R}_{\geq 0}$ such that $\boldsymbol{\varphi}_{\mathrm{AE}}$ and $\boldsymbol{\varrho}_{\mathrm{AE}}$ are *Lipschitz continuous*, i.e., there exists a constant $C_\varphi \geq 0$ such that for all points $\check{\boldsymbol{m}}, \check{\boldsymbol{w}} \in \mathbb{R}^n$

$$\left\| \boldsymbol{\varphi}_{\mathrm{AE}}\left(\check{\boldsymbol{m}}\right) - \boldsymbol{\varphi}_{\mathrm{AE}}\left(\check{\boldsymbol{w}}\right) \right\|_{\boldsymbol{g}} \leq C_\varphi \left\| \check{\boldsymbol{m}} - \check{\boldsymbol{w}} \right\|_{\check{\boldsymbol{g}}} \qquad (6.65)$$

and a constant $C_\varrho \geq 0$ such that for all points $\boldsymbol{m}, \boldsymbol{w} \in \mathbb{R}^N$

$$\left\| \boldsymbol{\varrho}_{\mathrm{AE}}\left(\boldsymbol{m}\right) - \boldsymbol{\varrho}_{\mathrm{AE}}\left(\boldsymbol{w}\right) \right\|_{\check{\boldsymbol{g}}} \leq C_\varrho \left\| \boldsymbol{m} - \boldsymbol{w} \right\|_{\boldsymbol{g}}. \qquad (6.66)$$

Theorem 6.30: *For a given tuple* $(\boldsymbol{\varphi}_{\mathrm{AE}}, \boldsymbol{\varrho}_{\mathrm{AE}}) \in \mathcal{F}_{\varphi,\varrho,\mathrm{AE}}$ *from the family of functions for MOR with autoencoders with an MSE value of* $L_{\mathrm{MSE}}\left(\boldsymbol{\varphi}_{\mathrm{AE}}, \boldsymbol{\varrho}_{\mathrm{AE}}\right) \geq 0$*, the point projection property* (6.15a) *is fulfilled approximately in the sense that for each* $\check{\boldsymbol{m}} \in \mathbb{R}^n$

$$\left\| \left(\boldsymbol{\varrho}_{\mathrm{AE}} \circ \boldsymbol{\varphi}_{\mathrm{AE}}\right)\left(\check{\boldsymbol{m}}\right) - \check{\boldsymbol{m}} \right\|_{\check{\boldsymbol{g}}} \leq C_\varrho \sqrt{|S_{\mathrm{train}}| L_{\mathrm{MSE}}\left(\boldsymbol{\varphi}_{\mathrm{AE}}, \boldsymbol{\varrho}_{\mathrm{AE}}\right)}$$
$$+ \left(C_\varrho C_\varphi + 1\right) \min_{\boldsymbol{w}_{\mathrm{train}} \in S_{\mathrm{train}}} \left\| \check{\boldsymbol{m}} - \boldsymbol{\varrho}_{\mathrm{AE}}\left(\boldsymbol{w}_{\mathrm{train}}\right) \right\|_{\check{\boldsymbol{g}}}.$$

Thus, for a bounded set $\check{M} \subset \mathbb{R}^n$, a fine sampling in S_{train} of $\check{M}$ and small values of the MSE functional such that the term $|S_{\text{train}}| L_{\text{MSE}} (\boldsymbol{\varphi}_{\text{AE}}, \boldsymbol{\varrho}_{\text{AE}})$ is small, the point projection property (6.15a) holds approximately on $\check{M}$, i.e., $\boldsymbol{\varrho}_{\text{AE}} \circ \boldsymbol{\varphi}_{\text{AE}}|_{\check{M}} \approx \text{id}_{\check{M}}$.

Proof. The proof is split in two parts. In the first part, we show that the inequality holds in the encoded training points $\check{\boldsymbol{w}}_{\text{train}} := \boldsymbol{\varrho}_{\text{AE}} (\boldsymbol{w}_{\text{train}})$ with $\boldsymbol{w}_{\text{train}} \in S_{\text{train}}$. Then, we show that the inequality holds for general $\check{\boldsymbol{m}} \in \mathbb{R}^n$ by applying Lipschitz continuity.

Consider a fixed but arbitrary training point $\boldsymbol{w}_{\text{train}} \in S_{\text{train}}$. Using (6.66) and (6.56), it holds

$$\|(\boldsymbol{\varrho}_{\text{AE}} \circ \boldsymbol{\varphi}_{\text{AE}}) (\check{\boldsymbol{w}}_{\text{train}}) - \check{\boldsymbol{w}}_{\text{train}}\|_{\check{\boldsymbol{g}}} = \|(\boldsymbol{\varrho}_{\text{AE}} \circ \boldsymbol{\varphi}_{\text{AE}} \circ \boldsymbol{\varrho}_{\text{AE}}) (\boldsymbol{w}_{\text{train}}) - \boldsymbol{\varrho}_{\text{AE}} (\boldsymbol{w}_{\text{train}})\|_{\check{\boldsymbol{g}}}$$
$$\leq C_\varrho \|(\boldsymbol{\varphi}_{\text{AE}} \circ \boldsymbol{\varrho}_{\text{AE}}) (\boldsymbol{w}_{\text{train}}) - \boldsymbol{w}_{\text{train}}\|_{\boldsymbol{g}}$$
$$\leq C_\varrho \sqrt{|S_{\text{train}}| L_{\text{MSE}} (\boldsymbol{\varphi}_{\text{AE}}, \boldsymbol{\varrho}_{\text{AE}})}.$$

This property can be generalized to points $\check{\boldsymbol{m}} \in \mathbb{R}^n \setminus \boldsymbol{\varrho}_{\text{AE}} (S_{\text{train}})$. The idea is that for a general Lipschitz continuous function $\boldsymbol{f} : \mathbb{R}^n \to \mathbb{R}^n$ with Lipschitz constant $C \geq 0$ and $\|\boldsymbol{f} (\check{\boldsymbol{w}}_{\text{train}})\|_{\check{\boldsymbol{g}}} \leq C_B$ for some $C_B \geq 0$, it holds for all $\check{\boldsymbol{m}} \in \mathbb{R}^n$ by adding a zero, triangle inequality, and Lipschitz continuity

$$\|\boldsymbol{f} (\check{\boldsymbol{m}})\|_{\check{\boldsymbol{g}}} \leq \|\boldsymbol{f} (\check{\boldsymbol{w}}_{\text{train}})\|_{\check{\boldsymbol{g}}} + \|\boldsymbol{f} (\check{\boldsymbol{m}}) - \boldsymbol{f} (\check{\boldsymbol{w}}_{\text{train}})\|_{\check{\boldsymbol{g}}} \leq C_B + C \|\check{\boldsymbol{m}} - \check{\boldsymbol{w}}_{\text{train}}\|_{\check{\boldsymbol{g}}}.$$

For our case, we use $\boldsymbol{f} (\check{\boldsymbol{m}}) = (\boldsymbol{\varrho}_{\text{AE}} \circ \boldsymbol{\varphi}_{\text{AE}}) (\check{\boldsymbol{m}}) - \check{\boldsymbol{m}}$ with Lipschitz constant $C = C_\varrho C_\varphi + 1$, bound $C_B = C_\varrho \sqrt{|S_{\text{train}}| L_{\text{MSE}} (\boldsymbol{\varphi}_{\text{AE}}, \boldsymbol{\varrho}_{\text{AE}})}$, and points $\check{\boldsymbol{w}}_{\text{train}} = \boldsymbol{\varrho}_{\text{AE}} (\boldsymbol{w}_{\text{train}})$. Thus, it holds

$$\|(\boldsymbol{\varrho}_{\text{AE}} \circ \boldsymbol{\varphi}_{\text{AE}}) (\check{\boldsymbol{m}}) - \check{\boldsymbol{m}}\|_{\check{\boldsymbol{g}}} \leq C_\varrho \sqrt{|S_{\text{train}}| L_{\text{MSE}} (\boldsymbol{\varphi}_{\text{AE}}, \boldsymbol{\varrho}_{\text{AE}})}$$
$$+ (C_\varrho C_\varphi + 1) \|\check{\boldsymbol{m}} - \boldsymbol{\varrho}_{\text{AE}} (\boldsymbol{w}_{\text{train}})\|_{\check{\boldsymbol{g}}}.$$

Taking the minimum over all $\boldsymbol{w}_{\text{train}} \in S_{\text{train}}$ on the right-hand side yields the result. $\square$

Remark 6.31 (Constrained autoencoders): *In [93], the authors introduce a novel autoencoder architecture, which aims at fulfilling the point projection property (6.15a) exactly. The architecture of the encoder is chosen to invert the decoder layer-wise based on the assumption that the linear layers of the decoder and encoder are pairwise biorthogonal. This biorthogonality is penalized in the loss functional with an additional term.*

One of the first works to combine autoencoders with projection-based MOR is [75]. As

discussed in Section 6.5.1, the time-continuous formulation in that work considers the GMG reduction for a state-independent Riemannian metric. A structure-preserving formulation for Hamiltonian systems in combination with autoencoders is discussed in [22]. As shown in Lemma 6.24, this work is based on the SMG reduction. In the subsequent chapter, we will investigate this case more closely.

Symplectic Model Order Reduction on Manifolds

7

In this final chapter, we intensify our study of structure-preserving MOR on manifolds for Hamiltonian systems, which we refer to as *symplectic MOR on manifolds*. Firstly, we present *theoretical findings* on preservation of energy and stability during the reduction and an error bound for the reduction error (Section 7.1). Secondly, we present the *weakly symplectic autoencoder*, a method to compute an approximately symplectic embedding from snapshot data (Section 7.2). A numerical example compares the newly introduced weakly symplectic autoencoder to classical symplectic MOR on subspaces and a nonlinear but non-symplectic embedding from literature for the challenging case of a thin moving pulse (Section 7.3). In this section, we assume that the reader is familiar with the basics of ANNs. For a more detailed introduction to ANNs, we refer, e.g., to [75]. The following is adapted from [22].

In relation to Chapter 6, we assume to be given two symplectic manifolds $(\mathcal{M}, \omega)$, $(\check{\mathcal{M}}, \check{\omega})$ which are even-dimensional $\dim(\mathcal{M}) = 2\bar{N}$, $\dim(\check{\mathcal{M}}) = 2\bar{n}$ and can both be described with one fixed chart (U, x), $(\check{U}, \check{x})$ with $U = \mathbb{R}^{2\bar{N}}$, $\check{U} = \mathbb{R}^{2\bar{n}}$. Moreover, we work in the bold notation and consider C^1 mappings instead of C^∞. For the sake of brevity, we omit the dependency on the parameter vector μ whenever possible. Then, an autonomous Hamiltonian FOM (6.37) and the SMG-ROM (Section 6.5.3) read

$$\begin{cases} \frac{\mathrm{d}}{\mathrm{d}t}\boldsymbol{\gamma}\big|_t = \boldsymbol{X}_{\mathscr{H}}\big|_{\boldsymbol{\gamma}(t)} = \boldsymbol{\omega}\big|_{\boldsymbol{\gamma}(t)}^{-1} \boldsymbol{D}\boldsymbol{\mathscr{H}}\big|_{\boldsymbol{\gamma}(t)}^{\top} \in \mathbb{R}^{2\bar{N}}, \\ \boldsymbol{\gamma}(t_0) = \boldsymbol{\gamma}_0, \end{cases} \tag{7.1}$$

$$\begin{cases} \frac{\mathrm{d}}{\mathrm{d}t}\check{\boldsymbol{\gamma}}\big|_t = \check{\boldsymbol{X}}_{\mathscr{H}}\big|_{\boldsymbol{\gamma}(t)} = \check{\boldsymbol{\omega}}\big|_{\check{\boldsymbol{\gamma}}(t)}^{-1} \boldsymbol{D}\check{\boldsymbol{\mathscr{H}}}\big|_{\check{\boldsymbol{\gamma}}(t)}^{\top} \in \mathbb{R}^{2\bar{n}}, \\ \check{\boldsymbol{\gamma}}(t_0) = \check{\boldsymbol{\gamma}}_0 = \boldsymbol{\varrho}(\boldsymbol{\gamma}_0) \end{cases} \tag{7.2}$$

with the Hamiltonian $\mathcal{H} \in C^1(\mathbb{R}^{2\bar{N}}, \mathbb{R})$, the symplectic form $\omega \in \Gamma(T^{(0,2)}(T\mathbb{R}^{2\bar{N}}))$, the embedding $\varphi \in C^1(\mathbb{R}^{2\bar{n}}, \mathbb{R}^{2\bar{N}})$, the reduced symplectic form $\tilde{\omega} = \varphi^*\omega \in \Gamma(T^{(0,2)}(T\mathbb{R}^{2\bar{n}}))$, and the reduced Hamiltonian $\check{\mathcal{H}} \equiv \mathcal{H} \circ \varphi$.

7.1 Theoretical Findings

We present theoretical findings on energy preservation (Section 7.1.1), stability preservation (Section 7.1.2) and error estimation (Section 7.1.3).

7.1.1 Energy Preservation

Proposition 7.1: *Let $\gamma \in C^1(\mathcal{I}, \mathbb{R}^{2\bar{N}})$ be the solution of the Hamiltonian FOM (7.1) at time t and let $\check{\gamma} \in C^1(\mathcal{I}, \mathbb{R}^{2\bar{n}})$ be the solution obtained from solving an SMG-ROM (7.2). Then, the error in the Hamiltonian*

$$\Delta\mathcal{H}(t) := |\mathcal{H}(\gamma(t)) - \check{\mathcal{H}}(\check{\gamma}(t))| = |\mathcal{H}(\gamma_0) - \check{\mathcal{H}}(\check{\gamma}_0)| \qquad (7.3)$$

is constant for all $t \in \mathcal{I}$.

Proof. In both models FOM and ROM the Hamiltonian evaluated the solution is constant over time. But then the difference of both is also constant over time. $\square$

Remark 7.2 (Exact preservation): *If the initial value is included in the image of the embedding $\varphi \in C^1(\mathbb{R}^{2\bar{n}}, \mathbb{R}^{2\bar{N}})$ (i.e., there exists a $\check{\gamma}_0 \in \mathbb{R}^{2\bar{n}}$ with $\gamma_0 = \varphi(\check{\gamma}_0)$), it follows from Proposition 7.1 that with the SMG projection, the Hamiltonian is exactly reproduced, $\Delta\mathcal{H} \equiv 0$. We discuss in Section 7.2.3, how an embedding can be constructed that is guaranteed to exactly reproduce the initial value.*

7.1.2 Stability Preservation

Under mild assumptions, it can be shown that symplectic MOR on manifolds preserves stability in the sense of Lyapunov. In the present subsection, we assume $\mathcal{H} \in C^2(\mathbb{R}^{2\bar{N}}, \mathbb{R})$ and $\varphi \in C^2(\mathbb{R}^{2\bar{n}}, \mathbb{R}^{2\bar{N}})$ such that $\check{\mathcal{H}} = \mathcal{H} \circ \varphi \in C^2(\mathbb{R}^{2\bar{n}}, \mathbb{R})$.

For an open set $V \subset \mathbb{R}^{2\bar{N}}$ and a vector field $\boldsymbol{X} \in C^1(V, TV)$, consider the system of ODEs

$$\frac{\mathrm{d}}{\mathrm{d}t}\gamma\Big|_t = \boldsymbol{X}\big|_{\gamma(t)} \in \mathbb{R}^{2\bar{N}} \qquad \text{for } t \in \mathcal{I}. \qquad (7.4)$$

We call a point $m_e \in V$ an *equilibrium point* if $X|_{m_e} = \mathbf{0}_{2\bar{N} \times 1}$. Lyapunov stability of the point m_e is defined as follows.

Definition 7.3 (Lyapunov stability [86, Sec. 12]): *An equilibrium point $m_e \in V$ of (7.4) is Lyapunov stable if for every $\epsilon > 0$, there exists $\delta > 0$ such that $\|m_e - \gamma(t; \gamma_0)\|_2 < \epsilon$ for all $t \in \mathcal{I}$ whenever $\|m_e - \gamma_0\|_2 < \delta$.*

In order to state sufficient conditions for an equilibrium point to be Lyapunov stable, we recall Lyapunov's stability theorem.

Theorem 7.4 (Lyapunov's stability theorem [86, Thm. 12.1.1]): *Assume that $m_e \in V$ is an equilibrium point of (7.4). If there exists $h \in C^2(V, \mathbb{R})$ such that (i) $Dh|_{m_e} = \mathbf{0}_{1 \times 2\bar{N}}$, (ii) the Hessian $D^2 h|_{m_e}$ of h is positive-definite, and (iii) $Dh|_m X|_m \leq 0$, for all $m \in V \subset \mathbb{R}^{2\bar{N}}$, then m_e is a Lyapunov stable point.*

The function h in Theorem 7.4 is called the *Lyapunov function*. For Hamiltonian systems, a suitable candidate for h is the Hamiltonian itself. In the case of an autonomous Hamiltonian considered in this paper, a point $m \in \mathbb{R}^{2\bar{N}}$ is an equilibrium point of (7.1) if and only if m is a critical point of $\mathcal{H}$, i.e., a point s.t. $D\mathcal{H}(m) = \mathbf{0}_{1 \times 2\bar{N}}$ [1, Prop. 3.4.16]. Following the well-known Dirichlet's stability theorem for Hamiltonian systems [86, Cor. 12.1.1], it suffices that the equilibrium point is a strict local maximum or minimum in order to be a Lyapunov stable point. Condition (iii) from Theorem 7.4 is automatically fulfilled for autonomous Hamiltonian systems which can be easily seen by

$$D\mathcal{H}|_m X_{\mathcal{H}}|_m = D\mathcal{H}|_m \omega|_m^{-1} D\mathcal{H}|_m^\top = 0 \quad \forall m \in V,$$

due to the skew-symmetry of $\omega|_m^{-1}$. Similar to [81, Thm. 18] in the special case of a linear embedding φ, we are now able to show that, if $\mathcal{H}$ (or $-\mathcal{H}$) is a Lyapunov function in an environment of the equilibrium point, then these equilibrium points for the FOM and ROM are Lyapunov stable. In the following we extend this theorem to hold for nonlinear embeddings φ.

Theorem 7.5 (Preservation of Lyapunov stability): *Assume that $m_e \in V$ is an equilibrium point of (7.1) and there exists $\check{m}_e \in \mathbb{R}^{2\bar{n}}$ such that $m_e = \varphi(\check{m}_e)$. If $\mathcal{H}$ (or $-\mathcal{H}$) is a Lyapunov function as defined in Theorem 7.4, then m_e and $\check{m}_e$ are Lyapunov stable equilibrium points for the FOM (7.1) and the SMG-ROM (7.2), respectively.*

Proof. As $\boldsymbol{m}_{\mathrm{e}}$ is an equilibrium point and $\mathcal{H}$ is a Lyapunov function, Theorem 7.4 implies that $\boldsymbol{m}_{\mathrm{e}}$ is Lyapunov stable. Evaluating the chain rule $D\breve{\mathcal{H}}\big|_{\breve{\boldsymbol{m}}} = D\mathcal{H}\big|_{\boldsymbol{\varphi}(\breve{\boldsymbol{m}})} D\boldsymbol{\varphi}\big|_{\breve{\boldsymbol{m}}}$ at $\breve{\boldsymbol{m}}_{\mathrm{e}}$ yields

$$D\breve{\mathcal{H}}\big|_{\breve{\boldsymbol{m}}_{\mathrm{e}}} = D\mathcal{H}\big|_{\boldsymbol{\varphi}(\breve{\boldsymbol{m}}_{\mathrm{e}})} D\boldsymbol{\varphi}\big|_{\breve{\boldsymbol{m}}_{\mathrm{e}}} = D\mathcal{H}\big|_{\boldsymbol{m}_{\mathrm{e}}} D\boldsymbol{\varphi}\big|_{\breve{\boldsymbol{m}}_{\mathrm{e}}} = \boldsymbol{0}_{1 \times 2\bar{n}},$$

where the last equivalence follows as $\boldsymbol{m}_{\mathrm{e}}$ is a critical point for $\mathcal{H}$, i.e., $D\mathcal{H}\big|_{\boldsymbol{m}_{\mathrm{e}}} = \boldsymbol{0}_{1 \times 2\bar{N}}$. Thus, $\breve{\boldsymbol{m}}_{\mathrm{e}}$ is an equilibrium point for (7.2). In order to show that $\breve{\boldsymbol{m}}_{\mathrm{e}}$ is a strict local minimum, we consider the Hessian matrix. Again, considering the chain rule, we get

$$D^2\breve{\mathcal{H}}\big|_{\breve{\boldsymbol{m}}_{\mathrm{e}}} = D\boldsymbol{\varphi}\big|_{\breve{\boldsymbol{m}}_{\mathrm{e}}}^{\top} D^2\mathcal{H}\big|_{\boldsymbol{\varphi}(\breve{\boldsymbol{m}}_{\mathrm{e}})} D\boldsymbol{\varphi}\big|_{\breve{\boldsymbol{m}}_{\mathrm{e}}}.$$

Therefore, for any $\boldsymbol{\xi} \in \mathbb{R}^{2\bar{n}} \setminus \{\boldsymbol{0}_{2\bar{n} \times 1}\}$, we obtain that $D^2\breve{\mathcal{H}}\big|_{\breve{\boldsymbol{m}}_{\mathrm{e}}}$ is positive-definite

$$\boldsymbol{\xi}^{\top} D^2\breve{\mathcal{H}}\big|_{\breve{\boldsymbol{m}}_{\mathrm{e}}} \boldsymbol{\xi} = \left(D\boldsymbol{\varphi}\big|_{\breve{\boldsymbol{m}}_{\mathrm{e}}}\boldsymbol{\xi}\right)^{\top} D^2\mathcal{H}\big|_{\boldsymbol{\varphi}(\breve{\boldsymbol{m}}_{\mathrm{e}})} \left(D\boldsymbol{\varphi}\big|_{\breve{\boldsymbol{m}}_{\mathrm{e}}}\boldsymbol{\xi}\right) > 0,$$

due to the positive definiteness of $D^2\mathcal{H}\big|_{\boldsymbol{m}_{\mathrm{e}}}$. With Dirichlet's stability theorem, we conclude that $\breve{\boldsymbol{m}}_{\mathrm{e}}$ is a Lyapunov stable point for (7.2). $\qquad\square$

7.1.3 Error Estimation

In this section, we deduce a rigorous a posteriori error bound for Runge–Kutta (RK) time integration schemes (see Section 2.3.2). For a linear embedding $\boldsymbol{\varphi}$, bounds have been derived in [30, Thm. 6.19], which we extend in the following to error bounds for nonlinear embeddings $\boldsymbol{\varphi}$. In the notation of the present chapter, the RK scheme for the FOM is for each time step $1 \leq k \leq K$ based on the *FOM RK residuals* $\boldsymbol{r}_{k,i}(\boldsymbol{w}_1, \dots, \boldsymbol{w}_s) := \boldsymbol{w}_i - \boldsymbol{X}_{\mathcal{H}}\big|_{\boldsymbol{\gamma}_{k-1}+\Delta t \sum_{j=1}^{s} a_{ij}\boldsymbol{w}_j}$ for $1 \leq i \leq s$ and solves

$$\boldsymbol{r}_{k,i}(\boldsymbol{w}_{k,1}, \dots, \boldsymbol{w}_{k,s}) = \boldsymbol{0}_{2\bar{N} \times 1}, \qquad \forall i \in \{1, \dots, s\},$$

$$\boldsymbol{\gamma}_k = \boldsymbol{\gamma}_{k-1} + \Delta t \sum_{i=1}^{s} b_i \boldsymbol{w}_{k,i}. \tag{7.5}$$

Analogously, the *ROM RK residuals* $\check{r}_{k,i}(\check{w}_1, \dots, \check{w}_s) := \check{w}_i - \check{X}_{\mathcal{H}}\big|_{\check{\gamma}_{k-1}+\Delta t \sum_{j=1}^{s} a_{ij}\check{w}_j}$ are defined for $1 \leq i \leq s$ and the RK scheme solves

$$\check{r}_{k,i}(\check{w}_{k,1}, \dots, \check{w}_{k,s}) = \mathbf{0}_{2\bar{n}\times 1}, \qquad \forall i \in \{1, \dots, s\},$$

$$\check{\gamma}_k = \check{\gamma}_{k-1} + \Delta t \sum_{i=1}^{s} b_i \check{w}_{k,i}. \tag{7.6}$$

Theorem 7.6 (Error bound): *Given a norm* $\|\cdot\| : \mathbb{R}^{2\bar{N}} \to \mathbb{R}_{\geq 0}$, *assume that* $\mathbf{X}_{\mathcal{H}}$ *is Lipschitz continuous, i.e., there exists a constant* $\kappa > 0$ *such that*

$$\left\| \mathbf{X}_{\mathcal{H}}\big|_{\mathbf{m}_1} - \mathbf{X}_{\mathcal{H}}\big|_{\mathbf{m}_2} \right\| \leq \kappa \|\mathbf{m}_1 - \mathbf{m}_2\|, \qquad \forall \mathbf{m}_1, \mathbf{m}_2 \in \mathbb{R}^{2\bar{N}},$$

and that Δt *is chosen sufficiently small such that*

(a1) *the matrix* $\mathbf{C} \in \mathbb{R}^{s\times s}$ *with entries* $[\mathbf{C}]_{ij} := \delta_{ij} - \kappa\Delta t |a_{ij}|$ *is invertible and*

(a2) *for every* $\mathbf{x}_s, \mathbf{y}_s \in \mathbb{R}_{\geq 0}^s$ *with* $\mathbf{C}\mathbf{x}_s \leq \mathbf{y}_s$, *it holds* $\mathbf{x}_s \leq \mathbf{C}^{-1}\mathbf{y}_s$.[1]

For $1 \leq k \leq K$, *consider the discrete FOM* γ_k *and ROM solution* $\check{\gamma}_k$ *of the RK schemes from* (7.5) *and* (7.6). *Then, it holds the error bound*

$$\|\gamma_k - \tilde{\gamma}_k\| \leq (c_1)^k \|\gamma_0 - \tilde{\gamma}_0\| + \sum_{\ell=0}^{k-1} (c_1)^\ell \left(\Delta t \sum_{m=1}^{s} |b_m| \sum_{i=1}^{s} [\mathbf{C}^{-1}]_{mi} \left\| \tilde{r}_{k-\ell,i}^{w} \right\| + \left\| \tilde{r}_{k-\ell}^{\gamma} \right\| \right),$$

with the reconstructed state $\tilde{\gamma}_k := \varphi(\check{\gamma}_k)$, *the reconstructed velocities* $\tilde{w}_{k,i} := \mathbf{D}\varphi\big|_{\check{\gamma}_{k-1}} \check{w}_{k,i}$, *for* $i = 1, \dots, s$, *the residual of the reconstructed state* *and the residuals of the reconstructed velocities*

$$\tilde{r}_k^{\gamma} := \tilde{\gamma}_k - \tilde{\gamma}_{k-1} - \Delta t \sum_{i=1}^{s} b_i \tilde{w}_{k,i}, \tag{7.7a}$$

$$\tilde{r}_{k,i}^{w} := \tilde{w}_{k,i} - \mathbf{X}_{\mathcal{H}}\big|_{\tilde{\gamma}_{k-1}+\Delta t \sum_{j=1}^{s} a_{ij}\tilde{w}_{k,j}}, \qquad i = 1, \dots, s, \tag{7.7b}$$

and the constant $c_1 := \left(1 + \kappa\Delta t \sum_{m=1}^{s} |b_m| \sum_{i=1}^{s} [\mathbf{C}^{-1}]_{mi} \right)$.

---

[1] For the implicit midpoint rule ($s = 1$), this condition holds if $C = 1 - (\kappa\Delta t)/2 \in \mathbb{R}_{>0}$, which can be ensured by choosing $\Delta t < 2/\kappa$. The condition can be verified for other (symplectic) RK methods, see Appendix A.3.

Proof. Subtracting $\tilde{\boldsymbol{r}}_{k,i}^{\boldsymbol{w}}$ from $\boldsymbol{r}_{k,i}(\boldsymbol{w}_{k,1}, \ldots, \boldsymbol{w}_{k,s})$ yields

$$\boldsymbol{r}_{k,i}(\boldsymbol{w}_{k,1}, \ldots, \boldsymbol{w}_{k,s}) - \tilde{\boldsymbol{r}}_{k,i}^{\boldsymbol{w}} = \boldsymbol{w}_{k,i} - \tilde{\boldsymbol{w}}_{k,i}$$
$$- \left(\boldsymbol{X}_{\mathcal{H}}|_{\boldsymbol{\gamma}_{k-1} + \Delta t \sum_{j=1}^{s} a_{ij} \boldsymbol{w}_{k,j}} - \boldsymbol{X}_{\mathcal{H}}|_{\tilde{\boldsymbol{\gamma}}_{k-1} + \Delta t \sum_{j=1}^{s} a_{ij} \tilde{\boldsymbol{w}}_{k,j}} \right).$$

Noting that $\boldsymbol{r}_{k,i}(\boldsymbol{w}_{k,1}, \ldots, \boldsymbol{w}_{k,s}) = \boldsymbol{0}_{2\bar{N} \times 1}$ for all $i = 1, \ldots, s$ due to (7.5), we arrive at

$$\boldsymbol{w}_{k,i} - \tilde{\boldsymbol{w}}_{k,i} = -\tilde{\boldsymbol{r}}_{k,i}^{\boldsymbol{w}} + \left(\boldsymbol{X}_{\mathcal{H}}|_{\boldsymbol{\gamma}_{k-1} + \Delta t \sum_{j=1}^{s} a_{ij} \boldsymbol{w}_{k,j}} - \boldsymbol{X}_{\mathcal{H}}|_{\tilde{\boldsymbol{\gamma}}_{k-1} + \Delta t \sum_{j=1}^{s} a_{ij} \tilde{\boldsymbol{w}}_{k,j}} \right).$$

Applying the norm on both sides, using Lipschitz continuity and the triangle inequality yields

$$\|\boldsymbol{w}_{k,i} - \tilde{\boldsymbol{w}}_{k,i}\| \le \|\tilde{\boldsymbol{r}}_{k,i}^{\boldsymbol{w}}\| + \kappa \|\boldsymbol{\gamma}_{k-1} - \tilde{\boldsymbol{\gamma}}_{k-1}\| + \kappa \Delta t \sum_{j=1}^{s} |a_{ij}| \|\boldsymbol{w}_{k,j} - \tilde{\boldsymbol{w}}_{k,j}\|.$$

Rearranging both sides leads to

$$\sum_{j=1}^{s} (\delta_{ij} - \kappa \Delta t |a_{ij}|) \|\boldsymbol{w}_{k,j} - \tilde{\boldsymbol{w}}_{k,j}\| \le \|\tilde{\boldsymbol{r}}_{k,i}^{\boldsymbol{w}}\| + \kappa \|\boldsymbol{\gamma}_{k-1} - \tilde{\boldsymbol{\gamma}}_{k-1}\|.$$

As Δt is small enough such that both assumptions (a1), (a2) hold, it holds for $m = 1, \ldots, s$

$$\|\boldsymbol{w}_{k,m} - \tilde{\boldsymbol{w}}_{k,m}\| \le \sum_{i=1}^{s} [\boldsymbol{C}^{-1}]_{mi} \left(\|\tilde{\boldsymbol{r}}_{k,i}^{\boldsymbol{w}}\| + \kappa \|\boldsymbol{\gamma}_{k-1} - \tilde{\boldsymbol{\gamma}}_{k-1}\| \right). \tag{7.8}$$

Evaluating the residual (7.7a) at $\tilde{\boldsymbol{\gamma}}_k$ and adding a zero by reformulating (7.5) yields

$$\|\boldsymbol{\gamma}_k - \tilde{\boldsymbol{\gamma}}_k\| \le \|\boldsymbol{\gamma}_{k-1} - \tilde{\boldsymbol{\gamma}}_{k-1}\| + \Delta t \sum_{m=1}^{s} |b_m| \|\boldsymbol{w}_{k,m} - \tilde{\boldsymbol{w}}_{k,m}\| + \|\tilde{\boldsymbol{r}}_k^{\boldsymbol{\gamma}}\|.$$

By inserting (7.8), it follows

$$\|\boldsymbol{\gamma}_k - \tilde{\boldsymbol{\gamma}}_k\| \le \left(1 + \kappa \Delta t \sum_{m=1}^{s} |b_m| \sum_{i=1}^{s} [\boldsymbol{C}^{-1}]_{mi} \right) \|\boldsymbol{\gamma}_{k-1} - \tilde{\boldsymbol{\gamma}}_{k-1}\|$$
$$+ \Delta t \sum_{m=1}^{s} |b_m| \sum_{i=1}^{s} [\boldsymbol{C}^{-1}]_{mi} \|\tilde{\boldsymbol{r}}_{k,i}^{\boldsymbol{w}}\| + \|\tilde{\boldsymbol{r}}_k^{\boldsymbol{\gamma}}\|.$$

Finally, an induction argument concludes the proof. $\qquad\square$

Note, that the Lipschitz condition on $\boldsymbol{X}_{\mathscr{H}}$ does not pose a severely limiting additional requirement, as it is a typical condition for the well-posedness of (7.1). Moreover, the quantities of the error bound are all computable and can be split into different categories, i.e., we have quantities from the underlying dynamical system such as the Lipschitz constant κ whereas other quantities depend on the chosen time-discretization such as $b_m, a_{ij}, \Delta t$. The embedding $\boldsymbol{\varphi}$ only enters the residual norm in form of the reconstructed state and velocity.

7.2 Data-based Generation of an Approximately Symplectic Embedding

As described in Section 6.6.5, autoencoders can be used to define an embedding $\boldsymbol{\varphi}$ and a point reduction map $\boldsymbol{\varrho}$. After revisiting autoencoders (Section 7.2.1), we discuss deep convolutional autoencoders (Section 7.2.2), explain how to exactly reproduce initial values (Section 7.2.3), and introduce our novel weakly symplectic deep convolutional autoencoder (Section 7.2.4).

7.2.1 Autoencoders

In this chapter, an autoencoder $\mathcal{A} := (\boldsymbol{e}(\cdot; \boldsymbol{\theta}), \boldsymbol{d}(\cdot; \boldsymbol{\theta}))$ is a tuple of two parametric functions, the *encoder* $\boldsymbol{e}(\cdot; \boldsymbol{\theta}) \in C^1(\mathbb{R}^{2\bar{N}}, \mathbb{R}^{2\bar{n}})$ and the *decoder* $\boldsymbol{d}(\cdot; \boldsymbol{\theta}) \in C^1(\mathbb{R}^{2\bar{n}}, \mathbb{R}^{2\bar{N}})$, with network parameters $\boldsymbol{\theta} \in \mathbb{R}^{n_\theta}$. The autoencoder is used to learn a low-dimensional representation of a given, finite dataset $\mathcal{X}_{\mathrm{train}} \subset \mathbb{R}^{2\bar{N}}, |\mathcal{X}_{\mathrm{train}}| < \infty$ by optimizing the *mean squared loss (MSE)*[2]

$$L_{\mathrm{data}}(\boldsymbol{\theta}) := \frac{1}{2\bar{N}|\mathcal{X}_{\mathrm{train}}|} \sum_{\boldsymbol{m} \in \mathcal{X}_{\mathrm{train}}} \|\boldsymbol{m} - \boldsymbol{d}(\boldsymbol{e}(\boldsymbol{m}; \boldsymbol{\theta}); \boldsymbol{\theta})\|^2 . \tag{7.9}$$

The embedding and the point reduction map are chosen as $\boldsymbol{\varphi} \equiv \boldsymbol{d}(\cdot; \boldsymbol{\theta}^*)$ and $\boldsymbol{\varrho} \equiv \boldsymbol{e}(\cdot; \boldsymbol{\theta}^*)$ for a (locally) optimal network parameter vector $\boldsymbol{\theta}^*$. In our case, the training data set are snapshots of the FOM, i.e.

$$\mathcal{X}_{\mathrm{train}} = S_{\mathrm{train}} := \{\boldsymbol{\gamma}_k(\mu) \mid 0 \le k \le K, \ \mu \in \mathcal{P}_{\mathrm{train}}\}, \tag{7.10}$$

where $\boldsymbol{\gamma}_k(\mu)$ is the solution of the RK scheme (7.5) and $\mathcal{P}_{\mathrm{train}} \subset \mathcal{P}, |\mathcal{P}_{\mathrm{train}}| < \infty$, is a finite training parameter set.

---

[2]In comparison to Chapter 6, the normalization factor in the MSE includes $2\bar{N}$ to be consistent with [22].

7.2.2 Deep Convolutional Autoencoders

For high-dimensional data, $2\bar{N} \gg 1$, autoencoders purely based on fully-connected ANNs (FNNs) might be too expensive to be trained since $n_{\boldsymbol{\theta}} \sim 2\bar{N}$ or even $n_{\boldsymbol{\theta}} \sim (2\bar{N})^2$. Moreover, FNNs do in general not make use of spatial correlation in the data. For such problems, the use of convolutional ANNs (CNNs) [73, 43, Cha. 9] is advantageous. These networks are based on the so-called cross-correlation which applies a filter matrix similarly to the discrete convolution. The dimension of the filter matrix is independent of the dimension of the input which makes it suitable for high-dimensional inputs. Moreover, this operation is invariant with respect to translations due to its convolutional structure. A combination of CNNs and autoencoders is introduced in [75] as so-called *deep convolutional autoencoders (DCAs)*. For details on DCA-based architectures we refer to [75, Sec. 5] and Section 7.3.2.

7.2.3 Exact Reproduction of Initial Value

Similarly to [75], we construct an embedding $\boldsymbol{\varphi}$ which exactly reproduces the initial value. To this end, we assume that the FOM has zero initial value $\boldsymbol{\gamma}_0(\mu) \equiv \mathbf{0}_{2\bar{N}\times 1}$ which can be achieved with a coordinate transformation $\boldsymbol{m}_{\text{new}} = \boldsymbol{m} - \boldsymbol{\gamma}_0(\mu)$ for any system with non-zero initial value. Furthermore, the decoder is set to

$$\boldsymbol{d}(\check{\boldsymbol{m}}; \boldsymbol{\theta}) = \boldsymbol{g}(\check{\boldsymbol{m}}; \boldsymbol{\theta}) - \boldsymbol{g}(\boldsymbol{e}(\mathbf{0}_{2\bar{N}\times 1}; \boldsymbol{\theta}); \boldsymbol{\theta}) \tag{7.11}$$

based on a trainable mapping $\boldsymbol{g}(\cdot, \boldsymbol{\theta}) \in C^1(\mathbb{R}^{2\bar{n}}, \mathbb{R}^{2\bar{N}})$. With $\boldsymbol{\varphi} \equiv \boldsymbol{d}(\cdot; \boldsymbol{\theta}^*)$ and $\boldsymbol{\varrho} \equiv \boldsymbol{e}(\cdot; \boldsymbol{\theta}^*)$, the initial value of the ROM is by definition $\check{\boldsymbol{\gamma}}_0 = \boldsymbol{\varrho}(\boldsymbol{\gamma}_0(\mu)) = \boldsymbol{e}(\mathbf{0}_{2\bar{N}\times 1}; \boldsymbol{\theta}^*)$ and the initial value is reconstructed exactly as

$$\tilde{\boldsymbol{\gamma}}_0 = \boldsymbol{d}(\check{\boldsymbol{\gamma}}_0; \boldsymbol{\theta}^*) = \boldsymbol{g}(\boldsymbol{e}(\mathbf{0}_{2\bar{N}\times 1}; \boldsymbol{\theta}^*); \boldsymbol{\theta}^*) - \boldsymbol{g}(\boldsymbol{e}(\mathbf{0}_{2\bar{N}\times 1}; \boldsymbol{\theta}^*); \boldsymbol{\theta}^*) = \mathbf{0}_{2\bar{N}\times 1} = \boldsymbol{\gamma}_0.$$

In the original formulation from [75], the term $\boldsymbol{g}(\boldsymbol{e}(\mathbf{0}_{2\bar{N}\times 1}; \boldsymbol{\theta}); \boldsymbol{\theta})$ in (7.11) is neglected during training. In contrast, we respect this term in the training in order to train the decoder in the same way it is used in the evaluation afterwards.

7.2.4 Weakly Symplectic Deep Convolutional Autoencoders

In general, the decoder $\boldsymbol{d}$ of the autoencoder learned with the DCA method will not be a symplectic map which is required for the SMG-ROM. Thus, we extend the DCAs to weakly symplectic DCAs by adding this constraint additionally to our loss function

$$L(\boldsymbol{\theta}) := \alpha L_{\text{data}}(\boldsymbol{\theta}) + (1 - \alpha) L_{\text{sympl}}(\boldsymbol{\theta}), \tag{7.12a}$$

$$L_{\text{sympl}}(\boldsymbol{\theta}) := \frac{1}{(2\bar{n})^2 |\mathcal{X}_{\text{train}}|} \sum_{\boldsymbol{m} \in \mathcal{X}_{\text{train}}} \left\| \boldsymbol{Dd}\big|_{(\boldsymbol{e}(\boldsymbol{m};\boldsymbol{\theta});\boldsymbol{\theta})}^{\top} \boldsymbol{\omega}\big|_{\boldsymbol{m}} \boldsymbol{Dd}\big|_{(\boldsymbol{e}(\boldsymbol{m};\boldsymbol{\theta});\boldsymbol{\theta})} - \mathbb{J}_{2\bar{n}}^{\top} \right\|_{\text{F}}^2, \tag{7.12b}$$

where $0 < \alpha < 1$ is a hyperparameter, $\|\cdot\|_{\text{F}}$ is the Frobenius norm, $(2\bar{n})^2 |\mathcal{X}_{\text{train}}|$ is again a normalizing constant, and $\boldsymbol{Dd}\big|_{(\boldsymbol{e}(\boldsymbol{m};\boldsymbol{\theta});\boldsymbol{\theta})} \in \mathbb{R}^{2\bar{N} \times 2\bar{n}}$ denotes the evaluation of the Jacobian of $\boldsymbol{d}(\cdot; \boldsymbol{\theta})$ at $\boldsymbol{e}(\boldsymbol{m}; \boldsymbol{\theta})$. The loss function L_{sympl} penalizes network parameters $\boldsymbol{\theta}$ for which $\boldsymbol{d}(\cdot; \boldsymbol{\theta})$ violates the canonical symplecticity (6.39) at the encoded data points $\boldsymbol{e}(\boldsymbol{m}; \boldsymbol{\theta})$ for $\boldsymbol{m} \in \mathcal{X}_{\text{train}}$.

Note that the symplecticity loss (7.12b) is more expensive to compute than the data loss (7.9) as it requires to compute the Jacobian of $\boldsymbol{d}$. In our framework, we use the Jacobian–vector product in pyTorch [96] to compute the Jacobian. For now, we ignore this additional cost as it is part of the training phase and it does not influence the computational cost to evaluate the encoder and its Jacobian after the training. Future work might investigate how to reduce the cost in (7.12b), e.g., by introducing another stochastic approximation such as Hutchinson's Trace Estimator [58].

7.3 Numerical Results

In this section, we perform numerical simulations of a linear wave equation that models the challenging transport of a thin pulse. First, we detail the Hamiltonian FOM. Then, we describe the training of the autoencoders and the construction of the reduced models. Subsequently, we compare our reduced model on the nonlinear (approximately) symplectic trial manifold to classical (non-)symplectic model reduction and to non-symplectic model reduction on manifolds in terms of the accuracy on training and test data. Moreover, we compare for all these MOR techniques the preservation of energy and symplecticity of the reduced model.

7.3.1 Full-Order Model

We consider a parametrized initial-boundary-value problem (IBVP) for the one-dimensional linear wave equation with homogeneous Dirichlet boundary conditions

$$
\begin{aligned}
\partial_{tt}^2 u(t,\xi;\mu) &= \mu^2 \partial_{\xi\xi}^2 u(t,\xi;\mu), && \text{for } (t,\xi) \in \mathcal{I} \times \Omega, \\
u(0,\xi;\mu) &= u_0(\xi;\mu), && \text{for } \xi \in \Omega, \\
\partial_t u(0,\xi;\mu) &= -\mu\,\partial_\xi u_0(\xi;\mu), && \text{for } \xi \in \Omega, \\
u(t,\xi;\mu) &= 0, && \text{for } t \in \mathcal{I}, \xi \in \{-1/2, 1/2\},
\end{aligned}
\tag{7.13}
$$

with the spatial domain $\Omega = (-1/2, 1/2)$ and time interval $\mathcal{I} = (0,1)$. The parameter $\mu \in \mathcal{P} := [5/12, 5/6] \subset \mathbb{R}$ is chosen to be the wave speed. The spline function

$$
h(s) := \begin{cases}
1 - 3/2 \cdot s^2 + 3/4 \cdot s^3, & 0 \le s \le 1, \\
(2-s)^3/4, & 1 < s \le 2, \\
0, & \text{otherwise,}
\end{cases}
$$

is used to formulate the parameter-dependent initial value with $u_0(\xi;\mu) := h\left(s(\xi;\mu)\right)$ and $s(\xi;\mu) := 20/\mu \cdot |\xi + 1/2 - \mu/10|$. The unique solution of this IBVP is a traveling wave solution $u(t,\xi;\mu) = u_0(\xi - \mu t;\mu)$. This model problem is similar to [81, 99] and the FOM from Section 5.3.1. Here, however, the problem is parametric, has nonzero initial velocity, and the support of the initial value compared to the domain length is much smaller. Thus, the system is very challenging for MOR on subspaces as it describes the transport of a thin pulse.

With the variables $q(t,\xi;\mu) := u(t,\xi;\mu)$ and $p(t,\xi;\mu) := \partial_t q(t,\xi;\mu) = \partial_t u(t,\xi;\mu)$, the PDE in (7.13) can be rewritten as a parametric Hamiltonian PDE [17]

$$
\begin{aligned}
\partial_t q(t,\xi;\mu) &= \left(\frac{\delta \mathcal{H}_{\text{PDE}}}{\delta p}[q,p;\mu] \right)(t,\xi;\mu) = p(t,\xi;\mu), \\
\partial_t p(t,\xi;\mu) &= -\left(\frac{\delta \mathcal{H}_{\text{PDE}}}{\delta q}[q,p;\mu] \right)(t,\xi;\mu) = -\mu^2 \partial_{\xi\xi} q(t,\xi;\mu), \\
\mathcal{H}_{\text{PDE}}[q,p;\mu] &:= \frac{1}{2} \int_\Omega \mu^2 (\partial_\xi q)^2 + p^2 \, \mathrm{d}\xi,
\end{aligned}
\tag{7.14}
$$

where $\frac{\delta(\cdot)}{\delta(\cdot)}$ denotes the variational derivative. We discretize the interior of Ω into $\bar{N} = 2048$ equidistantly spaced points which results for $i = 1, \dots, \bar{N}$ in $\xi_i := i\Delta_\xi - 1/2$ with step size

$\Delta_\xi := 1/(\bar{N}+1)$ and the two states $\boldsymbol{q}(t;\mu) := [q(t,\xi_i;\mu)]_{i=1}^{\bar{N}}$ and $\boldsymbol{p}(t;\mu) := [p(t,\xi_i;\mu)]_{i=1}^{\bar{N}}$. Discretizing (7.14) with a finite difference method, yields a $2\bar{N}$-dimensional Hamiltonian FOM (7.1) with a canonical symplectic form $\boldsymbol{\omega} \equiv \mathbb{J}_{2\bar{N}}^\top$ and $\boldsymbol{\gamma}(t;\mu) := [\boldsymbol{q}(t;\mu)^\top, \boldsymbol{p}(t;\mu)^\top]^\top \in \mathbb{R}^{2\bar{N}}$ and the separable, quadratic Hamiltonian

$$\mathcal{H}(\boldsymbol{m};\mu) := \frac{1}{2}\boldsymbol{m}^\top \begin{bmatrix} -\mu^2 \boldsymbol{D}_{\xi\xi} & \boldsymbol{0}_{\bar{N}\times\bar{N}} \\ \boldsymbol{0}_{\bar{N}\times\bar{N}} & \boldsymbol{I}_{\bar{N}} \end{bmatrix} \boldsymbol{m},$$

where $\boldsymbol{D}_{\xi\xi}$ is the central finite difference approximation for the second-order derivative $\partial_{\xi\xi}$. For symplectic time integration, we use the implicit midpoint rule (2.25) with $K = 4000$ steps. The training set $\mathcal{P}_{\text{train}}$ is chosen as 8 equidistant points in the parameter space $\mathcal{P}$ which results in $|\mathcal{P}_{\text{train}}| \cdot K = 32000$ snapshots.

7.3.2 Training of Deep Convolutional Autoencoders

In this subsection, we discuss all details on the architecture and training of the DCAs used in the numerical experiment. The settings specific for the different DCAs are listed in Table 7.1. For the training, the snapshot data is randomly split into two disjoint sets, (i) 80% training data $\mathcal{X}_{\text{train}}$ and (ii) 20% validation data $\mathcal{X}_{\text{val}}$. The network architectures are (weakly symplectic) DCAs as described in Section 7.2. For nine different reduced sizes $2\bar{n} \in \{2, 4, \ldots, 12, 18, 24, 30\} =: \mathcal{D}_r$, we train three different types of DCAs separately. The three investigated DCA types are (i) a weakly symplectic DCA $\mathcal{A}_{s,0}^{2\bar{n}}$, (ii) a non-symplectic DCA $\mathcal{A}_0^{2\bar{n}}$ with the same hyperparameter configuration as (i) but symplecticity is not included in the loss function (7.12a), i.e., $\alpha = 1$, and (iii) a completely different non-symplectic DCA architecture $\mathcal{A}_1^{2\bar{n}}$. In this context, we refer to a DCA as non-symplectic if symplecticity is not included in the loss function (7.12a), i.e., $\alpha = 1$. The hyperparameter configuration for $\mathcal{A}_{s,0}^{2\bar{n}}$ was decided by hyperparameter optimization with 250 candidates (with $\alpha < 1$) by minimizing the loss (7.12a) on the validation set $\mathcal{X}_{\text{val}}$. The hyperparameter configuration for the DCAs of type $\mathcal{A}_1^{2\bar{n}}$ was determined analogously in a separate run with $\alpha = 1$ over 400 candidates. In this setting, we provide a good baseline as we compare our approach to the same DCA without symplecticity in the loss function ($\mathcal{A}_0^{2\bar{n}}$) and a non-symplectic DCA optimized on its own ($\mathcal{A}_1^{2\bar{n}}$). For all different reduced dimensions $2\bar{n}$, the optimized hyperparameter configurations result in DCAs with a number of network parameters $n_{\boldsymbol{\theta}}$ between $93,000$ and $101,000$ for $\mathcal{A}_{s,0}^{2\bar{n}}, \mathcal{A}_0^{2\bar{n}}$ and between $248,000$ and $257,000$ for $\mathcal{A}_1^{2\bar{n}}$.

setting	$\mathcal{A}_{s,0}^{2\bar{n}}$	$\mathcal{A}_0^{2\bar{n}}$	$\mathcal{A}_1^{2\bar{n}}$
weight α in (7.12a)	0.9	1. (non-symplectic)	
num. conv. layer n_{conv}	6		5
conv. channels $\boldsymbol{c}$	$[2, 2, 4, 8, 16, 32, 64]$		$[2, 4, 8, 16, 32, 64]$
lengths, conv. layer $\boldsymbol{l}^{\mathrm{conv}}$	$[2048, 512, 256, 128, 64, 16, 2]$		$[2048, 1024, 512, 256, 128, 4]$
stride $\boldsymbol{s}$	$[4, 2, 2, 2, 4, 8]$		$[2, 2, 2, 2, 32]$
num. full layer n_{full}	1		2
lengths, full layer $\boldsymbol{l}^{\mathrm{full}}$	$[128, 2\bar{n}]$		$[256, 132, 2\bar{n}]$
learning rate	4.43e-4		1.05e-4
batch size	15		25
weight initialization	Kaiming normal [52]		Xavier uniform [42]

Table 7.1: Autoencoder-specific settings for the weakly symplectic DCAs $\mathcal{A}_{s,0}^{2\bar{n}}$ and the non-symplectic DCAs $\mathcal{A}_0^{2\bar{n}}, \mathcal{A}_1^{2\bar{n}}$. Note, that the DCAs $\mathcal{A}_{s,0}^{2\bar{n}}$ and $\mathcal{A}_0^{2\bar{n}}$ share all parameters except for the weight α. We only report the layout of the encoder part as the decoder uses a mirrored layout. The table is adapted from [22].

Both, encoder and decoder, are composed of multiple, sequential layers, see Figure 7.1. The sizes of the intermediate results are indicated in the upper part. Sizes with a $\times$-symbol indicate that the result is a second-order tensor. For such results, we call the first dimension the *channels* and the second dimension the *length*. The outermost layers (split, flat, dotted boundary around layers) convert the state $[\boldsymbol{q}; \boldsymbol{p}] \in \mathbb{R}^{2\bar{N}}$ to a second-order tensor $[\boldsymbol{q}, \boldsymbol{p}]^{\top} \in \mathbb{R}^{2 \times \bar{N}}$ (or $\mathbb{R}^{2 \times \bar{N}} \to \mathbb{R}^{2\bar{N}}$, respectively) such that both physical quantities, the configuration variables $\boldsymbol{q}$ and the conjugated momenta $\boldsymbol{p}$, occupy one separate channel. The next part is framed by a scaling operation and its inverse (scale, scale^{-1}, dashed boundary around layers). The scaling is chosen to scale each channel in the input data separately to the interval $[0, 1]$. This operation is typically applied directly to the data. In our approach, this operation is adopted in the network in order to ensure that this operation is respected in the symplecticity loss (7.12b). The other layers in Figure 7.1 are, in order, a block of convolutional layers (convblock), a flatten operation, a block of fully-connected layers (fullblock$_e$) in the encoder, a block of fully-connected layers (fullblock$_d$) in the decoder, a splitting operation and a block of transposed convolutions (convTblock). Each block consists of alternating (transposed) convolutional layers (or fully-connected layers, respectively) and nonlinear
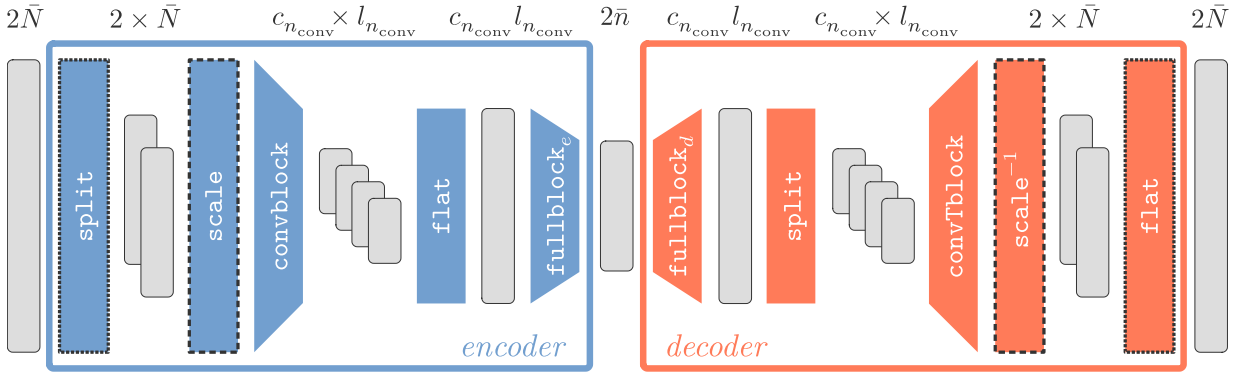
Figure 7.1: Schematic description of the network architecture of general DCAs composed of an encoder (blue) and a decoder part (orange). The sizes of the intermediate results (light gray) are indicated in the upper part. Sizes with a ×-symbol indicate that the result is a second-order tensor. This figure is adapted from [22].

activation layers. The activation function in all examples is the Exponential Linear Unit (ELU)

$$\sigma(x) := \begin{cases} x, & x \geq 0, \\ \exp(x) - 1, & x < 0. \end{cases}$$

The hyperparameters for a (transposed) convolutional layer are the kernel size, the stride value s_i, the number of output channels c_i and the padding. The length of the output $l^{\mathrm{conv}}_{i+1} \in \mathbb{N}$ of a (transposed) convolutional layer depends on all those hyperparameters and the length of the input l^{conv}_i. The hyperparameters for the fully-connected layers are the number of neurons described by the lengths l^{full}_i. We give an overview of the hyperparameters and the resulting lengths for each autoencoder in Table 7.1. Layer-specific hyperparameters are denoted as a vector $\boldsymbol{v} = [v_0, \dots, v_{n_{\boldsymbol{v}}}]$.

We use mini-batching in combination with the optimizer ADAM [64] with standard parameters except for the learning rate, which is given together with the batch size in Table 7.1 for each DCA type. The batches are reshuffled in every epoch. The DCAs are trained for 1000 epochs where one epoch is a full iteration over all training batches. The final parameter $\boldsymbol{\theta}^*$ is chosen as the minimizer of the total loss (7.12a) over the validation data set $\mathcal{X}_{\mathrm{val}}$ within those 1000 epochs. All biases are initialized with zeros. The weights are initialized with the method and corresponding distribution listed in Table 7.1. The DCAs are implemented with the pyTorch [96] framework. Moreover, the floating point precision is set to `double`-precision, as the FOM and ROM work with this precision.

reduction method	φ lin.	sympl.	approx.	ref.
Symplectic Manifold Galerkin (SMG)	no	yes	$\mathcal{A}_{s,0}^{2\bar{n}}$	Section 6.5.3, [22]
Manifold Galerkin (MG)	no	no	$\mathcal{A}_{0}^{2\bar{n}}, \mathcal{A}_{1}^{2\bar{n}}$	Section 6.5.1, [75]
Manifold LSPG (M-LSPG)	no	no		[75]
Symplectic Galerkin (SG)	yes	yes	$V_{\mathrm{CL}}^{2\bar{n}}$	Section 2.4.2, [99]
Galerkin (G)	yes	no	$V_{\mathrm{POD}}^{2\bar{n}}$	Section 2.2.2, [68]
least-squares Petrov–Galerkin (LSPG)	yes	no		[29]

Table 7.2: Summary of investigated reduction techniques. The table is adapted from [22].

7.3.3 Accuracy Based on Test Data

The DCAs described in the previous section are compared for three fixed parameter instances $\mathcal{P}_{\mathrm{test}} := \{\mu_1, \mu_2, \mu_3\}$ with $\mu_1 := 0.51$, $\mu_2 = 0.625$, $\mu_3 = 0.74$ that are all distinct from the training set $\mathcal{P}_{\mathrm{train}}$, i.e., we investigate how well the DCAs generalize to unseen data. For the weakly symplectic DCAs $\mathcal{A}_{s,0}^{2\bar{n}}$, we use the SMG reduction technique recited in Section 6.5.3. For the non-symplectic DCAs, we use the manifold Galerkin (MG) and the manifold LSPG (M-LSPG) both introduced in [75]. Additionally, we display the results for a classical symplectic MOR method, the cotangent lift (CL) with symplectic Galerkin (SG) projection, which was observed to be the best reduction technique in the experiments for the linear wave equation in [99]. Moreover, we present results for the proper orthogonal decomposition (POD) in combination with the Galerkin (G) and least-squares Petrov–Galerkin (LSPG) projection, which are classical (non-symplectic) MOR techniques. The different reduction techniques are summarized in Table 7.2. We quantify the quality of the reduced models on the test data with the (mean relative) projection error

$$e_{\mathrm{proj}} := \frac{1}{|\mathcal{P}_{\mathrm{test}}|} \sum_{\mu \in \mathcal{P}_{\mathrm{test}}} \sqrt{\frac{\sum_{k=0}^{K} \|(\boldsymbol{\varphi} \circ \boldsymbol{\varrho})(\boldsymbol{\gamma}_k(\mu)) - \boldsymbol{\gamma}_k(\mu)\|^2}{\sum_{k=0}^{K} \|\boldsymbol{\gamma}_k(\mu)\|^2}} \tag{7.15}$$

and the (mean relative) reduction error

$$e_{\mathrm{red}} := \frac{1}{|\mathcal{P}_{\mathrm{test}}|} \sum_{\mu \in \mathcal{P}_{\mathrm{test}}} \sqrt{\frac{\sum_{k=0}^{K} \|\boldsymbol{\varphi}(\check{\boldsymbol{\gamma}}_k(\mu)) - \boldsymbol{\gamma}_k(\mu)\|^2}{\sum_{k=0}^{K} \|\boldsymbol{\gamma}_k(\mu)\|^2}}, \tag{7.16}$$

where $\boldsymbol{\gamma}_k(\mu) \in \mathbb{R}^{2\bar{N}}$ is the FOM solution and $\check{\boldsymbol{\gamma}}_k(\mu) \in \mathbb{R}^{2\bar{n}}$ is the corresponding ROM solution at time t_k. The projection error is a measure how well a solution can be approximated by the respective DCA whereas the reduction error shows the error of the corresponding ROM.

Figure 7.2 illustrates both errors for all techniques from Table 7.2 for different reduced dimensions $2\bar{n} \in \mathcal{D}_r$. The errors are displayed separately for projection techniques based on symplectic (manifold) Galerkin (Figure 7.2, left), (manifold) Galerkin (Figure 7.2, center) and (manifold) LSPG (Figure 7.2, right). Errors are not depicted, (a) if the error is above 400% or (b) if the corresponding ROM simulation run did not reach the absolute tolerance of 1e-8 within the maximum number of 15 quasi-Newton iterations for some time step t_k, $0 \le k \le K$.

First, we comment on the classical MOR methods on subspaces, i.e., $V_{\mathrm{CL}}^{2\bar{n}}$ with SG and $V_{\mathrm{POD}}^{2\bar{n}}$ with G and LSPG (depicted by pentagon-symbols in each plot; left, middle, right). As expected from theory, the reduction error e_{red} of all these methods is always bounded from below by the projection error e_{proj} of the POD basis (black dash-dotted line). Moreover, all classical reduction methods show poor results in the reduction error, which is around or above 100% for most $2\bar{n} \in \mathcal{D}_r$. Overall, no reduction error is achieved below 39.5% with classical methods for $2\bar{n} \in \mathcal{D}_r$. Therefore, for the considered case of a thin moving pulse, classical MOR techniques on subspaces are not able to beneficially reduce the model for the investigated reduced dimensions.
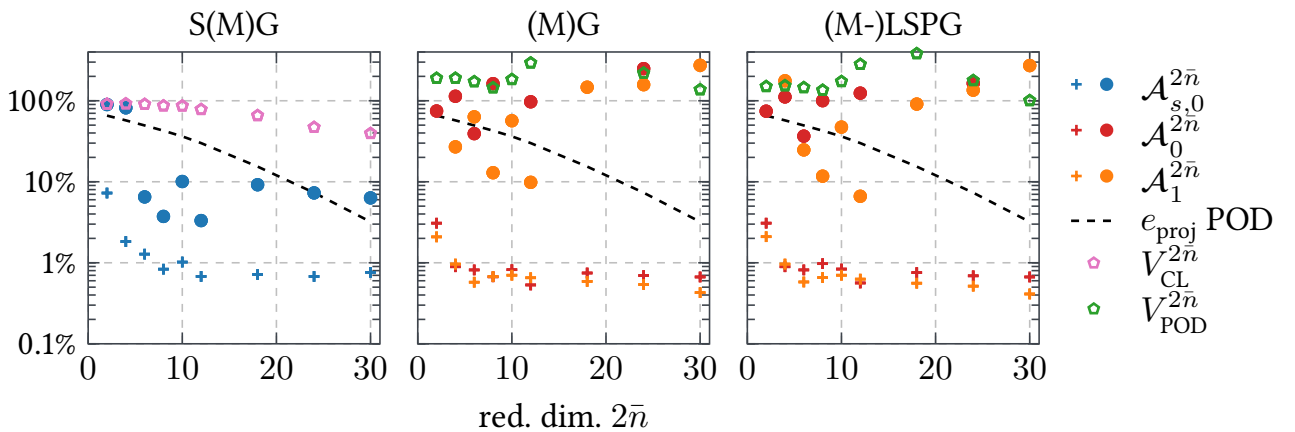
Figure 7.2: Reduction error e_{red} (7.16) (circles and pentagon-symbols) and projection error e_{proj} from (7.15) (plus-symbols and dash-dotted line) for different DCAs (see Table 7.1), and reduction techniques (see Table 7.2). We consider symplectic (manifold) Galerkin (left), (manifold) Galerkin (center) and (manifold) LSPG methods (right) separately. This figure is adapted from [22].

In contrast to that, all nonlinear projections based on the DCAs $\mathcal{A}_{s,0}^{2\bar{n}}$, $\mathcal{A}_0^{2\bar{n}}$, $\mathcal{A}_1^{2\bar{n}}$ attain lower projection errors e_{proj} (plus-symbols) than the projection error e_{proj} for the POD basis, and a lower reduction error e_{red} (circles) for at least one reduced dimension. The reduction errors provide results below and above the POD projection error, which aligns with previous experiments for model reduction on manifolds using autoencoders, see [75]. Furthermore, we observe that M-LSPG yields lower reduction errors than MG in average, which is in accordance with the results for Burgers' equation in [75]. Moreover, the architecture $\mathcal{A}_1^{2\bar{n}}$ hyperparameter-optimized for the non-symplectic setting (orange) yields in general better results than $\mathcal{A}_0^{2\bar{n}}$ (red) which is expected from the design of the two DCAs. In terms of numbers, the weakly symplectic DCAs $\mathcal{A}_1^{2\bar{n}}$ with SMG produce reduction errors below 11% for all reduced dimensions $2\bar{n} \in \mathcal{D}_r$. For the non-symplectic methods, however, only $2\bar{n} = 12$ is able to produce a reduction error lower than 11% for both reduction methods MG and M-LSPG. Especially for reduced dimensions $2\bar{n} \geq 18$, reduction errors above 90% render the non-symplectic DCAs impractical. In that sense, the non-symplectic DCAs yield less reliable results than $\mathcal{A}_{s,0}^{2\bar{n}}$ with SMG. Overall, the best reduction error is given by $\mathcal{A}_{s,0}^{2\bar{n}}$ with SMG with $2\bar{n} = 12$ with 3.3%.

In comparison to the results from [75] for the Burgers' equation, it is, however, surprising that the discrepancy between the reduction error and the projection error is very high for M-LSPG. This indicates that the lack of structure might impact M-LSPG which leads to higher reduction errors.[3]
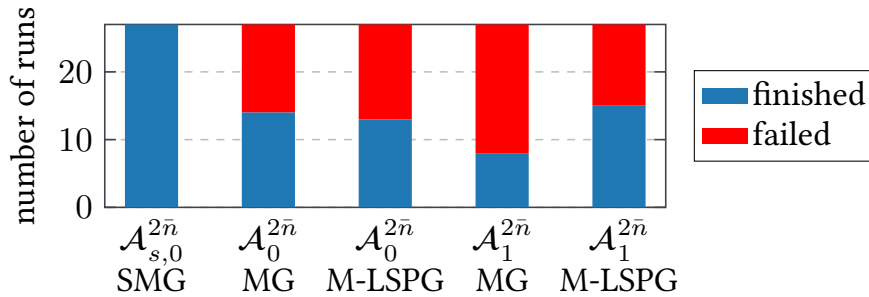
Figure 7.3: Number of successful (blue) compared to failed (red) reduced simulation runs for $\mathcal{A}_{s,0}^{2\bar{n}}$, $\mathcal{A}_0^{2\bar{n}}$, $\mathcal{A}_1^{2\bar{n}}$ with respective reduction technique, for μ_i, $i = 1, 2, 3$ and $2\bar{n} \in \mathcal{D}_r$. This figure is adapted from [22].

---

[3]The MG and M-LSPG in our implementation have been validated with the Burgers' example from [75] which leads to this conclusion.

Since Figure 7.2 excludes runs for which the Newton solver did not converge, we display the number of successful and failed runs in Figure 7.3. For the non-symplectic DCAs, we observe that non-converging reduced simulations occur, whereas all runs with the weakly symplectic DCAs converge. For $\mathcal{A}_1^{2\bar{n}}$, out of 27 simulations (9 reduced dimensions, 3 parameters) $8/27$ runs converged for MG and $15/27$ runs converged for M-LSPG. For $\mathcal{A}_0^{2\bar{n}}$, $14/27$ simulations converged for MG and $13/27$ simulations converged for M-LSPG. This means that, even in the best case, one third of the runs did not converge for the non-symplectic DCAs. This emphasizes the importance of structure-preservation in model reduction.

7.3.4 Quality in Terms of Structure

To showcase the quality in terms of structure, we investigate the error in the symplecticity of $\mathcal{A}_{s,0}^{2\bar{n}}$ with

$$e_{\text{symp}}(t_k;\mu) := \frac{1}{(2\bar{n})^2} \left\| \boldsymbol{D\varphi}|_{\check{\boldsymbol{\gamma}}_k(\mu)}^{\top} \mathbb{J}_{2\bar{N}}^{\top} \boldsymbol{D\varphi}|_{\check{\boldsymbol{\gamma}}_k(\mu)} - \mathbb{J}_{2\bar{n}}^{\top} \right\|_{\text{F}}, \tag{7.17}$$

where $\check{\boldsymbol{\gamma}}_k(\mu) \in \mathbb{R}^{2\bar{n}}$ denotes the solution of the SMG-ROM (7.2). Figure 7.4a depicts this error over time for different reduced dimensions $2\bar{n} \in \mathcal{D}_r$. It shows that the error in the symplecticity is comparable for $2\bar{n} > 4$, whereas for $2\bar{n} \leq 4$ higher errors might occur. In the latter case the reduced dimension may be too low in order to capture the essential properties of the set of all solutions. The following remark briefly comments on a possibility to enhance symplecticity in DCAs.

Remark 7.7 ((Strictly) symplectic embeddings): *In the present work, we determined approximately symplectic embeddings by penalizing symplecticity in the loss. This is advantageous in the scope of our work because it allows to compare the SMG-ROM with the MG-ROM on comparable architectures (which only differ in the penalization factor α).*

Future work might investigate (strictly) symplectic embeddings. To this end, the concept of DCAs could be paired with symplectic mappings such as the SympNets introduced in [60] (which has been proposed in a different context earlier in [34]). Moreover, the manifold cotangent lift introduced in [108] can be used to generate (strictly) symplectic mappings.

To numerically verify the preservation of the energy over time from Section 7.1.1, we plot in Figure 7.4b the evolution of the error in the Hamiltonian $\Delta\mathcal{H}(t;\mu_1)$ (7.3) for the DCAs $\mathcal{A}_{s,0}^{2\bar{n}}, \mathcal{A}_0^{2\bar{n}}$ and $\mathcal{A}_1^{2\bar{n}}$ (with SMG, MG, M-LSPG, whenever applicable). We illustrate the range
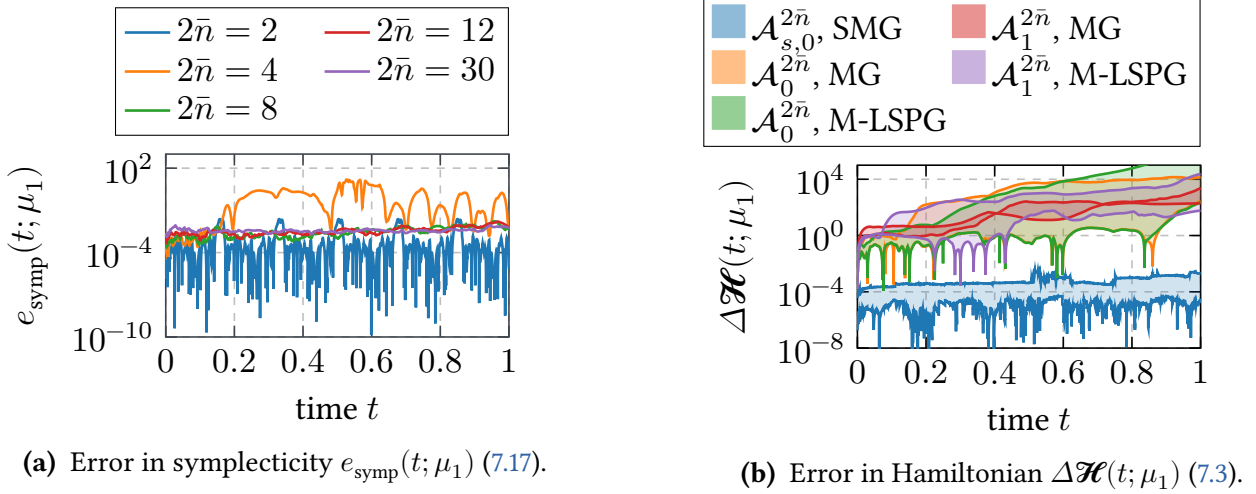
(a) Error in symplecticity $e_{\text{symp}}(t; \mu_1)$ (7.17).

(b) Error in Hamiltonian $\Delta\mathcal{H}(t; \mu_1)$ (7.3).

Figure 7.4: Error in the symplecticity $e_{\text{symp}}(t; \mu_1)$ (7.17) over time $t \in [0, 1]$ for the DCAs $\mathcal{A}_{s,0}^{2\bar{n}}$ with $2\bar{n} \in \mathcal{D}_r$ (left) and the minimum and maximum of the error in the Hamiltonian $\Delta\mathcal{H}(t; \mu_1)$ (7.3) over time $t \in [0, 1]$ for the DCAs $\mathcal{A}_{s,0}^{2\bar{n}}, \mathcal{A}_0^{2\bar{n}}, \mathcal{A}_1^{2\bar{n}}$ with different reduced dimensions $2\bar{n} \in \mathcal{D}_r$ (right). Both figures are taken from [22].

of $\Delta\mathcal{H}(t; \mu_1)$ over different reduced dimensions $2\bar{n} \in \mathcal{D}_r$ for each time step $t_k, 0 \leq k \leq K$. The minimum and maximum is plotted as solid lines and the area between both is shaded in the same color. Non-converging runs (red in Figure 7.3) are excluded, which is in favor of the non-symplectic DCAs $\mathcal{A}_0^{2\bar{n}}, \mathcal{A}_1^{2\bar{n}}$. We observe that the error in the Hamiltonian for small times $t \approx 0$ is very low in all cases. This is due to the exact reproduction of the initial value discussed in Section 7.2.3 which makes the DCAs match the Hamiltonian at $t = 0$, exactly with the idea from Remark 7.2. All runs of the weakly symplectic DCAs $\mathcal{A}_{s,0}^{2\bar{n}}$ are able to retain a low error in the Hamiltonian ($\Delta\mathcal{H}(t; \mu_1) < 4.2\text{e-}3$). The error is not exactly zero which we assume to stem from the fact that the symplectic midpoint rule conserves invariants exactly only up to quadratic order while the reduced Hamiltonian is of higher order than quadratic due to the nonlinearity of the embedding φ. However, the error is much lower than with the non-symplectic DCAs $\mathcal{A}_0^{2\bar{n}}, \mathcal{A}_1^{2\bar{n}}$. In the best case (for the non-symplectic DCAs), the minimum error in the Hamiltonian at the final time $t = 1$ is about 58 which is approximately four orders of magnitude higher than the maximal error of the symplectic method. In that sense, the additional constraint of weak symplecticity in (7.12b) in combination with the SMG projection shows its impact in this experiment with an improved preservation of the Hamiltonian compared to the non-symplectic DCAs.

Conclusion and Perspectives

8.1 Summary and Conclusion

In this thesis, we developed structure-preserving formulations and new algorithms for MOR on subspaces (Part I) and manifolds (Part II).

Part I focused on basis generation techniques for symplectic MOR. We introduced the PSD SVD-like decomposition as a powerful tool, that computes a non-orthogonal, symplectic basis. Furthermore, the PSD-greedy was formulated as a greedy method that is guaranteed to provide a symplectic basis in combination with a suitable basis generation technique. Lastly, we proved for the special case of canonizable systems with a periodic solution that an optimal symplectic basis in the time-continuous setting can be computed with the POD if the integration time is chosen accordingly. For each of these advancements, we deducted numerical experiments. We conclude from Part I that orthonormality of the basis is not required in symplectic MOR. All numerical experiments suggest that a non-orthogonal, symplectic basis allows to obtain the same accuracy as the orthogonal counterparts with less basis vectors. The resulting ROMs are smaller and thus more efficient.

Part II introduced a framework for structure-preserving MOR techniques based on differential geometry. Starting from a formulation of the FOM on manifolds, we introduced two MOR concepts (generalized manifold Galerkin and manifold Petrov–Galerkin). Adding more structure in the form of tensor fields allowed us to investigate Lagrangian and Hamiltonian systems together with structure-preserving MOR for such systems jointly in this framework. As a second step, we examined structure-preserving MOR for Hamiltonian systems on manifolds more closely. In terms of theoretical findings, we proved preservation of energy and stability and an error bound. As a practical algorithm, we introduced a technique to learn

an approximately symplectic embedding from snapshot data with the weakly symplectic autoencoders. Inspecting this new algorithm numerically for the challenging example of a moving thin pulse showed that both aspects of this thesis (structure-preservation and MOR on manifolds) are essential to obtain an accurate and robust ROM. We conclude from Part II that the differential geometric formulation is substantial to understand and preserve the structures present in the FOM. The main tool for structure-preservation is the pullback of covariant objects that transfers structure from the FOM to the ROM naturally. Moreover, a key insight from Part II is that many techniques existing in literature are included in the formalism of the presented framework. The differentiation between the generalized manifold Galerkin and the manifold Petrov–Galerkin helps to categorize these approaches.

8.2 Perspectives

Regarding the contents of this thesis, we see the following perspectives for future work: The methods developed in Part I for symplectic basis generation may be transferred to related fields such as MOR for port-Hamiltonian systems [114], which are a generalization of Hamiltonian systems. Current work [103] shows that the PSD SVD-like decomposition can also be beneficial in this case. However, the highest potential to inspire future work lies in the framework for structure-preserving MOR on manifolds from Part II. It provides a fertile basis to formulate and investigate structure-preserving MOR techniques for other structures as in port-Hamiltonian [114] or (port-)metriplectic [55, 89] systems. In terms of data-based embeddings, the framework should be extended to lifting [67, 101] and shifting [16, 59, 91, 102, 105, 112] operations, which are established approaches in MOR with nonlinear projections.

For the future of MOR and surrogate modelling in general, we anticipate further advances in both main aspects of this thesis, (i) structure-preservation methods and (ii) MOR on manifolds. The first aspect, (i) structure preservation, can be driven by the mathematical community that uses algebraic and geometric structures to formulate numerical techniques on the FOM level. The MOR community will closely follow this development and provide appropriate surrogate modelling techniques for the newly emerging structured models. The demand to improve the second aspect, (ii) MOR on manifolds, naturally emerges from the underlying assumption of MOR on subspaces that the Kolmogorov n-widths decay fast enough, which limits its applicability especially in FOMs with transport-dominated solutions.

Appendix

A Proofs

A.1 Topological Spaces and Topological Manifolds

A.1.1 Fundamentals

Consider a set $\mathcal{M}$. A *topology on $\mathcal{M}$* is a collection $\mathcal{T}$ of subsets of $\mathcal{M}$ (which are called *open subsets of $\mathcal{M}$*) that satisfy that (i) both the empty set $\emptyset$ and the set itself $\mathcal{M}$ are open, (ii) each union of open subsets is open, (iii) each intersection of finitely many open subsets is open. The pair $(\mathcal{M}, \mathcal{T})$ is called a *topological space*. If the specific topology is clear from the context or not particularly relevant for the discussion, then we simply write $\mathcal{M}$ instead of $(\mathcal{M}, \mathcal{T})$.

For two topological spaces $\mathcal{M}$ and $\mathcal{Q}$, a map $F\colon \mathcal{M} \to \mathcal{Q}$ is called *continuous*, if for every open subset $V \subset \mathcal{Q}$, the *preimage* $\{m \in \mathcal{M} \mid F(m) \in V\}$ is open in $\mathcal{M}$. We call F a *homeomorphism*, if (i) it is bijective (and thus the *inverse* $F^{-1}\colon \mathcal{Q} \to \mathcal{M}$ exists) and (ii) both F and F^{-1} are continuous. Correspondingly, two topological spaces $\mathcal{M}$ and $\mathcal{Q}$ are called *homeomorphic* if there exists a homeomorphism from $\mathcal{M}$ to $\mathcal{Q}$. Moreover, $\mathcal{M}$ is called *locally homeomorphic to* $\mathbb{R}^N$ for $N \in \mathbb{N}$ if for every point $m \in \mathcal{M}$ there exists an open set $U \subset \mathcal{M}$ with $m \in U$, which is homeomorphic to an open subset of $\mathbb{R}^N$. A topological space $\mathcal{M}$ is called a *topological manifold* of *dimension* N if it is locally homeomorphic to $\mathbb{R}^N$ (and additionally Hausdorff and second-countable, see e.g. [74, Cha. 1 and App. A]).

A.1.2 Proof of Lemma 6.1

By assumption, $\varphi \in C^\infty(\check{\mathcal{M}}, \mathcal{M})$ and $\varrho \in C^\infty(\mathcal{M}, \check{\mathcal{M}})$ are smooth maps. Then, the restrictions to $\varphi(\check{\mathcal{M}}) \subset \mathcal{M}$ are smooth maps $\varphi \in C^\infty(\mathcal{M}, \varphi(\check{\mathcal{M}}))$ and $\varrho|_{\varphi(\check{\mathcal{M}})} \in C^\infty(\varphi(\check{\mathcal{M}}), \check{\mathcal{M}})$

in the subspace topology. Thus, φ is a smooth diffeomorphism onto its image in the subspace topology. By [74, Prop. 4.8. (a)], φ is a smooth immersion and thus a smooth embedding.

A.2 Proofs for Lagrangian Systems

A.2.1 Derivation of the Reduced Euler-Lagrange Equations

In the following, we derive for the reduced Lagrangian system $(\check{Q}, \check{\mathscr{L}})$ the reduced Euler-Lagrange equations presented in (6.44). To begin with, we compute the derivatives of $\check{\mathscr{L}}$ for $\check{Y}_Q = \left(\check{q}, \check{v}^i \frac{\partial}{\partial \check{y}^i} \Big|_{\check{q}} \right) \in T\check{Q}$ with $1 \leq j \leq Q$ and $1 \leq i, k \leq \check{Q}$ as

$$
\begin{aligned}
\frac{\partial \check{\mathscr{L}}}{\partial \check{\xi}^{\underline{i}}} \bigg|_{\check{Y}_Q} &= \frac{\partial \mathscr{L}}{\partial \xi^{\underline{j}}} \bigg|_{\varphi(\check{Y}_Q)} \frac{\partial \varphi^{\underline{j}}}{\partial \check{\xi}^{\underline{i}}} \bigg|_{\check{Y}_Q} + \frac{\partial \mathscr{L}}{\partial \xi^{\underline{Q+j}}} \bigg|_{\varphi(\check{Y}_Q)} \frac{\partial \varphi^{\underline{Q+j}}}{\partial \check{\xi}^{\underline{i}}} \bigg|_{\check{Y}_Q} \\
&= \frac{\partial \mathscr{L}}{\partial \xi^{\underline{j}}} \bigg|_{\varphi(\check{Y}_Q)} \frac{\partial \varphi_Q^{\underline{j}}}{\partial \check{y}^{\underline{i}}} \bigg|_{\check{q}} + \frac{\partial \mathscr{L}}{\partial \xi^{\underline{Q+j}}} \bigg|_{\varphi(\check{Y}_Q)} \frac{\partial^2 \varphi_Q^{\underline{j}}}{\partial \check{y}^{\underline{i}} \partial \check{y}^{\underline{k}}} \bigg|_{\check{q}} \check{v}^k \\
\frac{\partial \check{\mathscr{L}}}{\partial \xi^{\underline{\check{Q}+i}}} \bigg|_{\check{Y}_Q} &= \frac{\partial \mathscr{L}}{\partial \xi^{\underline{j}}} \bigg|_{\varphi(\check{Y}_Q)} \frac{\partial \varphi^{\underline{j}}}{\partial \xi^{\underline{\check{Q}+i}}} \bigg|_{\check{Y}_Q} + \frac{\partial \mathscr{L}}{\partial \xi^{\underline{Q+j}}} \bigg|_{\varphi(\check{Y}_Q)} \frac{\partial \varphi^{\underline{Q+j}}}{\partial \xi^{\underline{\check{Q}+i}}} \bigg|_{\check{Y}_Q} \\
&= \frac{\partial \mathscr{L}}{\partial \xi^{\underline{Q+j}}} \bigg|_{\varphi(\check{Y}_Q)} \frac{\partial \varphi_Q^{\underline{j}}}{\partial \check{y}^{\underline{i}}} \bigg|_{\check{q}}.
\end{aligned}
$$

Evaluation for the lifted curve $\Gamma_{\check{\gamma}_Q} \in C^\infty(\mathcal{I}, T\check{Q})$ and derivation with respect to the time, yields for $1 \leq j, k \leq Q$ and $1 \leq i, \ell, p \leq \check{Q}$

$$
\begin{aligned}
\frac{\mathrm{d}}{\mathrm{d}t} \left(\frac{\partial \check{\mathscr{L}}}{\partial \xi^{\underline{\check{Q}+i}}} \bigg|_{\Gamma_{\check{\gamma}_Q(\cdot)}} \right) \bigg|_t &= \frac{\mathrm{d}}{\mathrm{d}t} \left(\frac{\partial \mathscr{L}}{\partial \xi^{\underline{Q+j}}} \bigg|_{\varphi(\Gamma_{\check{\gamma}_Q(\cdot)})} \frac{\partial \varphi_Q^{\underline{j}}}{\partial \check{y}^{\underline{i}}} \bigg|_{\check{\gamma}_Q(\cdot)} \right) \bigg|_t \\
&= \frac{\partial^2 \mathscr{L}}{\partial \xi^{\underline{k}} \partial \xi^{\underline{Q+j}}} \bigg|_{\varphi(\Gamma_{\check{\gamma}_Q(t)})} \frac{\partial \varphi_Q^{\underline{j}}}{\partial \check{y}^{\underline{i}}} \bigg|_{\check{\gamma}_Q(t)} \frac{\partial \varphi^{\underline{k}}}{\partial \check{\xi}^{\underline{\ell}}} \bigg|_{\Gamma_{\check{\gamma}_Q(t)}} \frac{\mathrm{d}}{\mathrm{d}t} \left(\Gamma_{\check{\gamma}_Q(\cdot)}^{\underline{\ell}} \right) \bigg|_t \\
&\quad + \frac{\partial^2 \mathscr{L}}{\partial \xi^{\underline{k}} \partial \xi^{\underline{Q+j}}} \bigg|_{\varphi(\Gamma_{\check{\gamma}_Q(t)})} \frac{\partial \varphi_Q^{\underline{j}}}{\partial \check{y}^{\underline{i}}} \bigg|_{\check{\gamma}_Q(t)} \frac{\partial \varphi^{\underline{k}}}{\partial \xi^{\underline{\check{Q}+\ell}}} \bigg|_{\Gamma_{\check{\gamma}_Q(t)}} \frac{\mathrm{d}}{\mathrm{d}t} \left(\Gamma_{\check{\gamma}_Q(\cdot)}^{\underline{\check{Q}+\ell}} \right) \bigg|_t \\
&\quad + \frac{\partial^2 \mathscr{L}}{\partial \xi^{\underline{Q+k}} \partial \xi^{\underline{Q+j}}} \bigg|_{\varphi(\Gamma_{\check{\gamma}_Q(t)})} \frac{\partial \varphi_Q^{\underline{j}}}{\partial \check{y}^{\underline{i}}} \bigg|_{\check{\gamma}_Q(t)} \frac{\partial \varphi^{\underline{Q+k}}}{\partial \check{\xi}^{\underline{\ell}}} \bigg|_{\Gamma_{\check{\gamma}_Q(t)}} \frac{\mathrm{d}}{\mathrm{d}t} \left(\Gamma_{\check{\gamma}_Q(\cdot)}^{\underline{\ell}} \right) \bigg|_t \\
&\quad + \frac{\partial^2 \mathscr{L}}{\partial \xi^{\underline{Q+k}} \partial \xi^{\underline{Q+j}}} \bigg|_{\varphi(\Gamma_{\check{\gamma}_Q(t)})} \frac{\partial \varphi_Q^{\underline{j}}}{\partial \check{y}^{\underline{i}}} \bigg|_{\check{\gamma}_Q(t)} \frac{\partial \varphi^{\underline{Q+k}}}{\partial \xi^{\underline{\check{Q}+\ell}}} \bigg|_{\Gamma_{\check{\gamma}_Q(t)}} \frac{\mathrm{d}}{\mathrm{d}t} \left(\Gamma_{\check{\gamma}_Q(\cdot)}^{\underline{\check{Q}+\ell}} \right) \bigg|_t \\
&\quad + \frac{\partial \mathscr{L}}{\partial \xi^{\underline{Q+j}}} \bigg|_{\varphi(\Gamma_{\check{\gamma}_Q(t)})} \frac{\partial^2 \varphi_Q^{\underline{j}}}{\partial \check{y}^{\underline{k}} \partial \check{y}^{\underline{i}}} \bigg|_{\check{\gamma}_Q(t)} \frac{\mathrm{d}}{\mathrm{d}t} \left(\Gamma_{\check{\gamma}_Q(\cdot)}^{\underline{k}} \right) \bigg|_t
\end{aligned}
$$

$$
\begin{aligned}
&= \frac{\partial^2 \mathscr{L}}{\partial \xi^{\underline{k}} \partial \xi^{\underline{Q+j}}}\bigg|_{\varphi(\Gamma_{\check{\gamma}_Q(t)})} \frac{\partial \varphi_Q^{\underline{j}}}{\partial \check{y}^{\underline{i}}}\bigg|_{\check{\gamma}_Q(t)} \frac{\partial \varphi_Q^{\underline{k}}}{\partial \check{y}^{\underline{\ell}}}\bigg|_{\check{\gamma}_Q(t)} \frac{\mathrm{d}}{\mathrm{d}t}\check{\gamma}_Q^{\underline{\ell}}\bigg|_t \\
&\quad + \frac{\partial^2 \mathscr{L}}{\partial \xi^{\underline{Q+k}} \partial \xi^{\underline{Q+j}}}\bigg|_{\varphi(\Gamma_{\check{\gamma}_Q(t)})} \frac{\partial \varphi_Q^{\underline{j}}}{\partial \check{y}^{\underline{i}}}\bigg|_{\check{\gamma}_Q(t)} \frac{\partial^2 \varphi_Q^{\underline{k}}}{\partial \check{y}^{\underline{\ell}} \partial \check{y}^{\underline{p}}}\bigg|_{\check{q}} \frac{\mathrm{d}}{\mathrm{d}t}\check{\gamma}_Q^{\underline{p}}\bigg|_t \frac{\mathrm{d}}{\mathrm{d}t}\check{\gamma}_Q^{\underline{\ell}}\bigg|_t \\
&\quad + \frac{\partial^2 \mathscr{L}}{\partial \xi^{\underline{Q+k}} \partial \xi^{\underline{Q+j}}}\bigg|_{\varphi(\Gamma_{\check{\gamma}_Q(t)})} \frac{\partial \varphi_Q^{\underline{j}}}{\partial \check{y}^{\underline{i}}}\bigg|_{\check{\gamma}_Q(t)} \frac{\partial \varphi_Q^{\underline{k}}}{\partial \check{y}^{\underline{\ell}}}\bigg|_{\check{\gamma}_Q(t)} \frac{\mathrm{d}^2}{\mathrm{d}t^2}\check{\gamma}_Q^{\underline{\ell}}\bigg|_t \\
&\quad + \frac{\partial \mathscr{L}}{\partial \xi^{\underline{Q+j}}}\bigg|_{\varphi(\Gamma_{\check{\gamma}_Q(t)})} \frac{\partial^2 \varphi_Q^{\underline{j}}}{\partial \check{y}^{\underline{\ell}} \partial \check{y}^{\underline{i}}}\bigg|_{\check{\gamma}_Q(t)} \frac{\mathrm{d}}{\mathrm{d}t}\check{\gamma}_Q^{\underline{\ell}}\bigg|_t.
\end{aligned}
$$

In total, it holds for $1 \le j, k \le Q$ and $1 \le i, \ell, p \le \check{Q}$

$$
\begin{aligned}
0 &= \frac{\partial \check{\mathscr{L}}}{\partial \check{\xi}^{\underline{i}}}\bigg|_{\Gamma_{\check{\gamma}_Q(t)}} - \frac{\mathrm{d}}{\mathrm{d}t}\left(\frac{\partial \check{\mathscr{L}}}{\partial \check{\xi}^{\underline{\check{Q}+i}}}\bigg|_{\Gamma_{\check{\gamma}_Q(\cdot)}}\right)\bigg|_t \\
&= \frac{\partial \varphi_Q^{\underline{j}}}{\partial \check{y}^{\underline{i}}}\bigg|_{\check{\gamma}_Q(t)}\left(\frac{\partial \mathscr{L}}{\partial \xi^{\underline{j}}}\bigg|_{\varphi(\Gamma_{\check{\gamma}_Q(t)})} - \frac{\partial^2 \mathscr{L}}{\partial \xi^{\underline{k}} \partial \xi^{\underline{Q+j}}}\bigg|_{\varphi(\Gamma_{\check{\gamma}_Q(t)})} \frac{\partial \varphi_Q^{\underline{k}}}{\partial \check{y}^{\underline{\ell}}}\bigg|_{\check{\gamma}_Q(t)} \frac{\mathrm{d}}{\mathrm{d}t}\check{\gamma}_Q^{\underline{\ell}}\bigg|_t \right. \\
&\quad - \frac{\partial^2 \mathscr{L}}{\partial \xi^{\underline{Q+k}} \partial \xi^{\underline{Q+j}}}\bigg|_{\varphi(\Gamma_{\check{\gamma}_Q(t)})} \frac{\partial^2 \varphi_Q^{\underline{k}}}{\partial \check{y}^{\underline{\ell}} \partial \check{y}^{\underline{p}}}\bigg|_{\check{\gamma}_Q|_t} \frac{\mathrm{d}}{\mathrm{d}t}\check{\gamma}_Q^{\underline{p}}\bigg|_t \frac{\mathrm{d}}{\mathrm{d}t}\check{\gamma}_Q^{\underline{\ell}}\bigg|_t \\
&\quad \left. - \frac{\partial^2 \mathscr{L}}{\partial \xi^{\underline{Q+k}} \partial \xi^{\underline{Q+j}}}\bigg|_{\varphi_Q(\Gamma_{\check{\gamma}_Q(t)})} \frac{\partial \varphi_Q^{\underline{k}}}{\partial \check{y}^{\underline{\ell}}}\bigg|_{\check{\gamma}_Q(t)} \frac{\mathrm{d}^2}{\mathrm{d}t^2}\check{\gamma}_Q^{\underline{\ell}}\bigg|_t\right).
\end{aligned}
$$

A.2.2 Proof of Theorem 6.18

In the following, we prove Theorem 6.18. In order to show that the systems are equivalent, we show that the underlying vector fields are identical, i.e., we show that the LMG reduction (6.49) of the Euler–Lagrange vector field (6.34) results in the reduced Euler–Lagrangian vector field (6.46). To simplify the notation, we use $\tau = \tau_{\mathsf{LMG}}$ and $\check{\tau} = \check{\tau}_{\mathsf{LMG}}$ in the following, with τ_{LMG} as in (6.47). Let $\check{Y}_Q = (\check{q}, \check{v}) = (\check{q}, \check{v}^{\underline{i}}\frac{\partial}{\partial \check{y}^{\underline{i}}}\big|_{\check{q}}) \in T\check{Q}$. The reduced tensor field $\check{\tau} = \mathrm{d}\varphi^*\tau$ reads for $1 \le \alpha, \beta \le 2Q$ and $1 \le k, \ell \le Q$ and $1 \le i, j, p \le \check{Q}$

$$
\begin{aligned}
\check{\tau}\big|_{\check{Y}_Q} &= \frac{\partial \varphi^{\underline{\gamma}}}{\partial \xi^{\underline{\alpha}}}\bigg|_{\check{Y}_Q}\left(\tau\big|_{\varphi(\check{Y}_Q)}\right)_{\underline{\gamma\delta}} \frac{\partial \varphi^{\underline{\delta}}}{\partial \xi^{\underline{\beta}}}\bigg|_{\check{Y}_Q} \mathrm{d}\xi^{\underline{\alpha}}\big|_{\check{Y}_Q} \otimes \mathrm{d}\xi^{\underline{\beta}}\big|_{\check{Y}_Q} \\
&= \left(\tau_q\big|_{\varphi(\check{Y}_Q)}\right)_{\underline{k\ell}}\left(\frac{\partial^2 \varphi_Q^{\underline{k}}}{\partial \check{y}^{\underline{p}} \partial \check{y}^{\underline{i}}}\bigg|_{\check{Y}_Q} \check{v}^{\underline{p}}\, \mathrm{d}\check{\xi}^{\underline{i}}\big|_{\check{Y}_Q} + \frac{\partial \varphi_Q^{\underline{k}}}{\partial \check{y}^{\underline{i}}}\bigg|_{\check{Y}_Q} \mathrm{d}\check{\xi}^{\underline{\check{Q}+i}}\big|_{\check{Y}_Q}\right) \otimes \left(\frac{\partial \varphi_Q^{\underline{\ell}}}{\partial \check{y}^{\underline{j}}}\bigg|_{\check{Y}_Q} \mathrm{d}\check{\xi}^{\underline{j}}\big|_{\check{Y}_Q}\right) \\
&\quad + \left(\tau_v\big|_{\varphi(\check{Y}_Q)}\right)_{\underline{k\ell}}\left(\frac{\partial \varphi_Q^{\underline{k}}}{\partial \check{y}^{\underline{i}}}\bigg|_{\check{Y}_Q} \mathrm{d}\check{\xi}^{\underline{i}}\big|_{\check{Y}_Q}\right) \otimes \left(\frac{\partial^2 \varphi_Q^{\underline{\ell}}}{\partial \check{y}^{\underline{p}} \partial \check{y}^{\underline{j}}}\bigg|_{\check{Y}_Q} \check{v}^{\underline{p}}\, \mathrm{d}\check{\xi}^{\underline{j}}\big|_{\check{Y}_Q} + \frac{\partial \varphi_Q^{\underline{\ell}}}{\partial \check{y}^{\underline{j}}}\bigg|_{\check{Y}_Q} \mathrm{d}\check{\xi}^{\underline{\check{Q}+j}}\big|_{\check{Y}_Q}\right)
\end{aligned}
$$

$$
= \left(\left.\breve{\tilde{\tau}}_q\right|_{\breve{Y}_Q}\right)_{\underline{ij}} \left.\mathrm{d}\breve{\xi}^{\underline{\breve{Q}+i}}\right|_{\breve{Y}_Q} \otimes \left.\mathrm{d}\breve{\xi}^{\underline{j}}\right|_{\breve{Y}_Q} + \left(\left.\breve{\tilde{\tau}}_{qv}\right|_{\breve{Y}_Q}\right)_{\underline{ij}} \left.\mathrm{d}\breve{\xi}^{\underline{i}}\right|_{\breve{Y}_Q} \otimes \left.\mathrm{d}\breve{\xi}^{\underline{j}}\right|_{\breve{Y}_Q}
$$

$$
+ \left(\left.\breve{\tilde{\tau}}_v\right|_{\breve{Y}_Q}\right)_{\underline{ij}} \left.\mathrm{d}\breve{\xi}^{\underline{i}}\right|_{\breve{Y}_Q} \otimes \left.\mathrm{d}\breve{\xi}^{\underline{\breve{Q}+j}}\right|_{\breve{Y}_Q}
$$

with the abbreviations

$$
\left(\left.\breve{\tilde{\tau}}_q\right|_{\breve{Y}_Q}\right)_{\underline{ij}} := \left.\frac{\partial \varphi_Q{}^k}{\partial \breve{y}^{\underline{i}}}\right|_{\breve{Y}_Q} \left(\left.\tau_q\right|_{\varphi(\breve{Y}_Q)}\right)_{\underline{k\ell}} \left.\frac{\partial \varphi_Q{}^\ell}{\partial \breve{y}^{\underline{j}}}\right|_{\breve{Y}_Q},
$$

$$
\left(\left.\breve{\tilde{\tau}}_v\right|_{\breve{Y}_Q}\right)_{\underline{ij}} := \left.\frac{\partial \varphi_Q{}^k}{\partial \breve{y}^{\underline{i}}}\right|_{\breve{Y}_Q} \left(\left.\tau_v\right|_{\varphi(\breve{Y}_Q)}\right)_{\underline{k\ell}} \left.\frac{\partial \varphi_Q{}^\ell}{\partial \breve{y}^{\underline{j}}}\right|_{\breve{Y}_Q},
$$

$$
\left(\left.\breve{\tilde{\tau}}_{qv}\right|_{\breve{Y}_Q}\right)_{\underline{ij}} := \left.\frac{\partial^2 \varphi_Q{}^k}{\partial \breve{y}^{\underline{p}} \partial \breve{y}^{\underline{i}}}\right|_{\breve{Y}_Q} \breve{v}^{\underline{p}} \left(\left.\tau_q\right|_{\varphi(\breve{Y}_Q)}\right)_{\underline{k\ell}} \left.\frac{\partial \varphi_Q{}^\ell}{\partial \breve{y}^{\underline{j}}}\right|_{\breve{Y}_Q} + \left.\frac{\partial \varphi_Q{}^k}{\partial \breve{y}^{\underline{i}}}\right|_{\breve{Y}_Q} \left(\left.\tau_v\right|_{\varphi(\breve{Y}_Q)}\right)_{\underline{k\ell}} \left.\frac{\partial^2 \varphi_Q{}^\ell}{\partial \breve{y}^{\underline{p}} \partial \breve{y}^{\underline{j}}}\right|_{\breve{Y}_Q} \breve{v}^{\underline{p}}.
$$

It is easy to verify that the inverse of $\breve{\tilde{\tau}}$ is given by

$$
\left.\breve{\tilde{\tau}}\right|^{-1}_{\breve{Y}_Q} = (\left.\breve{\tilde{\tau}}_q\right|_{\breve{Y}_Q})^{\underline{ij}} \left.\frac{\partial}{\partial \breve{\xi}^{\underline{i}}}\right|_{\breve{Y}_Q} \otimes \left.\frac{\partial}{\partial \breve{\xi}^{\underline{\breve{Q}+j}}}\right|_{\breve{Y}_Q}
$$

$$
- (\left.\breve{\tilde{\tau}}_v\right|_{\breve{Y}_Q})^{\underline{ik}} (\left.\breve{\tilde{\tau}}_{qv}\right|_{\breve{Y}_Q})_{\underline{k\ell}} (\left.\breve{\tilde{\tau}}_q\right|_{\breve{Y}_Q})^{\underline{\ell j}} \left.\frac{\partial}{\partial \breve{\xi}^{\underline{\breve{Q}+i}}}\right|_{\breve{Y}_Q} \otimes \left.\frac{\partial}{\partial \breve{\xi}^{\underline{\breve{Q}+j}}}\right|_{\breve{Y}_Q} \qquad \text{(A.1)}
$$

$$
+ (\left.\breve{\tilde{\tau}}_v\right|_{\breve{Y}_Q})^{\underline{ij}} \left.\frac{\partial}{\partial \breve{\xi}^{\underline{\breve{Q}+i}}}\right|_{\breve{Y}_Q} \otimes \left.\frac{\partial}{\partial \breve{\xi}^{\underline{j}}}\right|_{\breve{Y}_Q}
$$

with $1 \leq i, j, k, \ell \leq \breve{Q}$, which in bold notation reads

$$
\left.\breve{\boldsymbol{\tau}}\right|_{\breve{\boldsymbol{Y}}_Q} = \begin{bmatrix} \left.\breve{\boldsymbol{\tau}}_{qv}\right|_{\breve{\boldsymbol{Y}}_Q} & \left.\breve{\boldsymbol{\tau}}_v\right|_{\breve{\boldsymbol{Y}}_Q} \\ \left.\breve{\boldsymbol{\tau}}_q\right|_{\breve{\boldsymbol{Y}}_Q} & \mathbf{0}_{\breve{Q}\times\breve{Q}} \end{bmatrix} \qquad \text{and} \qquad \left.\breve{\boldsymbol{\tau}}\right|^{-1}_{\breve{\boldsymbol{Y}}_Q} = \begin{bmatrix} \mathbf{0}_{\breve{Q}\times\breve{Q}} & \left.\breve{\boldsymbol{\tau}}_q\right|^{-1}_{\breve{\boldsymbol{Y}}_Q} \\ \left.\breve{\boldsymbol{\tau}}_v\right|^{-1}_{\breve{\boldsymbol{Y}}_Q} & -\left.\breve{\boldsymbol{\tau}}_v\right|^{-1}_{\breve{\boldsymbol{Y}}_Q} \left.\breve{\boldsymbol{\tau}}_{qv}\right|_{\breve{\boldsymbol{Y}}_Q} \left.\breve{\boldsymbol{\tau}}_q\right|^{-1}_{\breve{\boldsymbol{Y}}_Q} \end{bmatrix}.
$$

Moreover, we obtain for the indices $1 \leq \beta, \gamma \leq 2Q$ and $1 \leq \alpha \leq 2\check{Q}$ and $1 \leq j, k \leq Q$ and $1 \leq \ell, p, r \leq \check{Q}$

$$
\begin{aligned}
\flat_{\check{\tau}}(R_{\text{LMG}}(X_{\mathscr{L}}))|_{\check{Y}_Q} &= \left(d\varphi^*|_{\check{Y}_Q}\left(\flat_{\tau}\left(X_{\mathscr{L}}|_{\varphi(\check{Y}_Q)}\right)\right)\right)_{\underline{\alpha}} d\check{\xi}^{\underline{\alpha}}\Big|_{\check{Y}_Q} \\
&= \frac{\partial\varphi^{\beta}}{\partial\check{\xi}^{\underline{\alpha}}}\Big|_{\check{Y}_Q}\left(\tau|_{\varphi(\check{Y}_Q)}\right)_{\underline{\beta\gamma}}\left(X_{\mathscr{L}}|_{\varphi(\check{Y}_Q)}\right)^{\underline{\gamma}} d\check{\xi}^{\underline{\alpha}}\Big|_{\check{Y}_Q} \\
&= \left(\frac{\partial\varphi^j}{\partial\check{\xi}^{\underline{\alpha}}}\Big|_{\check{Y}_Q}\left(\tau_v|_{\varphi(\check{Y}_Q)}\right)_{\underline{jk}}\left(X_{\mathscr{L}}|_{\varphi(\check{Y}_Q)}\right)^{\overline{Q+k}}\right. \\
&\quad \left. + \frac{\partial\varphi^{\check{Q}+j}}{\partial\check{\xi}^{\underline{\alpha}}}\Big|_{\check{Y}_Q}\left(\tau|_{\varphi(\check{Y}_Q)}\right)_{\underline{jk}}\frac{\partial\varphi_Q^k}{\partial\check{y}^{\ell}}\Big|_{\check{q}}\check{v}^{\underline{\ell}}\right) d\check{\xi}^{\underline{\alpha}}\Big|_{\check{Y}_Q} \\
&= \left(\frac{\partial\varphi_Q^j}{\partial\check{y}^r}\Big|_{\check{q}}\left(\tau_v|_{\varphi(\check{Y}_Q)}\right)_{\underline{jk}}\left(X_{\mathscr{L}}|_{\varphi(\check{Y}_Q)}\right)^{\overline{Q+k}}\right. \\
&\quad \left. + \frac{\partial^2\varphi_Q^j}{\partial\check{y}^r\partial\check{y}^p}\Big|_{\check{q}}\check{v}^{\underline{p}}\left(\tau_q|_{\varphi(\check{Y}_Q)}\right)_{\underline{jk}}\frac{\partial\varphi_Q^k}{\partial\check{y}^{\ell}}\Big|_{\check{q}}\check{v}^{\underline{\ell}}\right) d\check{\xi}^{\underline{r}}\Big|_{\check{Y}_Q} \\
&\quad + \frac{\partial\varphi_Q^j}{\partial\check{y}^r}\Big|_{\check{q}}\left(\tau_q|_{\varphi(\check{Y}_Q)}\right)_{\underline{jk}}\frac{\partial\varphi_Q^k}{\partial\check{y}^{\ell}}\Big|_{\check{q}}\check{v}^{\underline{\ell}} d\check{\xi}^{\overline{\check{Q}+r}}\Big|_{\check{Y}_Q}
\end{aligned}
\tag{A.2}
$$

and observe that the last term equals $\left(\check{\tau}_q|_{\check{Y}_Q}\right)_{\underline{r\ell}}\check{v}^{\underline{\ell}}$. Combining (A.2) with (A.1), the LMG reduction (6.49) of the Euler–Lagrange vector field (6.34) can be written (with the indices $1 \leq \alpha \leq 2\check{Q}$ and $1 \leq j, k \leq Q$ and $1 \leq i, \ell, p, r, s \leq \check{Q}$) as

$$
\begin{aligned}
R_{\text{LMG}}(X_{\mathscr{L}})|_{\check{Y}_Q} &= \left(\left(\sharp_{\check{\tau}} \circ d\varphi^*|_{\check{Y}_Q} \circ \flat_{\tau}\right)\left(X_{\mathscr{L}}|_{\varphi(\check{Y}_Q)}\right)\right)^{\underline{\alpha}} \frac{\partial}{\partial\check{\xi}^{\underline{\alpha}}}\Big|_{\check{Y}_Q} \\
&= \left(\check{\tau}_q|_{\check{Y}_Q}\right)^{\underline{ir}}\left(\check{\tau}_q|_{\check{Y}_Q}\right)_{\underline{r\ell}}\check{v}^{\underline{\ell}} \frac{\partial}{\partial\check{\xi}^{\underline{i}}}\Big|_{\check{Y}_Q} \\
&\quad + \left(\check{\tau}_v|_{\check{Y}_Q}\right)^{\underline{ir}}\left(\frac{\partial\varphi_Q^j}{\partial\check{y}^r}\Big|_{\check{q}}\left(\tau_v|_{\varphi(\check{Y}_Q)}\right)_{\underline{jk}}\left(X_{\mathscr{L}}|_{\varphi(\check{Y}_Q)}\right)^{\overline{Q+k}}\right. \\
&\quad + \frac{\partial^2\varphi_Q^j}{\partial\check{y}^r\partial\check{y}^p}\Big|_{\check{q}}\check{v}^{\underline{p}}\left(\tau_q|_{\varphi(\check{Y}_Q)}\right)_{\underline{jk}}\frac{\partial\varphi_Q^k}{\partial\check{y}^{\ell}}\Big|_{\check{q}}\check{v}^{\underline{\ell}} \\
&\quad \left. - \left(\check{\tau}_{qv}|_{\check{Y}_Q}\right)_{\underline{r\ell}}\left(\check{\tau}_q|_{\check{Y}_Q}\right)^{\underline{\ell p}}\left(\check{\tau}_q|_{\check{Y}_Q}\right)_{\underline{ps}}\check{v}^{\underline{s}}\right) \frac{\partial}{\partial\check{\xi}^{\overline{\check{Q}+i}}}\Big|_{\check{Y}_Q} \\
&= \check{v}^{\underline{i}} \frac{\partial}{\partial\check{\xi}^{\underline{i}}}\Big|_{\check{Y}_Q} + \left(\check{\tau}_v|_{\check{Y}_Q}\right)^{\underline{ir}}\left(\frac{\partial\varphi_Q^j}{\partial\check{y}^r}\Big|_{\check{q}}\left(\tau_v|_{\varphi(\check{Y}_Q)}\right)_{\underline{jk}}\left(X_{\mathscr{L}}|_{\varphi(\check{Y}_Q)}\right)^{\overline{Q+k}}\right. \\
&\quad \left. + \frac{\partial^2\varphi_Q^j}{\partial\check{y}^r\partial\check{y}^p}\Big|_{\check{q}}\check{v}^{\underline{p}}\left(\tau_q|_{\varphi(\check{Y}_Q)}\right)_{\underline{jk}}\frac{\partial\varphi_Q^k}{\partial\check{y}^{\ell}}\Big|_{\check{q}}\check{v}^{\underline{\ell}}\right.
\end{aligned}
$$

$$
-\frac{\partial^2 \varphi_Q{}^{\underline{j}}}{\partial \check{y}^{\underline{p}}\, \partial \check{y}^{\underline{r}}}\bigg|_{\check{q}}\, \check{v}^{\underline{p}} \left(\tau_q\big|_{\varphi(\check{Y}_Q)}\right)_{\underline{jk}} \frac{\partial \varphi_Q{}^{\underline{k}}}{\partial \check{y}^{\underline{\ell}}}\bigg|_{\check{q}}\, \check{v}^{\underline{\ell}}
$$

$$
-\frac{\partial \varphi_Q{}^{\underline{j}}}{\partial \check{y}^{\underline{r}}}\bigg|_{\check{q}} \left(\tau_v\big|_{\varphi(\check{Y}_Q)}\right)_{\underline{jk}} \frac{\partial^2 \varphi_Q{}^{\underline{k}}}{\partial \check{x}^{\underline{\ell}}\, \partial \check{y}^{\underline{p}}}\bigg|_{\check{q}}\, \check{v}^{\underline{\ell}}\, \check{v}^{\underline{p}} \right) \frac{\partial}{\partial \check{\xi}^{\check{Q}+i}}\bigg|_{\check{Y}_Q}
$$

$$
= \check{X}_{\check{\mathscr{L}}}\big|_{\check{Y}_Q}.
$$

Thus, the vector field obtained with the LMG reduction (6.49) with the LMG tensor field τ_{LMG} from (6.47) results in the reduced Euler–Lagrange vector field (6.46), which is equivalent to solving the reduced Euler–Lagrange equations (6.44) by construction.

A.3 Existence of Δt for Assumption (a2) in Theorem 7.6

Theorem A.1: *For all $C \in \mathbb{R}^{s \times s}$ with entries $[C]_{ij} := \delta_{ij} - \kappa \Delta t |a_{ij}|$ for $1 \le i, j \le s$, there exists $\Delta t > 0$ such that for every $x_s, y_s \in \mathbb{R}_{\ge 0}^s$ with $C x_s \le y_s$, it holds $x_s \le C^{-1} y_s$, i.e. assumption (a2) in Theorem 7.6 is fulfilled.*

Proof. We denote $C(\Delta t) := I_s - T(\Delta t)$ with $T(\Delta t) := \kappa \Delta t A \in \mathbb{R}_{\ge 0}^{s \times s}$, where the entries of A are given by $|a_{ij}|$, $1 \le i, j \le s$. We consider the inverse of $C(\Delta t)$ in terms of the Neumann series. If the series converges, it holds

$$
C^{-1}(\Delta t) = (I_s - T(\Delta t))^{-1} = \sum_{k=0}^{\infty} (T(\Delta t))^k .
$$

Let $\|\cdot\|_2$ be the two-norm on $\mathbb{R}^s$ and the (induced) spectral norm on $\mathbb{R}^{s \times s}$. The Neumann series converges on the Banach space $(\mathbb{R}^{s \times s}, \|\cdot\|_2)$, if $\|T(\Delta t)\|_2 < 1$ which is equivalent to

$$
\Delta t < \frac{1}{\kappa \|A\|_2}
$$

due to absolute homogeneity of the norm and $\kappa, \Delta t > 0$. Since both κ and $\|A\|_2$ are independent of Δt, we can always choose Δt small enough such that the Neumann series converges. For, e.g., the implicit midpoint rule ($s = 1$, $a_{11} = 1/2$), this results in the condition $\Delta t < 2/\kappa$.

We now assume that Δt is small enough such that the Neumann series converges and drop the dependency on Δt in the notation for the sake of brevity, i.e. we assume that $C^{-1} = \sum_{k=0}^{\infty} T^k$. Since the partial sums $\sum_{k=0}^{p} T^k \in \mathbb{R}_{\ge 0}^{s \times s}$ for all $p \in \mathbb{N}$ have non-negative

entries and $\mathbb{R}^{s \times s}_{\geq 0}$ is a closed subset of a metric space, we know that the limit $C^{-1} \in \mathbb{R}^{s \times s}_{\geq 0}$ also has non-negative entries.

But then, if for some $x_s, y_s \in \mathbb{R}^s_{\geq 0}$, the inequality $Cx_s \leq y_s$ holds, multiplication of the inequality with C^{-1} does not disrupt the inequality as for all $1 \leq i \leq s$

$$[x_s]_i = \left[C^{-1}Cx_s\right]_i = \sum_{j=1}^{s} \underbrace{[C^{-1}]_{ij}}_{\geq 0} \underbrace{[Cx_s]_j}_{\leq [y_s]_j} \leq \sum_{j=1}^{s} [C^{-1}]_{ij}[y_s]_j = [C^{-1}y_s]_i,$$

which is exactly the definition of $x_s \leq C^{-1}y_s$. $\square$

Bibliography

[1] R. Abraham and J. E. Marsden. *Foundations of mechanics*. 2nd edition. https://resolver.caltech.edu/CaltechBOOK:1987.001 (last accessed 5-Dec-2023). Addison-Wesley Publishing Company, 1987.

[2] S. Agoujil, A. H. Bentbib, and A. Kanber. *An iterative method for computing a symplectic SVD-like decomposition*. Computational and Applied Mathematics 37.1 (2018). DOI: 10.1007/s40314-016-0346-4.

[3] E. Al-Aidarous. *Symplectic Gram–Schmidt algorithm with re-orthogonalization*. Journal of King Abdulaziz University: Science 23.1 (2011). DOI: 10.4197/sci.23-1.2.

[4] M. Bachmayr and A. Cohen. *Kolmogorov widths and low-rank approximations of parametric elliptic PDEs*. Mathematics of Computation 86.304 (2017). DOI: 10.1090/mcom/3132.

[5] J. Barnett and C. Farhat. *Quadratic approximation manifold for mitigating the Kolmogorov barrier in nonlinear projection-based model order reduction*. Journal of Computational Physics 464 (2022). DOI: 10.1016/j.jcp.2022.111348.

[6] J. Barnett, C. Farhat, and Y. Maday. *Mitigating the Kolmogorov barrier for the reduction of aerodynamic models using neural-network-augmented reduced-order models*. AIAA SCITECH 2023 Forum. 2023. DOI: 10.2514/6.2023-0535.

[7] M. Barrault, Y. Maday, N. C. Nguyen, and A. T. Patera. *An 'empirical interpolation' method: Application to efficient reduced-basis discretization of partial differential equations*. Comptes Rendus Mathematique 339.9 (2004). DOI: 10.1016/j.crma.2004.08.006.

[8] T. Bendokat and R. Zimmermann. *The real symplectic Stiefel and Grassmann manifolds: Metrics, geodesics and applications*. Preprint. 2021. arXiv: 2108.12447 [math.DG].

[9] T. Bendokat and R. Zimmermann. *Geometric optimization for structure-preserving model reduction of Hamiltonian systems*. Proceedings of MATHMOD 2022. Vol. 55. 20. 2022. DOI: 10.1016/j.ifacol.2022.09.137.

[10] P. Benner and A. Salam. *The symplectic Lanczos process for Hamiltonian-positive matrices*. Talk at GAMM Annual Meeting, https://csc.mpi-magdeburg.mpg.de/mpcsc/benner/publications_fiona/talks/2013/Benner_GAMM2013.pdf (last accessed 5-Dec-2023). 2013.

[11] P. Benner, A. Cohen, M. Ohlberger, and K. Willcox. *Model reduction and approximation*. Society for Industrial and Applied Mathematics, 2017. DOI: 10.1137/1.9781611974829.

[12] P. Benner, P. Goyal, J. Heiland, and I. Pontes Duff. *A quadratic decoder approach to nonintrusive reduced-order modeling of nonlinear dynamical systems*. PAMM 23.1 (2023). DOI: 10.1002/pamm.202200049.

[13] P. Benner, P. Goyal, B. Kramer, B. Peherstorfer, and K. Willcox. *Operator inference for non-intrusive model reduction of systems with non-polynomial nonlinear terms*. Computer Methods in Applied Mechanics and Engineering 372 (2020). DOI: 10.1016/j.cma.2020.113433.

[14] P. Benner, S. Gugercin, and K. Willcox. *A survey of projection-based model reduction methods for parametric dynamical systems*. SIAM Review 57.4 (2015). DOI: 10.1137/130932715.

[15] R. Bishop and S. Goldberg. *Tensor analysis on manifolds*. Macmillan, 1968.

[16] F. Black, P. Schulze, and B. Unger. *Projection-based model reduction with dynamically transformed modes*. ESAIM: Mathematical Modelling and Numerical Analysis 54.6 (2020). DOI: 10.1051/m2an/2020046.

[17] T. J. Bridges and S. Reich. *Numerical methods for Hamiltonian PDEs*. Journal of Physics A: Mathematical and General 39.19 (2006). DOI: 10.1088/0305-4470/39/19/s02.

[18] P. Buchfink. *Structure-preserving model order reduction for linear elasticity*. Master's thesis. University of Stuttgart, 2017.

[19] P. Buchfink, A. Bhatt, and B. Haasdonk. *Symplectic model order reduction in RBmatlab*. 2019. DOI: 10.5281/zenodo.2578078.

[20] P. Buchfink, A. Bhatt, and B. Haasdonk. *Symplectic model order reduction with non-orthonormal bases.* Mathematical and Computational Applications 24.2 (2019). DOI: 10.3390/mca24020043.

[21] P. Buchfink, S. Glas, and B. Haasdonk. *Optimal bases for symplectic model order reduction of canonizable linear Hamiltonian systems.* Proceedings of MATHMOD 2022. Vol. 55. 20. 2022. DOI: 10.1016/j.ifacol.2022.09.138.

[22] P. Buchfink, S. Glas, and B. Haasdonk. *Symplectic model reduction of Hamiltonian systems on nonlinear manifolds and approximation with weakly symplectic autoencoder.* SIAM Journal on Scientific Computing 45.2 (2023). DOI: 10.1137/21M1466657.

[23] P. Buchfink, S. Glas, and B. Haasdonk. *Approximation bounds for model reduction on polynomially mapped manifolds.* Comptes Rendus. Mathématique (2024).

[24] P. Buchfink, S. Glas, B. Haasdonk, and B. Unger. *Model reduction on manifolds: A differential geometric framework.* Preprint. 2023. arXiv: 2312.01963 [math.NA].

[25] P. Buchfink and B. Haasdonk. *Experimental comparison of symplectic and non-symplectic model order reduction on an uncertainty quantification problem.* Numerical mathematics and advanced applications ENUMATH 2019. Springer International Publishing, 2020. DOI: 10.1007/978-3-030-55874-1_19.

[26] P. Buchfink, B. Haasdonk, and S. Rave. *PSD-greedy basis generation for structure-preserving model order reduction of Hamiltonian systems.* Proceedings of the conference Algoritmy 2020. http://www.iam.fmph.uniba.sk/amuc/ojs/index.php/algoritmy/article/view/1577/829 (last accessed 5-Dec-2023). Vydavateľstvo SPEKTRUM, 2020.

[27] A. Bunse-Gerstner. *Matrix factorizations for symplectic QR-like methods.* Linear Algebra and its Applications 83 (1986). DOI: 10.1016/0024-3795(86)90265-X.

[28] A. Cannas da Silva. *Lectures on symplectic geometry.* Springer Berlin Heidelberg, 2008. DOI: 10.1007/978-3-540-45330-7.

[29] K. Carlberg, C. Bou-Mosleh, and C. Farhat. *Efficient non-linear model reduction via a least-squares Petrov–Galerkin projection and compressive tensor approximations.* International Journal for Numerical Methods in Engineering 86.2 (2011). DOI: 10.1002/nme.3050.

[30]   K. Carlberg, M. Barone, and H. Antil. *Galerkin v. least-squares Petrov–Galerkin projection in nonlinear model reduction*. Journal of Computational Physics 330 (2017). DOI: [10.1016/j.jcp.2016.10.033](10.1016/j.jcp.2016.10.033).

[31]   K. Carlberg, R. Tuminaro, and P. Boggs. *Preserving Lagrangian structure in nonlinear model reduction with application to structural dynamics*. SIAM Journal on Scientific Computing 37.2 (2015). DOI: [10.1137/140959602](10.1137/140959602).

[32]   S. Chaturantabut and D. C. Sorensen. *Nonlinear model reduction via discrete empirical interpolation*. SIAM Journal on Scientific Computing 32.5 (2010). DOI: [10.1137/090766498](10.1137/090766498).

[33]   A. Cohen, C. Farhat, Y. Maday, and A. Somacal. *Nonlinear compressive reduced basis approximation for PDE's*. Comptes Rendus. Mécanique (2023). DOI: 10.5802/crmeca.191.

[34]   G. Deco and W. Brauer. *Nonlinear higher-order statistical decorrelation by volume-conserving neural architectures*. Neural Networks 8.4 (1995).

[35]   M. Drohmann, B. Haasdonk, and M. Ohlberger. *Reduced basis approximation for nonlinear parametrized evolution equations based on empirical operator interpolation*. SIAM Journal on Scientific Computing 34.2 (2012). DOI: [10.1137/10081157X](10.1137/10081157X).

[36]   J. L. Eftang, D. J. Knezevic, and A. T. Patera. *An hp certified reduced basis method for parametrized parabolic partial differential equations*. Mathematical and Computer Modelling of Dynamical Systems 17.4 (2011). DOI: [10.1080/13873954.2011.547670](10.1080/13873954.2011.547670).

[37]   A. Ern and J.-L. Guermond. *Theory and practice of finite elements*. Springer New York, 2004. DOI: [10.1007/978-1-4757-4355-5](10.1007/978-1-4757-4355-5).

[38]   B. Gao, N. T. Son, P.-A. Absil, and T. Stykel. *Geometry of the symplectic Stiefel manifold endowed with the Euclidean metric*. Geometric science of information. Springer International Publishing, 2021. DOI: [10.1007/978-3-030-80209-7_85](10.1007/978-3-030-80209-7_85).

[39]   B. Gao, N. T. Son, P.-A. Absil, and T. Stykel. *Riemannian optimization on the symplectic Stiefel manifold*. SIAM Journal on Optimization 31.2 (2021). DOI: [10.1137/20M1348522](10.1137/20M1348522).

[40]   B. Gao, N. T. Son, and T. Stykel. *Optimization on the symplectic Stiefel manifold: SR decomposition-based retraction and applications*. Linear Algebra and its Applications 682 (2023). DOI: [10.1016/j.laa.2023.10.025](10.1016/j.laa.2023.10.025).

[41] R. Geelen, S. Wright, and K. Willcox. *Operator inference for non-intrusive model reduction with quadratic manifolds*. Computer Methods in Applied Mechanics and Engineering 403 (2023). DOI: 10.1016/j.cma.2022.115717.

[42] X. Glorot and Y. Bengio. *Understanding the difficulty of training deep feedforward neural networks*. Proceedings of the thirteenth international conference on artificial intelligence and statistics. https://proceedings.mlr.press/v9/glorot10a.html (last accessed 5-Dec-2023). PMLR, 2010.

[43] I. Goodfellow, Y. Bengio, and A. Courville. *Deep learning*. https://www.deeplearningbook.org (last accessed 5-Dec-2023). MIT Press, 2016.

[44] C. Greif and K. Urban. *Decay of the Kolmogorov N-width for wave problems*. Applied Mathematics Letters 96 (2019). DOI: 10.1016/j.aml.2019.05.013.

[45] M. Grepl. *Reduced-basis approximations and a posteriori error estimation for parabolic partial differential equations*. PhD thesis, https://hdl.handle.net/1721.1/32387 (last accessed 5-Dec-2023). MIT, 2005.

[46] L. Grüne and O. Junge. *Gewöhnliche Differentialgleichungen*. 2nd edition. Springer Spektrum Wiesbaden, 2016. DOI: 10.1007/978-3-658-10241-8.

[47] B. Haasdonk. *Convergence rates of the POD-Greedy method*. ESAIM: Mathematical Modelling and Numerical Analysis 47.3 (2013). DOI: 10.1051/m2an/2012045.

[48] B. Haasdonk. *Model reduction and approximation*. SIAM, 2017. Chap. Reduced Basis Methods for Parametrized PDEs—A Tutorial Introduction for Stationary and Instationary Problems. DOI: 10.1137/1.9781611974829.ch2.

[49] B. Haasdonk and M. Ohlberger. *Reduced basis method for finite volume approximations of parametrized linear evolution equations*. ESAIM: Mathematical Modelling and Numerical Analysis 42.2 (2008). DOI: 10.1051/m2an:2008001.

[50] B. Haasdonk and M. Ohlberger. *Efficient reduced models and a posteriori error estimation for parametrized dynamical systems by offline/online decomposition*. Mathematical and Computer Modelling of Dynamical Systems 17.2 (2011). DOI: 10.1080/13873954.2010.514703.

[51] E. Hairer, G. Wanner, and C. Lubich. *Geometric numerical integration: Structure-preserving algorithms for ordinary differential equations*. Springer Berlin Heidelberg, 2006. DOI: 10.1007/3-540-30666-8.

[52]   K. He, X. Zhang, S. Ren, and J. Sun. *Delving deep into rectifiers: surpassing human-level performance on imagenet classification.* 2015 IEEE International Conference on Computer Vision (ICCV). 2015. DOI: 10.1109/ICCV.2015.123.

[53]   R. Herkert, P. Buchfink, and B. Haasdonk. *Dictionary-based online-adaptive structure-preserving model order reduction for parametric Hamiltonian systems.* Proceedings of Model Reduction and Surrogate Modeling (MORE 2022). 2024.

[54]   R. Herkert, P. Buchfink, B. Haasdonk, J. Rettberg, and J. Fehr. *Randomized symplectic model order reduction for Hamiltonian systems.* Large-scale scientific computing. Springer International Publishing, 2024.

[55]   Q. Hernández, A. Badías, F. Chinesta, and E. Cueto. *Port-metriplectic neural networks: Thermodynamics-informed machine learning of complex physical systems.* Computational Mechanics (2023). DOI: 10.1007/s00466-023-02296-w.

[56]   R. Horn and C. Johnson. *Matrix analysis.* Cambridge University Press, 1990.

[57]   H. Hotelling. *Analysis of a complex of statistical variables into principal components.* Journal of Educational Psychology 24.6 (1933). DOI: 10.1037/h0071325.

[58]   M. Hutchinson. *A stochastic estimator of the trace of the influence matrix for Laplacian smoothing splines.* Communications in Statistics - Simulation and Computation 18.3 (1989). DOI: 10.1080/03610918908812806.

[59]   O. Issan and B. Kramer. *Predicting solar wind streams from the inner-heliosphere to earth via shifted operator inference.* Journal of Computational Physics 473 (2023). DOI: 10.1016/j.jcp.2022.111689.

[60]   P. Jin, Z. Zhang, A. Zhu, Y. Tang, and G. Karniadakis. *SympNets: Intrinsic structure-preserving symplectic networks for identifying Hamiltonian systems.* Neural Networks 132 (2020). DOI: 10.1016/j.neunet.2020.08.017.

[61]   I. T. Jolliffe. *Principal component analysis.* Springer New York, 2002. DOI: 10.1007/b98835.

[62]   Y. Kajee, J-P. V. Pelteret, and B. D. Reddy. *The biomechanics of the human tongue.* International Journal for Numerical Methods in Biomedical Engineering 29.4 (2013). DOI: 10.1002/cnm.2531.

[63]   K. Karhunen. *Über lineare Methoden in der Wahrscheinlichkeitsrechnung.* Vol. 37. Annales Academiae Scientiarum Fennicae. Series A 1. 1947.

[64] D. P. Kingma and J. Ba. *Adam: A method for stochastic optimization.* Preprint. 2014. arXiv: 1412.6980 [cs.LG].

[65] A. W. Knapp. *Basic algebra.* 2nd edition. https://www.math.stonybrook.edu/~aknapp/download.html (last accessed 5-Dec-2023). Published by the Author, 2016.

[66] A. Kolmogorov. *Über die beste Annäherung von Funktionen einer gegebenen Funktionenklasse.* Annals of Mathematics 37.1 (1936). DOI: 10.2307/1968691.

[67] B. Kramer and K. E. Willcox. *Nonlinear model order reduction via lifting transformations and proper orthogonal decomposition.* AIAA Journal 57.6 (2019). DOI: 10.2514/1.J057791.

[68] K. Kunisch and S. Volkwein. *Galerkin proper orthogonal decomposition methods for parabolic problems.* Numerische Mathematik 90.1 (2001). DOI: 10.1007/s002110100282.

[69] S. Lall, P. Krysl, and J. E. Marsden. *Structure-preserving model reduction for mechanical systems.* Physica D: Nonlinear Phenomena 184.1 (2003). Complexity and Nonlinearity in Physical Systems – A Special Issue to Honor Alan Newell. DOI: 10.1016/S0167-2789(03)00227-6.

[70] C. Lanczos. *The variational principles of mechanics.* 2nd edition. Univ. of Toronto Press, 1962.

[71] H. P. Langtangen and A. Logg. *Solving PDEs in Python.* Springer, 2017. DOI: 10.1007/978-3-319-52462-7.

[72] H. P. Langtangen and G. K. Pedersen. *Scaling of differential equations.* 1st edition. Springer Publishing Company, 2016. DOI: 10.1007/978-3-319-32726-6.

[73] Y. LeCun, L. Bottou, Y. Bengio, and P. Haffner. *Gradient-based learning applied to document recognition.* Proceedings of the IEEE. Vol. 86. 11. 1998. DOI: 10.1109/5.726791.

[74] J. M. Lee. *Introduction to smooth manifolds.* Springer New York, 2012. DOI: 10.1007/978-1-4419-9982-5.

[75] K. Lee and K. Carlberg. *Model reduction of dynamical systems on nonlinear manifolds using deep convolutional autoencoders.* Journal of Computational Physics 404 (2020). DOI: 10.1016/j.jcp.2019.108973.

[76] B. Leimkuhler and S. Reich. *Simulating Hamiltonian dynamics.* Cambridge Monographs on Applied and Computational Mathematics. Cambridge University Press, 2005. DOI: 10.1017/CBO9780511614118.

[77]   R. Leiteritz, P. Buchfink, B. Haasdonk, and D. Pflüger. *Surrogate-data-enriched physics-aware neural networks*. Proceedings of the northern lights deep learning workshop 2022. Vol. 3. 2022. DOI: 10.7557/18.6268.

[78]   M. Loève. *Probability theory*. Van Nostrand, 1955.

[79]   J. L. Lumley. *The structure of inhomogeneous turbulent flows*. Atmospheric Turbulence and Radio Wave Propagation (1967).

[80]   B. Maboudi Afkham, A. Bhatt, B. Haasdonk, and J. S. Hesthaven. *Symplectic model reduction with a weighted inner product*. Preprint. 2018. arXiv: 1803.07799 [math.NA].

[81]   B. Maboudi Afkham and J. S. Hesthaven. *Structure preserving model reduction of parametric Hamiltonian systems*. SIAM Journal on Scientific Computing 39.6 (2017). DOI: 10.1137/17M1111991.

[82]   B. Maboudi Afkham and J. S. Hesthaven. *Structure-preserving model-reduction of dissipative Hamiltonian systems*. Journal of Scientific Computing (2019). DOI: 10.1007/s10915-018-0653-6.

[83]   Y. Maday, A. T. Patera, and G. Turinici. *Global a priori convergence theory for reduced-basis approximations of single-parameter symmetric coercive elliptic partial differential equations*. Comptes Rendus Mathematique 335.3 (2002). DOI: 10.1016/S1631-073X(02)02466-4.

[84]   Y. Maday, A. T. Patera, and G. Turinici. *A priori convergence theory for reduced-basis approximations of single-parameter elliptic partial differential equations*. Journal of Scientific Computing 17.1 (2002). DOI: 10.1023/A:1015145924517.

[85]   J. E. Marsden and T. S. Ratiu. *Introduction to mechanics and symmetry*. Springer New York, 1999. DOI: 10.1007/978-0-387-21792-5.

[86]   K. Meyer and D. Offin. *Introduction to Hamiltonian dynamical systems and the N-body problem*. 3rd edition. Springer, 2017. DOI: 10.1007/978-3-319-53691-0.

[87]   R. Milk, S. Rave, and F. Schindler. *PyMOR – generic algorithms and interfaces for model order reduction*. SIAM Journal on Scientific Computing 38.5 (2016). DOI: 10.1137/15M1026614.

[88]   P. J. Morrison. *The Maxwell–Vlasov equations as a continuous Hamiltonian system*. Physics Letters A 80.5 (1980). DOI: 10.1016/0375-9601(80)90776-8.

[89]   P. J. Morrison. *A paradigm for joined Hamiltonian and dissipative systems.* Physica D: Nonlinear Phenomena 18.1 (1986). DOI: 10.1016/0167-2789(86)90209-5.

[90]   M. Oechsner, K.-H. Kloos, B. Pyttel, C. Berger, M. Kübler, A. K. Müller, K.-H. Habig, and M. Woydt. *Anhang E: Diagramme und Tabellen. Dubbel: Taschenbuch für den Maschinenbau.* Springer Berlin Heidelberg, 2014. DOI: 10.1007/978-3-642-38891-0_40.

[91]   M. Ohlberger and S. Rave. *Nonlinear reduced basis approximation of parameterized evolution equations via the method of freezing.* Comptes Rendus Mathematique 351.23 (2013). DOI: 10.1016/j.crma.2013.10.028.

[92]   M. Ohlberger and S. Rave. *Reduced basis methods: Success, limitations and future challenges.* Proceedings of the conference Algoritmy. http://www.iam.fmph.uniba.sk/amuc/ojs/index.php/algoritmy/article/view/389, (last accessed 5-Dec-2023). 2016.

[93]   S. E. Otto, G. R. Macchio, and C. W. Rowley. *Learning nonlinear projections for reduced-order modeling of dynamical systems using constrained autoencoders.* Preprint. 2023. arXiv: 2307.15288 [math.DS].

[94]   S. E. Otto, A. Padovan, and C. W. Rowley. *Optimizing oblique projections for nonlinear systems using trajectories.* SIAM Journal on Scientific Computing 44.3 (2022). DOI: 10.1137/21M1425815.

[95]   C. Paige and C. V. Loan. *A Schur decomposition for Hamiltonian matrices.* Linear Algebra and its Applications 41 (1981). DOI: 10.1016/0024-3795(81)90086-0.

[96]   A. Paszke, S. Gross, F. Massa, A. Lerer, J. Bradbury, G. Chanan, T. Killeen, Z. Lin, N. Gimelshein, L. Antiga, A. Desmaison, A. Köpf, E. Yang, Z. DeVito, M. Raison, A. Tejani, S. Chilamkurthy, B. Steiner, L. Fang, J. Bai, and S. Chintala. *PyTorch: An imperative style, high-performance deep learning library.* Neural information processing systems. https://proceedings.neurips.cc/paper_files/paper/2019/file/bdbca288fee7f92f2bfa9f7012727740-Paper.pdf (last accessed 5-Dec-2023). 2019.

[97]   B. Peherstorfer. *Model order reduction of parametrized systems with sparse grid learning techniques.* PhD thesis, https://nbn-resolving.de/urn/resolver.pl?urn:nbn:de:bvb:91-diss-20130918-1163421-0-8 (last accessed 5-Dec-2023). Technische Universität München, 2013.

[98]   B. Peherstorfer and K. Willcox. *Data-driven operator inference for nonintrusive projection-based model reduction.* Computer Methods in Applied Mechanics and Engineering 306 (2016). DOI: 10.1016/j.cma.2016.03.025.

[99]   L. Peng and K. Mohseni. *Symplectic model reduction of Hamiltonian systems.* SIAM Journal on Scientific Computing 38.1 (2016). DOI: 10.1137/140978922.

[100]   L. Peng and K. Mohseni. *Structure-preserving model reduction of forced Hamiltonian systems.* Preprint. 2016. arXiv: 1603.03514 [math.NA].

[101]   E. Qian, B. Kramer, B. Peherstorfer, and K. Willcox. *Lift & Learn: Physics-informed machine learning for large-scale nonlinear dynamical systems.* Physica D: Nonlinear Phenomena 406 (2020). DOI: 10.1016/j.physd.2020.132401.

[102]   J. Reiss, P. Schulze, J. Sesterhenn, and V. Mehrmann. *The shifted proper orthogonal decomposition: A mode decomposition for multiple transport phenomena.* SIAM Journal on Scientific Computing 40.3 (2018). DOI: 10.1137/17M1140571.

[103]   J. Rettberg, D. Wittwar, P. Buchfink, A. Brauchler, P. Ziegler, J. Fehr, and B. Haasdonk. *Port-Hamiltonian fluid–structure interaction modelling and structure-preserving model order reduction of a classical guitar.* Mathematical and Computer Modelling of Dynamical Systems 29.1 (2023). DOI: 10.1080/13873954.2023.2173238.

[104]   J. Rettberg, D. Wittwar, P. Buchfink, R. Herkert, J. Fehr, and B. Haasdonk. *Improved a posteriori error bounds for reduced port-Hamiltonian systems.* Preprint. 2023. arXiv: 2303.17329 [math.NA].

[105]   D. Rim, S. Moe, and R. J. LeVeque. *Transport reversal for model reduction of hyperbolic partial differential equations.* SIAM/ASA Journal on Uncertainty Quantification 6.1 (2018). DOI: 10.1137/17M1113679.

[106]   T. Ruiner, J. Fehr, B. Haasdonk, and P. Eberhard. *A-posteriori error estimation for second order mechanical systems.* Acta Mechanica Sinica 28 (2012). DOI: 10.1007/s10409-012-0114-7.

[107]   H. Sharma and B. Kramer. *Preserving Lagrangian structure in data-driven reduced-order modeling of large-scale dynamical systems.* Preprint. 2022. arXiv: 2203.06361 [math.NA].

[108]   H. Sharma, H. Mu, P. Buchfink, R. Geelen, S. Glas, and B. Kramer. *Symplectic model reduction of Hamiltonian systems using data-driven quadratic manifolds*. Computer Methods in Applied Mechanics and Engineering 417 (2023). DOI: 10.1016/j.cma.2023.116402.

[109]   H. Sharma, Z. Wang, and B. Kramer. *Hamiltonian operator inference: Physics-preserving learning of reduced-order models for canonical Hamiltonian systems*. Physica D: Nonlinear Phenomena 431 (2022). DOI: 10.1016/j.physd.2021.133122.

[110]   S. Shuva, P. Buchfink, O. Röhrle, and B. Haasdonk. *Reduced basis methods for efficient simulation of a rigid robot hand interacting with soft tissue*. Large-scale scientific computing. Springer International Publishing, 2022. DOI: 10.1007/978-3-030-97549-4_46.

[111]   L. Sirovich. *Turbulence the dynamics of coherent structures. Part I: Coherent structures*. Quarterly of Applied Mathematics 45 (1987). DOI: 10.1090/qam/910462.

[112]   T. Taddei. *A registration method for model order reduction: Data compression and geometry reduction*. SIAM Journal on Scientific Computing 42.2 (2020). DOI: 10.1137/19M1271270.

[113]   B. Unger and S. Gugercin. *Kolmogorov n-widths for linear dynamical systems*. Advances in Computational Mathematics 45.5-6 (2019). DOI: 10.1007/s10444-019-09701-0.

[114]   A. van der Schaft and D. Jeltsema. *Port-Hamiltonian systems theory: An introductory overview*. Foundations and Trends® in Systems and Control 1.2-3 (2014). DOI: 10.1561/2600000002.

[115]   S. Volkwein. *Proper orthogonal decomposition: Theory and reduced-order modelling*. https://www.math.uni-konstanz.de/numerik/personen/volkwein/teaching/POD-Book.pdf (last accessed 5-Dec-2023). University of Konstanz, 2013.

[116]   H. Xu. *A numerical method for computing an SVD-like decomposition*. SIAM Journal on Matrix Analysis and Applications 26.4 (2005). DOI: 10.1137/S0895479802410529.

[117]   H. Xu. *An SVD-like matrix decomposition and its applications*. Linear Algebra and its Applications 368 (2003). DOI: 10.1016/S0024-3795(03)00370-7.

Abstract

Mathematical models are a key enabler to understand complex processes across all branches of research and development since such models allow us to simulate the behavior of the process without physically realizing it. However, detailed models are computationally demanding and, thus, are frequently prohibited from being evaluated (a) multiple times for different parameters, (b) in real time or (c) on hardware with low computational power. The field of model (order) reduction (MOR) aims to approximate such detailed models with more efficient surrogate models that are suitable for the tasks (a-c). In classical MOR, the solutions of the detailed model are approximated in a problem-specific, low-dimensional subspace, which is why we refer to it as MOR on subspaces. The subspace is characterized by a reduced basis that can be computed from given data with a so-called basis generation technique.

The two key aspects in this thesis are: (i) structure-preserving MOR techniques and (ii) MOR on manifolds. Preserving given structures throughout the reduction is important to obtain physically consistent reduced models. We demonstrate this for Lagrangian and Hamiltonian systems, which are dynamical systems that guarantee preservation of energy over time. MOR on manifolds, on the other hand, broadens the applicability of MOR to problems that cannot be treated efficiently with MOR on subspaces.